

Multicomponent cyclization strategies to novel  
conformationally constrained peptides



# “Multicomponent cyclization strategies to novel conformationally constrained peptides”

## Dissertation

zur Erlangung des Doktorgrades der  
Naturwissenschaften (Dr. rer. nat.)

der

Naturwissenschaftlichen Fakultät II Chemie, Physik  
und Mathematik

der Martin-Luther-Universität Halle-Wittenberg

vorgelegt von

**Herrn M.Sc. Aldrin Vasco Vidal**

Geb. Am 15.11.1989 in La Habana, Kuba

Halle (Saale) 2019

The work described in this dissertation has been developed at the Leibniz-Institute of Plant Biochemistry (IPB) in cooperation with Martin-Luther Halle-Wittenberg University and the University of Havana.



**Supervisor and thesis editor:** Prof. Dr. Ludger A. Wessjohann

**International co-supervisor:** Prof. Dr. Daniel G. Rivera

1<sup>st</sup> Reviewer: Prof. Dr. Ludger A. Wessjohann (IPB-Halle)

2<sup>nd</sup> Reviewer: Prof. Dr. Hans-Dieter Arndt (Universität Jena)

Date of Public Defense: March 12<sup>th</sup>, 2020

## **Declaration**

“I declare that I have completed this dissertation without unauthorized help of a second party and only with the assistance acknowledged therein. I have appropriately acknowledged and referenced all text passages that are derived literally from or based on the content of published or unpublished work of other authors.”

Aldrin Vasco Vidal

*But how could you live and have no story to tell?*

*Fyodor Dostoevsky*

***To Yani,  
for all the love, for all the joy***



## Acknowledgments

The long ride that comprises the culmination of a Ph.D. cannot be traveled without a lot of extraordinary people without whom, all this work wouldn't have been achieved. I need to first express my innermost gratitude to Daniel G. Rivera, for being both, scientific guide and dear friend; joining his working group in Havana was the best choice I could have ever made. I owe to him my passion for research and my enthusiasm in exploring new projects and ideas. To Prof. Wessjohann many thanks for allowing me to join the IPB and for his confidence in my work. The independence he offered me had noticeably improved my scientific capacity and planning. I appreciate that in one way or another he always managed to find some time for me in his tight schedule whenever I needed it. The vast knowledge and great ideas, as well as the love and enthusiasm for science transmitted from these two extraordinary researchers, are the foundation of my forthcoming scientific career. Feeling how proud and satisfied both of you were with my scientific development was an infinite source of strength and enthusiasm.

My passion for NMR is intrinsically connected to two persons who I deeply admire: Prof. Carlos Pérez and Dr. Andrea Porzel. Carlos is the best lecturer any student could ever have and for me was lifechanging to have become his master student and coworker. To Andrea my greatest gratitude for teaching me the technical details of operating an NMR spectrometer and for her dedication and patience every time a new question appeared.

My sincere thanks to all members of the Leibniz Institute of Plant Biochemistry (IPB-Halle) particularly to the members of the Bioorganic Chemistry department (NWC), and to the team at the Center for Natural Products Research in Havana. I keep special gratitude to Prof. Bernhard Westermann for his continuous support inside and outside the lab and the many hours of scientific discussion. To all my labmates, colleagues and friends in the IPB, Alfredo, Annegret, Anja E., Anja K., Antonio, Bruno, Carlos, Daniela, David, Dayma, Dube, Frank, Haider, Janoi, Katya, Leo, Martin, Mathias, Micjel, Nalin, Paul, Renata, Thomas, Tuvshin and Yanira many many thanks for all the good memories and the unique working atmosphere. Having so many friends from all around the world was also a way of feeling like being at home. Especial thanks to Manuel for his friendship and for being the consultant in so many moments of unexpected results in the lab. To my co-supervised students in Havana Mario, Leo, Gaby, Fidel, and Celia many thanks for the good work.

Likewise, I would like to extend my gratitude to the many collaborators, inside and outside the IPB, that supported my work during this time. To Prof. Jochen Balbach and Dr. Stefan Gröger for the NMR characterization in water solution; to Dr. Robert Rennert and Prof. Goran Kaluderović for the anticancer assays; to Dr. Silke Pienkny for the design of protein inhibitors; and to Dr. Andreas Kerth for the DLS studies of some of the peptides. My greater appreciation to Wolfgang Brandt for opening the doors of his lab to me and support me in the molecular modeling of my compounds.

To all the technical staff in NWC many thanks for doing our work much easier. I must particularly thank Anja Ehrlich for sharing her expertise in HPLC with me and assist with the purification of several compounds. Also special thanks to Gudrun Hahn for her unconditional disposition to help when needed and for doing always her best to understand my primitive German. To Martina Brode many thanks for performing the antifungal assays for several compounds. To Ines Stein my gratitude for her disposition to help in every bureaucratic issue. To Mandy Dorn and Dr. Andrej Frolov many thanks for the MS characterization.

I will also like to thank the German Academic Exchange Service (DAAD) for the doctoral scholarship which allowed me to come to Germany.

No success in the world worth anything without the people to share it with, those who, no matter what, will be there for you. To my parents Marcela Vidal and Mario Vasco my eternal gratefulness for being the examples that shaped my character and encouraged me to follow my dreams. Thank you so much for so many sacrifices, including understanding that the road conducting me to my Ph.D. needed to be traveled far away from home. To my brothers and my sister thanks a lot for being always so proud of your little brother, this feeling is something I carry always with me wherever I go. Finally, I need to thank the person who from the very beginning has been the co-pilot in this travel and whose support and love have been a foothold in every moment. To Yani, my best partner and my best friend, is dedicated this thesis. No success in my life does not carry your name and no joy is complete if you are not there to live it with me.

To all, including those I could have forgotten, many many thanks.

Aldrin Vasco Vidal

Halle, 02.09.2019

## Abstract

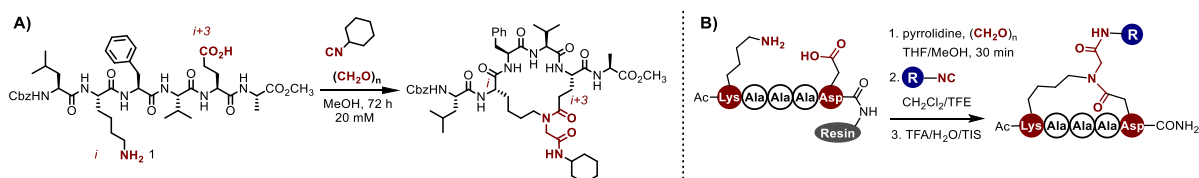
Peptides represent a unique class of bioactive molecules which occupy a special space between small molecules and biologics, often combining the best of both but yet behaving biochemically and therapeutically different from them.<sup>[1-3]</sup> The recent development of new methodologies for the synthesis of modified peptides, particularly constrained peptides, is reflected in the greater number of peptide-based drugs and candidates in clinical evaluation. Most peptide properties such as binding affinity and specificity, solubility and metabolic stability can be optimized and tailored to a desired application by the introduction of conformational restraints *via* derivatization of the peptide skeleton.<sup>[4]</sup> Currently, macrocyclization stands as the most effective way of introducing conformational constraints in short and medium-sized peptides designed for biological and medicinal applications.

The present thesis describes the development of new strategies for the synthesis of constrained peptides based on multicomponent reactions (MCRs). Using this special class of chemical transformation, the simultaneous derivatization and folding of a variety of peptide sequences are achieved. Special attention is given to describe the structural implications of utilizing the multicomponent processes for the stabilization of peptide secondary structures such as  $\beta$ -turns,  $\alpha$ -helixes, and  $\beta$ -hairpins.

**Chapter 1** contains up-to-date literature regarding the use of MCRs for the synthesis of constrained peptides. Likewise, the main advantages of MCRs-based cyclization methodologies over traditional strategies including one or two components are described.

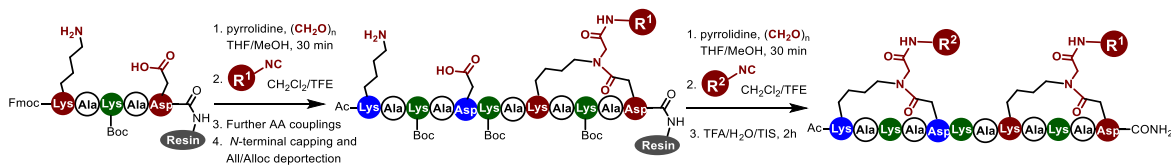
**Chapter 2** describes the first report on Ugi-4CR macrocyclization including peptide side chains. The work was thought to expand the scope of the already reported Ugi head-to-tail macrocyclization of tri- and hexapeptides<sup>[5]</sup> and to evaluate its suitability for the stabilization of relevant peptide secondary structures. The Ugi side chain-to-side chain cyclization proves to be effective for the stabilization of tight turns in hexa- hepta- and octapeptides, with the subsequent installation of an exocyclic *N*-substituted lactam bridge. The main limitation of this solution-phase approach is the lack of orthogonality of the Ugi-reactive side chains towards other amino and carboxylic acid groups usually found in a peptide sequence.

In **Chapter 3**, a solid phase approach for the Ugi side chain-to-side chain macrocyclization of peptides is described. As compared with the solution-phase approach, this methodology enables the access to more complex peptide sequences since the desired Ugi-reacting side chains could be orthogonally deprotected before cyclization. In an endeavor to mimic the helical-occurring model peptide Ac-(cyclo-1,5)-[KAAAD]-NH<sub>2</sub>,<sup>[6]</sup> a series of Ugi-derived pentapeptides bearing different *N*-substituents were prepared. In contrast with the model helical peptide, the Ugi-cyclized pentapeptides occur as a mixture of two conformers in water, i.e. *s-cis/s-trans* conformers around the tertiary amide, both possessing a  $\beta$ -turn conformation. Neither the secondary structure nor the conformer distribution seems to be dramatically influenced by the nature of the *N*-substituent at the exocyclic lactam. For Ugi-cyclized dodecapeptides with helical propensity, the helical content seems to be related to variations in the population of *s-cis* and *s-trans* conformers.



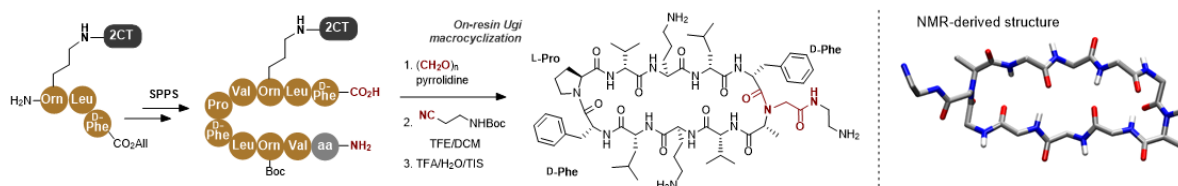
Scheme 1. A) Solution-phase and B) solid-phase strategy for the Ugi-4CR macrocyclization of peptides

The scope of the Ugi-based side chain-to-side chain cyclization in the stabilization of  $\alpha$ -helical conformations is expanded for the synthesis of more complex stapled peptides, as described in **Chapter 4**. A series of helical dodecapeptides bearing one or two Ugi-cyclizations are synthesized. As compared with “classical” stapling methodologies,<sup>[7–9]</sup> the multicomponent nature of the Ugi-4CR allows the readily installation of pharmacologically relevant functionalities at the lactam bridge, i.e. PEGs, sugars, fluorescent labels, and reactive handles. The suitability of this methodology in bioconjugation strategies is proven by the design of a helical peptide bearing a maleimide functionalization, which further enables the conjugation to a carrier protein.



Scheme 2. Solid-phase strategy for bicyclic Ugi-stapled peptides

A final part of the work addresses the design of Ugi-based strategies for the stabilization of  $\beta$ -hairpins (**Chapter 5**). The insertion of an *N*-substituted amino acid – arising from the Ugi-4CR – within the peptide skeleton proves effective in mimicking the proline residue in naturally occurring  $\beta$ -hairpins. The method is employed in the synthesis of mimetics of Gramicidin S bearing one or two *N*-functionalizations at the  $\beta$ -turn motif while conserving the  $\beta$ -hairpin structure.



Scheme 3. Synthesis of Ugi-derived analogs of Gramicidin S

The main scientific achievement of the present thesis is to demonstrate the suitability of Ugi-based cyclization methods for the stabilization of the most relevant peptide secondary structures. As compared with alternative approaches, a key advantage of the present strategy is the combination of functionalization and conformational locking in the same step. From a structural point of view, the insertion of functionalized tertiary amides allows the occurrence of *s-cis/s-trans* isomerization, which constitutes the most distinctive characteristic of these compounds. Current efforts are directed to exploit the synthetic potential of this strategy in the development of new inhibitors of protein-protein interactions, ligands for plant protein receptors and antimicrobial agents.

## References

- [1] J. L. Lau, M. K. Dunn, *Bioorganic Med. Chem.* **2018**, *26*, 2700–2707.
- [2] C. Morrison, *Nat. Rev. Drug Discov.* **2018**, *17*, 531–533.
- [3] K. Fosgerau, T. Hoffmann, *Drug Discov. Today* **2015**, *20*, 122–128.
- [4] A. F. B. Räder, M. Weinmüller, F. Reichart, A. Schumacher-Klinger, S. Merzbach, C. Gilon, A. Hoffman, H. Kessler, *Angew. Chem., Int. Ed.* **2018**, *57*, 14414–14438.
- [5] A. Failli, H. Immer, M. Götz, *Can. J. Chem.* **1979**, *57*, 3257–3261.
- [6] A. D. De Araujo, H. N. Hoang, W. M. Kok, F. Diness, P. Gupta, T. A. Hill, R. W. Driver, D. A. Price, S. Liras, D. P. Fairlie, *Angew. Chem., Int. Ed.* **2014**, *53*, 6965–6969.
- [7] T. A. Hill, N. E. Shepherd, F. Diness, D. P. Fairlie, *Angew. Chem., Int. Ed.* **2014**, *53*, 13020–13041.
- [8] M. Pelay-Gimeno, A. Glas, O. Koch, T. N. Grossmann, *Angew. Chem., Int. Ed.* **2015**, *54*, 8896–8927.
- [9] S. P. Brown, A. B. Smith, *J. Am. Chem. Soc.* **2015**, *137*, 4034–4037.



# Zusammenfassung

Peptide stellen eine einzigartige Klasse von bioaktiven Molekülen dar, die einen speziellen Platz zwischen kleinen Moleküle und Biomolekülen einnehmen. Dabei vereinigen sie die bevorzugten Eigenschaften beider und verhalten sich dabei jedoch biochemisch und therapeutisch unterschiedlich.<sup>[1-3]</sup> Die aktuelle Entwicklung neuer synthetischer Methoden von modifizierten Peptiden, im Speziellen von konformationell eingeschränkten Peptiden, zeigt sich in einer Vielzahl an peptid-basierten Medikamenten und deren Anwendung in klinischen Studien. Peptideigenschaften wie Bindungsaffinität, Spezifität, Löslichkeit und metabolische Stabilität können optimiert werden und für die gewünschte Anwendungen durch Einführung von Konformationseinschränkungen durch die Derivatisierung des Peptidgrundgerüsts angepasst werden.<sup>[4]</sup> Momentan gehört die Makrozyklisierung zu den effektivsten Methoden für die Einführung dieser Konformationseinschränkungen in kurzen sowie mittelkettigen Peptiden für die biologische und medizinische Anwendung.

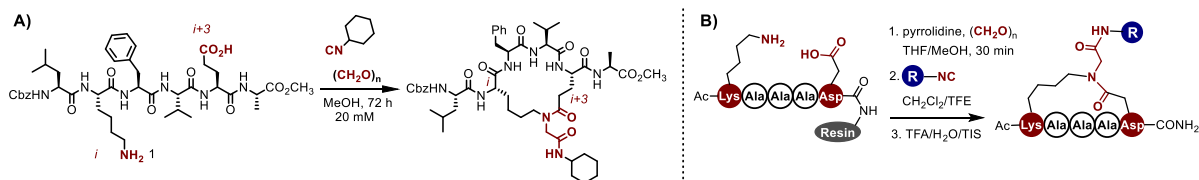
Die vorliegende Dissertation beinhaltet die Entwicklung neuer Synthesestrategien von konformationell eingeschränkten Peptiden mittels Multikomponentenreaktionen (MCRs). Durch Verwendung dieser speziellen Art der chemischen Transformation kann simultan die Derivatisierung und die Faltung einer Vielzahl von Peptidsequenzen erreicht werden. Ein spezielles Augenmerk liegt dabei auf den strukturellen Auswirkungen, die durch die Verwendung des Multikomponentenprozesses für die Stabilisierung von Peptidsekundärstrukturen wie  $\beta$ -*turns*,  $\alpha$ -Helices und  $\beta$ -*hairpins* hervorgehen.

**Kapitel 1** umfasst die aktuelle Literatur bezüglich der Verwendung von MCRs für die Synthese von konformationell eingeschränkten Peptiden. Weiterhin ist der Hauptvorteil der MCR-basierten Zyklisierung gegenüber traditionellen Methoden sowie Ein- oder Zwei-Komponentenstrategien beschrieben.

Das **zweite Kapitel** befasst sich mit einer erstmals durchgeführten Ugi-4-CR Makrozyklisierung unter Einbindung der Peptidseitenketten. Diese Arbeit diente der Spektrumserweiterung der bereits bekannten Ugi-Kopf-zu-Schwanz-Zyklisierung von Tri- und Hexapeptiden<sup>[5]</sup> sowie der Anwendbarkeitsprüfung für die Stabilisierung von relevanten Peptidsekundärstrukturen. Die Ugi-Seitenketten-zu-Seitenketten-Zyklisierung bietet eine effektive Methode zur Stabilisierung von gespannten *turns* in Hexa-, Hepta- und Oktapeptiden mit der stufenweisen Einführung von exozyklischen *N*-substituierten Lactambrücken. Die

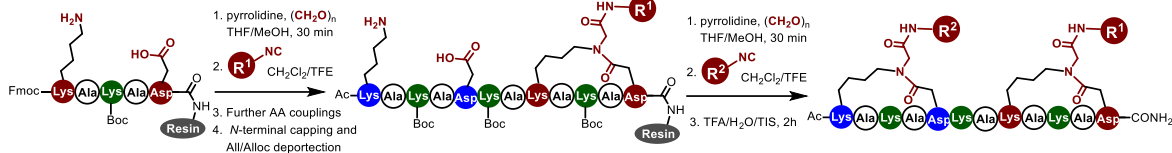
Hauptlimitierung von diesem in Lösung durchgeführten Ansatz ist der Mangel an Orthogonalität von der Ugi-reaktiven Seitenkette zu anderen Amino- und Carboxylgruppen, die sonst in Peptidsequenzen vorkommen.

Im **dritten Kapitel** wird ein Festphasenansatz für die Ugi-Seitenketten-zu-Seitenketten-Zyklisierung beschrieben. Verglichen zum In-Lösung-Verfahren ermöglicht diese Methode den Zugang zu komplexeren Peptidsequenzen aufgrund der gewünschten Ugi-reaktiven Seitenkette, die orthogonal vor der Zyklisierung geschützt wird. In Bemühungen zur Nachahmung des helikal vorkommenden Modellpeptids Ac-(cyclo-1,5)-[KAAAD]-NH<sub>2</sub>,<sup>[6]</sup> wurde eine Reihe von Pentapeptiden, welche verschiedene *N*-Substitutionen aufweisen, mittels Ugi-Reaktion hergestellt. Im Gegensatz zum helikalen Modellpeptid zeigen die Ugi-zyklisierten Pentapeptide eine Mischung von zwei Konformeren in Wasser, die *s-cis* und *s-trans* Konformation um tertiäre Amide - wobei beide eine  $\beta$ -turn Konformation besitzen. Weder die Sekundärstruktur noch die Konformerverteilung sind dramatisch von der Natur der *N*-Substitution des exozyklischen Lactams beeinflusst. Für Ugi-zyklisierte Dodecapeptide mit helikaler Tendenz scheint es, dass der helikale Inhalt im Zusammenhang mit der Variation der Population von *s-cis* und *s-trans* Konformeren steht.



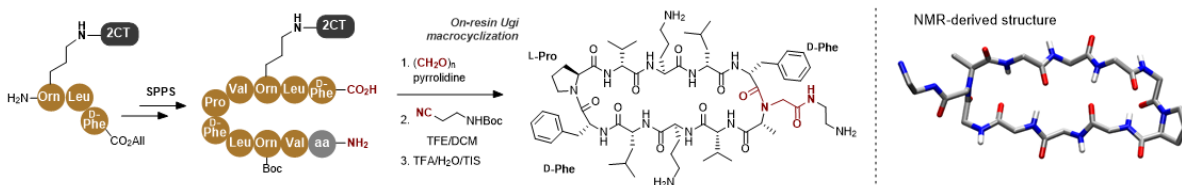
Schema 1. A) In-Lösung- und B) Festphasenstrategie für die Ugi-4CR Makrozyklisierung von Peptiden

Der Umfang der Ugi-basierten Seitenketten-zu-Seitenketten-Zyklisierung für die Stabilisierung von  $\alpha$ -helikalen Konformationen wurde durch die Synthese von komplex gestapelten Peptiden (*stapled peptides*) erweitert, was in **Kapitel 4** erläutert wird. Eine Serie von helikalen Dodecapeptiden wurde mittels ein oder zwei Ugi-Zyklisierungen synthetisiert. Im Vergleich zu den „klassischen“ Stapelmethoden<sup>[7–9]</sup> erlaubt der Multikomponentenansatz der Ugi-4CR eine finale Einführung der pharmakologisch relevanten Funktionalisierung an der Lactambrücke, z.B. PEGs, Zucker, fluoreszierende Sonden und reaktive *handles*. Die Anwendbarkeit dieser Methode für Biokonjugationsstrategien wurde durch das Design von helikalen und mit Maleimid-funktionalisierte Peptiden, welche weiterhin die Konjugation zu einem Transportprotein ermöglicht, bestätigt.



Schema 2. Festphasenstrategie für bizyklische Ugi-gestapelte Peptide

Im finalen Teil dieser Arbeit wird das Design einer Ugi-basierten Strategie für die Stabilisierung von  $\beta$ -hairpins beschrieben (**Kapitel 5**). Die Einführung von einer *N*-substituierten Aminosäure, entstanden durch die Ugi-4CR, innerhalb eines Peptidgrundgerüsts beweist die effektive Nachahmung eines Prolinrestes in natürlich vorkommenden  $\beta$ -hairpins. Dieser Ansatz wurde für die Synthese von Gramicidin S Mimetika angewendet, wobei ein oder zwei *N*-Funktionalisierungen am  $\beta$ -turn Gerüst verwendet werden konnten, um die  $\beta$ -hairpin Struktur zu bewahren.



Schema 3. Synthese durch Ugi-4CR erhaltene Analoga von Gramicidin S

Der größte wissenschaftliche Gewinn der vorliegenden Dissertation ist die Demonstration über die Anwendbarkeit der Ugi-basierten Zyklisierungsmethoden für die Stabilisierung der relevantesten Peptidsekundärstrukturen. Im Vergleich zu alternativen Herangehensweisen ist der wesentliche Vorteil der vorgestellten Strategie die Kombination aus Funktionalisierung und Einführung einer Sekundärstruktur in einem Schritt. Strukturell betrachtet erlaubt die Einführung von funktionalisierten tertiären Amiden das Vorkommen von *s-cis/s-trans* Isomerisierung, welche den unverwechselbaren Charakter dieser Verbindungen ausmacht. Aktuelle Bemühungen zielen auf das synthetische Potenzial dieser Strategie in der Entwicklung neuer Inhibitoren für Protein-Protein Interaktionen, Liganden für Pflanzenproteinrezeptoren und antimikrobiellen Wirkstoffen ab.

## Referenzen

- [1] J. L. Lau, M. K. Dunn, *Bioorganic Med. Chem.* **2018**, *26*, 2700–2707.
- [2] C. Morrison, *Nat. Rev. Drug Discov.* **2018**, *17*, 531–533.
- [3] K. Fosgerau, T. Hoffmann, *Drug Discov. Today* **2015**, *20*, 122–128.
- [4] A. F. B. Räder, M. Weinmüller, F. Reichart, A. Schumacher-Klinger, S. Merzbach, C. Gilon, A. Hoffman, H. Kessler, *Angew. Chem., Int. Ed.* **2018**, *57*, 14414–14438.

- [5] A. Failli, H. Immer, M. Götz, *Can. J. Chem.* **1979**, *57*, 3257–3261.
- [6] A. D. De Araujo, H. N. Hoang, W. M. Kok, F. Diness, P. Gupta, T. A. Hill, R. W. Driver, D. A. Price, S. Liras, D. P. Fairlie, *Angew. Chem., Int. Ed.* **2014**, *53*, 6965–6969.
- [7] T. A. Hill, N. E. Shepherd, F. Diness, D. P. Fairlie, *Angew. Chem., Int. Ed.* **2014**, *53*, 13020–13041.
- [8] M. Pelay-gimeno, A. Glas, O. Koch, T. N. Grossmann, *Angew. Chem., Int. Ed.* **2015**, *54*, 8896–8927.
- [9] S. P. Brown, A. B. Smith, *J. Am. Chem. Soc.* **2015**, *137*, 4034–4037.

# Table of Contents

<b>Chapter 1.</b>	1
1.1. Constrained peptides: current status and future directions	2
1.2. Peptide Macrocyclization by Multicomponent Reactions	4
1.3. Head-to-tail cyclization by isocyanide-based MCRs	6
1.4. Multicomponent side chain-to-side chain cyclization	11
1.5. Other MCR-based strategies to constrained peptides	15
1.6. Remarks and future perspectives	16
1.7. Aims of this PhD work	16
1.8. References	17
<b>Chapter 2.</b>	21
2.1. Introduction	22
2.2. Synthetic Plan	22
2.3. Macrocyclization of peptide side chains by Ugi reaction	24
2.4. Three-dimensional structure of side chain-to-side chain cross-linked peptides	26
2.5. Conclusions	31
2.6. Experimental Section	32
General	32
NMR structure determination	35
Molecular Dynamics Simulations	36
2.7. References	37
<b>Chapter 3.</b>	39
3.1. Introduction	40
3.2. Synthetic Plan	40
3.3. Synthesis of analogs of Ac-(cyclo-1,5)-[KAAAD]-NH <sub>2</sub>	42
3.4. Influence of the s-cis/s-trans isomerism on the helical content of dodecapeptides	45
3.5. Conclusions	47
3.6. Experimental part	48
3.6.1 Spectroscopic characterization	48
3.6.2 Chromatographic methods	48
3.6.3 High resolution mass spectrometry characterization	49
3.6.4 General methods for Peptide Synthesis	49
3.6.5 General protocol for the synthesis of isocyanides from amines	50
3.6.6 Synthesis of peptides	51
3.6.7 NMR structure determination	58

3.7.	References .....	60
<b>Chapter 4.</b>	.....	61
4.1.	Introduction .....	62
4.2.	Synthetic Plan .....	62
4.3.	Synthesis of Ugi-stapled dodecapeptides .....	63
4.4.	Synthesis of bicyclic peptides .....	67
4.5.	Ligation-enabling peptide stapling .....	68
4.6.	Conclusions .....	69
4.7.	Experimental part .....	70
	4.7.1 Spectroscopic characterization .....	70
	4.7.2 Chromatographic methods .....	70
	4.7.3 Mass spectrometry characterization .....	70
	4.7.4 General methods for Peptide Synthesis .....	71
	4.7.5 Synthesis of isocyanides .....	73
	4.7.6 Synthesis of peptides .....	73
	4.7.7 Molecular Dynamics Simulations .....	87
4.8.	References .....	88
<b>Chapter 5.</b>	.....	91
5.1.	Introduction .....	92
5.2.	Synthetic plan .....	93
5.3.	Mono-substituted GS analogs .....	93
5.4.	Di-substituted GS analogs .....	95
5.5.	Conclusions .....	99
5.6.	Experimental part .....	99
	5.6.1 General Information .....	99
	5.6.2 General methods for the Solid Phase Peptide Synthesis .....	100
	5.6.3 Synthesis of tripeptide Fmoc-Orn(NH-2CT)-Leu-D-Phe-OH .....	101
	5.6.4 Synthesis of isocyanides .....	102
	5.6.5 Synthesis of cyclic peptides .....	103
	5.6.6 NMR-based structure calculations .....	108
5.7.	References .....	110
<b>Annexes</b>	.....	113

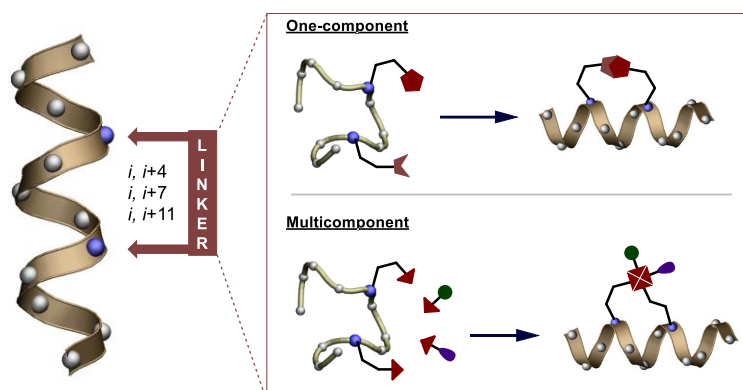
## List of abbreviations

aa	amino acid	NMM	<i>N</i> -Methylmorpholine
Alloc	allyloxycarbonyl	NMP	<i>N</i> -Methyl-2-pyrrolidon
Ac	acetate	NMR	nuclear magnetic resonance
AcN	acetonitrile	NOE	nuclear Overhauser effect
Boc	<i>tert</i> -butyl carbamate	PEG	polyethylene glycol
calcd.	calculated	Ph	phenyl
CD	circular dichroism	PPI	protein-protein interaction
COSY	correlation spectroscopy	PRESAT	presaturation
CuAAC	copper(I)-catalyzed alkyne-azide cycloaddition	PyAOP	(7-azabenzotriazol-1-yloxy) tripyrrolidinophosphonium hexafluorophosphate
DCM	dichloromethane	PyBOP	benzotriazol-1-yl-oxytripyrrolidinophosphonium hexafluorophosphate
DIC	diisopropylcarbodiimide	RMSD	root-mean-square deviation
DIPEA	diisopropylethylamine	ROE	rotating-frame Overhauser enhancement
DMF	dimethylformamide	ROESY	Rotating frame nuclear Overhauser effect spectroscopy
DMSO	dimethyl sulfoxide	RP-HPLC	reverse-phase high performance liquid chromatography
ES	excitation sculpting	RP-UHPLC	reverse-phase ultra-high performance liquid chromatography
ESI-MS	electrospray ionization mass spectrometry	RT	room temperature
EtOAc	ethyl acetate	R <sub>t</sub>	retention time
FA	formic acid	SPPS	solid phase peptide synthesis
Fmoc	9-fluorenylmethyloxycarbonyl	<i>t</i> Bu	<i>tert</i> -butyl
FT-ICR	Fourier transform ion cyclotron resonance	TFA	trifluoroacetic acid
GHRP	growth hormone-releasing peptide	TFE	2,2,2-trifluoroethanol
HMBC	heteronuclear multiple bond correlation spectroscopy	TG-S-RAM	tentagel resin-bound Rink amide
HOBt	1-hydroxybenzotriazole	THF	tetrahydrofuran
HR-MS	high resolution mass spectrometry	TIS	triisopropylsilane
HSQC	heteronuclear single quantum coherence spectroscopy	TLC	thin layer chromatography
IR	infrared	TMS	tetramethyl silane
MALDI-MS	matrix-assisted laser desorption-ionization mass spectrometry	TOCSY	total correlation spectroscopy
MCR	multicomponent reaction	Trt	triphenylmethyl
Me	methyl	TSP	3-(trimethylsilyl)propionic-2,2,3,3-d <sub>4</sub> acid sodium salt
MeOH	methanol	Ugi-4CR	Ugi-four components reaction
MD	molecular dynamics		
min.	minute		
MWD	multi wavelength detector		



## Chapter 1.

# Multicomponent strategies to conformationally-constrained peptides



**ABSTRACT:** Constraining peptides into bioactive conformations stands as one of the most successful strategies to design novel peptidomimetics with improved stability and physicochemical characteristics for therapeutic effect. The utilization of multicomponent reactions for such purposes provides a key advantage over the established methods: a diversity-generating character which enables the exploration of a broader chemical space at the same time that conformational rigidity is efficiently incorporated into the target molecule.

## 1.1. Constrained peptides: current status and future directions

Peptides represent a unique class of bioactive molecules which occupy a special space between small chemicals and large biologics, theoretically combining the best from both but yet behaving biochemically and therapeutically distinct from them.<sup>[1–3]</sup> As intrinsic signaling molecules for many physiological functions, peptides possess an enormous potential for the design of drugs which interfere with protein-protein interactions (PPIs)<sup>[4–6]</sup> or serve as ligands for membrane-bound receptors. Nevertheless, native peptides are limited as therapeutics due to their frequent low membrane permeability, and insufficient bioavailability due to fast proteolytic degradation. Since these properties are directly connected to conformational instability,<sup>[7]</sup> a plethora of synthetic methodologies has been developed for the introduction of structural motifs to selectively tune the peptide skeleton into favored conformations (Figure 1.1). Cyclization<sup>[8]</sup> (either by the covalent linkage of peptide's side chains or termini), *N*-methylation of the peptide skeleton,<sup>[9–11]</sup> the introduction of non-proteinogenic amino acids (e.g. D-amino acids,<sup>[12]</sup> retro-inverse peptides,<sup>[13]</sup> peptide bond surrogates<sup>[14–16]</sup> and the use of building blocks bearing amino and carboxylic groups as amino acid substitutes<sup>[17–19]</sup> have proven success to introduce conformational constraints and to reduce enzymatic degradation. A systematic classification of peptidomimetics according to their degree of similarity with native peptides has been recently proposed by Grossmann and collaborators.<sup>[20]</sup>

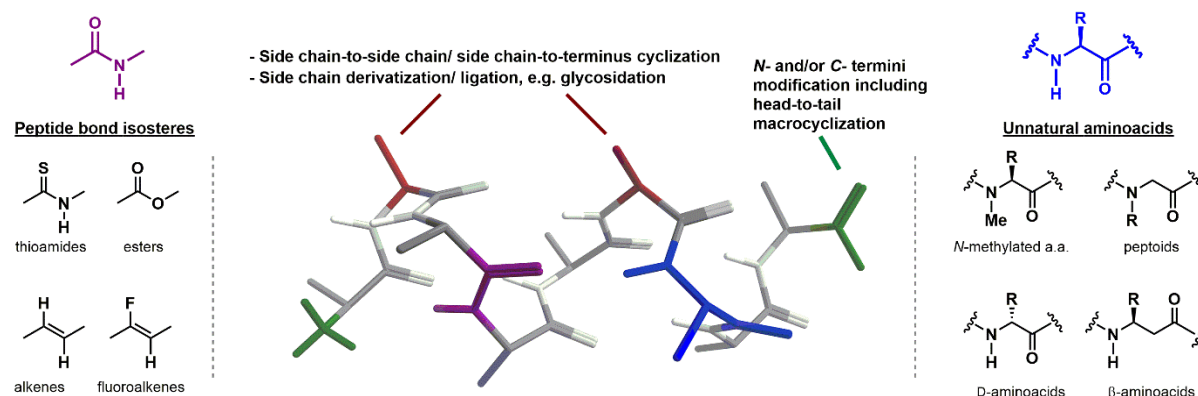


Figure 1.1. Structural modifications commonly employed to introduce conformational constraints in peptides

Motivated by the growing capabilities to understand the molecular basis of PPI-triggered biological responses, the development of mimetics of peptide binding epitopes – including the reproduction of protein motifs within small peptide sequences – has been boosted in the last decade.<sup>[3,8,17,20]</sup> Particularly, macrocyclic peptides have garnered a lot of attention from the scientific community since they are synthetically accessible and amenable to be optimized

towards its binding affinity and specificity, as well as its solubility or proteolytic stability.<sup>[21]</sup> Furthermore, several cyclic peptides have proven bioavailable even violating to different extents the limits traditionally considered to be important for oral bioavailability of drug-like small molecules.<sup>[22,23]</sup> Nowadays, it is generally accepted that macrocyclization – also employed by nature to improve stability and bioactivity of peptides –<sup>[9,24]</sup> is the most effective method towards achieving the conformational rigidity capable to mimic the common peptide's secondary structures in small and medium peptidic sequences.<sup>[8]</sup>

The covalent linkage between reactive groups present in a peptide skeleton can intuitively conduct to four possible combinations for achieving macrocycles: head-to-tail, side chain-to-side chain, and side chain-to- C- or N-terminus (Figure 1.2). Nevertheless, the continuous optimization of peptide sequences towards a better target affinity or pharmacological profile has raised novel cyclopeptides including multicyclic<sup>[2,21,25]</sup> and backbone-cyclized peptides.<sup>[26,27]</sup>

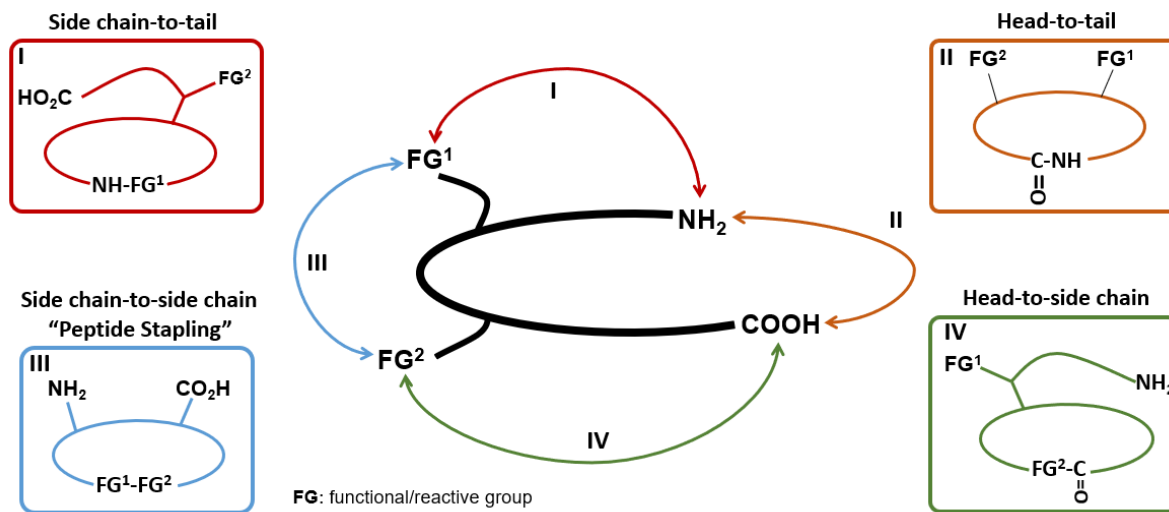


Figure 1.2. Traditional strategies to achieve peptide macrocyclization. Adapted from Yudin and co-workers, *Nature Chemistry*, 2011.<sup>[28]</sup>

This flowering has been also reflected in the pharmaceutical sector by an increased amount of constrained peptide drug candidates in clinical-stages as well as the higher investment in such projects.<sup>[2]</sup> The development of new methodologies enabling the synthesis of constrained peptides, particularly macrocycles, constitutes therefore a field with growing impact in the future of medicinal chemistry.

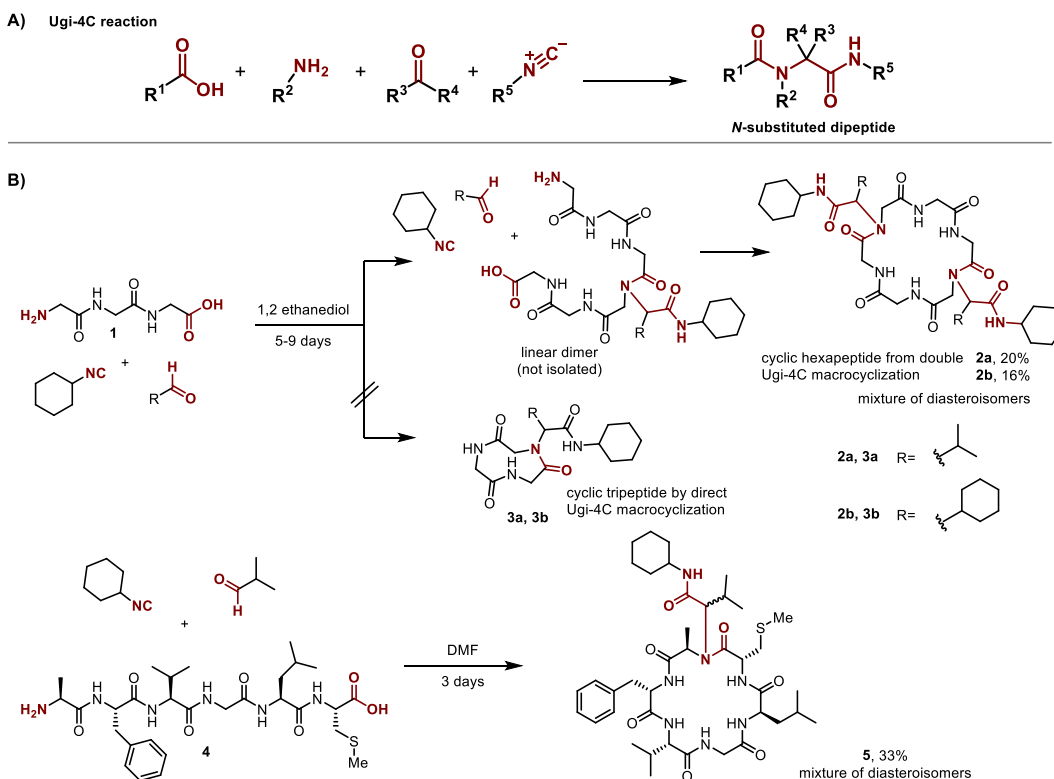
## 1.2. Peptide Macrocyclization by Multicomponent Reactions

Naturally occurring cyclic peptides possess dissimilar medicinal applications ranging from antimicrobial,<sup>[29,30]</sup> anticancer,<sup>[7,31]</sup> immunosuppressive,<sup>[32]</sup> hormonal properties,<sup>[33]</sup> among others. In contrast to ribosomal peptides, macrocyclic peptides isolated from fungi and bacteria very frequently present structural features such as *N*-methylation and non-proteinogenic amino acids. In order to mimic those features, synthetic methodologies capable to generate chemical diversity elements are needed.

Multicomponent reactions (MCRs) are highly efficient chemical processes in which three or more molecules converge in one-pot into a final product with the subsequent generation of high levels of molecular complexity and diversity.<sup>[34–37]</sup> These reactions are also characterized by a high atom economy, a reason why they have been implemented in almost all fields of synthetic and biological chemistry.<sup>[34]</sup> MCRs have proven great value for the synthesis of heterocycles,<sup>[37,38]</sup> natural products<sup>[39]</sup> and polymers<sup>[40]</sup> while its applicability in the chemical modification of proteins, e.g. glycoconjugation<sup>[41]</sup> and labeling,<sup>[41]</sup> is growing in interest.

Even when limited examples of MCRs are described for peptide cyclization, a wide repertoire of ring closing strategies has been developed for the synthesis of steroid-based supramolecular receptors,<sup>[42–44]</sup> topologically defined macromulticycles,<sup>[45,46]</sup> macrocyclic peptoids<sup>[47,48]</sup> and peptidomimetics.<sup>[49–52]</sup> In this field, the groups of Wessjohann<sup>[9,42–46,53]</sup> and Zhu<sup>[54,55]</sup> have pioneered the development of multicomponent macrocyclization strategies while Dömling's,<sup>[49–51]</sup> Andrade's<sup>[47,48]</sup> and Rivera's<sup>[56,57]</sup> groups have actively extended this catalogue. The Ugi-4component reaction (Ugi-4CR) – probably the most universal of all MCRs – was the first one applied to any type of multicomponent macrocyclization approach. As depicted in scheme 1.1A, it comprises the condensation of an amine, a carbonyl compounds, a carboxylic acid and an isocyanide to produce a *N*-substituted dipeptide motif. The Ugi reaction proceeds through the formation of the corresponding Schiff base, followed by the addition of the iminium and the carboxylate to the isocyanide to form the so-called  $\alpha$ -adduct. The final step is the Mumm type rearrangement, i.e., an intramolecular acylation of the amine nitrogen atom followed by the subsequent hydroxylimine→amide tautomeric conversion. The utilization of MCRs for peptide macrocyclization was firstly reported by Failli *et al.* in 1979.<sup>[58]</sup> The authors utilized the Ugi-4CR to cyclize tri- and hexapeptides in a head-to-tail fashion. When cyclization of the tripeptide Gly-Gly-Gly **1** in the presence of a commercial aldehyde and cyclohexyl isocyanide was attempted, only cyclohexapeptides **2a** and **2b** were isolated

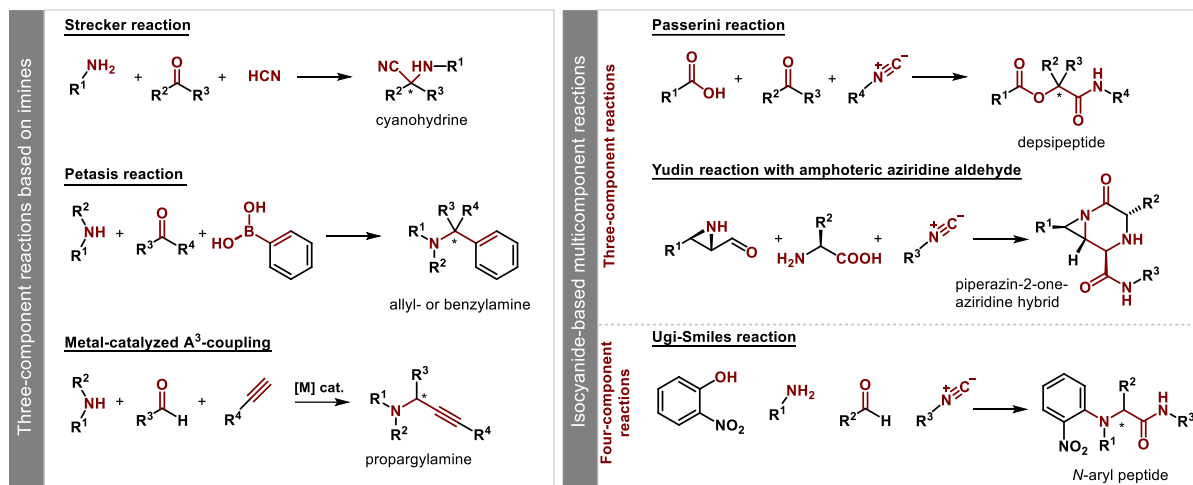
(Scheme 1.1B). Apparently, in this case the dimerization of the peptide backbone is favored over the ring closure yielding to the 9 membered ring. In order to overcome the strain-derived difficulties which made it impossible to obtain the expected cyclotripeptide, the authors performed the direct Ugi macrocyclization from the linear hexapeptide **4** to obtain cyclic hexapeptide **5** in 33% yield.



Scheme 1.1. A) Mechanism of the Ugi-4C reaction and B) First report of MCRs-based macrocyclization of peptides

Intriguingly, it took 30 years before another MCR was used for the cyclization of oligopeptides.<sup>[59]</sup> A recent review analyzing the advances in the field is available from the group of Rivera.<sup>[60]</sup> Despite the advantages of such processes for the generation of molecular complexity and diversity, some MCRs intrinsically possess slow kinetics, which can be usually overcome by using high concentrations of the reactants. Nevertheless, as a general rule, macrocyclizations are conducted under high dilution conditions in order to avoid oligomerization. This latter, combined with the low stereocontrol of some MCRs, could have led peptide chemists to choose other common ring-closing reactions such as Copper-catalyzed alkyne-azide cycloaddition<sup>[61,62]</sup> and macrolactamization.<sup>[63]</sup> The current renaissance of MCRs in the field of peptide macrocyclization was initiated by Yudin and co-workers in 2010

when the authors proved the suitability of a new reaction based on the use of an amphoteric amino aldehyde for the head-to-tail cyclization of small peptides. Afterwards, works describing the utilization of peptide macrocyclization strategies based on the Strecker,<sup>[64]</sup> Petasis,<sup>[65]</sup> Passerini,<sup>[66]</sup> Ugi (and some of its variants)<sup>[66–70]</sup> reactions, as well as the metal-catalyzed A<sup>3</sup>-coupling of aldehydes, alkynes, and amines<sup>[71]</sup> have been reported (Scheme 1.2).



Scheme 1.2. Multicomponent reactions utilized in peptide macrocyclization strategies

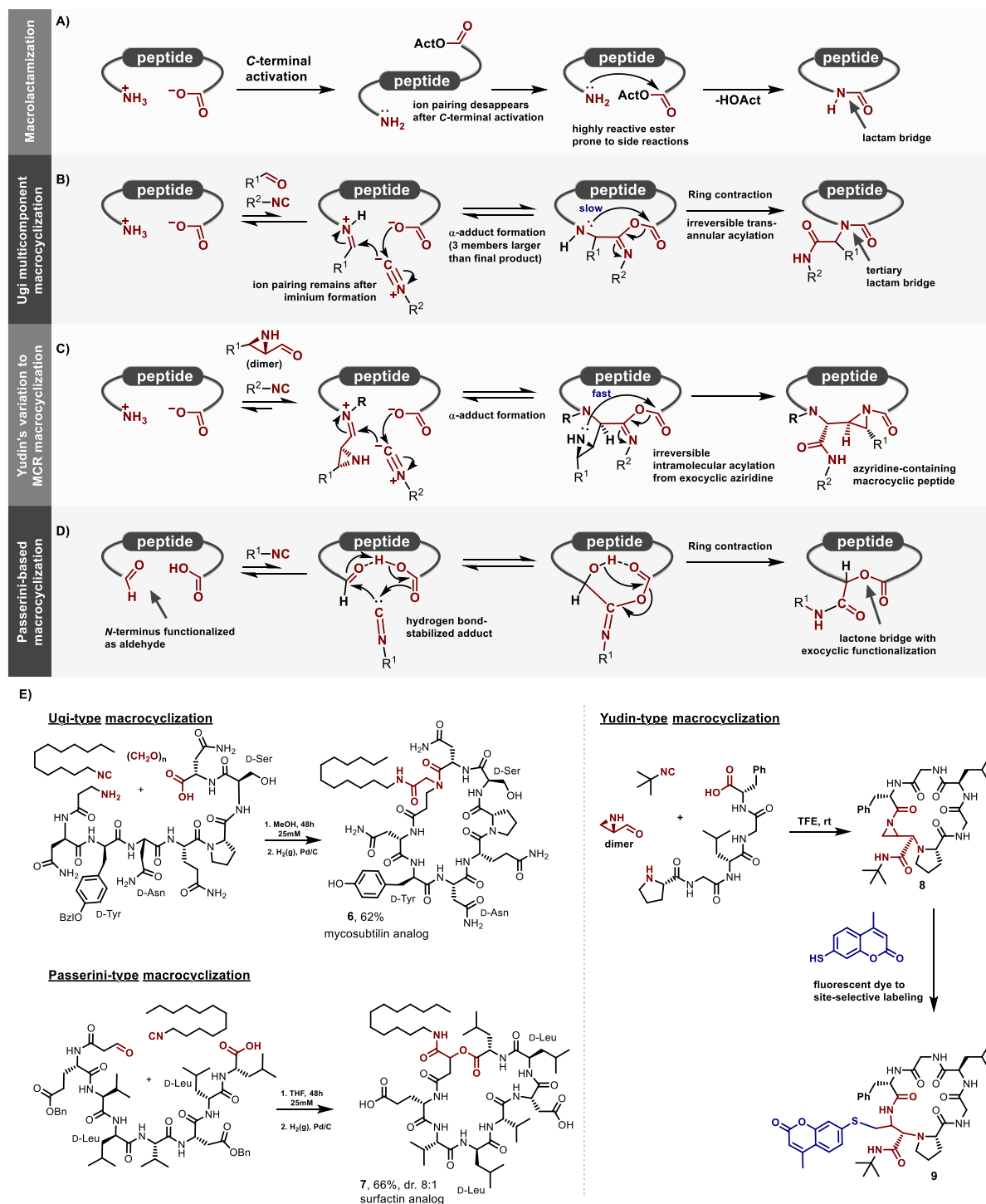
### 1.3. Head-to-tail cyclization by isocyanide-based MCRs

Probably one of the most challenging chemical modifications to be performed in a peptide skeleton is the covalent tethering of its *N*- and *C*- termini. It is well documented that such macrocyclization processes – despite the chemical reaction behind them – are intrinsically disfavored from an entropic point of view, since only in a relatively restricted number of conformations the involved reactive groups are close enough to propitiate the ring closure.<sup>[28]</sup> Competing processes such as dimerization or oligomerization possess faster kinetics – particularly at high concentrations – making the use of extreme dilution conditions to avoid them almost mandatory (usually submillimolar concentration). Additionally, the steric hindrance of the amino acids involved in the cyclization can lead to significant levels of epimerization at the *C*-terminus due to the long half-life time of the highly activated ester species (Scheme 1.3A).<sup>[72]</sup> The latter can be improved with the development of highly specialized coupling reagents that have been widely utilized for the synthesis of lactam-bridged cyclic peptides. The using of templates that help the peptide termini to prevail closer in space – i.e. metals capable to coordinate the peptide skeleton, or temporarily *N*-substituted amides to favor turn structures – is another proven strategy to achieve the tethering of the termini.<sup>[28]</sup>

A direct benefit of the utilization of the Ugi reaction for head-to-tail macrocyclization over macrolactamization is the fact that the reaction proceeds through the formation of an  $\alpha$ -adduct three members larger than the final cyclic peptide (Scheme 1.3B). In this way, the ring strain caused for the approximation of the peptide termini could be expected to be lower than for the direct amide formation.<sup>[73]</sup> Furthermore, Yudin has postulated that the ion pairing coming from the oppositely charged termini of the peptide and maintained according to the mechanism of the Ugi even after formation of the iminium ion, could be seen as an important enthalpy contribution which aids to maintain the termini in spatial proximity.<sup>[59]</sup> This ion pairing is absent during the typical C-terminal activation employed in macrolactamization procedures. Nevertheless, this factor is competing with many other structural, hydrophobic or electrostatic interactions (e.g. interchain hydrogen-bonding,  $\beta$ -turn-favoring sequences, ion-pairing from side chains, etc...) and its generalization should not be lightly presumed. Another factor to be considered is that the multicomponent nature of the process implies the participation of three molecules in order to produce the product. While the imine formation is usually straightforward (even though it is an equilibrium), formation of the  $\alpha$ -adduct is a process involving three reaction centers (being the reaction pathway so far not fully clarified) and is therefore expected to be disfavored towards unimolecular processes involving two reaction centers as the macrolactamization. Additionally, the transannular attack of the amine onto the mixed anhydride is slow, allowing intermolecular processes such as the nucleophilic attack of the solvent to be kinetically competitive.<sup>[74]</sup>

The main advantage of Ugi-mediated macrocyclizations of peptides is the possibility to readily access tertiary lactam bridges in one-pot which could lead to further peptide derivatization and functionalization. This is an idea that has been exploited by our working group and constitutes one of the main topics to be described in the present thesis. The utilization of such macrocyclizations proved to be suitable for the introduction of a convertible isocyanide that could be further activated towards acylation for the chemoselective labeling of cyclopeptides.<sup>[75]</sup> Furthermore, a methodology allowing the one-pot cyclization and lipidation was successfully applied to the synthesis of cyclolipopeptide analogs of mycosubtilin as compound **6** in scheme 1.3E. Remarkably, the use of lipidic isocyanides and aldehydes also allowed the simultaneous insertion of two lipidic tails while cyclization was achieved. For short peptide sequences (*i.e.* tetrapeptides), partial cyclodimerization was observed when the peptide cyclization was attempted at a 10 mM concentration. The resulting compounds showed improved cytotoxic activity *in vitro*, as compared with the natural surfactin, against

B16F10 melanoma cells with an IC<sub>50</sub> value in the low micromolar range as determined by MTT and CV assays.<sup>[66]</sup>

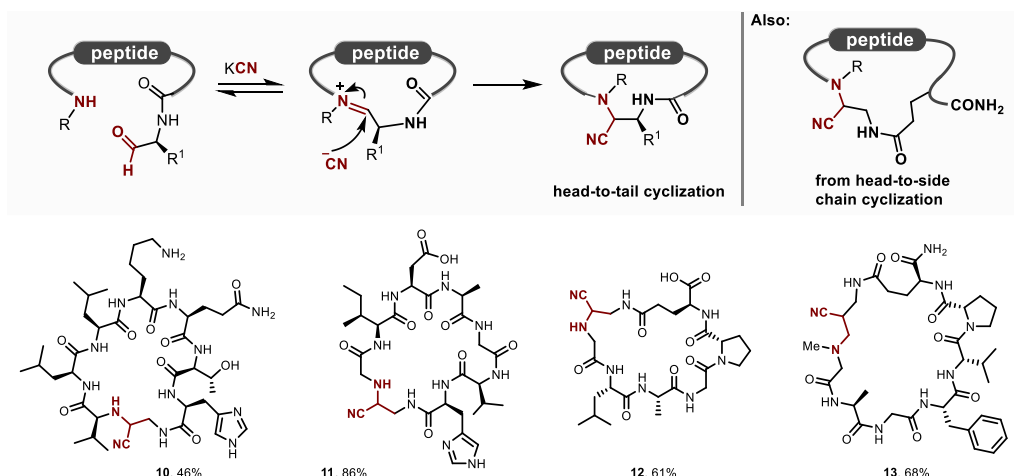


Scheme 1.3. Mechanism for head-to-tail cyclization of peptides by means of A) Macrolactamization, B) Ugi-4C reaction C) Yudin multicomponent reaction with amphoteric aziridine aldehydes and D) Passerini reaction. E) Examples of cyclic peptides synthesized by the different strategies.

In contrast to traditional Ugi macrocyclizations, the use of Yudin's aziridine aldehydes (Scheme 1.3C) is advantageous in two senses: 1) the slow intramolecular transannular acylation (commonly referred as Mumm rearrangement) occurs with a remarkable faster kinetics since it is the result of a favored intramolecular attack of an exocyclic aziridine moiety; and 2) the attack of the chiral aziridine is highly diastereoselective, which overcomes the biggest drawback of Ugi-type reactions. This methodology performs noticeably well for the head-to-tail cyclization of small peptides reporting high yields in remarkable short time and concentrations as high as 0.2 M. The resulting in-backbone aziridine insertion could be thought to be one of the downsides of this variant, but it was proven to be suitable for the site-selective labeling of peptides through reaction with sulfur-containing fluorescent labels and subsequent ring opening.<sup>[59]</sup>

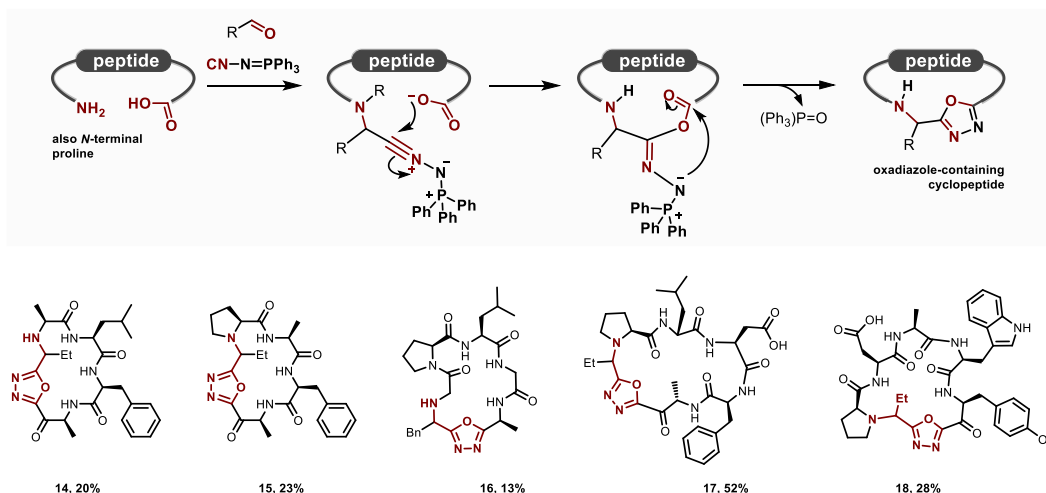
The Passerini reaction consists on the condensation of a carbonyl compound, a carboxylic acid and an isocyanide to afford an  $\alpha$ -acyloxy amide and is believed to follow a non-ionic mechanism (Scheme 1.3D).<sup>[74]</sup> This reaction is the most popular for its efficient access to constrained depsipeptides.<sup>[76]</sup> Wessjohann and co-workers were the first reporting a Passerini-based macrocyclization methodology including the condensation of bifunctional isocyanides and carboxylic acids in the presence of isobutyraldehyde. The same working group successfully developed a head-to-tail protocol for the synthesis of analogs of surfactin as in compound **7**. In contrast with the natural lipopeptide, the utilization of a lipidic isocyanide leads to a cyclic depsipeptide with an *exo*-cyclic amide bearing the lipidic tail.<sup>[66]</sup>

Another well-known MCR which only recently has been employed for macrocyclization is the Strecker reaction. Inspired in natural non-ribosomal peptide synthesis, Baran and co-workers prepared macrocyclic imines in water from totally unprotected peptides, which were subsequently trapped by means of an internal or external nucleophilic addition comprising cyanides. As illustrated in scheme 1.4, the imine formation is a reversible step and the ratio of cyclic product highly depends on the amino acid sequence and size of the peptide to be cyclized. Nevertheless, the nucleophilic attack of a cyanide irreversibly leads to the formation of the final cyclic  $\alpha$ -aminonitrile. The method afforded not only head-to-tail but also head-to-side-chain macrocyclic peptides in good yields after 24 to 72 hrs.<sup>[64]</sup>



Scheme 1.4. Strecker reaction-mediated multicomponent cyclization of peptides

An interesting example of MCR-mediated synthesis to rapidly access structurally diverse macrocyclic peptides has been recently reported by Yudin and co-workers.<sup>[77]</sup> The authors exploited the unusual reactivity of an (*N*-isocyanimino)-phosphorane for the one-pot synthesis of heterocyclic-containing head-to-tail macrocyclic peptides. Upon isocyanide addition to the imine and subsequent formation of the  $\alpha$ -adduct expected for an Ugi-type mechanism, the nucleophilic nitrogen within the (*N*-isocyanimino)-triphenylphosphorane moiety attacks intramolecularly the C-terminal carboxylic acid to form an in-backbone-grafted 1,3,4-oxadiazole ring (Scheme 1.5).



Scheme 1.5. Yudin's MCR for the synthesis of oxadiazole-containing macrocyclic peptides

As in the case of Yudin's previous approaches comprising the utilization of aziridine-containing aldehydes, the insertion of an exocyclic nucleophile which could perform a favored intramolecular attack over the mixed anhydride formed during the "classical" Ugi mechanism

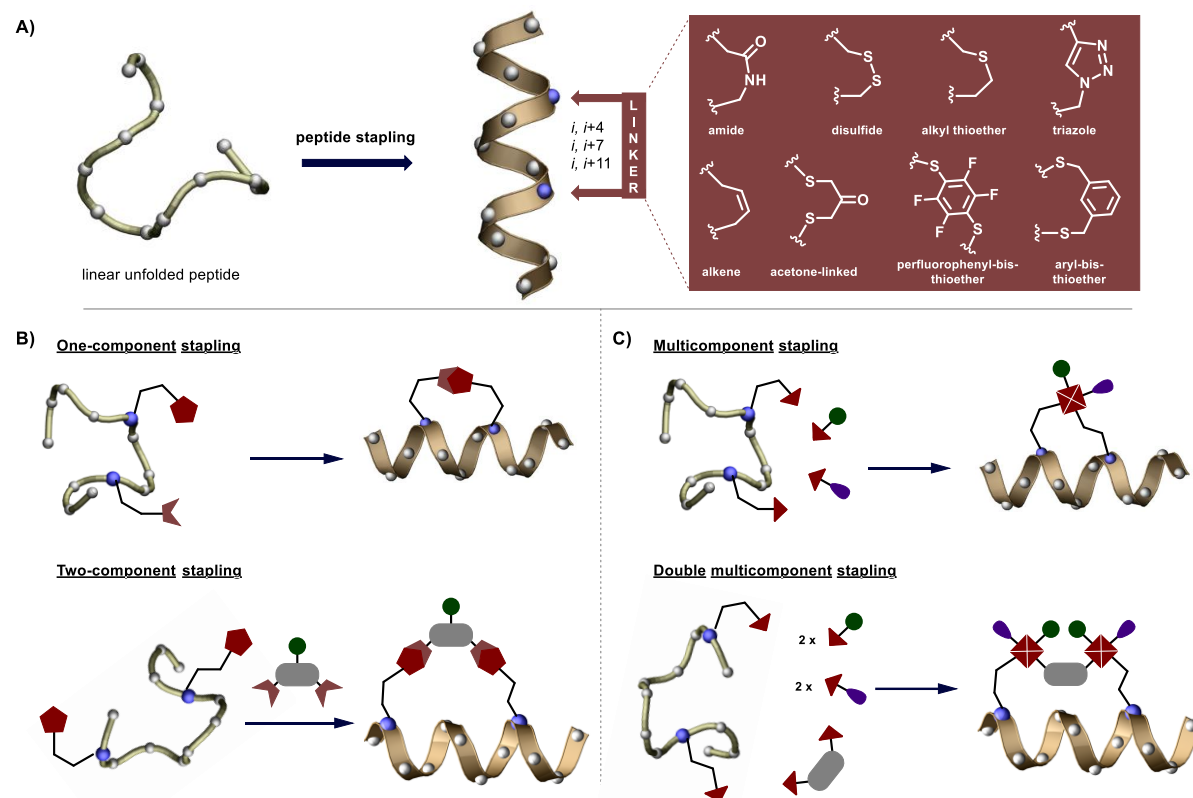
seems to significantly improve the kinetics of the reaction. In this way, macrocyclic peptides ranging from 4 to 7 amino acids (e.g., **14,15,16,17** and **18**) were prepared in moderate to good yields after 3 hours of reaction. Additionally, the synthesized peptides displayed a high passive membrane permeability, which could be considered an advantage for the development of bioavailable peptide-based therapeutics.<sup>[77]</sup>

#### 1.4. Multicomponent side chain-to-side chain cyclization

Peptide stapling is probably the most powerful tool towards the development of novel therapeutics based on peptides. This term was firstly employed as a denomination for the synthesis of all-hydrocarbon bridged peptides by ring-closing metathesis<sup>[78]</sup> and has been extended to those synthetic methodologies which employ covalent side chain-to-side chain tethering to conformationally constrain peptides. This latter includes CuAAC,<sup>[61,79]</sup> Lys/Orn to Asp/Glu lactamization,<sup>[80,81]</sup> Lys *N*<sup>ε</sup>- and Cys *S*- arylation,<sup>[82,83]</sup> Cys alkylation<sup>[84]</sup> and Pd-catalyzed C-H activation<sup>[85,86]</sup> (Scheme 1.6A). Even when stapling is mainly associated with the stabilization of  $\alpha$ -helices, side chain-to-side chain tethering has proven valuable for the synthesis of bioactive peptides with irregular secondary structure.<sup>[87]</sup> A classical stapling approach for the stabilization of helical peptides consists on reaction between two functional groups situated on side chains usually separated by 4, 7 or 11 amino acids, corresponding to the occurrence of the chains on the same face of an ideal helical-folded peptide. While this “one component approach” (Scheme 1.6B) has proven effective towards the synthesis of biologically relevant cyclic peptides,<sup>[78,80]</sup> two-component based strategies have been growing up in the literature.<sup>[88]</sup> This approach is mandatory for such cases in which the distance of the ring-closing side chains is too short to achieve the optimal distance for helical stabilization (e.g. when linking two cysteines separated in a *i, i+7* fashion; where *i* refers to the position of an amino acid in the sequence) and therefore a second component – bearing bifunctional reacting groups complementary to those in the peptide side chains – is needed to reach the helix-stabilizing distance.<sup>[89]</sup> This two-component approach has been recognized as advantageous by some authors, who have exploited the possibility of introducing an additional functionalization with the second component to allow further derivatization or functionalization of the resulting stapled peptide.<sup>[90]</sup>

In contrast to the described approaches, the introduction of multicomponent reactions for peptide stapling can be seen as an opportunity to effectively address diversity to the existing

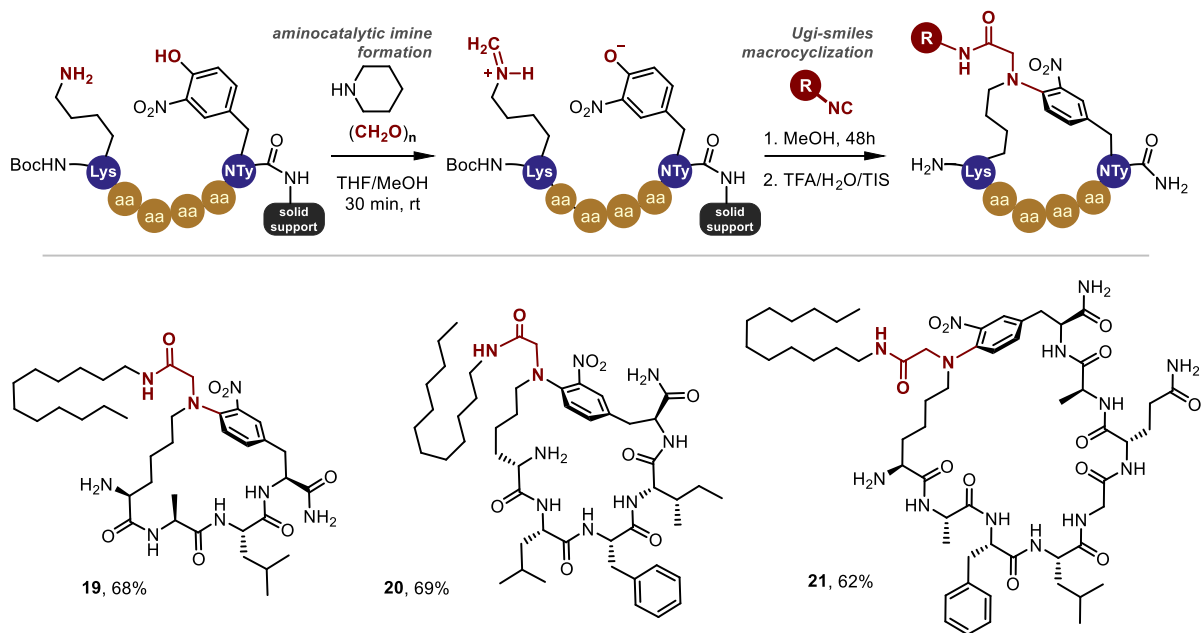
methodologies. In a “normal” approach a four-component reaction (Scheme 1.6C) could lead to the insertion of two elements of diversity, i.e. two components are combined to achieve the peptide cyclization while the other two can provide structural diversity to the tethering moiety. Furthermore, this approach is also compatible with the use of two bifunctional components towards a double MCR stapling methodology.<sup>[68]</sup>



Scheme 1.6. A) Common linkers employed for  $\alpha$ -helical stabilization. B) One and two component strategies for peptide stapling and C) Multicomponent stapling methodologies.

In an endeavor to extend the success of MCR-based strategies in the synthesis of cyclolipopeptides, Wessjohann and co-workers applied the Ugi-Smiles reaction for the head-to-tail and side chain-to-side chain cyclization of short peptide sequences (Scheme 1.7).<sup>[67]</sup> The strategy comprises the insertion of an *N*-aryl moiety from *o*-nitro-tyrosine which confers rigidity and lipophilicity to the tether while the advantages of Ugi- and Passerini-based strategies – i.e. the simultaneous cyclization and derivatization from the use of lipidic isocyanide – are also met. Aside from the solution-phase approach, the authors also showed the suitability of the protocol to be conducted on-resin. In this way, the desired peptide sequence can be built by standard solid phase peptide synthesis and the groups participating

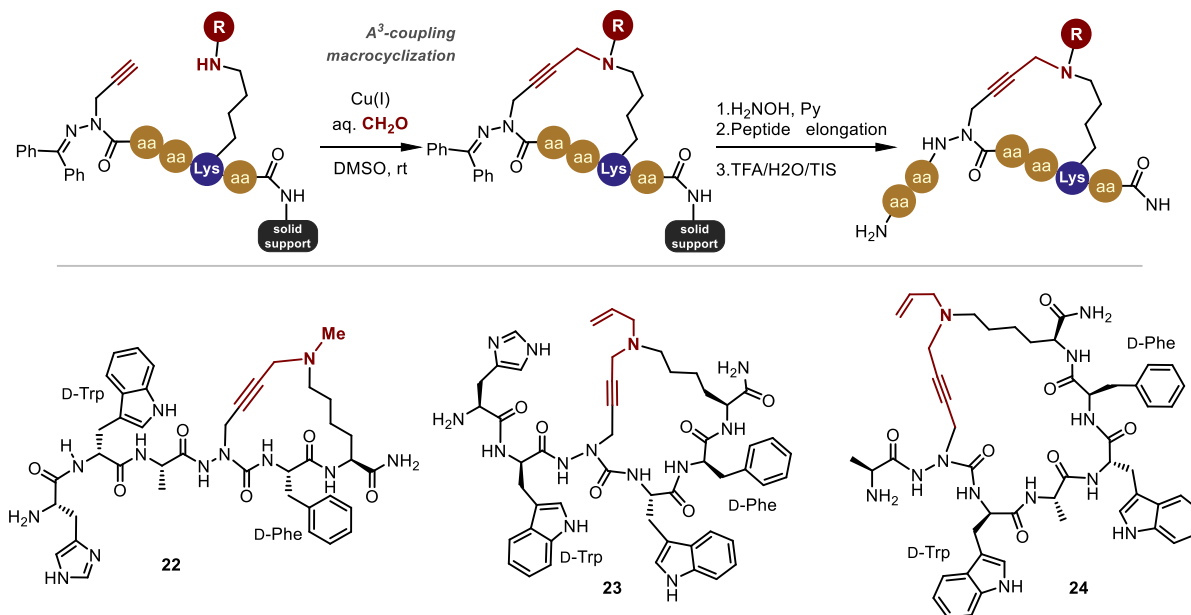
in the cyclization can be selectively deprotected avoiding undesirable side reactions from Ugi-reactive side chains. The spontaneous 1,4-diazepanedione formation occurring during *N*-Fmoc deprotection on a Lys-Asp *N*-terminal sequence was employed as turn-inducing motif to facilitate cyclization. Nevertheless, the authors only reported examples bearing a lysine residue at the *N*-terminus and no examples of helical peptides were attempted.



Scheme 1.7. Ugi-Smiles approach to cyclic-lipopeptides

Peptidomimetics containing aza-amino acids – i.e. peptides in which at least in one amino acid the  $\alpha$ -carbon has been substituted by a nitrogen atom – have proven applicability for the development of bioactive compounds.<sup>[91]</sup> An on-resin stapling methodology comprising the A<sup>3</sup>-coupling reaction of alkyne-functionalized azapeptides has been reported by Ong, Lubell and co-workers (Scheme 1.8).<sup>[71]</sup> In order to perform the A<sup>3</sup>-coupling macrocyclization, a peptide chain containing an *N*<sup>F</sup>-*o*-nitrobenzenesulfonyl protected lysine and an *N*-terminal *N*<sup>α</sup>-propargyl semicarbazone residue is assembled on-resin. After selective side chain deprotection, the cyclization between *N*<sup>F</sup>-alkylated lysine, alkyne, and formaldehyde in the presence of copper(I) iodide is achieved in 24 h. Semicarbazone removal allows further elongation of the peptide chain. The protocol was employed for the preparation of 15 growth hormone-releasing peptide-6 (GHRP-6) analogs exemplified by macrocyclic azapeptides **22**, **23** and **24**. Compound **24** resulted in the highest ever reported affinity for CD36 for a GHRP-6 analogue. The multicomponent character of the A<sup>3</sup>-macrocyclization enables the possibility to incorporate an additional component which could modulate the biological activity of the

target peptide sequence. The incorporation of aza-residues into the sequence favors reverse turn conformations, which in addition to the coordination of imine and alkyne by the metal, facilitates the cyclization process.

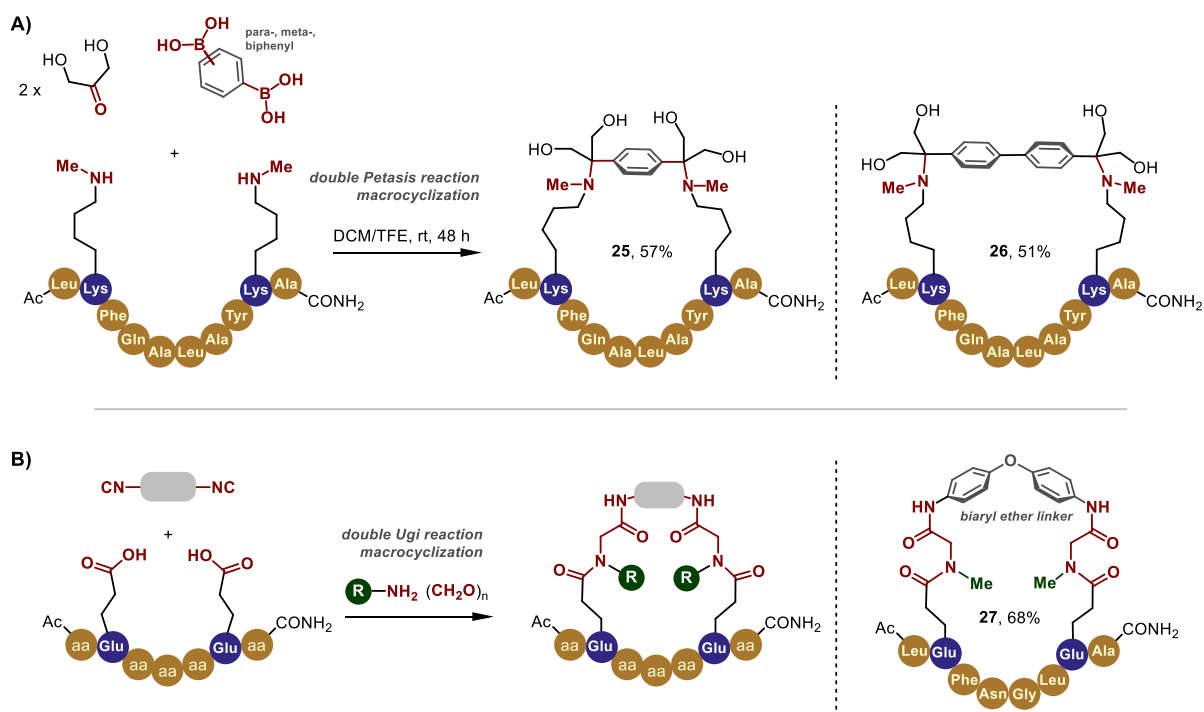


Scheme 1.8.  $A^3$ -coupling-based macrocyclization reported by Ong, Lubell and co-workers

In analogy to stapling protocols using two double-functionalized components, Wessjohann, Rivera and co-workers have reported multicomponent strategies involving homo-double-functionalized peptides. As observed in scheme 1.9A, the authors successfully achieved the ( $i, i+7$ ) Petasis-mediated stapling of decapeptides.<sup>[65]</sup> The double condensation between boronic acids, carbonyl compounds and  $N^{\epsilon}$ -methyl lysine is conducted under *pseudo*-dilution conditions for 48 hours at room temperature. Even for short peptide sequences, the method proved suitable to stabilize helical structures. Rigidity-inducing moieties coming from di-boronic acids could be conveniently inserted into the tether while exocyclic diversity is easily achievable by variation of the oxo-component.

An alternative approach from the same authors comprises the double Ugi condensation between two carboxylic group-containing side chains, paraformaldehyde, an amine and an aryl-*bis*-isocyanide (Scheme 1.9B). The best results were achieved by using syringe pumps for the slow addition of both, the *bis*-isocyanide and peptide, to a solution of the amine and the paraformaldehyde. The method proved suitable for the side chain-to-side chain as well as for the side chain-to-tail macrocyclization of small peptides. In this approach, both the amine and the carbonyl group are responsible for providing structural diversity to the final product.

Remarkably, the method comprises achieves the formation of eight covalent bonds in one-pot.<sup>[68]</sup>

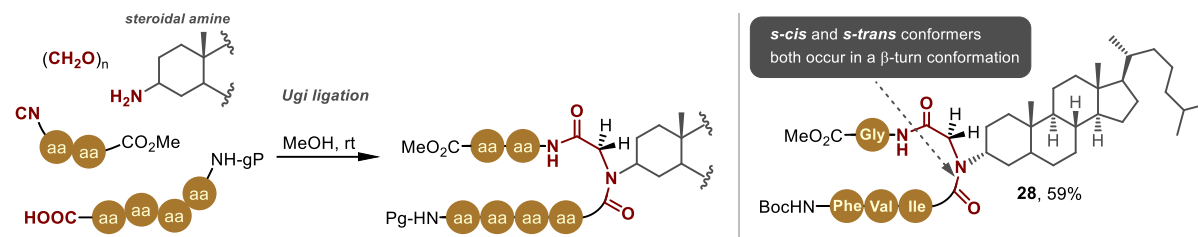


Scheme 1.9. Strategies based on double multicomponent reactions

## 1.5. Other MCR-based strategies to constrained peptides

Beyond the obvious capacity of multicomponent macrocyclizations to deliver peptides bearing skeletons with restricted conformational space, the backbone modification in linear peptides by MCRs is another valid approach to achieve this goal. Several reports describe the potential of MCR-based approaches for the reproduction of topological templates (i.e.  $\beta$ -turns) in small peptidomimetics.<sup>[92,93]</sup> Nevertheless, the potential MCRs possess for the synthesis of small cyclic molecules – and which could ultimately be applied to obtain modified peptide skeletons – has not yet been extensively employed for the modification of peptides themselves, but mostly was applied to obtain small peptidomimetics usually shorter than four amino acids. An interesting approach which proved successful in diminishing a linear peptide's conformational freedom consisted of the direct *N*-ligation of peptides to steroids at one of the backbone's amide bond reported by Rivera *et. al.*<sup>[94]</sup> The condensation of a steroidal imine with a peptidic isocyanide and a *C*-terminal carboxylic acid from a peptide, led to penta- and hexapeptides bearing an *N*-steroidal backbone substitution (Scheme 1.10). Most of the compounds showed

two major conformers by NMR coming from *s-cis/s-trans* isomerization around the tertiary amide. NMR-based three-dimensional structure determination of one of the compounds revealed that the steroid moiety forced both conformers in a  $\beta$ -turn conformation.



Scheme 1.10. Ugi-based *N*-steroid ligation strategy towards constrained peptides

## 1.6. Remarks and future perspectives

Virtually, any biophysical property of a peptide – e.g. its binding affinity and specificity, solubility and proteolytic stability– can be optimized and tailored to a desired application by the introduction of conformational restraints or derivatization of the peptide skeleton. In this sense, expanding the existing repertoire of synthetic methods that enable access to structurally-diverse peptides can exponentially impact the future development of peptide-based therapeutics. Multicomponent reactions, particularly those based on isonitriles, enjoy several characteristics which make them suitable tools for developing new methodologies to access modified peptides:

- easy implementation
- high efficiency and atom economy
- high diversity-generating character
- high occurrence of reacting groups available in peptide skeletons and side chains

The success of future MCR-based strategies for rational tailoring of peptides is inevitably linked to the capacity of understanding the main structural differences between parent and MCR-modified peptides. Only the structure-based application of such strategies could unleash the full potential of MCRs on the road to an improved chemistry of peptides.

## 1.7. Aims of this PhD work

The present thesis aims the development of new strategies for the synthesis of constrained peptides based on multicomponent reactions, with special emphasis on the conformational aspects resulting from those structural modifications. The main objectives to be fulfilled are:

- To develop new peptide macrocyclization strategies based on isocyanide-based MCRs capable to either induce or stabilize regular secondary structures such as helices,  $\beta$ -strands, reverse turns and loops.
- To implement solid-phase synthesis methodologies that include on-resin MCR cyclization steps leading to helical and  $\beta$ -hairpin scaffolds of biological relevance.
- To determine the solution-phase three-dimensional structure of the synthesized cyclic peptides by means of spectroscopic and molecular modelling studies.
- To employ the multicomponent macrocyclization strategies for the functionalization of conformationally constrained peptides with reactive handles suitable for further conjugation approaches.

## 1.8. References

- [1] J. L. Lau, M. K. Dunn, *Bioorganic Med. Chem.* **2018**, *26*, 2700–2707.
- [2] C. Morrison, *Nat. Rev. Drug Discov.* **2018**, *17*, 531–533.
- [3] K. Fosgerau, T. Hoffmann, *Drug Discov. Today* **2015**, *20*, 122–128.
- [4] G. Zinzalla, D. E. Thurston, *Future Med. Chem.* **2009**, *1*, 65–93.
- [5] D. E. Scott, A. R. Bayly, C. Abell, J. Skidmore, *Nat. Rev. Drug Discov.* **2016**, *15*, 533–550.
- [6] Z. Qian, P. G. Dougherty, D. Pei, *Curr. Opin. Chem. Biol.* **2017**, *38*, 80–86.
- [7] A. F. B. Räder, M. Weinmüller, F. Reichart, A. Schumacher-Klinger, S. Merzbach, C. Gilon, A. Hoffman, H. Kessler, *Angew. Chemie - Int. Ed.* **2018**, *57*, 14414–14438.
- [8] T. A. Hill, N. E. Shepherd, F. Diness, D. P. Fairlie, *Angew. Chemie - Int. Ed.* **2014**, *53*, 13020–13041.
- [9] L. A. Wessjohann, C. Andrade, O. Vercillo, D. Rivera, in *TARGETS Heterocycl. Syst.*, **2006**, pp. 24–53.
- [10] J. Chatterjee, F. Rechenmacher, H. Kessler, *Angew. Chemie Int. Ed.* **2013**, *52*, 254–269.
- [11] A. F. B. Räder, F. Reichart, M. Weinmüller, H. Kessler, *Bioorganic Med. Chem.* **2018**, *26*, 2766–2773.
- [12] R. Mahalakshmi, P. Balam, in *D-Amino Acids A New Front. Amin. Acid Protein Res.*, **2006**, pp. 415–430.
- [13] M. Chorev, M. Goodman, *Acc. Chem. Res.* **1993**, *26*, 266–273.
- [14] V. D. Bock, D. Speijer, H. Hiemstra, J. H. van Maarseveen, *Org. Biomol. Chem.* **2007**, *5*, 971–5.
- [15] A. Choudhary, R. T. Raines, *ChemBioChem* **2011**, *12*, 1801–1807.
- [16] A. F. Spatola, K. Darlak, *Tetrahedron* **1988**, *44*, 821–833.
- [17] J. A. Robinson, *Acc. Chem. Res.* **2008**, *41*, 1278–1288.
- [18] S. A. W. Gruner, E. Locardi, E. Lohof, H. Kessler, *Chem. Rev.* **2002**, *102*, 491–514.
- [19] A. Mizuno, K. Matsui, S. Shuto, *Chem. - A Eur. J.* **2017**, *23*, 14394–14409.
- [20] M. Pelay-Gimeno, A. Glas, O. Koch, T. N. Grossmann, *Angew. Chem. Int. Ed* **2015**, *54*, 8896–8927.
- [21] A. A. Vinogradov, Y. Yin, H. Suga, *J. Am. Chem. Soc.* **2019**, *141*, 4167–4181.

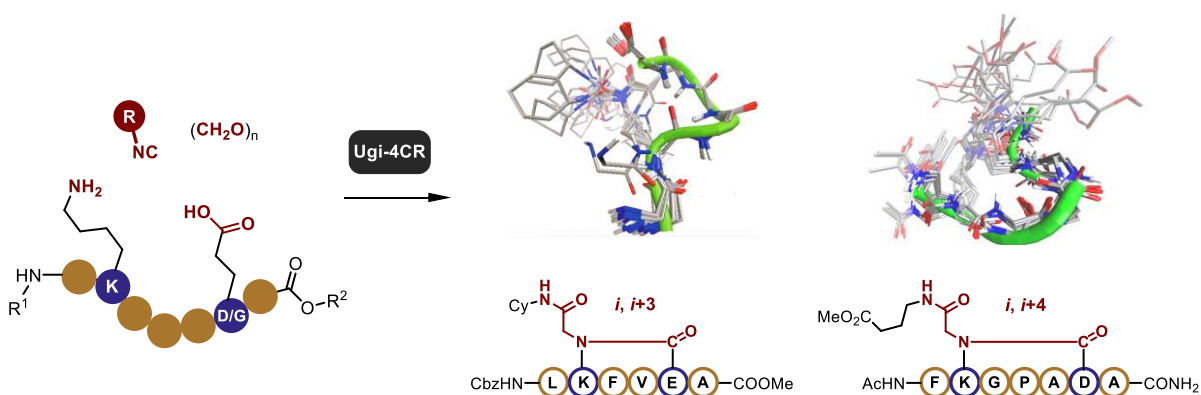
- [22] D. S. Nielsen, R. J. Lohman, H. N. Hoang, T. A. Hill, A. Jones, A. J. Lucke, D. P. Fairlie, *ChemBioChem* **2015**, *16*, 2289–2293.
- [23] D. S. Nielsen, N. E. Shepherd, W. Xu, A. J. Lucke, M. J. Stoermer, D. P. Fairlie, *Chem. Rev.* **2017**, *117*, 8094–8128.
- [24] M. A. Abdalla, L. J. McGaw, *Molecules* **2018**, *23*, 2080–2099.
- [25] T. Passioura, T. Katoh, Y. Goto, H. Suga, *Annu. Rev. Biochem.* **2014**, *83*, 727–752.
- [26] M. G. Ricardo, J. F. Marrero, O. Valdes, D. G. Rivera, L. A. Wessjohann, *Chem. - A Eur. J.* **2018**, *346250000*, 769–774.
- [27] S. J. S. Rubin, N. Qvit, *Curr. Top. Med. Chem.* **2018**, *18*, 526–555.
- [28] C. J. White, A. K. Yudin, *Nat. Chem.* **2011**, *3*, 509–524.
- [29] A. J. Park, J. P. Okhovat, J. Kim, *Curr. Biol.* **2016**, *26*, R1–R21.
- [30] K. Sato, U. Nagai, *J. Chem. Soc. Perkin Trans. 1* **1986**, *1*, 1231–1234.
- [31] D. Gaspar, A. Salomé Veiga, M. A. R. B. Castanho, *Front. Microbiol.* **2013**, *4*, 1–16.
- [32] K. Thell, R. Hellinger, G. Schabbauer, C. W. Gruber, *Drug Discov. Today* **2014**, *19*, 645–653.
- [33] S. Qiu, G. Pellino, F. Fiorentino, S. Rasheed, A. Darzi, P. Tekkis, C. Kontovounisios, *Gastroenterol. Res. Pract.* **2017**, *2017*, 1–8.
- [34] A. Dömling, W. Wang, K. Wang, *Chem. Rev.* **2012**, *112*, 3083–3135.
- [35] J. Zhu, Q. Wang, M. X. Wang, *Multicomponent Reactions in Organic Synthesis*, Wiley-VCH Verlag GmbH & Co. KGaA, Weinheim, Germany, **2015**.
- [36] S. Brauch, S. S. van Berkel, B. Westermann, *Chem. Soc. Rev.* **2013**, *42*, 4948–4962.
- [37] E. Ruijter, R. Scheffelaar, R. V. A. Orru, *Angew. Chemie - Int. Ed.* **2011**, *50*, 6234–6246.
- [38] B. H. Rotstein, S. Zaretsky, V. Rai, A. K. Yudin, *Chem. Rev.* **2014**, *114*, 8323–8359.
- [39] B. B. Touré, D. G. Hall, *Chem. Rev.* **2009**, *109*, 4439–4486.
- [40] O. Kreye, T. Tóth, M. A. R. Meier, *J. Am. Chem. Soc.* **2011**, *133*, 1790–1792.
- [41] Y. Méndez, J. Chang, A. R. Humpierre, A. Zanuy, R. Garrido, A. V. Vasco, J. Pedroso, D. Santana, L. M. Rodríguez, D. García-Rivera, et al., *Chem. Sci.* **2018**, *9*, 2581–2588.
- [42] L. A. Wessjohann, B. Voigt, D. G. Rivera, *Angew. Chemie - Int. Ed.* **2005**, *44*, 4785–4790.
- [43] L. A. Wessjohann, D. G. Rivera, F. Coll, *J. Org. Chem.* **2006**, *71*, 7521–7526.
- [44] D. G. Rivera, L. A. Wessjohann, *Molecules* **2007**, *12*, 1890–1899.
- [45] D. G. Rivera, L. A. Wessjohann, *J. Am. Chem. Soc.* **2006**, *128*, 7122–7123.
- [46] D. G. Rivera, L. A. Wessjohann, *J. Am. Chem. Soc.* **2009**, *131*, 3721–3732.
- [47] A. de F. S. Barreto, O. E. Vercillo, M. A. Birkett, J. C. Caulfield, L. A. Wessjohann, C. K. Z. Andrade, *Org. Biomol. Chem.* **2011**, *9*, 5024.
- [48] O. E. Vercillo, C. K. Z. Andrade, L. A. Wessjohann, *Org. Lett.* **2008**, *10*, 205–8.
- [49] G. P. Liao, E. M. M. Abdelraheem, C. G. Neochoritis, K. Kurpiewska, J. Kalinowska-Tłuścik, D. C. McGowan, A. Dömling, *Org. Lett.* **2015**, *17*, 4980–4983.
- [50] E. M. M. Abdelraheem, K. Kurpiewska, J. Kalinowska-Tłuścik, A. Dömling, *J. Org. Chem.* **2016**, *81*, 8789–8795.
- [51] R. Madhavachary, E. M. M. Abdelraheem, A. Rossetti, A. Twarda-Clapa, B. Musielak, K. Kurpiewska, J. Kalinowska-Tłuścik, T. A. Holak, A. Dömling, *Angew. Chemie - Int. Ed.* **2017**, *56*, 10725–10729.
- [52] O. Kreye, B. Westermann, D. G. Rivera, D. V. Johnson, R. V. A. Orru, L. A. Wessjohann, *QSAR Comb. Sci.* **2006**, *25*, 461–464.
- [53] L. A. Wessjohann, D. G. Rivera, O. E. Vercillo, *Chem. Rev.* **2009**, *109*, 796–814.
- [54] G. Masson, L. Neuville, C. Bughin, A. Fayol, J. Zhu, **2010**, pp. 1–24.
- [55] P. Janvier, M. Bois-Choussy, H. Bienaymé, J. Zhu, *Angew. Chemie - Int. Ed.* **2003**, *42*, 811–814.
- [56] D. G. Rivera, O. Pando, R. Bosch, L. A. Wessjohann, D. G. Rivera, O. Pando, R. Bosch, L. A. Wessjohann, **2008**, 6229–6238.

- [57] R. Echemendía, W. F. Rabêlo, E. R. López, J. Coro, M. Suárez, M. W. Paixão, D. G. Rivera, *Tetrahedron Lett.* **2018**, *59*, 4050–4053.
- [58] A. Failli, H. Immer, M. Götz, *Can. J. Chem.* **1979**, *57*, 3257–3261.
- [59] R. Hili, V. Rai, A. K. Yudin, *J. Am. Chem. Soc.* **2010**, *132*, 2889–91.
- [60] L. Reguera, D. G. Rivera, *Chem. Rev.* **2019**, DOI 10.1021/acs.chemrev.8b00744.
- [61] K. Holland-Nell, M. Meldal, *Angew. Chemie - Int. Ed.* **2011**, *50*, 5204–5206.
- [62] Y. Wu, L. B. Olsen, Y. H. Lau, C. H. Jensen, M. Rossmann, Y. R. Baker, H. F. Sore, S. Collins, D. R. Spring, *ChemBioChem* **2016**, *17*, 689–692.
- [63] N. E. Shepherd, R. S. Harrison, G. Ruiz-Gomez, G. Abbenante, J. M. Mason, D. P. Fairlie, *Org. Biomol. Chem.* **2016**, *14*, 10939–10945.
- [64] L. R. Malins, J. N. Degruyter, K. J. Robbins, P. M. Scola, M. D. Eastgate, M. R. Ghadiri, P. S. Baran, *J. Am. Chem. Soc.* **2017**, *139*, 5233–5241.
- [65] M. G. Ricardo, D. Llanes, L. A. Wessjohann, D. G. Rivera, *Angew. Chemie - Int. Ed.* **2019**, *58*, 2700–2704.
- [66] M. C. Morejón, A. Laub, G. N. Kaluđerović, A. R. Puentes, A. N. Hmedat, A. J. Otero-González, D. G. Rivera, L. A. Wessjohann, *Org. Biomol. Chem.* **2017**, *15*, 3628–3637.
- [67] M. C. Morejón, A. Laub, B. Westermann, D. G. Rivera, L. A. Wessjohann, *Org. Lett.* **2016**, *18*, 4096–4099.
- [68] M. G. Ricardo, F. E. Morales, H. Garay, O. Reyes, D. Vasilev, L. A. Wessjohann, D. G. Rivera, *Org. Biomol. Chem.* **2015**, *13*, 438–446.
- [69] A. V. Vasco, Y. Méndez, A. Porzel, J. Balbach, L. A. Wessjohann, D. G. Rivera, *Bioconjug. Chem.* **2019**, *30*, 253–259.
- [70] A. V. Vasco, C. S. Pérez, F. E. Morales, H. E. Garay, D. Vasilev, J. A. Gavín, L. A. Wessjohann, D. G. Rivera, *J. Org. Chem.* **2015**, *80*, 6697–6707.
- [71] J. Zhang, M. Mulumba, H. Ong, W. D. Lubell, *Angew. Chemie - Int. Ed.* **2017**, *56*, 6284–6288.
- [72] J. S. Davies, *J. Pept. Sci.* **2003**, *9*, 471–501.
- [73] L. A. Wessjohann, D. G. Rivera, O. E. Vercillo, *Chem. Rev.* **2009**, *109*, 796–814.
- [74] A. Dömling, I. Ugi, *Angew. Chemie* **2000**, *39*, 3168–3210.
- [75] L. A. Wessjohann, M. C. Morejón, G. M. Ojeda, C. R. B. Rhoden, D. G. Rivera, *J. Org. Chem.* **2016**, *81*, 6535–6545.
- [76] M. Paravidino, R. Scheffelaar, R. F. Schmitz, F. J. J. De Kanter, M. B. Groen, E. Ruijter, R. V. A. Orru, *J. Org. Chem.* **2007**, *72*, 10239–10242.
- [77] J. R. Frost, C. C. G. Scully, A. K. Yudin, *Nat. Chem.* **2016**, *8*, 1105–1111.
- [78] L. D. Walensky, A. L. Kung, I. Escher, T. J. Malia, S. Barbuto, R. D. Wright, G. Wagner, G. L. Verdine, S. J. Korsmeyer, *Science* **2004**, *305*, 1466–70.
- [79] Y. H. Lau, P. de Andrade, S.-T. Quah, M. Rossmann, L. Laraia, N. Sköld, T. J. Sum, P. J. E. Rowling, T. L. Joseph, C. Verma, et al., *Chem. Sci.* **2014**, *5*, 1804.
- [80] A. D. de Araujo, J. Lim, K.-C. Wu, Y. Xiang, A. C. Good, R. Skerlj, D. P. Fairlie, *J. Med. Chem.* **2018**, *61*, 2962–2972.
- [81] N. E. Shepherd, H. N. Hoang, G. Abbenante, D. P. Fairlie, *J. Am. Chem. Soc.* **2005**, *127*, 2974–2983.
- [82] G. Lautrette, F. Touti, H. G. Lee, P. Dai, B. L. Pentelute, *J. Am. Chem. Soc.* **2016**, *138*, 8340–8343.
- [83] A. M. Spokoyny, Y. Zou, J. J. Ling, H. Yu, Y. S. Lin, B. L. Pentelute, *J. Am. Chem. Soc.* **2013**, *135*, 5946–5949.
- [84] H. Jo, N. Meinhardt, Y. Wu, S. Kulkarni, X. Hu, K. E. Low, P. L. Davies, W. F. Degrado, D. C. Greenbaum, *J. Am. Chem. Soc.* **2012**, *134*, 17704–17713.
- [85] L. Mendive-Tapia, S. Preciado, J. García, R. Ramón, N. Kielland, F. Albericio, R. Lavilla, *Nat.*

- Commun.* **2015**, *6*, 7160.
- [86] A. F. M. Noisier, J. García, I. A. Ionuț, F. Albericio, *Angew. Chemie - Int. Ed.* **2017**, *56*, 314–318.
- [87] P. M. Cromm, K. Wallraven, A. Glas, D. Bier, A. Fürstner, C. Ottmann, T. N. Grossmann, *ChemBioChem* **2016**, *17*, 1915–1919.
- [88] S. P. Brown, A. B. Smith, *J. Am. Chem. Soc.* **2015**, *137*, 4034–4037.
- [89] A. Muppidi, K. Doi, S. Edwardraja, E. J. Drake, A. M. Gulick, H. G. Wang, Q. Lin, *J. Am. Chem. Soc.* **2012**, *134*, 14734–14737.
- [90] K. Sharma, D. L. Kunciw, W. Xu, M. M. Wiedmann, Y. Wu, H. F. Sore, W. R. J. D. Galloway, Y. H. Lau, L. S. Itzhaki, D. R. Spring, in *Cycl. Pept. From Bioorganic Synth. to Appl.*, The Royal Society Of Chemistry, **2017**, pp. 164–187.
- [91] R. Chingle, C. Proulx, W. D. Lubell, *Acc. Chem. Res.* **2017**, *50*, 1541–1556.
- [92] A. Rossetti, A. Sacchetti, M. Gatti, A. Pugliese, G. Roda, *Chem. Heterocycl. Compd.* **2017**, *53*, 1214–1219.
- [93] G. Koopmanschap, E. Ruijter, R. V. A. Orru, *Beilstein J. Org. Chem.* **2014**, *10*, 544–598.
- [94] D. G. Rivera, A. V. Vasco, R. Echemendía, O. Concepción, C. S. Pérez, J. A. Gavín, L. A. Wessjohann, *Chem. - A Eur. J.* **2014**, *20*, 13150–13161.

## Chapter 2.

# Macrocyclization of Peptide Side Chains by Ugi Reaction: Achieving Peptide Folding and Exocyclic *N*- Functionalization in One Shot



**ABSTRACT:** The utilization of the Ugi reaction for the side chain-to-side chain and side chain-to-termini macrocyclization of peptides is described. In contrast to traditional methodologies comprising the one-component intramolecular cyclization of peptides, a multicomponent approach enables the access not only to stable folded structures but also the simultaneous incorporation of exocyclic functionalities as *N*-substituents. Analysis of the NMR-derived structures revealed the formation of helical turns,  $\beta$ -bulges, and  $\alpha$ -turns in cyclic peptides cross-linked at  $i \rightarrow i+3$  and  $i \rightarrow i+4$  positions, proving the folding effect of the multicomponent Ugi macrocyclization. Molecular dynamics simulation provided further insights on the stability and molecular motion of the side chain cross-linked peptides.

\* The content within this chapter has been published as: A. V. Vasco, C. S. Pérez, F. E. Morales, H. E. Garay, D. Vasilev, J. A. Gavín, L. A. Wessjohann, D. G. Rivera, *J. Org. Chem.* **2015**, *80*, 6697–6707. Author contribution: synthesis of side chain-to-side chain cyclic peptides, NMR analysis and structure refinement of all compounds.

## 2.1. Introduction

Development of effective synthetic approaches to access short peptides mimicking protein-like bioactive conformations remains as one of the most recurrent targets of modern medicinal chemistry.<sup>[1]</sup> Whereas cyclization<sup>[2–4]</sup> and conjugation to topological templates<sup>[2,5–9]</sup> have both proven effective to introduce conformational constraints in small peptides, cyclization have prevailed as the most versatile way to design peptide-based protein ligands and mimetics of protein epitopes.<sup>[5,10]</sup> Cyclic peptides can effectively mimic the most common secondary structures (i.e.,  $\beta$ -hairpins,  $\beta$ -strands,  $\alpha$ -helix and turns) while significantly enhancing the binding affinity to the biological target and improving the pharmacological properties of the linear sequence.<sup>[11,12]</sup>

As previously discussed, the incorporation of multicomponent reactions to the existing repertoire of chemical modifications allowing the synthesis of constrained peptides could broaden the scope of such methodologies towards diversity-generating chemistries. In an effort to deeper understand the synthetic and structural particularities of MCR-based approaches, we decided to expand the scope of the Ugi-based macrocyclization reported by Failli and co-workers in 1979 towards side chain-involving Ugi macrocyclizations.<sup>[13]</sup> Therefore, our main goal was to demonstrate that the Ugi-4CR is a suitable procedure for the macrocyclization of peptide side chains, thus leading to cyclic peptides bearing a tertiary lactam bridge instead of a secondary one, i.e., *N*-substituted cyclic peptides. In order to prove the suitability of the methodology to introduce conformational constraints in the peptide skeleton, NMR-based three-dimensional structures of the *N*-substituted cyclic peptides in solution were proposed. It should be noted that the work contained in this chapter<sup>[14]</sup> was reported before other Ugi-based macrocyclization approaches published by our working group already described in Chapter 1.

## 2.2. Synthetic Plan

Several reports have shown the scope and limitations of the Ugi reaction in the macrocyclization of dissimilar substrates,<sup>[15–19]</sup> including peptidic ones.<sup>[20–22]</sup> According to the mechanism of the Ugi-4CR – in which the initially formed  $\alpha$ -adduct evolves through an intramolecular acylation (Mumm rearrangement) to the final product – the migration capacity of the amino component is crucial for the reaction extension and efficiency.<sup>[23,24]</sup>

In this sense, Yudin *et. al.* have proposed that the slow kinetics of the Ugi macrocyclization in short peptides may be due to the slow transannular attack of the amine to the mixed anhydride.<sup>[3]</sup> As an alternative, this group introduced the use of amphoteric aziridine aldehydes<sup>[23]</sup> and (*N*-isocyanimino)-phosphoranes<sup>[25]</sup> for two new MCR-based peptide macrocyclizations deviating from the Mumm rearrangement allowing the highly efficient and stereoselective head-to-tail cyclization of short and medium-size peptides. In contrast to linear peptides, small pentapeptoids (i.e., *N*-alkylated pentaglycines) have been successfully cyclized by the Ugi reaction,<sup>[20,21]</sup> confirming that a greater flexibility of the amine moiety facilitates the macrocyclic Ugi-based ring closure.

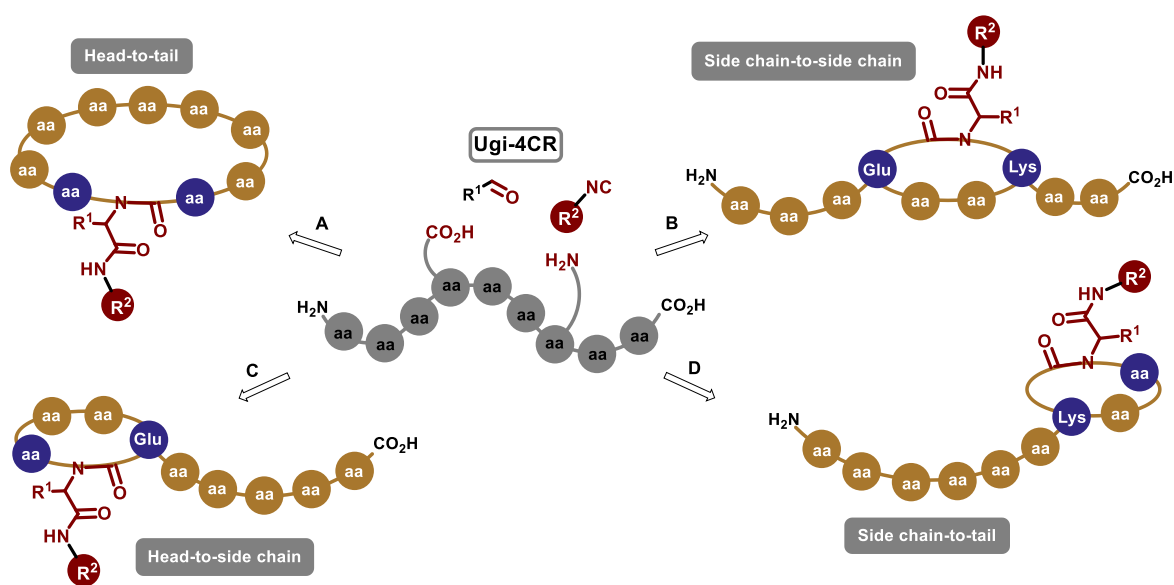


Figure 2.1. Peptide macrocyclization strategies by the Ugi-4 components reaction

Despite the discussed limitations of Ugi-4CR-based head-to-tail macrocyclizations of peptides, we thought that the use of peptide side chains could effectively deliver the cyclized peptide due to a higher flexibility of the functional groups taking part on the multicomponent cyclization. Figure 2.1 illustrates the four possibilities of peptide macrocyclization by means of the Ugi reaction, including the head-to-tail cyclization (A) previously reported.<sup>[13]</sup> As this reaction is the condensation of an amino and a carboxylic group with a carbonyl component and an isocyanide, cyclization strategies B, C and D rely on the presence of Glu/Asp and Lys/Orn along the peptide sequence. Perhaps the most important feature of this strategy – and the one that distinguishes it more from the classic peptide coupling – is the generation of an exocyclic functionality at the *N*-substituted amide formed during the ring closing step. We

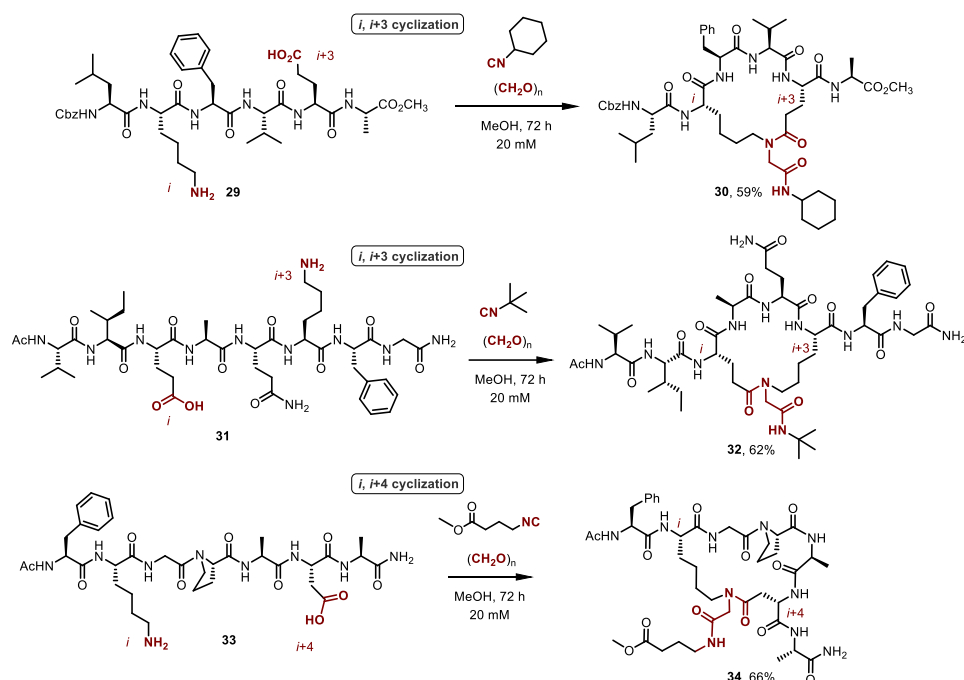
envisioned that the exploitation of such a characteristic may provide a variety of applications not so easily available for conventional cyclization methods based on lactam formation.

### 2.3. Macrocyclization of peptide side chains by Ugi reaction

Our first goal was to exploit the relatively higher flexibility – as compared with peptide termini – of carboxylic acid- and amino-containing peptide side chains as two of the four components of the Ugi reaction (Scheme 2.1). In this direction, oligopeptides **29**, **31** and **33** were prepared following in the first case a stepwise solution-phase synthesis and a standard Fmoc/*t*Bu solid-phase protocol for the last two compounds. The strategy consisted on the introduction of amino acids with Ugi-reactive side chains located at  $i$ ,  $i + 3$  and  $i$ ,  $i + 4$  (where  $i$  is a residue number) positions, as these combinations are known to stabilize both turns and helical structures.<sup>[5,26–28]</sup> Thus, peptides **29** and **31** bear the Lys/Glu and Glu/Lys pairs located at the  $i$  and  $i + 3$  positions running from the *N* to *C*-terminus direction, while peptide **33** has the Lys and Asp residues located at  $i$  and  $i + 4$  positions. However, the amino acid sequences were not designed to favor any periodic secondary structure (e.g.,  $\alpha$ -helix and  $\beta$ -sheet), since the goal was to assess the effect of the Ugi macrocyclization on the peptide folding. In order to avoid the formation of several diastereoisomers, paraformaldehyde was employed as the oxo component.

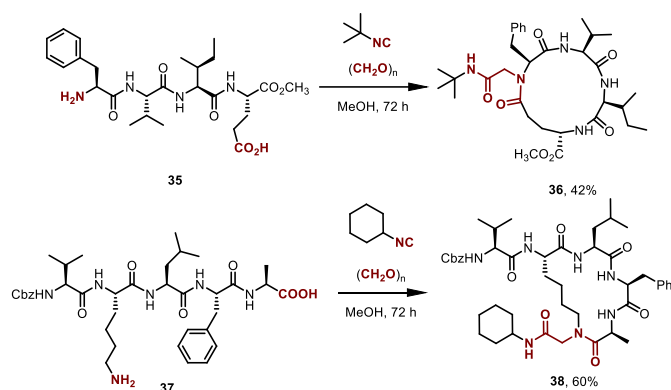
In an attempt to favor the partial formation of the imine, the first step in the macrocyclization protocol is the reaction of the peptide with a small excess of paraformaldehyde during two hours at a concentration of 20 mM in dry methanol. Afterwards, the mixture is diluted ten times in methanol until a final concentration of 2 mM and the isocyanide is added. HPLC monitoring of the Ugi macrocyclization affording **30** proved high conversion ( $\geq 80\%$ ) after 72 h of reaction. Thus, the general reaction time was fixed to 72 h for all macrocyclizations to enable comparison of efficiency among the different approaches. Cyclic peptides **30**, **32** and **34** were obtained in good yield (ca. 60%) and high purity ( $> 95\%$ ) after preparative HPLC purification, which renders enough material for assessing the solution three-dimensional structure through NMR analysis. It should be noted that even when the obtained yields seem to be lower than those of lactamization protocols with coupling agents, four covalent bonds are formed in the multicomponent reaction, while only one is formed during peptide coupling. Synthesis of cyclic peptide **34** demonstrates the possibility of incorporating an exocyclic reactive functionality arising from the isocyanide component, suitable for further derivatization.

*Macrocyclization of Peptide Side Chains by Ugi Reaction: Achieving Peptide Folding and Exocyclic N-Functionalization in One Shot*



Scheme 2.1. Side chain-to-side chain macrocyclization by Ugi reaction

To expand the scope of the Ugi macrocyclization, two examples including the reaction between one side chain of a peptide and one terminus were implemented. As depicted in Scheme 2.2, head-to-side chain and side chain-to-tail macrocyclizations from tetrapeptide **35** and pentapeptide **37** successfully delivered peptides **36** and **38**. The yield of isolated cyclic peptide **36** was the lowest among all macrocyclizations, but there were no great differences between the yields obtained for **38**, **30** and **32**. Noticeably, the most efficient Ugi macrocyclizations are those employing the amino group of the flexible Lys side chain, despite of the fact that macrocycles **30**, **32**, **34** and **38** feature different ring sizes. Most likely, the high flexibility of the lysine side chains circumvents further hampering of the already slow transannular attack of the amine to the mixed anhydride which leads to the Ugi product. In contrast, Ugi macrocyclization affording cyclic peptide **36** comprises the reaction of a backbone terminal amino group, which seems to share with the head-to-tail approach the mechanistic complications derived from a slow transannular Mumm type rearrangement in small peptides.



Scheme 2.2. Side chain-to-termini macrocyclization by Ugi reaction

## 2.4. Three-dimensional structure of side chain-to-side chain cross-linked peptides

Probably the most important outcome of the utilization of Ugi macrocyclization protocols is the possibility to access folded peptides bearing exocyclic functionalizations. Therefore, it was necessary to have an idea about the effect of the Ugi macrocyclization on the three-dimensional solution-phase structures of the side chain cross-linked peptides. It should be noted that even for such small constrained peptides, a significant number of rotatable bonds are present. Additionally, the lack of a tertiary structure makes that the conformation in solution could be dramatically influenced by external factors such as solvent and temperature. The latter, joined to the presence of *non*-proteinogenic motifs – i.e. the *N*-substituted lactam bridge –, made us think that the proposal of a structure generated exclusively *in silico* could be meaningless. Consequently, we chose compounds **30**, **32** and **34** to be studied by means of NMR-based molecular dynamics simulations. The goal was to utilize information from coupling constants ( $^3J_{\text{NHCH}_\alpha}$ ) and ROE crosspeaks as constraints for simulated annealing and refinement protocols in *Xplor-NIH*, in order to generate three dimensional structures in agreement with the observed experimental spectroscopic parameters.<sup>[29,30]</sup> Figure 2.2 illustrates a standard workflow for the structure elucidation of peptides by means of NMR-based Molecular Dynamics.<sup>[31]</sup> Enough spectroscopic information should be recorded in order to achieve the fully unambiguous assignment of all the resonance signals. Once all the spin systems are known and connected, coupling constants and NOE/ROE contacts containing relevant structural information are chosen and employed as restraints for simulated annealing regularization and refinement protocols within XPLOR-NIH. In order to evaluate the conformational stability of the molecules in time, the best NMR structures can be utilized as

starting point in further Molecular Dynamics simulations without NMR restraints. It should be noted that this is the standard workflow which was used for other NMR-based structure elucidations included in further chapters. Special emphasis should be made in the fact that XPLOR-NIH, as well as many other software allowing NMR-based structure elucidation of biomolecules,<sup>[32–35]</sup> is highly optimized for reproducing native structures of peptides and proteins which are mostly favored for relatively large sequences of non-modified peptides. Since our molecules lay far away from being native peptides but mostly peptidomimetics, special attention should be addressed during the NMR refinement process to disable as many extra features as possible, included in the software to deliver “better” peptide-like structures, e.g. amino acids torsion databases, etc.

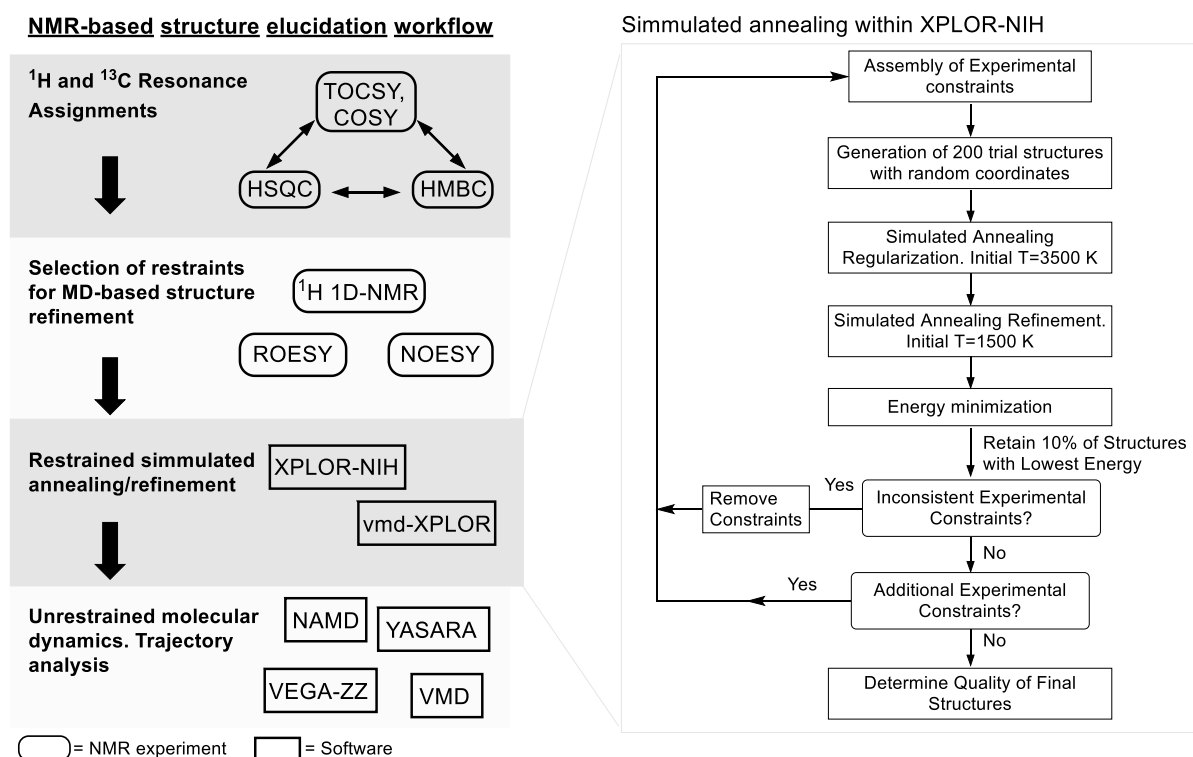


Figure 2.2. Strategy for the NMR-based three dimensional structure elucidation of compounds **30**, **32** and **34**

Similarly to other Lys-Asp/Glu cross-linked peptides made by classic lactamization, we hypothesized that the Ugi macrocyclization could introduce significant conformational constraints onto the small peptides which could ultimately also induce the folding of the peptide into turn structures.<sup>[5]</sup> Due to low solubility in water, the structural characterization of these compounds was assessed based on 1D and 2D <sup>1</sup>H NMR spectroscopy in DMSO-d<sub>6</sub> at 298 K.

For cyclic peptides **30** and **32** – featuring a crosslink between Lys and Glu separated by two residues, i.e. including four amino acids – a folded structure with a  $C^{\alpha}_i-C^{\alpha}_{i+3}$  distance lower than 7 Å typical of reverse turns might be expected. In the case of cyclic peptide **30**, coupling constants  $^3J_{\text{NHCH}\alpha}$  were higher than 8 Hz for all residues, with exception of C-terminal Ala. These values are indicative of a well-structured peptide skeleton with low conformational freedom, and commonly are associated to the occurrence of  $\beta$ -strand structures.<sup>[31,36]</sup> Only three signals are present in the  $C^{\alpha}\text{H}$  region of the  $^1\text{H}$  NMR spectrum, consequence of an overlapping of  $\alpha$ -hydrogen resonances of Lys2, Val4 and Glu5 at 4.30 ppm as evidenced in the HSQC spectrum. This latter made impossible the unequivocal assignment of several ROE cross-peaks involving these hydrogens and, consequently, their use as experimental restraints during the structure refinement. The superimposition of the 20 lowest energy structures of cyclic peptide **30** are shown in Figure 2.3A (top), featuring 0.14 Å average RMSD to the mean structure for the peptide backbone which reflects the conformational rigidity previously suggested by the  $^3J_{\text{NHCH}\alpha}$  values. These structures reflect a total of 37 distance constraints (5 strong, 18 medium and 14 weak; 22 inter-residual: 10 of them sequential and 12 non-sequential) resulted from analysis of ROESY spectrum as well as six dihedral restraints, 5  $\phi$  angles from the  $^3J_{\text{NHCH}\alpha}$  data and one  $\chi_1$  angle from the Phe residue. Stereospecific assignment of the methylene hydrogens of Phe3, the  $\text{H}^{\epsilon}$  of Lys3, and methyl groups of Val4 was introduced after three rounds of simulation.

The NMR-derived solution structures of **30** comprise a reverse turn with certain propensity to helicity, i.e., the  $\phi$  and  $\psi$  angles of Phe3, Val4 and Glu5 lay within the helical region of the Ramachandran plot. To further determine whether such a behavior remains in time or not, MD simulation during 80 ns from the average NMR-derived structure was performed. As observed in Figure 2.3B (top), the  $\phi/\psi$  distribution in time for the four central amino acids obtained from MD, confirms that the helical zone of the Ramachandran plots is indeed the most populated. Also shown are three of the most representative structures obtained during the simulation time, evidencing the major deviations from each other, and therefore the major mobility, at the first two residues Leu1 and Lys2. This comprises the two *N*-terminal residues visiting a *pseudo*-planar conformation, while residues Phe3, Val4, and Glu5 mostly remain in an helical one. Furthermore, various relevant hydrogen bonds were detected during MD simulation, including  $\text{CO}_{\text{Lys2}}\cdots\text{NH}_{\text{Ala6}}$  (6% in time; *i, i+4* characteristic of  $\alpha$ -helix),  $\text{CO}_{\text{Lys2}}\cdots\text{NH}_{\text{Glu5}}$  (2% in time) and  $\text{CO}_{\text{Phe3}}\cdots\text{NH}_{\text{Ala6}}$  (3% in time).

In contrast to **30**, cyclic peptide **32** also contains a *N*-substituted lactam bridge of Glu and Lys side chains at *i* and *i*+3 positions, but with opposed directionality. This directionality is known to play an important role in bridged peptides with helical propensity when cross-linked at *i*, *i*+4 positions.<sup>[37]</sup> In this direction, we sought it could be meaningful to evaluate whether the change in the amide position might be important also in the folding of Ugi cross-linked peptides at *i*, *i*+3 positions.

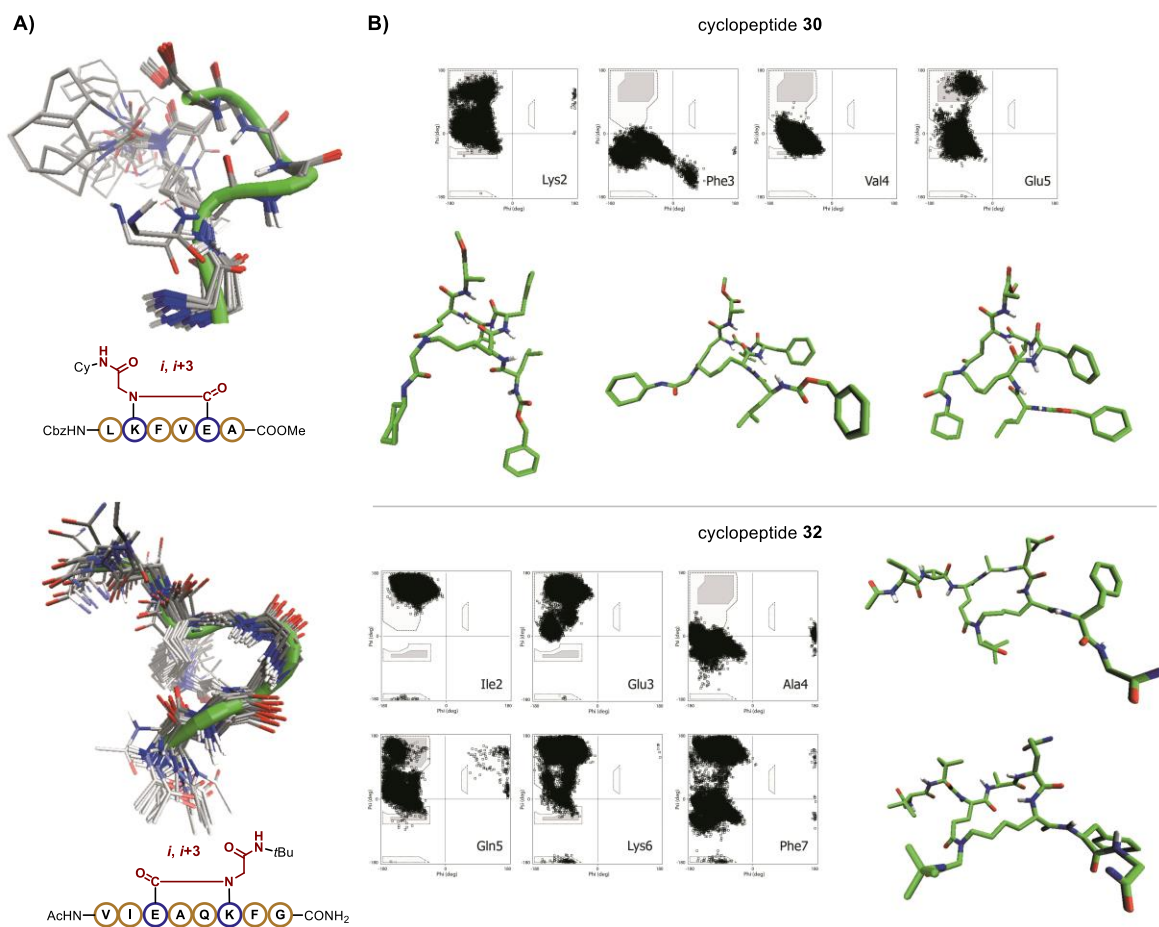


Figure 2.3. A) Superimposition of 20 lowest energy structures of cyclic peptides **30** and **32**. B) Distribution in time of  $\phi$  and  $\psi$  angles (Ramachandran plots) for central amino acids of peptides **30** and **32**, and some representative structures as obtained from MD simulation.

Figure 2.3A (bottom) depicts the superimposition of the final 20 lowest energy structures of **32** which results from a total of 43 distance constraints (13 strong, 16 medium and 14 weak; 28 inter-residual: 22 of them sequential and only 6 non-sequential) and 5  $^3J_{\text{NHCH}\alpha}$  coupling constants restraints. In this case,  $^3J_{\text{NHCH}\alpha}$  coupling constants of residues Val1, Ile2, Lys6 and Phe7 were higher than 8 Hz, while  $^3J_{\text{NHCH}\alpha}$  values of central residues Glu3, Ala4 and Gln5

were between 6 Hz and 7 Hz. Noticeably, intense  $H^\alpha$ - $H^N(i, i+1)$  ROE crosspeaks were abundant, which is indicative of  $\beta$ -sheet structures. However,  $H^\alpha$ - $H^N(i, j)$  and  $H^N$ - $H^N(i, j)$  ROEs for residues separated more than two amino acids (i.e. medium-range) were absent. Along with the high  $^3J_{NHCH\alpha}$  values of residues Val1, Ile2, Lys6 and Phe7, ROESY-derived information suggests  $\beta$ -strand conformations for sequences flanking the central amino acids Ala4 and Gln5. The analysis of the final structures (0.68 Å RMSD difference to the mean structure for the backbone) suggests a conformation which comprises a  $\beta$ -strand with a change in the directionality due to the presence of a reverse turn at the central residues. Further MD simulations carried out during 80 ns of simulation from the NMR-derived average structure, revealed that the reverse turn transits from a tighter (17% in time) to a looser disposition (most populated), as shown in the representative conformations illustrated in Figure 2.3B (bottom). The average distance  $C^{\alpha}_{Glu3}$ - $C^{\alpha}_{Lys6}$  during the simulation time is around 7 Å ( $6.77 \pm 0.51$  Å) which is considered the limit for the classification of open tight turns. In the looser conformations of the central turn of peptide **32**, the irregularity in the  $\beta$ -strand chain caused by residues Ala4 and Gln5 resembles a  $\beta$ -bulge, i.e., a protuberance that affects the directionality of  $\beta$ -strands but in a less drastic manner than tight turns.<sup>[38]</sup> This is supported by the fact that  $\phi$  and  $\psi$  angles of residue Ala4 lay within the right-handed helical region of Ramachandran plot, while the remaining residues mostly populate the  $\beta$ -sheet space (Figure 2.3B), which is a common characteristic of classic  $\beta$ -bulges.<sup>[38]</sup>

Combined NMR/MD analysis was also performed for peptide **34**, which is cross-linked at  $i, i + 4$  residues by a  $N$ -substituted lactam bridge. Previously, it has been reported that lactamization of Lys and Asp residues located at  $i, i + 4$  positions is a very effective way to stabilize an  $\alpha$ -helix in small peptides.<sup>[5]</sup> Nevertheless, we chose to introduce the turn-inducing amino acids Pro and Gly at the middle of the peptide sequence instead of using other sequences favoring helicity (e.g., poly-Ala or poly-Leu). Accordingly, we anticipated that cyclic peptide **34** could fold onto a *pseudo*-planar  $\alpha$ -turn rather than in a  $\alpha$ -helical conformation. For peptide **34**,  $^3J_{NHCH\alpha}$  coupling constants higher than 8 Hz were only found for residues Phe1 and Lys2, while  $^3J_{NHCH\alpha}$  values of the remaining residues were between 6 and 8 Hz. As a result, there is no clear inclination either to helical or to  $\beta$ -strand structures. A total of 42 distance constraints (6 strong, 7 medium and 29 weak; 19 inter-residual: 16 of them sequential and only 3 non-sequential) resulted from ROESY spectrum. As most inter-residual ROE

contacts were between sequential amino acids, these evidences indicate low propensity to either helical or tight turn conformations.

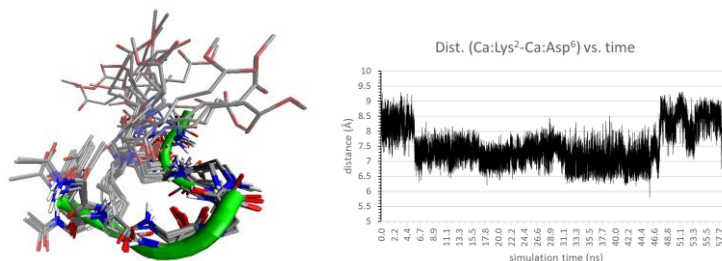


Figure 2.4. Superimposition of the 20 best NMR-derived structures of **34** and MD-derived plot of the  $C^{\alpha}_{Lys2}-C^{\alpha}_{Asp6}$  distance vs. simulation time

Figure 2.4 shows the superimposition of the 20 lowest energy NMR-derived structures of **34** (0.86 Å RMSD difference to the mean structure for the backbone), illustrating that this peptide occurs in a rather loose reverse turn including five residues ( $\alpha$ -turn). Analysis of the distance  $C^{\alpha}_{Lys2}-C^{\alpha}_{Asp6}$  reveals that, in fifteen of the twenty lowest energy structures, the value is lower than 7 Å, whilst five structures had a distance greater than 7 Å. To get deeper insight into the loose character of the  $\alpha$ -turn, we performed a MD simulation during 60 ns starting from the NMR-derived lowest energy structure. Figure 2.4B depicts the plot of  $C^{\alpha}_{Lys2}-C^{\alpha}_{Asp6}$  distances *versus* time, indicating that such distances varies from 6.5 Å to around 9 Å. However, most populated states lay within a distance of 7-7.5 Å, confirming the relatively loose character of the reverse turn.

An important remark is the fact that none of the bridged peptides studied show *s-cis/s-trans* isomerization around the tertiary lactam bridge which has been described as a characteristic of peptide mimetics synthesized by Ugi reactions.<sup>[6]</sup>

## 2.5. Conclusions

We have proven that the Ugi reaction is also a suitable approach for the macrocyclization of peptide side chains, enabling the simultaneous access to folded peptide conformations and exocyclic *N*-functionalization at the resulting lactam bridge. Macrocyclization efficiency is higher for side chain-to-side chain combinations based on Glu/Asp and Lys residues, while the cyclization of a carboxylic side chain with an *N*-terminal amine provided poorer results. One big limitation of the described approach is the lack of orthogonality of the tethering side

chains towards other Ugi-reacting side chains, making its implementation difficult for application in natural peptides.

Side chain-to-side chain cross-linked peptides were analyzed by NMR and MD simulation to assess the folding effect of the Ugi macrocyclization. Thus, cyclization at  $i \rightarrow i+3$  positions led to folded structures such as a helical turn and a loose  $\beta$ -turn resembling a  $\beta$ -bulge, while the  $i \rightarrow i+4$  combination resulted in formation of a loose  $\alpha$ -turn. Nevertheless, in order to get a deeper insight about the effect of the *N*-substituent nature on the stability of specific secondary structures as well as the potential utilization of such exocyclic appendages as derivatization sites, e.g., for lipidation or glycosylation, further conformational studies on water soluble Ugi-cyclized peptides need to be done.

## 2.6. Experimental Section

### **General**

$^1\text{H}$  NMR and  $^{13}\text{C}$  NMR spectra were recorded at 400/600 MHz for  $^1\text{H}$ , 100/150 MHz for  $^{13}\text{C}$ , at 300 K. Chemical shifts ( $\delta$ ) are reported in parts per million relative to TMS using the residual solvent signals as secondary standards. Coupling constants ( $J$ ) are reported in Hertz. Splitting patterns that could not be easily interpreted are designated as multiplet (m) or broad singlet (br. s). Carbon resonances were assigned using additional information provided by DEPT spectra recorded with phase angles of  $135^\circ$ . For compounds subjected to structure determination, NMR peak assignments were accomplished by analysis of standard TOCSY (mixing time 60 ms), g-COSY, g-HSQC, HMBC and tr-ROESY (500 ms spin-lock) spectra. Peptides were characterized by electrospray ionization mass spectrometry (ESI-MS) in a hybrid quadrupole-time-of-flight instrument (QTOF1, Waters, USA) fitted with a nanospray ion source. All reagents and solvents were used as received, with the exception of  $\text{CH}_2\text{Cl}_2$ , DMF and DIPEA that were dried by distillation from  $\text{CaH}_2$  over argon prior to use as reaction solvent, and DMF was stored over  $4\text{\AA}$  molecular sieves. Flash column chromatography was carried out using silica gel 60 (230-400 mesh) and analytical thin layer chromatography (TLC) was performed using silica gel aluminum sheets.

**General procedure for the Ugi reaction-based macrocyclization:** A solution of paraformaldehyde (0.13 mmol, 1.3 equiv.),  $\text{Et}_3\text{N}$  (0.1 mmol, 1 equiv) and the peptide (0.1 mmol, 1 equiv.) in MeOH (5 mL) was stirred for 1 h at room temperature and next diluted to 50 mL of MeOH. The isocyanide (0.2 mmol, 2 equiv.) was added and the reaction mixture

was stirred for 96 h and then concentrated under reduced pressure. The crude peptide was dissolved in the minimum amount of TFA, precipitated from frozen diethyl ether, then taken up in 1:1 acetonitrile/water and lyophilized. Peptides were purified by preparative RP-HPLC on the HPLC system LaChrom (Merck Hitachi, Germany). Separation was achieved by RP C18 column (Vydac, 25 × 250 mm, 25 μm). A linear gradient from 15% to 45% of solvent B over 50 min at a flow rate of 5 mL/min was used. Detection was accomplished at 226 nm. Solvent A: 0.1% (v/v) TFA in water. Solvent B: 0.05% (v/v) TFA in acetonitrile.

**N-Substituted cyclic peptide 30:** Peptide **29** (85 mg, 0.1 mmol), cyclohexylisocyanide (20 μL, 0.15 mmol), paraformaldehyde (4 mg, 0.13 mmol) were reacted according to the general cyclization procedure. Purification by preparative RP-HPLC afforded the cyclic peptide **30** (55 mg, 56%) as a white amorphous solid. Purity of 98% as determined by analytical RP-HPLC.  $R_t = 14.96$  min.  $^1\text{H NMR}$  (600 MHz, DMSO- $d_6$ ):  $\delta$  8.72 (d,  $J = 8.9$  Hz, 1H), 8.31 (d,  $J = 8.8$  Hz, 1H), 8.23 (d,  $J = 3.9$  Hz, 1H), 7.87 (d,  $J = 8.2$  Hz, 1H), 7.55 (d,  $J = 8.0$  Hz, 1H), 7.40 – 7.26 (m,  $J = 6.8$  Hz, 5H), 7.24 – 7.08 (m,  $J = 24.6$  Hz, 5H), 6.72 (d,  $J = 9.0$  Hz, 1H), 5.02 (d,  $J = 12.9$  Hz, 1H), 4.99 (d,  $J = 13.0$  Hz, 1H), 4.45 – 4.39 (m, 1H), 4.32 – 4.26 (m, 3H), 4.05 – 3.99 (m, 2H), 3.90 (d,  $J = 16.0$  Hz, 1H), 3.72 (d,  $J = 16.1$  Hz, 1H), 3.64 (s, 3H), 3.54 – 3.41 (m, 2H), 3.15 (dd,  $J = 14.1, 3.0$  Hz, 1H), 2.95 – 2.86 (m, 1H), 2.77 (dd,  $J = 14.0, 10.8$  Hz, 1H), 2.44 – 2.30 (m, 2H), 2.25 – 2.17 (m, 1H), 2.03 – 1.96 (m, 1H), 1.75 – 1.47 (m, 8H), 1.46 – 1.29 (m,  $J = 13.5$  Hz, 7H), 1.21 (d,  $J = 7.0$  Hz, 3H), 1.28 – 1.01 (m,  $J = 7.0$  Hz, 6H), 0.89 (d,  $J = 6.7$  Hz, 3H), 0.85 (d,  $J = 6.6$  Hz, 3H), 0.83 (d,  $J = 7.4$  Hz, 3H), 0.81 (d,  $J = 7.2$  Hz, 3H).  $^{13}\text{C NMR}$  (150 MHz, DMSO- $d_6$ ):  $\delta$  172.5, 172.4, 171.8, 171.4, 170.4, 170.2, 167.3, 155.8 (CO); 137.9, 137.1 (C), 128.8, 128.4, 128.2, 127.8, 127.7, 127.0, 126.2 (CH); 65.3 (CH<sub>2</sub>); 56.0, 54.3, 52.9, 52.4 (CH); 52.1 (CH<sub>3</sub>); 49.0 (CH); 48.7, 48.4 (CH<sub>2</sub>); 47.5, 40.9 (CH); 37.3, 32.9, 32.4, 32.3 (CH<sub>2</sub>); 31.4 (CH); 28.1, 27.7, 27.1, 25.2, 24.7, 24.7 (CH<sub>2</sub>); 24.2 (CH); 23.2 (CH<sub>3</sub>); 22.6 (CH<sub>2</sub>); 21.3, 19.2, 17.4, 17.0 (CH<sub>2</sub>). ESI-MS  $m/z$ : 997.59 [M+H]<sup>+</sup>, calcd. for C<sub>51</sub>H<sub>74</sub>O<sub>11</sub>N<sub>8</sub>Na: 997.55.

**N-Substituted cyclic peptide 32:** Peptide **31** (93 mg, 0.1 mmol), *tert*-butylisocyanide (17 μL, 0.15 mmol), paraformaldehyde (4 mg, 0.13 mmol) were reacted according to the general cyclization procedure. Purification by preparative RP-HPLC afforded the pure cyclic peptide **32** (58 mg, 56%) as a white amorphous solid. Purity of 97% as determined by analytical RP-HPLC.  $R_t = 15.53$  min.  $^1\text{H NMR}$  (600 MHz, DMSO- $d_6$ ):  $\delta$  8.53 (s, 1H), 8.31 (t,  $J = 5.6$  Hz, 1H), 8.15 (d,  $J = 6.4$  Hz, 1H), 8.03 (d,  $J = 7.9$  Hz, 1H), 7.96 (d,  $J = 7.6$  Hz, 1H), 7.94 (d,  $J = 9.0$  Hz, 1H), 7.91 (d,  $J = 9.0$  Hz, 1H), 7.84 (d,  $J = 8.9$  Hz, 1H), 7.82 (d,  $J = 6.7$  Hz, 1H), 7.40 (s, 1H), 7.31 (s, 1H), 7.25 – 7.20 (m, 4H), 7.18 – 7.14 (m, 1H), 7.08 (s, 1H), 6.79 (s, 1H), 4.51 – 4.46

(m, 1H), 4.28 – 4.22 (m, 2H), 4.19 – 4.12 (m, 2H), 4.09 – 4.06 (m, 1H), 4.05 – 3.99 (m, 1H), 3.85 (d,  $J = 15.7$  Hz, 1H), 3.70 (d,  $J = 15.9$  Hz, 1H), 3.65 (dd,  $J = 16.7, 5.9$  Hz, 1H), 3.56 (dd,  $J = 16.8, 5.5$  Hz, 1H), 3.21 (m, 2H), 3.03 (dd,  $J = 13.7, 4.9$  Hz, 1H), 2.80 (dd,  $J = 13.8, 9.5$  Hz, 1H), 2.65 – 2.57 (m, 1H), 2.30 – 2.22 (m, 1H), 2.11 – 2.03 (m, 2H), 1.97 – 1.89 (m, 1H), 1.85 (s, 3H), 1.88-1.82 (m, 1H) 1.80 – 1.72 (m, 3H), 1.71 – 1.65 (m, 1H), 1.60 – 1.30 (m, 5H), 1.26 (d,  $J = 6.8$  Hz, 3H), 1.23 (s, 9H), 1.20 – 1.00 (m, 3H), 0.84 – 0.75 (m, 12H).  $^{13}\text{C}$  NMR (150 MHz, DMSO- $d_6$ ):  $\delta$  173.8, 171.9, 171.8, 171.7, 171.3, 171.2, 171.1, 170.7, 170.4, 170.3, 169.2, 167.7, 165.9 (CO); 137.6 (C), 129.2, 128.1, 126.3 (CH); 57.7, 56.7, 54.0, 53.0, 51.9, 51.7 (CH); 50.1 (C); 48.9 (CH); 47.9, 47.5, 41.9, 37.4 ( $\text{CH}_2$ ); 36.6 (CH), 31.9, 31.3 ( $\text{CH}_2$ ); 30.4 (CH), 28.6 ( $\text{CH}_3$ ); 28.3, 27.7, 27.4, 27.1, 24.4 ( $\text{CH}_2$ ); 22.5 ( $\text{CH}_3$ ); 21.9 ( $\text{CH}_2$ ); 19.3, 18.2, 17.8, 15.2, 11.1 ( $\text{CH}_3$ ). ESI-MS  $m/z$ : 1027.59  $[\text{M}+\text{H}]^+$ , calcd. for  $\text{C}_{49}\text{H}_{78}\text{O}_{12}\text{N}_{12}$ : 1027.59.

**N-Substituted cyclic peptide 34:** Peptide **33** (89 mg, 0.1 mmol), methyl 4-isocyanobutanoate (21  $\mu\text{L}$ , 0.15 mmol), paraformaldehyde (4 mg, 0.13 mmol) were reacted according to the general cyclization procedure. Purification by preparative RP-HPLC afforded the pure cyclic peptide **34** (32 mg, 36%) as a white amorphous solid. Purity of 95% as determined by analytical RP-HPLC.  $R_t = 14.65$  min.  $^1\text{H}$  NMR (600 MHz, DMSO- $d_6$ ):  $\delta$  8.46 – 8.41 (bs, 1H), 8.22 (d,  $J = 6.2$  Hz, 1H), 8.05 (d,  $J = 7.9$  Hz, 1H), 8.03 (d,  $J = 8.4$  Hz, 1H), 7.67 – 7.63 (m, 1H), 7.60 (d,  $J = 7.4$  Hz, 1H), 7.52 (d,  $J = 7.6$  Hz, 1H), 7.27 – 7.21 (m, 4H), 7.19 – 7.15 (m, 1H), 7.04 (d,  $J = 9.4$  Hz, 1H), 7.00 (d,  $J = 10.0$  Hz, 1H), 4.62 – 4.56 (m, 1H), 4.54 – 4.48 (m, 1H), 4.41 – 4.30 (m, 2H), 4.19 – 4.04 (m, 4H), 3.77 – 3.67 (m, 2H), 3.57 (s, 3H), 3.67 – 3.46 (m, 2H), 3.45 – 3.36 (m, 1H), 3.15 – 2.97 (m, 4H), 2.93 (dd,  $J = 13.9, 3.9$  Hz, 1H), 2.68 (dd,  $J = 13.7, 10.3$  Hz, 1H), 2.55 – 2.52 (m, 1H), 2.23 – 2.15 (m, 3H), 1.96 – 1.85 (m, 2H), 1.84 – 1.78 (m, 1H), 1.73 (s, 3H), 1.71 – 1.59 (m, 4H), 1.47 – 1.38 (m, 2H), 1.31 (d,  $J = 7.4$  Hz, 3H), 1.33 – 1.27 (m, 2H), 1.23 (d,  $J = 7.2$  Hz, 3H).  $^{13}\text{C}$  NMR (150 MHz, DMSO- $d_6$ ):  $\delta$  173.8, 173.2, 172.7, 172.6, 171.6, 171.0, 170.9, 170.4, 169.6, 169.1, 168.0 (CO); 138.0 (C); 129.2, 128.0, 126.2 (CH); 61.4, 53.8, 52.1 (CH); 51.3 ( $\text{CH}_3$ ); 50.6 (s), 49.7 (CH); 48.6, 48.5 ( $\text{CH}_2$ ); 48.4 (CH); 46.6, 41.1, 38.0, 37.7, 34.0, 32.5, 30.6, 29.1, 27.4, 24.5, 24.4 ( $\text{CH}_2$ ); 22.5 ( $\text{CH}_3$ ); 22.2 ( $\text{CH}_2$ ); 17.9, 16.2 ( $\text{CH}_3$ ). ESI-MS  $m/z$ : 885.44  $[\text{M}+\text{H}]^+$ , calcd. for  $\text{C}_{41}\text{H}_{60}\text{O}_{12}\text{N}_{10}$ : 885.44.

**N-substituted cyclic peptide 36:** Peptide **35** (56 mg, 0.1 mmol), *tert*-butylisocyanide (17  $\mu\text{L}$ , 0.15 mmol), paraformaldehyde (6 mg, 0.2 mmol) were reacted according to the general cyclization procedure. Purification by Flash column chromatography afforded the pure cyclic peptide **36** (27 mg, 44%) as a white amorphous solid.  $^1\text{H}$  NMR (600 MHz, acetone- $d_6$ ):  $\delta$  7.73

(bs, 1H), 7.51 (bs, 1H), 7.38 (bs, 1H), 7.36 – 6.98 (m, 6H), 5.10-5.01 (m, 1H), 4.84-4.76 (m, 1H), 4.38-4.30 (m, 1H), 4.23-4.17 (m, 1H), 3.90 – 3.79 (m, 2H), 3.66 (s, 3H), 3.50-3.41(m,1H), 3.15 – 3.05 (m, 1H), 2.63 (m, 1H), 2.54 – 1.88 (m, 4H), 1.70-1.60 (m, 1H), 1.34 (s, 9H), 1.41 – 1.14 (m, 2H), 1.04 – 0.81 (m, 12H).  $^{13}\text{C}$  NMR (150 MHz, acetone- $d_6$ ):  $\delta$  176.0, 173.8, 173.1, 172.0, 171.5, 170.6 (CO); 138.9 (C); 129.7, 129.3, 127.7 (CH); 63.5, 63.2, 62.6 (CH); 53.3 (C), 51.9 (CH); 50.7 (CH<sub>3</sub>); 48.0 (CH<sub>2</sub>); 36.8 (CH<sub>2</sub>), 36.6 (CH); 34.6 (CH<sub>2</sub>); 31.5 (CH); 28.7 (CH<sub>3</sub>); 25.7, 25.3 (CH<sub>2</sub>), 19.9, 19.8, 16.1, 12.3 (CH<sub>3</sub>). ESI-MS (ESI-FT-ICR)  $m/z$ : 638.36 [M+Na]<sup>+</sup>, calcd. for C<sub>32</sub>H<sub>49</sub>O<sub>7</sub>NaN<sub>5</sub>: 638.35.

**N-Substituted cyclic peptide 38:** Peptide **37** (71 mg, 0.1 mmol), cyclohexylisocyanide (20  $\mu\text{L}$ , 0.15 mmol), paraformaldehyde (6 mg, 0.2 mmol) were reacted according to the general cyclization procedure. Purification by flash column chromatography afforded the pure cyclic peptide **38** (42 mg, 51%) as a white amorphous solid.  $^1\text{H}$  NMR (600 MHz, CDCl<sub>3</sub>/CD<sub>3</sub>OD 95:5):  $\delta$  7.51 – 7.29 (m, 10H), 5.26 (d,  $J$  = 12.4 Hz, 1H), 5.22 (d,  $J$  = 12.4 Hz, 1H), 4.77 (dd,  $J$  = 10.2, 3.7 Hz, 1H), 4.69 (dd,  $J$  = 9.5, 3.1 Hz, 1H), 4.47 (d,  $J$  = 6.0 Hz, 1H), 4.35 (m, 1H), 4.21 (q,  $J$  = 5.7 Hz, 1H), 4.12 (d,  $J$  = 16.0 Hz, 1H), 3.97 (d,  $J$  = 16.0 Hz, 1H), 3.84-3.77 (m, 1H), 3.59 – 3.50 (m, 1H), 3.33 – 3.23 (m, 1H), 3.07 (dd,  $J$  = 14.3, 10.4 Hz, 1H), 2.08 – 2.00 (m, 1H), 1.98-1.90 (m, 2H), 1.89 – 1.69 (m, 7H), 1.69- 1.24 (m, 10H), 1.52 (d,  $J$  = 7.2 Hz, 3H), 1.12 (d,  $J$  = 6.7 Hz, 3H), 1.08 (d,  $J$  = 6.4 Hz, 6H), 1.05 (d,  $J$  = 6.5 Hz, 3H).  $^{13}\text{C}$  NMR (150 MHz, CDCl<sub>3</sub>/CD<sub>3</sub>OD 95:5):  $\delta$  173.1, 172.8, 171.6, 171.4, 171.1, 168.3, 156.8 (CO); 136.6, 135.9 (C); 128.3, 127.9, 127.9, 127.5, 127.1, 126.2 (CH), 66.3 (CH<sub>2</sub>), 57.5, 55.1, 53.5, 50.9, 49.3 (CH); 49.2 (CH<sub>2</sub>), 48.9 (CH), 48.3, 40.3, 36.4, 32.0, 31.9 (CH<sub>2</sub>); 30.9 (CH); 27.4, 26.4 (CH<sub>2</sub>), 24.9 (CH), 24.4, 24.1 (CH<sub>2</sub>), 21.9, 20.7, 18.4, 17.2, 16.2 (CH<sub>3</sub>). ESI-MS (ESI-FT-ICR)  $m/z$ : 854.50 [M+Na]<sup>+</sup>, calcd. for C<sub>45</sub>H<sub>65</sub>O<sub>8</sub>NaN<sub>7</sub>: 854.48.

### **NMR structure determination**

Cross-peaks in t-ROESY spectra were assigned and integrated in *Sparky NMR*.<sup>[39]</sup> Distance constraints from ROE intensities were generated using pseudo-atoms corrections where needed, and placed into three groups: strong (2.8 Å upper limit), medium (3.5 Å upper limit) and weak (5.0 Å upper limit). The lower limit for NOE restraints was always maintained at 1.8 Å. Backbone dihedral angle restraints were inferred from  $^3J_{\text{NHCH}_\alpha}$  coupling constants in 1D spectrum at 300 K,  $\varphi$  was restrained to  $-120 \pm 30^\circ$  for  $^3J_{\text{NHCH}_\alpha} \geq 8$  Hz as reported by Fairlie *et al.*<sup>8e</sup> Peptide bond  $\omega$  angles were all set *trans*. Structure calculations were carried out using *Xplor-NIH 2.33* package.<sup>[30]</sup> The calculations were performed using the standard force field

parameter set (PARALLHDG.PRO) and topology file (TOPALLHDG.PRO) within *Xplor-NIH* with in-house modifications to ensure peptide cyclization and amide *N*-substitution. Structures were visualized and analyzed using *VMD-Xplor*.<sup>[29]</sup>

NMR structure determination was performed through simulated annealing regularization and refinement in torsion angle space, using experimental data as inter-proton distances and dihedral angles restraints. For simulated annealing regularization, 200 starting structures were randomly generated. A 100 ps molecular dynamics simulation at 3500 K was performed with a time-step of 3 fs. The system was cooled from 3500 to 25 K, with a temperature step of 12.5 K. At each temperature step, 0.2 ps of molecular dynamics simulation was performed. A 500 steps torsion angle minimization was performed and finally the system was optimized by means of 500 steps of conjugated gradient Powell Cartesian minimization.

The refinement protocol consisted in a slow cooling simulated annealing from the regularized structures. A 10 ps molecular dynamics simulation at 1500 K was achieved with a time-step of 3 fs. The system was cooled with a temperature step of 12.5 K and a simulation time of 0.2 ps at each temperature. A 500 torsion angle minimization was performed afterwards a second 500 steps minimization was achieved in Cartesian coordinates. A finally 1000 steps Powell minimization with an energy function non-dependent of experimental restraints was executed.

### **Molecular Dynamics Simulations**

Molecular dynamics simulation was performed with the NAMD<sup>[40]</sup> software taking as starting coordinates the corresponding NMR structure. The CHARMM-36<sup>[41]</sup> force field was used with convenient parameterizations for non-standard residues, i.e. peptide *N*-functionalized cyclization, with the help of Paratool plugin within *VMD* molecular package.<sup>[42]</sup> Before each simulation, 60 ps MD equilibration was performed. All simulations were achieved using periodic boundary conditions in a cubic box with explicit solvent. The model proposed by Laaksonen<sup>[43]</sup> was employed for the treatment of DMSO molecules. Simulation temperature was always set to 310 K, using Langevin dynamics for temperature control (damping coefficient of 1/ps). Langevin piston was utilized for maintaining a pressure of 1 atm. A 12 Å cutoff with a switching function was employed for non-bonded van der Waals and electrostatics interactions. A 2 fs time-step was always used with the SHAKE algorithm for freeze hydrogen-heavy atom interatomic distances. Final trajectories were analyzed and visualized in *VMD*<sup>[29]</sup> and *Vega ZZ*<sup>[44]</sup> software.

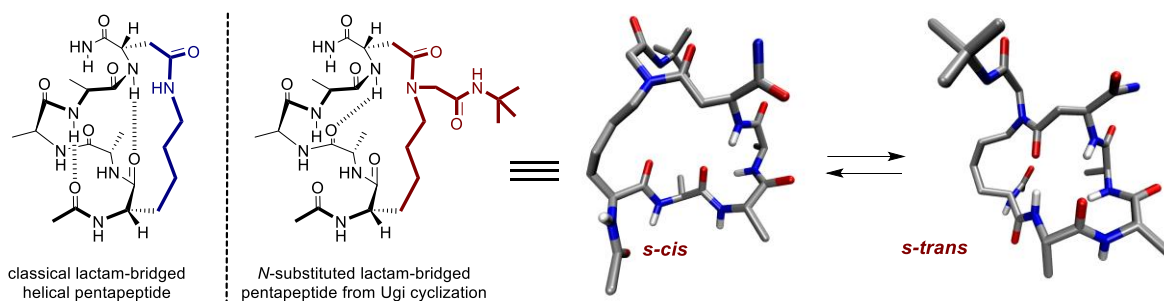
## 2.7. References

- [1] A. K. Yudin, *Chem. Sci.* **2015**, *6*, 30–49.
- [2] V. J. Hruby, *Nat. Rev. Drug Discov.* **2002**, *1*, 847–858.
- [3] C. J. White, A. K. Yudin, *Nat. Chem.* **2011**, *3*, 509–524.
- [4] E. Marsault, M. L. Peterson, *J. Med. Chem.* **2011**, *54*, 1961–2004.
- [5] T. A. Hill, N. E. Shepherd, F. Diness, D. P. Fairlie, *Angew. Chem., Int. Ed.* **2014**, *53*, 13020–13041.
- [6] D. G. Rivera, A. V. Vasco, R. Echemendía, O. Concepción, C. S. Pérez, J. A. Gavín, L. A. Wessjohann, *Chem. - A Eur. J.* **2014**, *20*, 13150–13161.
- [7] C. A. Bodé, T. Bechet, E. Prodhomme, K. Gheysen, P. Gregoir, J. C. Martins, C. P. Muller, A. Madder, *Org. Biomol. Chem.* **2009**, *7*, 3391–3399.
- [8] G. Tuchscherer, D. Grell, M. Mathieu, M. Mutter, *J. Pept. Res.* **1999**, *54*, 185–194.
- [9] Y. Singh, G. T. Dolphin, J. Razkin, P. Dumy, *ChemBioChem* **2006**, *7*, 1298–1314.
- [10] C. Morrison, *Nat. Rev. Drug Discov.* **2018**, *17*, 531–533.
- [11] L. G. Milroy, T. N. Grossmann, S. Hennig, L. Brunsveld, C. Ottmann, *Chem. Rev.* **2014**, *114*, 4695–4748.
- [12] M. Pelay-gimeno, A. Glas, O. Koch, T. N. Grossmann, *Angew. Chem., Int. Ed.* **2015**, *54*, 8896–8927.
- [13] A. Failli, H. Immer, M. Götz, *Can. J. Chem.* **1979**, *57*, 3257–3261.
- [14] A. V. Vasco, C. S. Pérez, F. E. Morales, H. E. Garay, D. Vasilev, J. A. Gavín, L. A. Wessjohann, D. G. Rivera, *J. Org. Chem.* **2015**, *80*, 6697–6707.
- [15] D. G. Rivera, L. A. Wessjohann, *J. Am. Chem. Soc.* **2009**, *131*, 3721–3732.
- [16] D. G. Rivera, O. E. Vercillo, L. A. Wessjohann, *Org. Biomol. Chem.* **2008**, *6*, 1787.
- [17] D. G. Rivera, L. A. Wessjohann, *J. Am. Chem. Soc.* **2006**, *128*, 7122–7123.
- [18] L. A. Wessjohann, D. G. Rivera, F. Coll, *J. Org. Chem.* **2006**, *71*, 7521–7526.
- [19] L. A. Wessjohann, B. Voigt, D. G. Rivera, *Angew. Chem., Int. Ed.* **2005**, *44*, 4785–4790.
- [20] A. de F. S. Barreto, O. E. Vercillo, M. A. Birkett, J. C. Caulfield, L. A. Wessjohann, C. K. Z. Andrade, *Org. Biomol. Chem.* **2011**, *9*, 5024.
- [21] O. E. Vercillo, C. K. Z. Andrade, L. A. Wessjohann, *Org. Lett.* **2008**, *10*, 205–8.
- [22] M. G. Ricardo, F. E. Morales, H. Garay, O. Reyes, D. Vasilev, L. A. Wessjohann, D. G. Rivera, *Org. Biomol. Chem.* **2015**, *13*, 438–446.
- [23] R. Hili, V. Rai, A. K. Yudin, *J. Am. Chem. Soc.* **2010**, *132*, 2889–91.
- [24] A. Dömling, I. Ugi, *Angew. Chemie* **2000**, *39*, 3168–3210.
- [25] J. R. Frost, C. C. G. Scully, A. K. Yudin, *Nat. Chem.* **2016**, *8*, 1105–1111.
- [26] K. Estieu-Gionnet, G. Guichard, *Expert Opin. Drug Discov.* **2011**, *6*, 937–963.
- [27] L. K. Henchey, A. L. Jochim, P. S. Arora, *Curr. Opin. Chem. Biol.* **2008**, *12*, 692–697.
- [28] A. D. De Araujo, H. N. Hoang, W. M. Kok, F. Diness, P. Gupta, T. A. Hill, R. W. Driver, D. A. Price, S. Liras, D. P. Fairlie, *Angew. Chem., Int. Ed.* **2014**, *53*, 6965–6969.
- [29] C. D. Schwieters, J. J. Kuszewski, G. Marius Clore, *Prog. Nucl. Magn. Reson. Spectrosc.* **2006**, *48*, 47–62.
- [30] C. D. Schwieters, J. J. Kuszewski, N. Tjandra, G. M. Clore, *J. Magn. Reson.* **2003**, *160*, 65–73.
- [31] G. S. Rule, T. K. Hitchens, *Fundamentals of Protein NMR Spectroscopy*, Springer Netherlands, Berlin/Heidelberg, **2006**.
- [32] W. Rieping, B. Bardiaux, A. Bernard, T. E. Malliavin, M. Nilges, *Bioinformatics* **2007**, *23*, 381–382.
- [33] A. K. Downing, P. Güntert, in *Protein NMR Tech.*, **2004**, pp. 353–378.
- [34] Y. Shen, F. Delaglio, G. Cornilescu, A. Bax, *J. Biomol. NMR* **2009**, *44*, 213–223.

- [35] A. T. Brunger, *Nat. Protoc.* **2007**, *2*, 2728–2733.
- [36] A. C. Gibbs, T. C. Bjorndahl, R. S. Hodges, D. S. Wishart, *J. Am. Chem. Soc.* **2002**, *124*, 1203–1213.
- [37] N. E. Shepherd, H. N. Hoang, G. Abbenante, D. P. Fairlie, *J. Am. Chem. Soc.* **2005**, *127*, 2974–2983.
- [38] A. W. E. Chan, E. G. Hutchinson, D. Harris, J. M. Thornton, *Protein Sci.* **1993**, *2*, 1574–1590.
- [39] T. D. Goddard, D. G. Kneller, **2007**.
- [40] J. C. Phillips, R. Braun, W. Wang, J. Gumbart, E. Tajkhorshid, E. Villa, C. Chipot, R. D. Skeel, L. Kalé, K. Schulten, *J. Comput. Chem.* **2005**, *26*, 1781–1802.
- [41] A. D. MacKerell, M. Feig, C. L. Brooks, *J. Am. Chem. Soc.* **2004**, *126*, 698–699.
- [42] W. Humphrey, A. Dalke, K. Schulten, *J. Mol. Graph.* **1996**, *14*, 33–38.
- [43] A. Vishnyakov, A. P. Lyubartsev, A. Laaksonen, *J. Phys. Chem. A* **2001**, *105*, 1702–1710.
- [44] A. Pedretti, L. Villa, G. Vistoli, *J. Mol. Graph. Model.* **2002**, *21*, 47–49.

## Chapter 3.

# On the influence of the lactam bridge *N*-substituent and *cis/trans* isomerism on the secondary structure of Ugi-stapled peptides



**ABSTRACT:** The chapter describes the first insights into the structural influence of the *s-cis/s-trans* isomerism of lactam bridged peptides derived from the Ugi reaction. On-resin Ugi macrocyclizations allowed the synthesis of a small family of pentapeptides derived from Fairlie's model peptide Ac-(cyclo-1,5)-[KAAAD]-NH<sub>2</sub> bearing *N*-substituents of different nature. The nature of the substituent doesn't show a high influence in the solution 3D structure of these compounds as demonstrated by means of NMR. The latter is not the case for dodecapeptides prone to helicity, where the insertion of a lipidic *N*-substituent increases the presence of helical conformations.

\* The information contained in this chapter was eventually submitted in a different form for publication. It was split in two papers and amended by additional data. The first part already is published as: Vasco, A.V.; Brode, M.; Méndez, Y.; Valdés, O.; Rivera, D.G.; Wessjohann, L.A. *Molecules* **2020**, *25*, 811. The second part is under preparation for submission later in 2020 with the draft title: "Insights into *s-cis/s-trans* isomerism and the influence of the lactam bridge *N*-substituent in the secondary structure of Ugi-stapled peptides" Author contribution: Synthesis of stapled peptides, partial NMR analysis, Molecular Dynamics Simulations.

### 3.1. Introduction

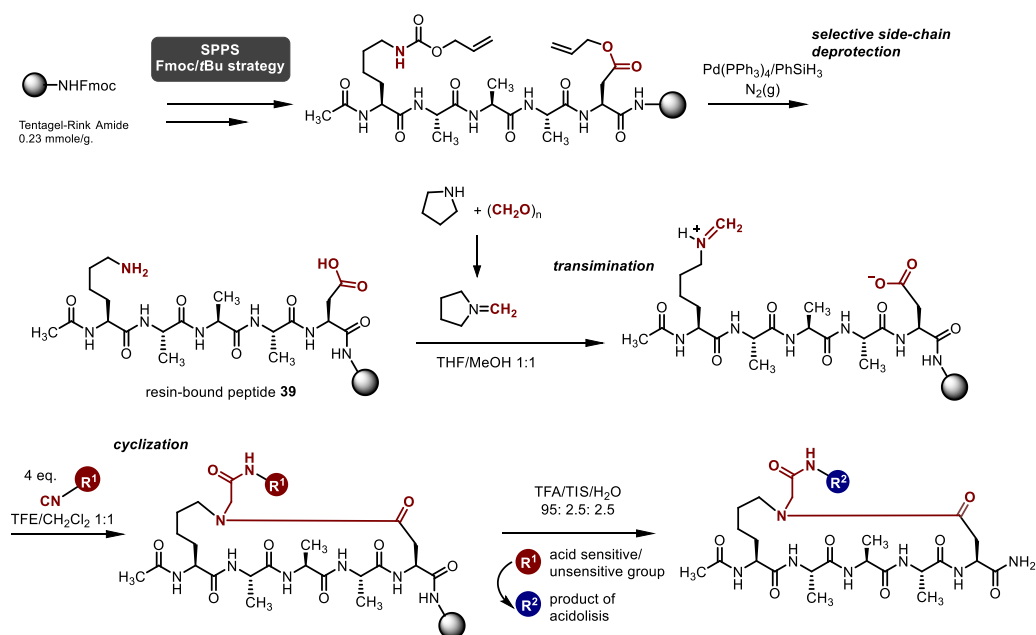
Stapled peptides in which the side-chain cross-linkages have been created by means of multicomponent reactions (MCRs) have recently emerged as an interesting type of cyclic peptides. MCRs such as the metal-catalyzed amine/alkyne/aldehyde coupling,<sup>[1]</sup> the Ugi<sup>[2-4]</sup> and the Petasis<sup>[5]</sup> reactions have proven successful in introducing conformational constraints by tethering amino acid side chains, at the same time that incorporate additional exocyclic fragments in a diversity-generating manner.<sup>[6]</sup> Several other MCRs also have been employed to macrocyclize peptides by their termini, thus enabling the insertion of unique peptidomimetic or heterocyclic moieties that provide distinctive conformational properties to the peptide skeleton.<sup>[7,8]</sup>

Ugi-stapled peptides are compounds in which amine (Lys) and carboxylic acid (Asp and Glu)-containing side chains have been tethered by the Ugi reaction, with the subsequent formation of a tertiary lactam bridge.<sup>[2,3,9]</sup> In comparison with secondary lactam bridges arising from traditional peptide coupling,<sup>[10,10,11]</sup> the presence of a tertiary amide could dramatically influence the secondary structure of this stapled peptides. Therefore, the initial goal of our study was to assess the conformational features of cyclic peptides derived from the Ugi-cyclization, in comparison with those produced by macrolactamization. As starting point, we chose the model peptide Ac-(cyclo-1,5)-[KAAAD]-NH<sub>2</sub>, which, as extensively described by Fairlie and co-workers by means of CD and NMR-based studies,<sup>[12,13]</sup> occurs in an  $\alpha$ -helical conformation in aqueous solution. Additionally, this sequence has been previously employed to compare the helical stabilization capabilities of several stapling methodologies.<sup>[13]</sup> Therefore, in order to assess the influence of the Ugi-inserted *N*-substitution, it seemed a good strategy to compare the helicity of such model peptide with that of analogous peptides derived from the Ugi cyclization.

### 3.2. Synthetic Plan

As compared with other synthetic stapling technologies such as alkene metathesis<sup>[14,15]</sup> and Cu(I) catalyzed azide-alkyne dipolar cycloaddition,<sup>[16,17]</sup> a clear disadvantage of Ugi-cyclization is the impossibility to be carried it out in the presence of other Ugi-reacting peptide side chains, i.e. carboxylic acids and amino groups. Therefore, an Ugi macrocyclization protocol based on

solid support had to be developed in which the reactive side chains are selectively deprotected and cyclized on resin while the rest of the peptide side chains - and those labile protecting groups inserted in the *N*-functionalization – are only deprotected during peptide cleavage. As depicted in scheme 3.1, we chose a classical Fmoc/*t*Bu strategy for the assembly of the peptide sequence while inserting the Ugi-reacting Lys1 and Asp5 side chains protected as Alloc carbamate and Allyl ester respectively. The latter enables the selective, concomitant deprotection in the presence of Pd(0) of both amino and carboxylic acid to be involved in the Ugi macrocyclization. This strategy affords resin-bound peptide **39**, which is further subjected to the multicomponent macrocyclization protocol.



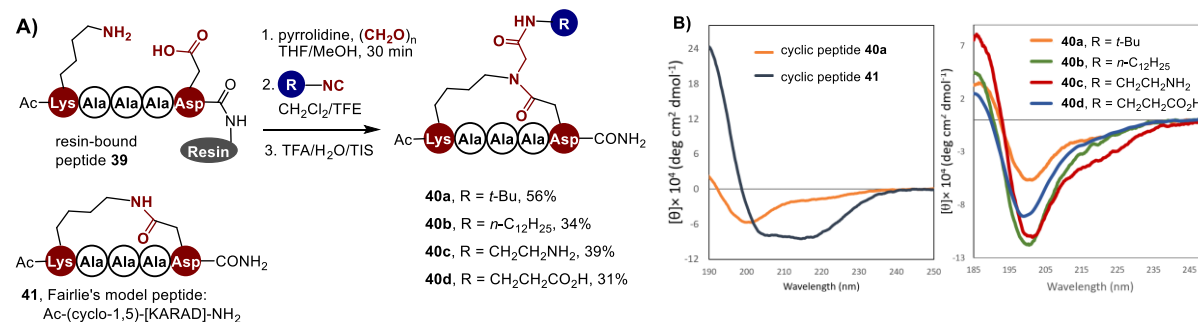
Scheme 3.1. General protocol for the on-resin Ugi macrocyclization of pentapeptides

In contrast with the solution-phase approach, the on-resin version of the Ugi macrocyclization requires two specific synthetic steps. First, the Lys1 side chain is submitted to a catalytic transimination protocol by reaction with a pre-mixed suspension of paraformaldehyde and pyrrolidine which quantitatively yields the corresponding imine. This step is crucial for the success of on-solid support Ugi-4CR since the low solubility of the aldehyde component in the reaction mixture and the slow diffusion into the resin, considering its oligomeric equilibrium nature, could lead to incomplete or none formation of the imine and the subsequent failure of the multicomponent process.<sup>[18]</sup> After imine formation, the resin is washed and the peptide is

further reacted with four equivalents of the isocyanide during 18 hours. Analysis of the conversion of the linear peptides after 18 hours by means of HPLC led us to choose the mixture TFE/DCM 1:1 as the solvent mixture to be employed in the cyclization process.

### 3.3. Synthesis of analogs of Ac-(cyclo-1,5)-[KAAAD]-NH<sub>2</sub>

Scheme 3.2A depicts the synthesis of cyclic pentapeptides **40a-d** by means of the Ugi macrocyclization strategy as previously discussed. In order to provide some structural comparison, the installation of a bulky group (*t*-Bu, **40a**), a lipidic tail (C12, **40b**), a cationic group (**40c**) and an anionic (**40d**) at the *N*-substituent was conducted. After HPLC purification, the obtained yields ranged between 30% and 56% which is comparable to those obtained in a solution phase approach.<sup>[2]</sup> As a reference, Fairlie's model peptide **41** was also synthesized.<sup>[13]</sup>



Scheme 3.2. A) Synthesis of cyclopentapeptides **40a-d**. B) CD spectra of the synthesized peptides in aqueous phosphate buffer at pH 7.2.

Analysis of the CD spectra in aqueous phosphate buffer at pH 7.2 (Scheme 3.2B) shows a clear deviation from the helical structure for peptide **40a** when compared with Fairlie's model pentapeptide **41**. A shift of the band at 205 nm towards 200 nm as well as a lower intensity of the band at 215 nm and 190 nm are indicative of a higher population of 3<sub>10</sub>-helix (in this case a single  $\beta$ -turn). This marked difference was unexpected, since Fairlie and co-workers have previously reported Ac-(*N*-methyl-cyclo-1,5)-[KLLLLD]-NH<sub>2</sub> – i.e. the analog of peptide **41** bearing an *N*-methylation at the lactam bridge and three leucine instead of alanine – to also occur in a helical conformation as inferred from its CD spectrum under similar conditions.<sup>[13]</sup> Also unexpected was the fact that, as observed in the recorded CD spectra, the synthesized pentapeptides seem to possess high structural similarity. Furthermore, none of the

compounds showed significant improvement of the helicity when CD spectra were recorded in 50% TFE. Deeper structural analysis by means of NMR revealed that all the peptides occur as a mixture of two major conformers in solution. Full assignment of the NMR resonances was assessed for compounds **40a**, **40c** and **40d** and analysis of the spectra exposed a major population of the *s-cis* conformer (i.e. that in which the two amino acid side chains are on the same side of the amide bond formed during the Ugi cyclization). Despite the differences in the nature of the *N*-substituents, the chemical shift of amide protons and  $\alpha$ -carbons, as well as the ratio of the two major conformers were very similar for all the compounds. The latter indicates that the overall three dimensional structure of the peptide is not considerably affected by the nature of the *N*-substituent. Even when full resonances assignment for cyclic peptide **40b** was impossible to achieve due to broadening of the NMR signals, it was assessed that a 7:3 *s-cis/s-trans* ratio was occurring in solution.

A NMR-based structure in water was proposed for peptide **40a** where 5:3 *s-cis/s-trans* ratio in solution was found (Figure 3.1) The temperature dependence of amide protons was evaluated, suggesting that protons from the Asp5 amide and the terminal carboxamide for both conformers, as well as the Ala2 and Ala4 amide protons for the minor conformer, could be involved in hydrogen bonding interactions. The final models obtained after simulated annealing and refinement protocols from ROE-derived distance restraints, agreed with this experimental data (Figure 3.1). Both conformers appear to occur in a  $\beta$ -turn conformation defined by the  $CO_i-HN_{i+3}$  hydrogen bond between Ala2 and Asp5 residues.

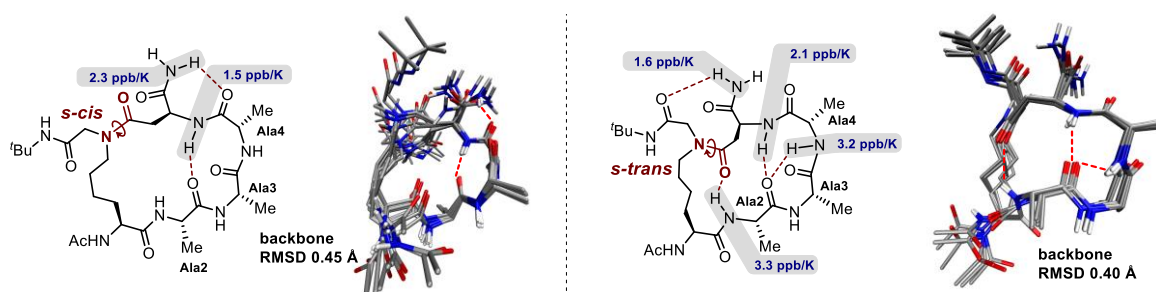
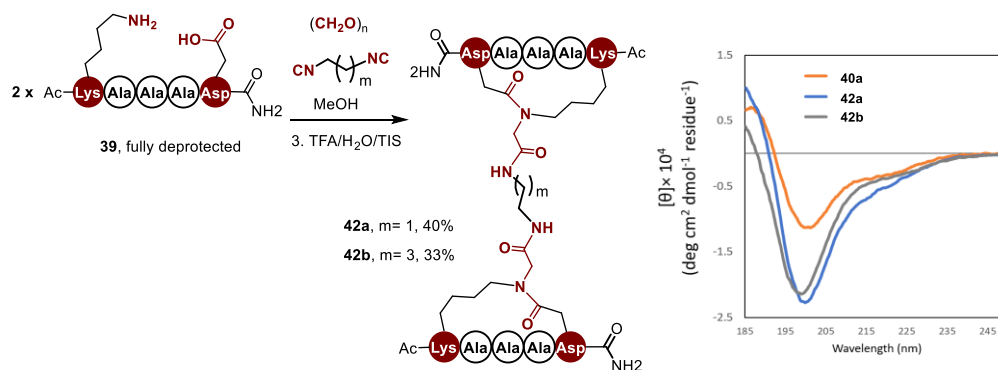


Figure 3.1. Superimposition of the 10 lowest energy NMR structures in aqueous solution for A) *s-cis* and B) *s-trans* conformers of cyclopeptide **40a**.

The observed *s-cis/s-trans* isomerism hasn't been found in previous reports, where the NMR 3D structure of Ugi-stapled peptides was determined in DMSO.<sup>[2]</sup> For both conformers of peptide **40a**, the *t*-butyl acetamide moiety introduced as *N*-substituent of the lactam bridge is

directed towards the outer region of the molecule and does not appear to be involved in any type of intramolecular interactions. This observation could explain why variations on the nature of the *N*-substituent – i.e. insertion of amino groups or carboxylic acids – does not cause significant differences in the chemical shifts of amide protons and  $\alpha$ -carbons in compounds **40c** and **40d**. Even when low temperature coefficients of the amide hydrogens in conformer *s-trans* – indicative of hydrogen bond formation – are in correspondence with those observed in helical pentapeptides reported by Fairlie and co-workers,<sup>[13,19]</sup> the strong medium-range NOEs which characterize these structures were not observed. A deeper look into the proposed 3D structure of the *s-trans* conformer shows the occurrence of a hydrogen bond involving the carbonyl group at the exocyclic amide, which could explain the rupture of the helicity in these small peptides.

Additionally, the possibility of accessing dimeric structures in one-pot reaction from linear peptides was assessed with the synthesis of compounds **42a-b**. A solution phase macrocyclodimerization protocol enabled by the use of diisocyanides, allowed the efficient synthesis of bis-stapled peptides from the fully deprotected peptide **39**. In this case, the *N*-substitution inserted in the multicomponent tethering has a peptidic nature. This example stands out the high potential of Ugi-based macrocyclization strategies as powerful tools to generate complexity in one-pot. Remarkably, 8 covalent bonds are formed in one synthetic step. As depicted in scheme 3.3, no further tendency to random coil or helical conformations as compared with peptide **40a** is observed. Furthermore, analysis of the NMR data of compound **42a** confirmed the presence of 3 major conformers – i.e. *cis-cis*, *trans-trans* and *trans-cis=cis-trans* – in a 9:2:1 ratio.



Scheme 3.3. Synthesis of bis-stapled peptides by double Ugi macrocyclization

### 3.4. Influence of the *s-cis/s-trans* isomerism on the helical content of dodecapeptides

To further study how the *N*-substituent's nature influences helicity, three more compounds – designed as amphiphilic helical peptides – were prepared (Figure 3.2A). Observed from an helical wheel projection (Figure 3.2B),<sup>[20]</sup> the sequence was designed to possess a polycationic face bearing three lysine side chains with an opposite face bearing the Ugi cyclization. In this way, we expected to evaluate whether the enthalpic contribution of the helix nucleation could influence the *s-cis/s-trans* isomerization and *vice versa*.

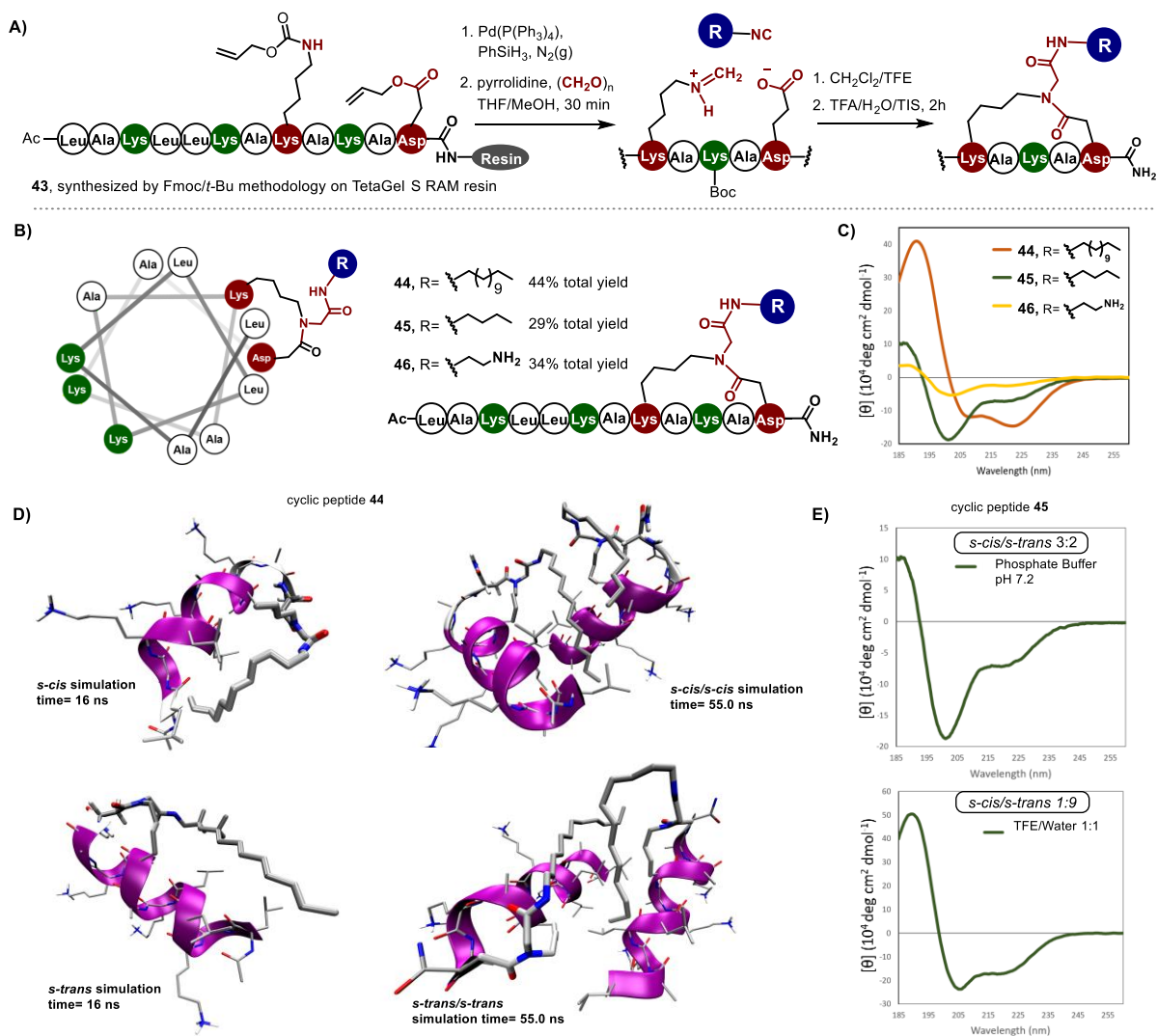


Figure 3.2. A) Synthesis, B) structure and helical wheel representation, and C) CD spectra of *N*-functionalized amphiphilic dodecapeptides. D) Representative snapshots from MD simulations including one (left) or two (right) molecules of cyclopeptides **44**. Top: assuming *s-cis* configuration. Bottom: assuming *s-trans* configuration E) CD spectra in water and water/TFE of peptide **45**.

The Ugi macrocyclization between Lys8 and Asp12 residues was used to introduce a *n*-dodecyl acetamide moiety in compound **44**. As a result, the helical conformation of the peptide skeleton is obtained (Figure 3.2C). As depicted in Figure 3.2B, this molecule was designed to possess the higher amphiphilic character, having three positively charged side chains in the opposite face of a lipidic *N*-substitution. Diminishing the alkyl chain at the *N*-substitution from twelve to four carbons as in compound **45**, results in a shift in the CD spectrum towards a  $3_{10}$ -helical structure as evidenced by the deeper minimum at 200 nm and the lower intensity at 222 nm. The replacement of the *n*-butyl chain for 2-amino propane leads to an overall decrease of the intensity of the CD signals of peptide **46**, but the location of the minima remains at the same wavelength as in **45**. These results seem to indicate that conformational changes occur when the length of the lipid moiety is decreased.  $^1\text{H-NMR}$  spectrum of compound **44** is characterized by broad signals even at low concentrations ( $\sim 1\text{mM}$ ), probably due to certain tendency to micelles formation in solution. Even when one main conformer seems to be present in solution, to determine whether this corresponds to the *s-cis* or *s-trans* was not possible.

Molecular Dynamics simulations from the ideal helical structures of both conformers of **44** suggest that the high  $\alpha$ -helicity could be favored by hydrophobic interactions of the lipidic tails with the non-polar face of the molecule, also rich in Leu side chains (Figure 3.2D, left). Such interactions seem to stabilize the helical structure in both conformers, leading to a prevalence of the  $\alpha$ -helical content during the 100 ns of explored simulation time. The enhanced helicity could, however, be also the result of intermolecular interactions, as suggested by MD simulations involving two molecules of stapled peptide **44** (Fig. 3.2D, right). During the 100 ns of simulation, a bimolecular association was observed comprising the hydrophobic side chains and the lipid tail of both molecules interacting intermolecularly, while the cationic side chains (Lys) are exposed to the solvent. Thus, despite it is difficult to determine which of the amide isomer is predominant, MD indicates that any of them may occur as  $\alpha$ -helix in solution.

On the other hand, stapled peptide **45** occurs in a 3:2 *s-cis/s-trans* ratio in water as observed by NMR. We hypothesize that the poorer helicity of compound **45** could be due either to the lower number of stabilizing hydrophobic interactions between the short aliphatic chain and the hydrophobic side chains, which is also linked to a worst amphiphilic character. However, such a conformational heterogeneity in water changes in 50%  $\text{H}_2\text{O/TFE}$ , a solvent mixture in which

a major conformer (> 85%) of **45** occur, as confirmed by NMR. As a consequence of this shift in the conformer population of **45** in 50% H<sub>2</sub>O/TFE, the helicity of this peptide is notably enhanced (Fig. 3.2E). Such evidence suggests that the differences observed in the *s-cis/s-trans* population for borderline cases can also significantly influence the overall helicity observed in CD. As seen in the shorter peptides **40a-d**, the conformational mixture derived from the rotation around the tertiary lactam bridge is detrimental for the  $\alpha$ -helical character, while any environmental or structural variation (e.g., solvent change or enhanced amphiphilicity) favoring one of the rotamers seems to lead to an overall increment in the peptide helicity.

### 3.5. Conclusions

For the first time, *s-cis/s-trans* isomerism in *N*-substituted amide-bridged peptides in water is described. Such compounds can be efficiently prepared by on-resin Ugi macrocyclization with the use of isocyanides of different nature as source of structural diversity. Solution phase macrocyclodimerization of linear peptides can be performed when diisocyanides are used, generating dimeric cyclopeptides in one-pot reaction.

We proved that Ugi-derived cyclic pentapeptides occur as a mixture of the *s-cis* and *s-trans* rotamers of the tertiary lactam bridge and that the nature of the *N*-functionality does not significantly influence the secondary structure of short cyclic peptides. An NMR/MD study of a model compound suggests that both conformers occur in  $\beta$ -turn conformations, which correspond to a single turn of a  $3_{10}$  helix rather than an  $\alpha$ -helix.

Alternatively, for longer lactam-bridged peptides, the nature and position of Ugi-derived *N*-functionalization does have a marked effect on the overall solution-phase three-dimensional structure. Thus, insertion of a lipidic tail at a lactam bridge suitably placed at a position favoring amphiphilicity (i.e., facially opposed to cationic residues) comprises a significant enhancement of the  $\alpha$ -helical content as compared with non-lipidic or charged Ugi-derived exocyclic moieties. It seems that the combination of the stabilizing hydrophobic interactions between the lipid and other aliphatic side chains and the reinforcement of the amphiphilicity – when properly placed along the sequence – contributes to the stabilization of a major conformer in an  $\alpha$ -helix secondary structure. Overall, the general trend was that the occurrence in solution

of both the *s-cis* and *s-trans* isomers is detrimental to the  $\alpha$ -helicity of both short and long Ugi-stapled peptides.

## 3.6. Experimental part

### **3.6.1 Spectroscopic characterization**

NMR spectra were recorded at 298 K either on a Varian Mercury 400 NMR spectrometer at 399.94 MHz and 100.57 MHz for  $^1\text{H}$  and  $^{13}\text{C}$  respectively, or on an Agilent (Varian) VNMRs 600 NMR spectrometer at 599.83 MHz and 150.83 MHz, respectively. Chemical shifts ( $\delta$ ) for intermediates characterized in common organics solvents are reported in ppm relative to the TMS ( $^1\text{H}$  NMR) and to the solvent signal ( $^{13}\text{C}$  NMR). For water-recorded NMR spectra, the chemical shifts are reported relative to TSP-d4 and  $^{13}\text{C}$  chemical shifts were inferred from  $^1\text{H}$ -1D spectra according to IUPAC recommendations.<sup>[21]</sup> IR spectra were obtained on a Thermo Nicolet 5700 FT-IR spectrometer. Circular dichroism spectra were recorded on a Jasco J-815 spectropolarimeter equipped with a temperature controller at 20°C. A total of 16 accumulations from 260 to 185 nm at 50 nm/sec using 1 mm cuvettes were done.

### **3.6.2 Chromatographic methods**

Analytical and preparative RP-HPLC of crude peptides was carried out with an Agilent 1260 Infinity series system equipped with two preparative pumps and one analytical quaternary pump, coupled to an MWD detector and an Agilent 6120 Quadrupole LC/MS detector using API-ES as ion source. Reverse phase YMC-ODS-A column (150 × 4.6 mm I.D., 5  $\mu\text{m}$  particle size) and YMC-ODS-A (150 × 20 mm I.D., 5  $\mu\text{m}$  particle size) columns were used for analytical and preparative scale respectively. Analyses of pure peptides were performed on a Waters Acquity UHPLC BEH C18 column (1.7  $\mu\text{m}$ , 2.1 mm × 50 mm) using a Waters Acquity UHPLC system coupled to a LCQ Deca XP MAX (Thermo Scientific) mass spectrometer. The ESI IT mass spectra were recorded with a 4.0 kV spray voltage; sheath gas nitrogen; capillary temperature, 275 °C; capillary voltage, 30 V. The column was maintained at 40 °C. Unless otherwise stated, a linear gradient from 5% to 90% of solvent B (0.1% (v/v) formic acid (FA) in acetonitrile) in solvent A (0.1% (v/v) formic acid (FA) in water) over 10 min at a flow rate of

0.15 mL min<sup>-1</sup> was used. The mass spectra were evaluated by the Thermo software Xcalibur 2.0.7.

### **3.6.3 High resolution mass spectrometry characterization**

High resolution ESI mass spectra were obtained from a Bruker Apex III Fourier transform ion cyclotron resonance (FT-ICR) mass spectrometer equipped with an Infinity<sup>TM</sup> cell, a 7.0 Tesla superconducting magnet, an RF-only hexapole ion guide and an external electrospray ion source (Agilent, off axis spray).

### **3.6.4 General methods for Peptide Synthesis**

**Solid Phase Peptide Synthesis:** Coupling reactions were carried out automatically on an INTAVIS ResPepSL automated peptide synthesizer by a stepwise Fmoc/tBu strategy using a 5-fold excess of amino acid and PyBop and a 10-fold excess of NMM at R.T. for 15 min. A 50  $\mu$ mol scale on TG-S-RAM (Iris Biotech) resin (217 mg, 0.23 mmol/mg) was utilized. **Swelling:** The resin is swelled for 20 min in dichloromethane before bring it into the synthesizer. After the coupling of all amino acids, the resin is manually washed with DCM (3 $\times$ 1 min) and DMF (2 $\times$ 1 min) and reacted with 10 eq. of Ac<sub>2</sub>O/DIEA in 2 mL of DMF for 30 min. The completeness of the reaction is confirmed through the Kaiser test and the resin is manually washed with DCM (3 $\times$ 1 min). **Alloc/Allyl Removal:** The resin is washed with dry dichloromethane (2 $\times$ 2 min) under a stream of nitrogen. A solution of phenylsilane (20 eq.) in dry dichloromethane and tetrakis(triphenylphosphine) palladium(0) (0.2 eq.) are added to the resin under a continuous stream of nitrogen. The mixture is stirred in the dark for 10 min, and the procedure is repeated once more. Finally, the resin is washed with 0.5% of sodium diethyldithiocarbamate trihydrate in DMF (5 $\times$ 2 min) and DCM (2 $\times$ 2 min). **Aminocatalysis-mediated Ugi-4C cyclization:** The side chain deprotected resin-bound peptide is washed with THF (4 $\times$ 1 min) and treated with a suspension of paraformaldehyde (4 eq.) and pyrrolidine (4 eq.) in THF/MeOH (1:1) for 30 min. The excess of reagents is removed by washing the beads with THF (4 $\times$ 1min). The resin is then washed with DCM (4 $\times$ 1min) and DCM/TFE 1:1 solution (2 $\times$ 1min). A solution of the isocyanide (4 eq.) in 2 mL DCM/TFE 1:1 (or THF:MeOH 1:1 for relative polar isocyanides) is added to the resin and the suspension is stirred overnight (18hrs). Completion is evaluated by ESI-MS or RP-HPLC monitoring after mini-cleavages.

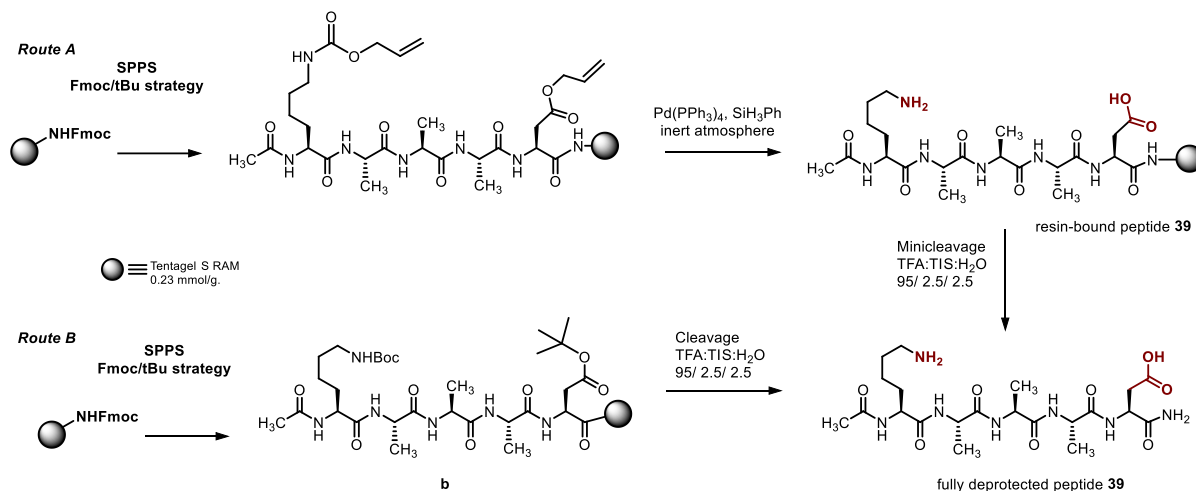
Afterwards, the resin is washed with DCM (3×1 min) and DMF (2×1 min). Finally, the resin is washed with DCM (5×2 min) and Et<sub>2</sub>O (3×1 min). **Minicleavage:** A small amount of the dry resin (less than 10 mg) is transferred to an Eppendorf vial and 400 µL of the cleavage cocktail (TFA/TIS/H<sub>2</sub>O 95:2.5:2.5) is added. The suspension is gently agitated during 45 min and afterwards the cleavage cocktail is concentrated under N<sub>2</sub> flow and the remaining oil is precipitated by addition of 500 µL diethyl ether. The suspension is centrifuged for 5 min after what the solid and liquid phases are separate by settling. The precipitated peptide is dissolved in a mixture AcN/H<sub>2</sub>O in order to be analyzed by HPLC. **Cleavage:** The resin is treated with the cocktail TFA/TIS/H<sub>2</sub>O (95:2.5:2.5). The peptide is precipitated from frozen diethyl ether, then taken up in 1:2 AcN/H<sub>2</sub>O and lyophilized. **Solution Phase Ugi-4C cyclization:** A solution of paraformaldehyde (0.13 mmol, 1.3 eq.), Et<sub>3</sub>N (0.1 mmol, 1 eq.) and the peptide (0.1 mmol, 1 eq.) in MeOH (5 mL) was stirred for 1 h at room temperature and next diluted to 50 mL of MeOH. The isocyanide (0.2 mmol, 2 eq.) was added and the reaction mixture was stirred for 96 h and then concentrated under reduced pressure. The crude peptide was dissolved in the minimum amount of TFA, precipitated from frozen diethyl ether, then taken up in 1:1 AcN/H<sub>2</sub>O and lyophilized.

### **3.6.5 General protocol for the synthesis of isocyanides from amines**

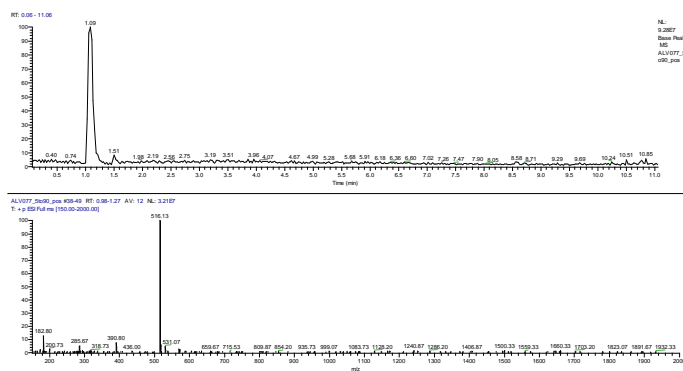
A solution of the amine (25 mmol) in ethyl formate (20 mL) is heated at reflux temperature for 12 h to afford the formamide. The resulting solution is concentrated under vacuum and used without further purification. The formamide in 40 mL of dry THF, mixed with Et<sub>3</sub>N (4 eq.) and under N<sub>2</sub> atmosphere is cooled to 0 °C and a solution of POCl<sub>3</sub> (1.3 eq.) in 15 mL of THF is added dropwise during 30 minutes. The resulting mixture is stirred at 0 °C for 1 h, then allowed to reach room temperature and stirred for additional 2 h. The reaction mixture is quenched with 50 mL of 10% aqueous NaHCO<sub>3</sub> and extracted with EtOAc (2×50 mL). The combined organic phases are washed with brine (20 mL), dried over anh. Na<sub>2</sub>SO<sub>4</sub>, and concentrated under reduced pressure to dryness. The crude product is purified by column chromatography. The details of the synthesis of isocyanides are enclosed in the annexes at the end of the manuscript.

### 3.6.6 Synthesis of peptides

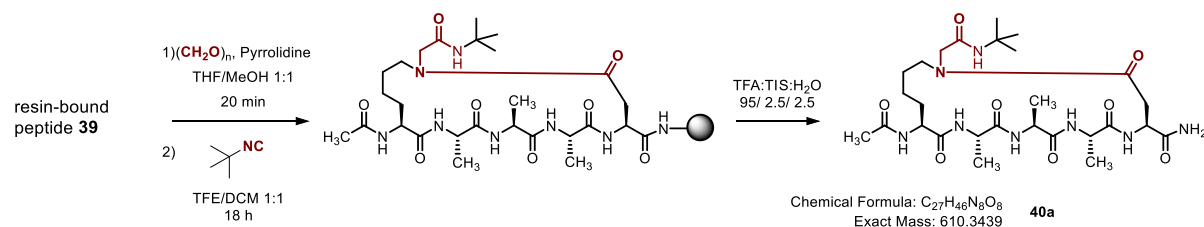
#### Ac-Lys-Ala-Ala-Ala-Asp-NH<sub>2</sub>(**39**)



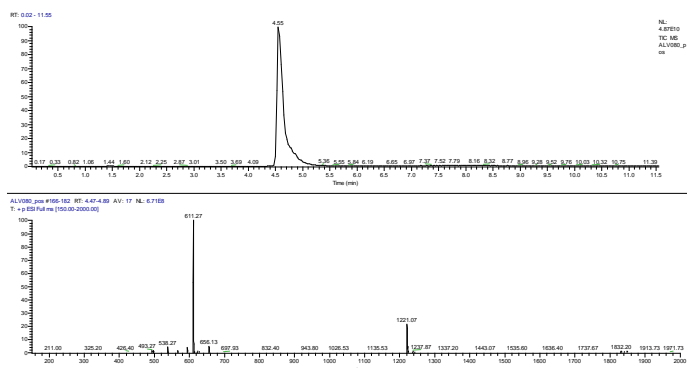
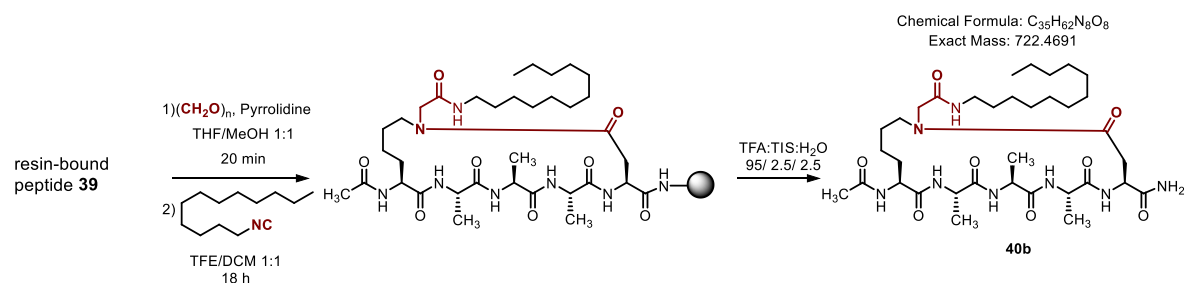
Resin-bound peptide **39** was synthesized in 50  $\mu$ mol scale on Tentagel S RAM resin (217 mg, 0.23 mmol/mg) (*Route A*) according to the protocols described in section 3.6.4. The purity of the resin-bound peptide was evaluated through minicleavages according to the protocol described in 3.6.4 ( $R_t$  1.09 min). In order to synthesize the fully deprotected peptide **39** to be cyclized on solution



phase, a 100  $\mu$ mol scale on Tentagel S RAM (435 mg) resin was employed to assemble the resin bound peptide **b** (Ac-Lys(Boc)-Ala-Ala-Ala-(Asp(*t*Bu)-resin) (*Route B*) which after cleavage with TFA/H<sub>2</sub>O/TIS 95:2.5:2.5 for 2h according to the protocol described in 3.6.4 afforded the fully deprotected peptide **39** (92% cleavage yield), which was characterized by analytical UHPLC ( $R_t$  1.07 min, > 95% purity (crude)). ESI-HRMS, calcd for C<sub>21</sub>H<sub>38</sub>N<sub>7</sub>O<sub>8</sub>: 516.2782 [M+H]<sup>+</sup>; Found: *m/z* 516.2774 [M + H]<sup>+</sup>. The peptide was employed in the solution phase macrocyclization without further purification.

Ac-(*N*-(2-(*tert*-butylamino)-2-oxoethyl)-(cyclo-1,5))-[KAAAD]-NH<sub>2</sub> (**40a**)

Cyclic peptide **40a** was produced by on-resin cyclization in a 50 μmol scale from resin-bound peptide **39** according to the aminocatalysis-mediated Ugi macrocyclization protocol described in 3.6.4, in the presence of *tert*-butylisocyanide. Cleavage with TFA/H<sub>2</sub>O/TIS 95:2.5:2.5 for 2 h afforded peptide **40a** (88% cleavage yield), which was purified by semi-preparative RP-HPLC (17.1 mg, 56% isolated yield); *R*<sub>t</sub> 4.55 min, > 95% purity. ESI-HRMS, calcd. for C<sub>27</sub>H<sub>47</sub>N<sub>8</sub>O<sub>8</sub>: 611.3517 [M + H]<sup>+</sup> Found: *m/z* 611.3502 [M + H]<sup>+</sup>.

Ac-(*N*-(2-(*n*-dodecylamino)-2-oxoethyl)-(cyclo-1,5))-[KAAAD]-NH<sub>2</sub> (**40b**)

Cyclic peptide **40b** was produced by on-resin cyclization in a 50 μmol scale from resin-bound peptide **39** according to the aminocatalysis-mediated Ugi macrocyclization protocol described in 3.6.4, in the presence of *n*-dodecylisocyanide. Cleavage with TFA/H<sub>2</sub>O/TIS 95:2.5:2.5 for 2 h afforded peptide **40b** (78% cleavage yield), which was purified by semi-preparative RP-

HPLC (12.4 mg, 34% isolated yield);  $R_t$  9.03 min, > 95% purity. ESI-HRMS, calcd. for  $C_{35}H_{63}N_8O_8$ : 723.4769 [M + H]<sup>+</sup> Found:  $m/z$  723.4744 [M + H]<sup>+</sup>.

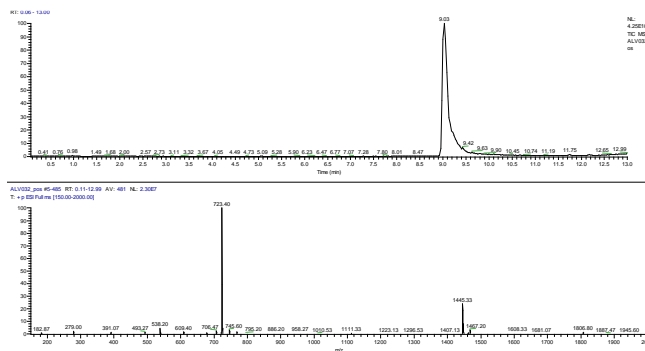
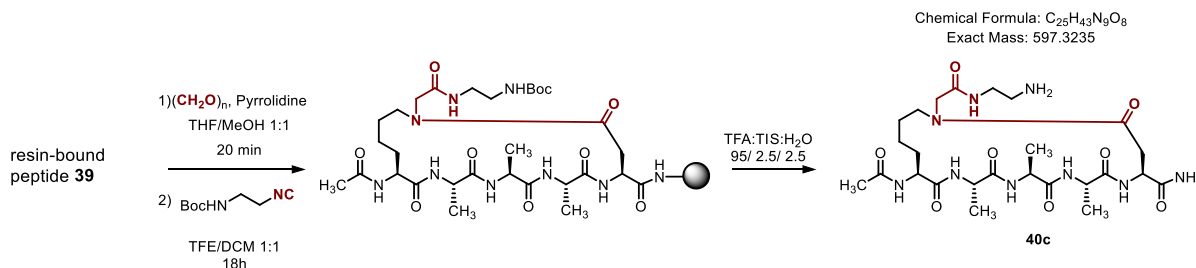
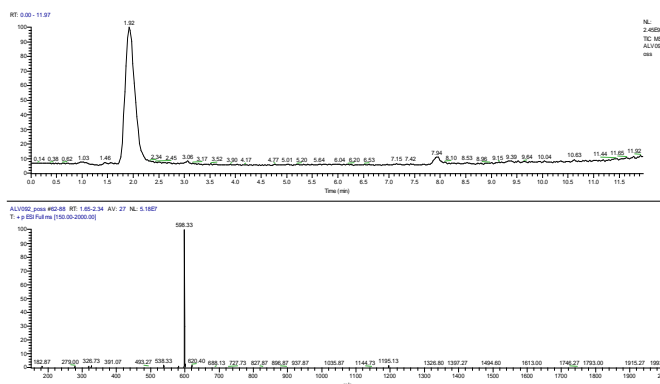


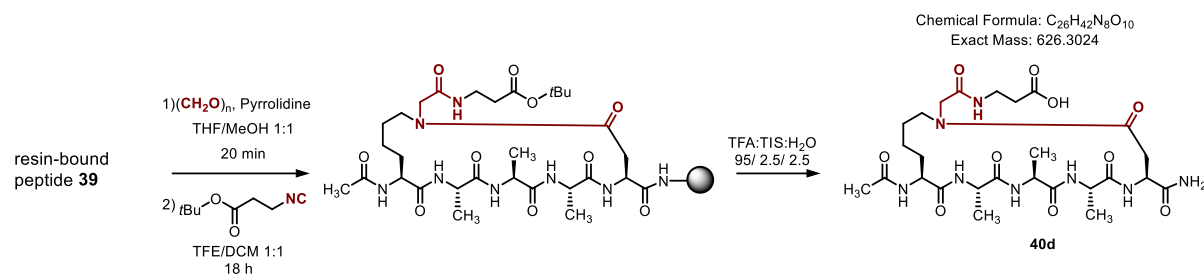
Figure 3.5. UHPLC-MS chromatogram of pure peptide **40b**

### Ac-(*N*-((2-(aminoethyl)amino)-2-oxoethyl)-(cyclo-1,5))-[KAAAD]-NH<sub>2</sub> (**40c**)

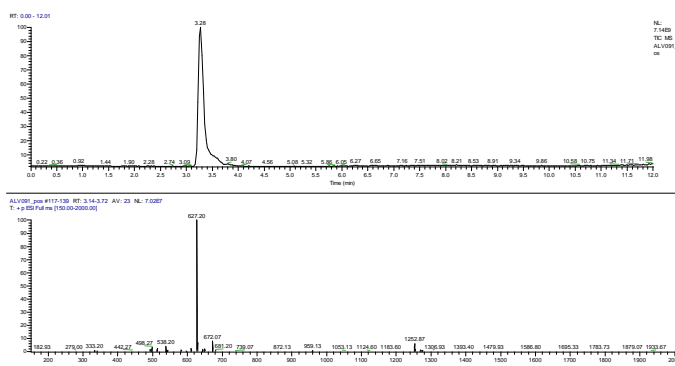
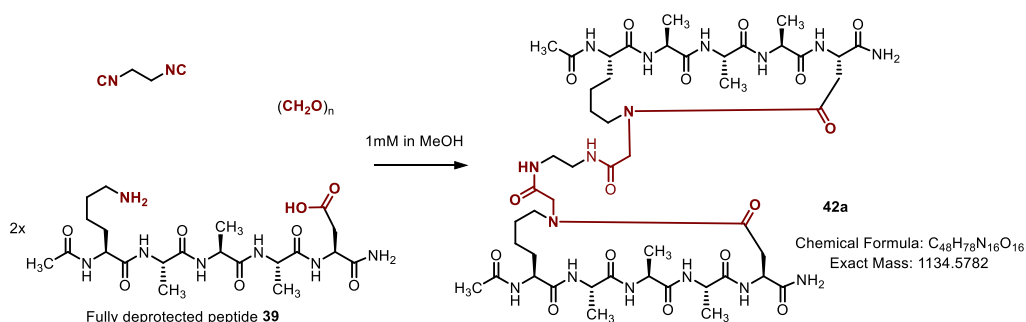


Cyclic peptide **40c** was produced by on-resin cyclization in a 50  $\mu\text{mol}$  scale from resin-bound peptide **39** according to the aminocatalysis-mediated Ugi macrocyclization protocol described in 3.6.4, in the presence of (*N*-Boc)-aminoethyl isocyanide. Cleavage with TFA/H<sub>2</sub>O/TIS 95:2.5:2.5 for 2 h



Ac-*N*-((2-(carboxyethyl)amino)-2-oxoethyl)-(cyclo-1,5))-[KAAAD]-NH<sub>2</sub> (**40d**)

Cyclic peptide **40d** was produced by on-resin cyclization in a 50 μmol scale from resin-bound peptide **39** according to the aminocatalysis-mediated Ugi macrocyclization protocol described in 3.6.4, in the presence of *tert*-butyl-3-isocyanopropionate. Cleavage with TFA/H<sub>2</sub>O/TIS 95:2.5:2.5 for 2 h afforded peptide **40d** (83% cleavage yield), which was purified by semi-preparative RP-HPLC (9.8 mg, 31% isolated yield); *R*<sub>t</sub> 3.28 min, > 93% purity. ESI-HRMS, calcd. for C<sub>26</sub>H<sub>43</sub>N<sub>8</sub>O<sub>10</sub>: 626.3024 [M + H]<sup>+</sup> Found: *m/z* 627.3091 [M + H]<sup>+</sup>.

Figure 3.7. UHPLC-MS chromatogram of pure peptide **40d**bis-[Ac-*N*-((2-(aminomethyl)-2-oxoethyl)-(cyclo-1,5))-[KAAAD]-NH<sub>2</sub>] (**42a**)

Cyclic peptide **42a** was produced by solution phase cyclization from fully deprotected peptide **39** according to the solution-phase Ugi macrocyclization protocol described in 3.6.4, in the presence of 1,2-diisocynoethane. The crude peptide was purified by semi-preparative RP-HPLC (38.1 mg, 33% isolated yield);  $R_t$  3.75 min, > 95% purity. ESI-HRMS, calcd. for  $C_{48}H_{79}N_{16}O_{16}$ : 1135.5860 [M + H]<sup>+</sup> Found:  $m/z$  1135.5856 [M + H]<sup>+</sup>.

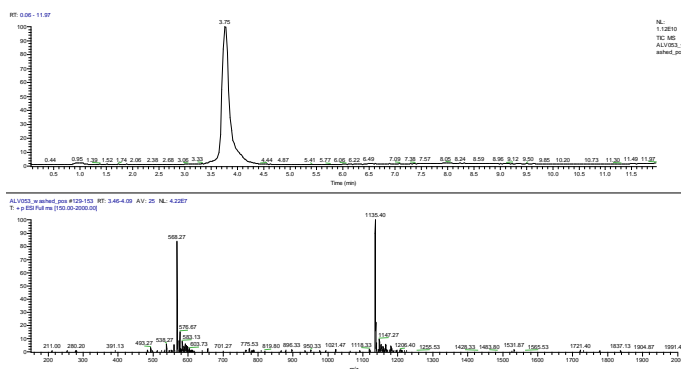
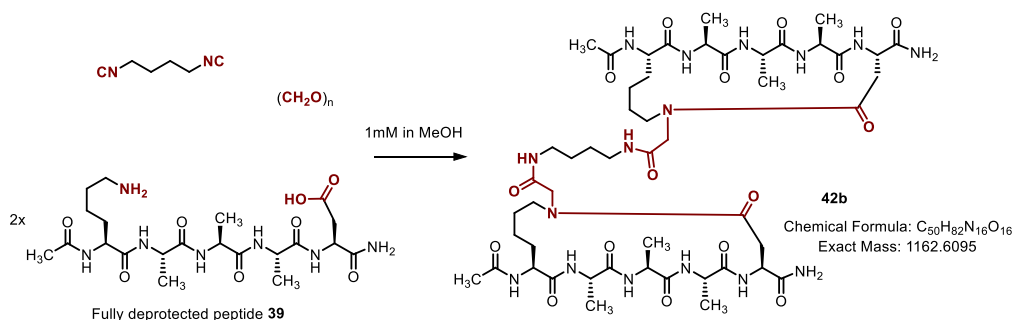


Figure 3.8. UHPLC-MS chromatogram of pure peptide **42a**

### bis-[Ac-(*N*-(2-(aminoethyl)-2-oxoethyl)-(cyclo-1,5))-[KAAAD]-NH<sub>2</sub>)] (**42b**)



Cyclic peptide **42b** was produced by solution phase cyclization from fully deprotected peptide **39** according to the solution-phase macrocyclization protocol described in 3.6.4, in the presence of 1,4-diisocyanobutane. The crude peptide was purified by semi-preparative RP-HPLC (7.6 mg, 6% isolated yield);  $R_t$  3.89 min, > 89% purity. ESI-HRMS, calcd. for  $C_{50}H_{83}N_{16}O_{16}$ : 1163.6173 [M + H]<sup>+</sup> Found:  $m/z$  1163.6160 [M + H]<sup>+</sup>.

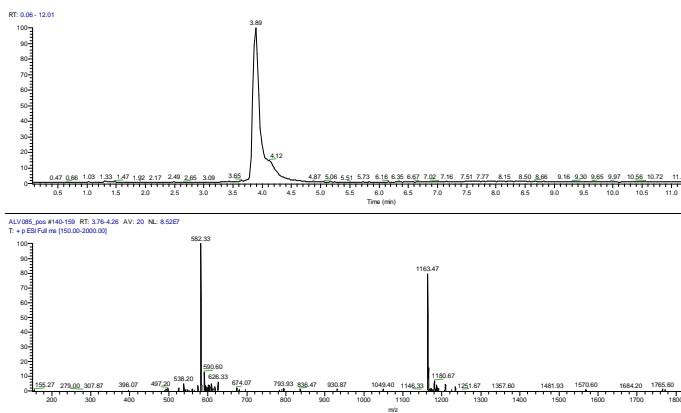
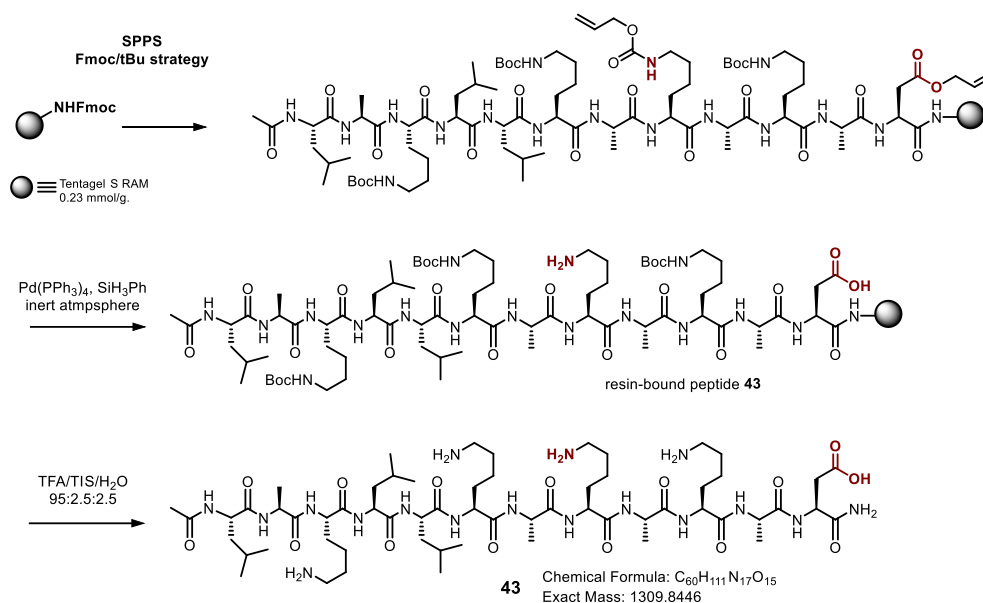


Figure 3.9. UHPLC-MS chromatogram of pure peptide **42b**

## Linear Peptide 43



Resin-bound peptide **43** was synthesized in 50  $\mu\text{mol}$  scale on TentaGel S RAM resin (217 mg, 0.23 mmol/mg) according to the protocols described in section 3.6.4. The purity of the resin-bound peptide was evaluated through minicleavages according to the protocol described in 3.6.4. Analytical UHPLC:  $R_t$  4.54 min, > 87% purity (crude); ESI-HRMS, calcd for C<sub>60</sub>H<sub>112</sub>N<sub>17</sub>O<sub>15</sub>/2: 655.9301 [M+2H]<sup>2+</sup>; Found:  $m/z$  655.9333 [M + 2H]<sup>2+</sup>.

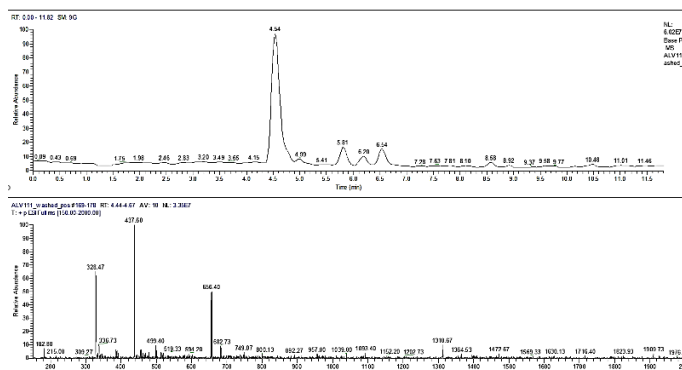
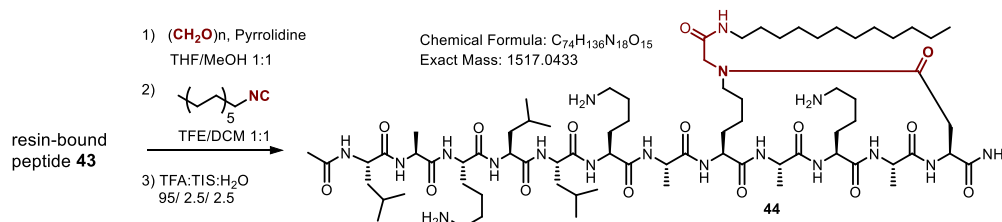


Figure 3.10. UHPLC-MS chromatogram of crude peptide **43**

Ac-(N-(2-(*n*-dodecylamino)-2-oxoethyl)-(cyclo-8,12))-[LAKLLKAKAKAD]-NH<sub>2</sub> (**44**)

Cyclic peptide **44** was produced by on-resin cyclization in a 50  $\mu$ mol scale from resin-bound peptide **43** according to the aminocatalysis-mediated Ugi macrocyclization protocol described in 3.6.4.4, in the presence of *n*-dodecylisocyanide. Cleavage with TFA/H<sub>2</sub>O/TIS 95:2.5:2.5 for 2 h afforded peptide **44**

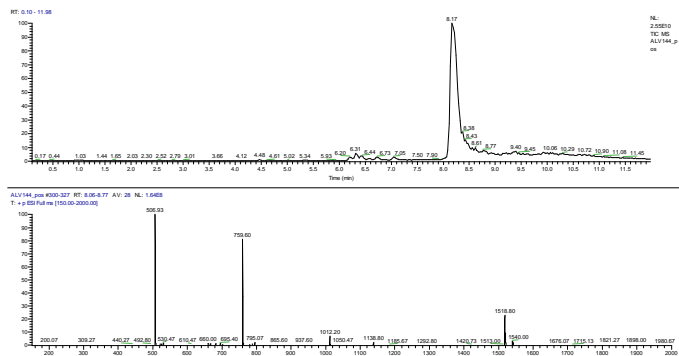
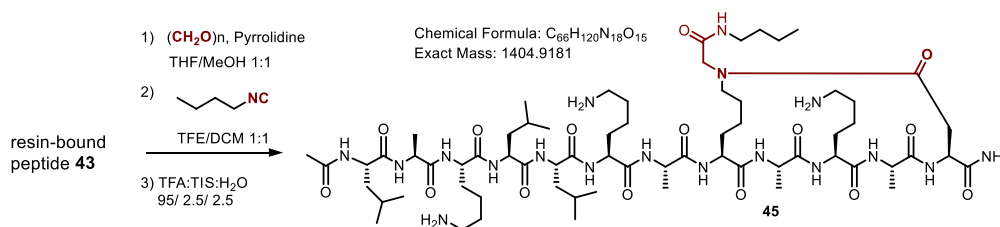


Figure 3.11. UHPLC-MS chromatogram of pure peptide **44**

(87% cleavage yield), which was purified by semi-preparative RP-HPLC (32.3 mg, 43% isolated yield); *R*<sub>t</sub> 8.17 min, > 91% purity. ESI-HRMS, calcd. for C<sub>74</sub>H<sub>138</sub>N<sub>18</sub>O<sub>15</sub>: 759.5295 [M + 2H]<sup>2+</sup> Found: *m/z* 759.5273 [M + 2H]<sup>2+</sup>.

### Ac-(*N*-(2-(*n*-butylamino)-2-oxoethyl)-(cyclo-8,12))-[LAKLLKAKAKAD]-NH<sub>2</sub> (**45**)



Cyclic peptide **45** was produced by on-resin cyclization in a 50  $\mu$ mol scale from resin-bound peptide **43** according to the aminocatalysis-mediated Ugi macrocyclization protocol described in 3.6.4.4, in the presence of *n*-butylisocyanide. Cleavage with TFA/H<sub>2</sub>O/TIS 95:2.5:2.5 for 2 h afforded peptide **45**

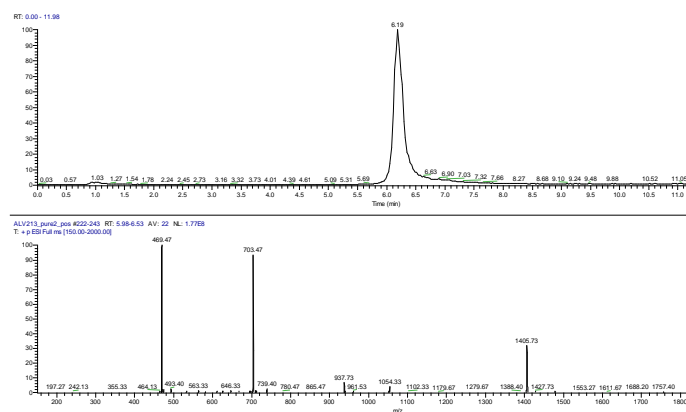
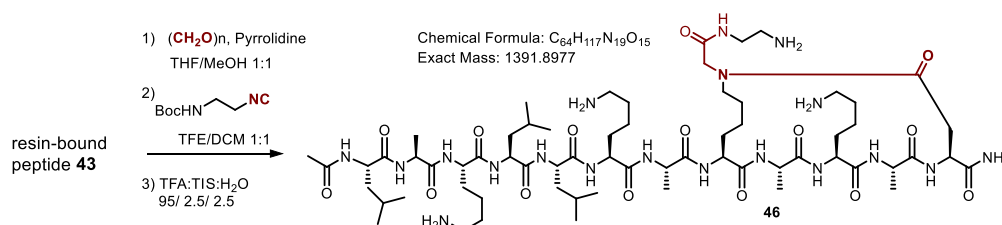


Figure 3.12. UHPLC-MS chromatogram of pure peptide **45**

(83% cleavage yield), which was purified by semi-preparative RP-HPLC (27.9 mg, 40% isolated yield); *R*<sub>t</sub> 6.19 min, > 94%

purity. ESI-HRMS, calcd. for  $C_{66}H_{122}N_{18}O_{15}$ : 703.4669  $[M + 2H]^{2+}$  Found:  $m/z$  703.4676  $[M + 2H]^{2+}$ .

### Ac-(N-((2-(aminoethyl)amino)-2-oxoethyl)-(cyclo-1,5))-[LAKLLKAKAKAD]-NH<sub>2</sub> (46)



Cyclic peptide **46** was produced by on-resin cyclization in a 50  $\mu$ mol scale from resin-bound peptide **43** according to the aminocatalysis-mediated Ugi macrocyclization protocol described in 3.6.4.4, in the presence of *n*-butylisocyanide. Cleavage with TFA/H<sub>2</sub>O/TIS 95:2.5:2.5 for 2 h afforded peptide **45** (82% cleavage yield), which was

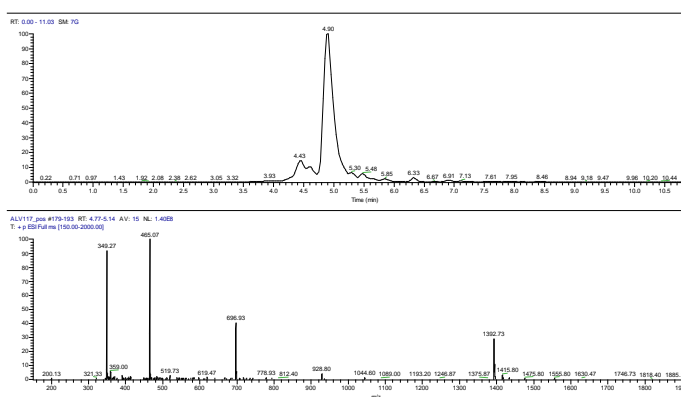


Figure 3.13. UHPLC-MS chromatogram of pure peptide **46**

purified by semi-preparative RP-HPLC (27.9 mg, 40% isolated yield);  $R_t$  4.90 min, > 86% purity. ESI-HRMS, calcd. for  $C_{64}H_{119}N_{19}O_{15}/2$ : 696.9567  $[M + 2H]^{2+}$  Found:  $m/z$  696.9561  $[M + 2H]^{2+}$ .

### 3.6.7 NMR structure determination

Cross-peaks in ROESY spectra were assigned and integrated in NMRFAM-SPARKY.<sup>[22]</sup> Distance constraints from ROE intensities were generated using pseudo-atoms corrections where needed, and placed into three groups: strong (2.8 Å upper limit), medium (3.5 Å upper limit) and weak (5.0 Å upper limit). The lower limit for distance restraints was always maintained at 1.8 Å. Backbone dihedral angle restraints were inferred from  $^3J_{NHCHa}$  coupling constants in 1D spectrum at 300 K,  $\varphi$  was restrained to  $-120 \pm 30^\circ$  for  $^3J_{NHCHa} \geq 8$  Hz as reported by Fairlie and co-workers.<sup>[19]</sup> Peptide backbone bond  $\omega$  angles were all set *trans*.

Structure calculations were carried out using *Xplor-NIH 2.43* package.<sup>[23]</sup> The calculations were performed using the standard force field parameter set and topology file within *Xplor-NIH* with in-house modifications to allow peptide cyclization and amide *N*-substitution. Structures were visualized and analyzed using *VMD-Xplor*. The *s-cis* or *s-trans* conformation around the tertiary amide was unequivocally inferred from the NMR data and fixed during the MD simulations.

NMR structure determination was performed through simulated annealing regularization and refinement in torsion angle space, using experimental data as inter-proton distances and dihedral angles restraints. For simulated annealing regularization 200 starting structures were randomly generated. A 100 ps molecular dynamics simulation at 3500 K was performed with a time-step of 3 fs. The system was cooled from 3500 to 25 K, with a temperature step of 12.5 K. At each temperature step, 0.2 ps of molecular dynamics simulation was performed. A 500 steps torsion angle minimization was performed and finally the system was optimized by means of 500 steps conjugated gradient Powell Cartesian minimization.

The refinement protocol consisted in a slow cooling simulated annealing from the regularized structures. A 10 ps molecular dynamics simulation at 1500 K was achieved with a time-step of 3 fs. The system was cooled with a temperature step of 12.5 K and a simulation time of 0.2 ps at each temperature. A 500 torsion angle minimization was performed afterwards a second 500 steps minimization was achieved in Cartesian coordinates. A finally 1000 steps Powell minimization with an energy function non-dependent of experimental restraints was executed.

### **Molecular Dynamics Simulations**

MD simulations were conducted within YASARA ([www.yasara.org](http://www.yasara.org)). For dodecapeptides **44** and **45**, a structure was created within MOE ([www.chemcomp.com](http://www.chemcomp.com)) and further imported into YASARA. For the modeling of compound **44** including two cyclolipopeptides, two molecules in an ideal helical conformation were built in MOE and a protein-protein docking using Rigid Body refinement was assessed in order to determine the best intermolecular fitting. In all cases, the structures imported into YASARA were firstly optimized and the obtained coordinates were employed as starting point for a 100 ns MD simulation using AMBER 12 force field. The starting model was placed in a water box with a physiological NaCl concentration of 0.9%. Periodic boundary conditions with pressure control at 298 K were

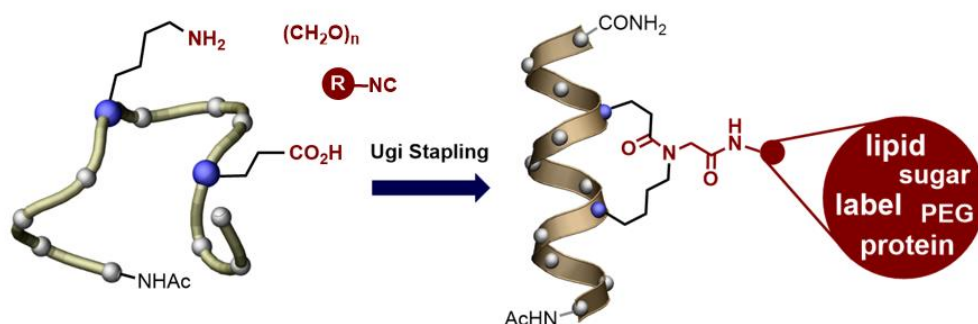
utilized. Force field parametrizations for the novel residues based on semi-empirical calculations were automatically calculated. The final trajectory was analyzed within YASARA, as well as VMD.<sup>[24]</sup>

### 3.7. References

- [1] J. Zhang, M. Mulumba, H. Ong, W. D. Lubell, *Angew. Chem., Int. Ed.* **2017**, *56*, 6284–6288.
- [2] A. V. Vasco, C. S. Pérez, F. E. Morales, H. E. Garay, D. Vasilev, J. A. Gavín, L. A. Wessjohann, D. G. Rivera, *J. Org. Chem.* **2015**, *80*, 6697–6707.
- [3] A. V. Vasco, Y. Méndez, A. Porzel, J. Balbach, L. A. Wessjohann, D. G. Rivera, *Bioconjug. Chem.* **2019**, *30*, 253–259.
- [4] M. C. Morejón, A. Laub, B. Westermann, D. G. Rivera, L. A. Wessjohann, *Org. Lett.* **2016**, *18*, 4096–4099.
- [5] M. G. Ricardo, D. Llanes, L. A. Wessjohann, D. G. Rivera, *Angew. Chem., Int. Ed.* **2019**, *58*, 2700–2704.
- [6] L. Reguera, Y. Méndez, A. R. Humpierre, O. Valdés, D. G. Rivera, *Acc. Chem. Res.* **2018**, *51*, 1475.
- [7] J. R. Frost, C. C. G. Scully, A. K. Yudin, *Nat. Chem.* **2016**, *8*, 1105–1111.
- [8] B. K. W. Chung, C. J. White, A. K. Yudin, *Nat. Protoc.* **2017**, *12*, 1277–1287.
- [9] M. G. Ricardo, F. E. Morales, H. Garay, O. Reyes, D. Vasilev, L. A. Wessjohann, D. G. Rivera, *Org. Biomol. Chem.* **2015**, *13*, 438–446.
- [10] M. E. Houston, C. L. Gannon, C. M. Kay, R. S. Hodges, *J. Pept. Sci.* **1995**, *1*, 274–282.
- [11] N. E. Shepherd, H. N. Hoang, V. S. Desai, E. Letouze, P. R. Young, D. P. Fairlie, *J. Am. Chem. Soc.* **2006**, *128*, 13284–13289.
- [12] N. E. Shepherd, H. N. Hoang, G. Abbenante, D. P. Fairlie, *J. Am. Chem. Soc.* **2005**, *127*, 2974–2983.
- [13] A. D. De Araujo, H. N. Hoang, W. M. Kok, F. Diness, P. Gupta, T. A. Hill, R. W. Driver, D. A. Price, S. Liras, D. P. Fairlie, *Angew. Chem., Int. Ed.* **2014**, *53*, 6965–6969.
- [14] Y. W. Kim, T. N. Grossmann, G. L. Verdine, *Nat. Protoc.* **2011**, *6*, 761–771.
- [15] P. M. Cromm, J. Spiegel, T. N. Grossmann, *ACS Chem. Biol.* **2015**, *10*, 1362–1375.
- [16] K. Holland-Nell, M. Meldal, *Angew. Chem., Int. Ed.* **2011**, *50*, 5204–5206.
- [17] K. Sharma, D. L. Kunciw, W. Xu, M. M. Wiedmann, Y. Wu, H. F. Sore, W. R. J. D. Galloway, Y. H. Lau, L. S. Itzhaki, D. R. Spring, in *Cycl. Pept. From Bioorganic Synth. to Appl.*, The Royal Society Of Chemistry, **2017**, pp. 164–187.
- [18] F. E. Morales, H. E. Garay, D. F. Muñoz, Y. E. Augusto, A. J. Otero-González, O. Reyes Acosta, D. G. Rivera, *Org. Lett.* **2015**, *17*, 2728–2731.
- [19] N. E. Shepherd, H. N. Hoang, G. Abbenante, D. P. Fairlie, *J. Am. Chem. Soc.* **2005**, *127*, 2974–2983.
- [20] M. Schiffer, A. B. Edmundson, *Biophys. J.* **1967**, *7*, 121–135.
- [21] R. K. Harris, E. D. Becker, S. M. Cabral De Menezes, R. Goodfellow, P. Granger, *Concepts Magn. Reson. Part A Bridg. Educ. Res.* **2002**, *14*, 326–346.
- [22] W. Lee, M. Tonelli, J. L. Markley, *Bioinformatics* **2015**, *31*, 1325–1327.
- [23] C. D. Schwieters, J. J. Kuszewski, N. Tjandra, G. M. Clore, *J. Magn. Reson.* **2003**, *160*, 65–73.
- [24] W. Humphrey, A. Dalke, K. Schulten, *J. Mol. Graph.* **1996**, *14*, 33–38.

## Chapter 4.

# Multicomponent Peptide Stapling to Lactam-Bridged Exocyclic *N*-Functionalized Helical Peptides



**ABSTRACT:** The present chapter describes a multicomponent approach to peptide stapling which enables the simultaneous stabilization of helical secondary structures and the exocyclic *N*-functionalization of the side chain-tethering lactam bridge. This is accomplished by means of a solid-phase methodology comprising the on-resin Ugi reaction-based macrocyclization of peptide side chains bearing amino and carboxylic acid groups. The exocyclic diversity elements arising from the isocyanide component used in the Ugi multicomponent stapling protocol allows the incorporation of relevant fragments such as lipids, sugars, polyethylene glycol, fluorescent labels, and reactive handles. We prove the utility of such exocyclic reactive groups, for example, in the bioconjugation of a maleimide-armed lactam-bridged peptide to a carrier protein. The on-resin multicomponent stapling proved efficient for the installation of not only one, but also two consecutive lactam bridges having either identical or dissimilar *N*-functionalities. The easy access to helical peptides with a diverse set of exocyclic functionalities shows prospect for applications in peptide drug discovery and chemical biology.

\* The content within this chapter has been published as: A. V Vasco, Y. Méndez, A. Porzel, J. Balbach, L. A. Wessjohann, D. G. Rivera, *Bioconjug. Chem.* **2019**, *30*, 253–259. Author contribution: Synthesis of stapled peptides, NMR analysis, Molecular Dynamics simulations.

## 4.1. Introduction

The concept “peptide stapling” was introduced for the first time to describe the synthesis of all-hydrocarbon bridged peptides by ring-closing metathesis.<sup>[1–3]</sup> Even before, helical structures had been successfully induced in short peptide sequences by the introduction of lactam bridges.<sup>[4–10]</sup> Since then, both macrocyclization techniques have furnished a variety of helical synthetic peptides with remarkable biological and medicinal applications.<sup>[11–16]</sup> Furthermore, several synthetic methodologies have emerged as successful approaches for the side chain-to-side chain tethering.<sup>[17–19]</sup> This includes the Cu<sup>I</sup>-catalyzed alkyne-azide cycloaddition (click),<sup>[20–22]</sup> Lys N<sup>ε</sup>- and Cys S-arylations,<sup>[23–25]</sup> Cys alkylation,<sup>[26]</sup> and Pd-catalyzed C-H activation.<sup>[27,28]</sup> Additionally, there is a special type of ‘two-component’ stapling approach,<sup>[20]</sup> in which the side chain-bridging moiety is designed to bear an additional handle suitable for the modulating bioactivity, labeling or conjugation. Thus, Spring and co-workers have introduced a double-click, two-component stapling with functionalized dialkyne linkages.<sup>[29–31]</sup> Similarly, Dawson and co-workers described an acetone-linked side-chain bridge capable of stabilizing a helical structure and providing the carbonyl functional group for further labeling and conjugation through oxime ligation.<sup>[32]</sup>

The possibility of accessing helical structures from side chain-to-side chain Ugi-macrocyclization described in previous chapters, encouraged us to further study the suitability of this approach as stapling methodology. Thus, we aimed at proving that this multicomponent macrocyclization could do the double purpose of locking a helical peptide conformation and providing a varied set of exocyclic moieties at the lactam bridge, all in one step.

## 4.2. Synthetic Plan

Never before, the helical inducing lactam-bridge strategy has been combined with the synchronized installation of biologically relevant exocyclic functionalities such as lipid, polyethylene glycol (PEG), carbohydrate and fluorescent label. The latter is unfeasible by the classic lactamization approach which leads to a lactam-bridge with a secondary amide, but achievable by means of Ugi-macrocyclization between Lys and Asp/Glu side chains in the presence of an appropriate isocyanide and/or aldehyde bearing the desired functionality.

As previously discussed, the scope of the solution-phase Ugi macrocyclization is very limited, as this reaction is not a bioorthogonal process like, e.g., click chemistry. Nevertheless, a solid-

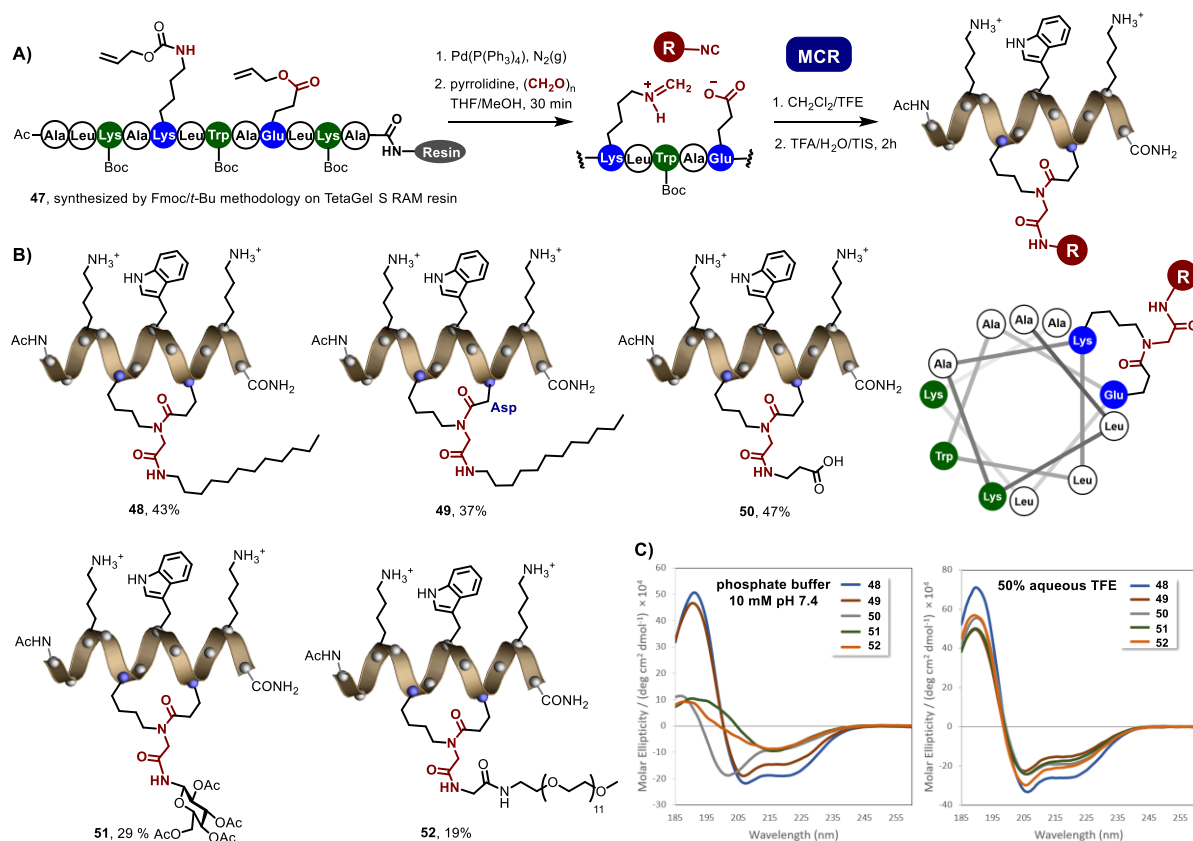
phase protocol – enabling the growth of longer peptides and the multicomponent cyclization/functionalization all being executed on resin – could be a straightforward approach for the synthesis of functionalized helical peptides. In this direction, the carboxylic acid and amino group components of the Ugi reaction were decided to come from the peptide side chains – i.e. side chain tethering combinations Lys/Glu and Lys/Asp – while paraformaldehyde was chosen as oxo-component in order to avoid undesired racemization. In consequence, the diversity-generating motif was established to arise from the isocyanide component.

### 4.3. Synthesis of Ugi-stapled dodecapeptides

A solid-phase methodology based on three degrees of orthogonality was employed for the preparation of peptide **47**. As depicted in scheme 4.1, after Alloc/Allyl deprotection of the Lys and Glu/Asp side chains chosen to be cyclized, the imine formation at the Lys  $\epsilon$ -NH<sub>2</sub> was undertaken by transimination for 30 min with fourfold excess of pyrrolidinium ion arising from the reaction of paraformaldehyde and pyrrolidine. This step is crucial to ensure the complete conversion of the free amine into the imine, as it is the washing of the resin prior to the addition of the isocyanide component to avoid basic conditions during the Ugi cyclization.<sup>[33]</sup> TentaGel S RAM resin with low loading (0.24 mmol/g) was used, while a careful screening of solvents proved that the mixture DCM/trifluoroethanol (TFE) 1:1 (v/v) is the best option for this multicomponent macrocyclization step. Intriguingly, DCM/TFE showed better results than the mixtures THF/MeOH – used in the transamination step – and DCM/MeOH, both previously employed for on-resin Ugi reaction at the peptide *N*-terminus.<sup>[33]</sup> We hypothesize that the helical-inducing effect of TFE facilitates the engagement of the reacting carboxylic (Glu/Asp) and imine groups (Lys) by positioning them in spatial proximity.

Mini-cleavages and HPLC/ESI-MS analyses after 12 h of reaction often showed complete consumption of the linear peptide. In cases of incomplete on-resin macrocyclization after 12 h, a second cycle of imine formation and Ugi reaction for additional 12 h was required. Thus, the criterion for ending the process after either one or two macrocyclization cycles was the disappearance of the linear peptide in HPLC. The isolated yields reported in scheme 4.1 can be considered as good, as they correspond to the overall solid-phase process including all peptide couplings, deprotections and the final on-resin multicomponent macrocyclization.

In order to address the influence of the exocyclic *N*-functionality in the stability of the helical peptide, we initially chose an amino acid sequence with helical propensity, and bearing two Lys alternating with a Trp at *i*, *i*+4 positions to favor further helical stabilization by cation- $\pi$  interactions. Nevertheless, we initially demonstrated that linear peptide **47** (in the deprotected form) does not feature a purely  $\alpha$ -helical structure, as evident from its CD spectrum (see the experimental section). As illustrated in scheme 4.1, the lactam bridge *N*-functionality does have certain influence on the helical stability of the stapled peptides. For example, lipidated peptides **48** and **49** show a typical  $\alpha$ -helical CD spectra in aqueous solution (10 mM, phosphate buffer, pH 7.4), evidenced by the maximum at 191 nm and double minimum at 207 and 222 nm. Even when in our case it didn't resulted in significant differences in the yield, from a synthetic point of view the use of the Lys/Glu instead of the Lys/Asp combination is advised in order to avoid the occurrence of aspartimide formation. As observed from comparison of the CD spectra of peptides **48** and **49**, the latter doesn't impact dramatically the helical content.



Scheme 4.1. Multicomponent stapling approach to lactam-bridged *N*-functionalized helical peptides A) On-resin Ugi macrocyclization enabling the lactam bridge formation and *N*-functionalization with exocyclic appendages. B) Ugi-derived helical peptides with diverse lactam bridge *N*-functionalities. C) CD spectra of the stapled peptides

The CD spectrum of stapled peptide **50** – which bears a carboxylate as exocyclic appendage – shows in phosphate buffer a slight shift in its minima to lower wavelengths compared to **48** and **49** (i.e., 222 nm→218 nm, 207 nm→202 nm). For peptide **50**, a marked decrease in the intensity of the maximum and a slight shift to 187 nm is also observed. These features are commonly found in  $3_{10}$ -helical peptides, showing the change from an  $\alpha$ -helix when the lactam *N*-substituent is a lipid to a  $3_{10}$ -helix when it is a carboxylate group. A more drastic change is observed in the CD spectra of stapled peptides **51** and **52**, bearing peracetylated D-glucose and a PEG chain, respectively, as exocyclic *N*-substituents of the lactam bridge. For both compounds, there is a significant loss of helical content in aqueous solution compared to the stapled lipopeptides. To address the further capacity of stapled peptides **48-52** for helical stabilization, the CD spectra were measured in 50% aqueous TFE. As depicted in Scheme 4.1C, a notable improvement in the  $\alpha$ -helicity was found for the stapled **50**, **51** and **52**, which are those bearing more polar exocyclic lactam *N*-functionalities. The rationale for the excellent  $\alpha$ -helicity of peptides **48** and **49**, even in water, could be the reinforcement of their amphiphilic character due to the presence of the lipid tail in the opposed face to the cationic side chains, observed in cyclic lipododecapeptides described in previous chapters. Based on these results, we were interested in addressing the influence of both the exocyclic lactam *N*-functionality and the amino acid sequence on the helical stability of this novel system.

As depicted in figure 4.1, the change of the two Lys by two Arg leading to stapled peptide **53** does not affect the  $\alpha$ -helical character of this type of amphiphilic structure. However, the replacement of Trp by Lys to produce peptide **54** – also having the exocyclic lipid tail in opposed face to three Lys – gives rise to a  $3_{10}$ -helix CD spectrum in phosphate buffer. This latter might be due to the loss of cation- $\pi$  interactions and subsequent appearance of repulsive electrostatic interactions between the three cationic side chains of peptide **54**. Similarly, the installation of a positive charge at the lactam *N*-substitution in both stapled peptides **55** and **56** also provokes a shift towards  $3_{10}$ -helix. Analysis of the CD spectra of the four peptides in 50% aqueous TFE shows peptides **53**, **54** and **55** displaying a marked  $\alpha$ -helicity, while peptide **56** shows a much lower  $\alpha$ -helical content.

To get a deeper insight into the three-dimensional structure in water of this class of stapled peptides, we turned to study a model compound by means of NMR and molecular dynamics (MD) simulation. Whereas the lipidic stapled peptides showed the higher  $\alpha$ -helical character according to CD, their analysis by NMR proved difficult due to the presence of broad

resonance signals in the  $^1\text{H}$  NMR spectra. As a result, we prepared peptide **57** having a shorter aliphatic chain, and therefore, a lower tendency for aggregation and micelle formation.

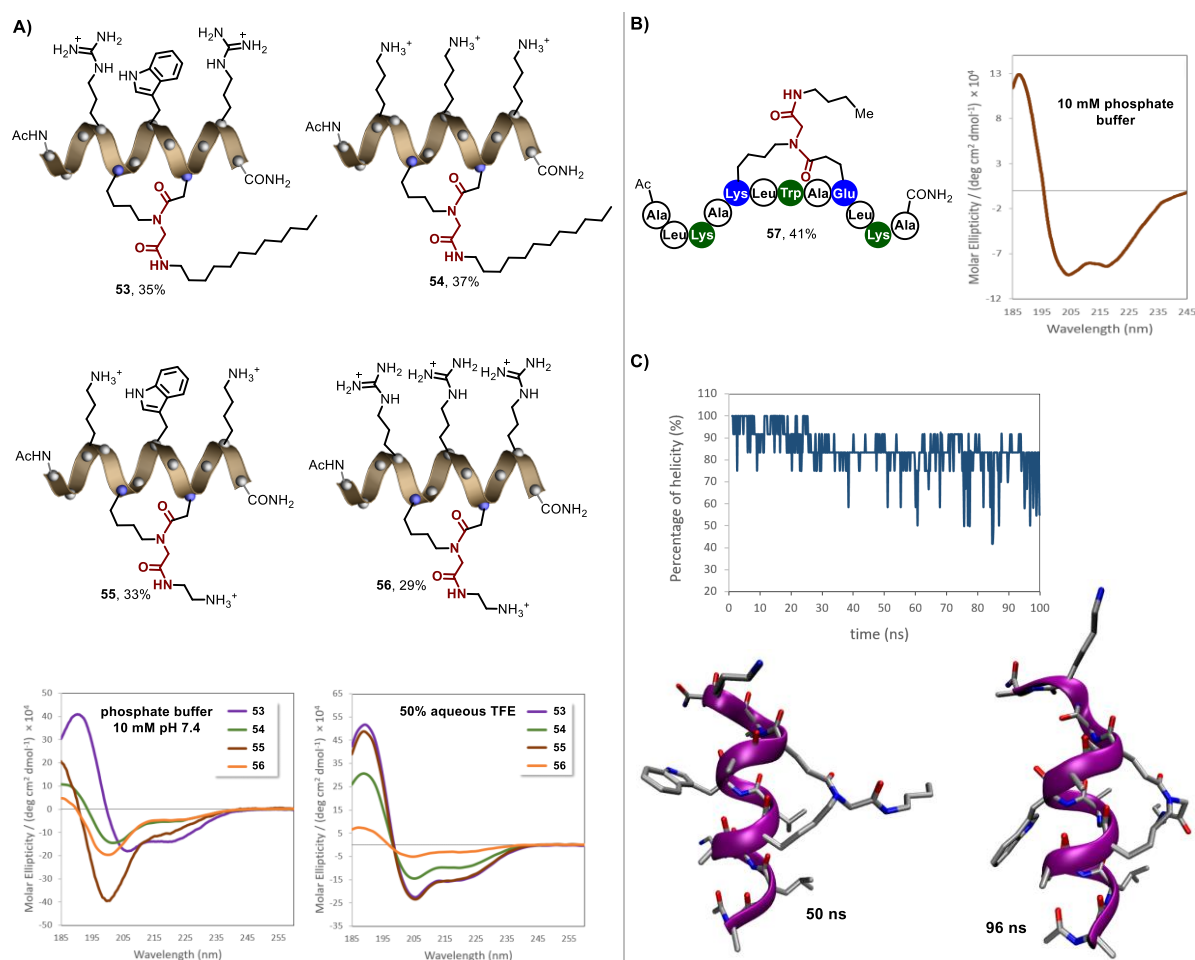


Figure 4.1. A) Structures and CD spectra of Ugi-derived stapled peptides with lactam bridge *N*-functionalities of lipidic and cationic nature. B) Structure and CD spectrum in phosphate buffer of peptide **57**. C) Analysis of the  $\alpha$ -helical population by Molecular Dynamics simulation (program: YASARA, force field: AMBER 14, solvent: explicit water at pH 7.4, T= 298 K, simulation time: 100 ns).

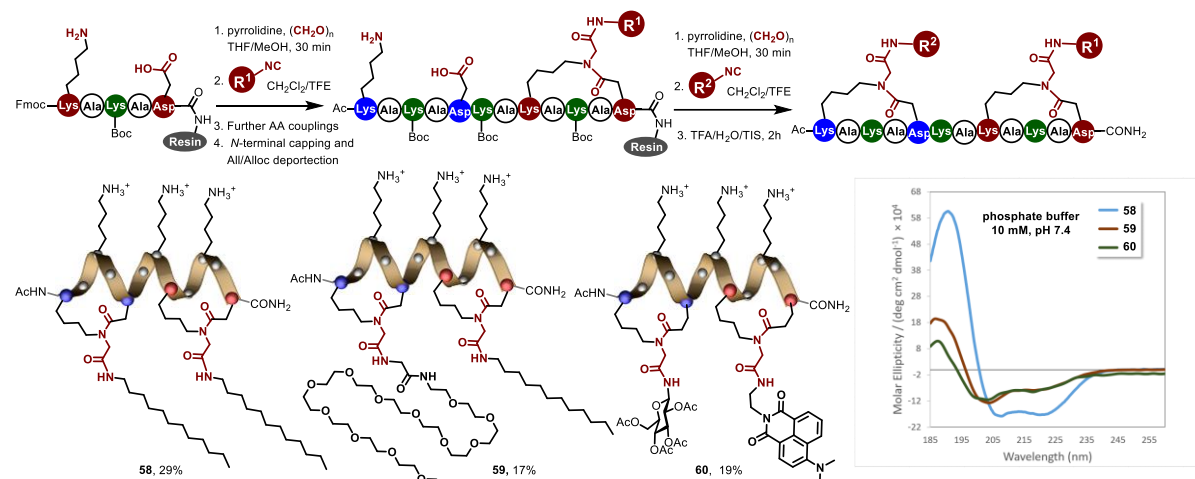
As depicted in figure 4.1B, the CD spectrum of this peptide also shows a typical  $\alpha$ -helical behavior in phosphate buffer, thus serving as a model compound to study the  $\alpha$ -helical stability. Full assignment of the NMR resonances was achieved, confirming the presence of a major conformer in more than 90%. Due to the tertiary nature of the Ugi-derived amide at the lactam bridge, it was important to know whether the major conformer occurs in the *s-cis* or *s-trans* amide configuration. The NOE data unequivocally proved the major presence of the *s-cis* rotamer at the bridge amide bond, with the consequent positioning of both the Glu and Lys side chains toward the same side. The  $^3J_{\text{NHCH}\alpha}$  coupling constants of most residues were lower

than 6 Hz, which is characteristic of  $\alpha$ -helices. However, long-range NOEs were not detected probably due to low signal-to-noise ratio derived from the low concentration required to avoid peptide aggregation. Despite of this, the combined CD and NMR information enabled to build an  $\alpha$ -helical model as starting point for studying the helical stability by MD simulation. Figure 4.1C illustrates the evolution in time of the  $\alpha$ -helical content calculated as the percentage of residues having their  $\phi$  and  $\psi$  angles in the  $\alpha$ -helical region. Snapshots at 50 ns and 96 ns are representative conformations populated during the MD simulation time, showing a well-conserved helical structure up to 50 ns and a tendency towards a partial unfolding of the C-terminus at later simulation times.

#### 4.4. Synthesis of bicyclic peptides

After proving the capacity of the Ugi multicomponent stapling to lock peptide sequences in helical conformation and to introduce at the same type exocyclic fragments of biological (e.g., lipid, sugar) and pharmacological (e.g., PEG) relevance, we looked at demonstrating that more complex modified peptides are available through this solid-phase methodology. In this sense, a traditional approach for the stabilization of longer helical structures is the installation of not only one but also two lactam bridges along the sequence. These bicyclic helical peptides are commonly produced in solid-phase by implementing a first on-resin lactamization, followed by peptide growth and a second lactamization. Thus, we sought to extend the scope of our strategy to allow for the multicomponent incorporation of two *N*-functionalized lactam bridges. As shown in scheme 4.2, a solid-phase protocol comprising two subsequent on-resin Ugi multicomponent macrocyclizations was implemented to incorporate the exocyclic lactam *N*-substituents  $R^1$  and  $R^2$ . Again, three degrees of orthogonality were required to enable the first on-resin Ugi macrocyclization at one Lys side chain, while having other amino groups protected as Fmoc (*N*-terminus) and Boc (Lys). The sequence was designed to construct the lactam bridges by suitable positioning two Asp/Lys pairs separated at *i*, *i*+4 residues. This methodology provides a unique type of bicyclic peptides with either identical or different exocyclic *N*-functionalities. For example, peptide **58** features a bilipidated bicyclic structure resulting from the employment of lipidic isocyanides in both cyclization steps. Alternatively, peptides **59** and **60** were produced using the lipid/PEG and fluorescent label/sugar combinations, respectively, derived from using different isocyanides for the consecutive Ugi macrocyclizations.

Analysis of the CD spectra of peptides **58-60** in phosphate buffer reinforces the idea that the amphiphilic nature of the Ugi-stapled peptide favors the  $\alpha$ -helical character. Thus, peptide **58** bearing three cationic Lys side chains at the opposed face of the lipidated lactam bridges, shows a typical  $\alpha$ -helical CD spectrum. In comparison, the incorporation of the PEG chain on peptide **59**, as well as a fluorescent tag and a sugar in peptide **60**, results in a partial loss of  $\alpha$ -helicity.

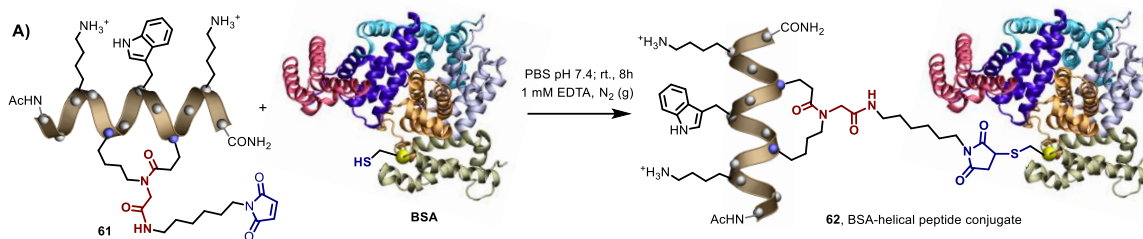


Scheme 4.2. Solid-phase methodology to bicyclic lactam-bridged peptides with exocyclic *N*-functionalities derived from sequential Ugi multicomponent macrocyclizations

#### 4.5. Ligation-enabling peptide stapling

To extend further the potential of the multicomponent stapling concept, we sought to implement an approach comprising the stabilization of an  $\alpha$ -helix at the time that a reactive handle is installed as exocyclic appendage. Previously, we introduced amino and carboxylic groups as exocyclic appendages of the lactam bridge, albeit the presence of other Lys and Glu/Asp residues avoids using the exocyclic lactam *N*-functionalities for further derivatization, e.g., conjugation. As a result, we sought to show the possibility of incorporating a reactive handle suitable for a bioorthogonal conjugation to other biomolecules. Thus, peptide **61** was prepared by means of the on-resin Ugi macrocyclization using a maleimide-functionalized isocyanide. As depicted in scheme 4.3, this type of  $\alpha$ -helical structure (see experimental part for CD) can be readily conjugated to a thiol-containing protein like bovine serum albumin (BSA), which has a Cys at position 34. MALDI-MS analysis proves the formation of helical peptide-BSA conjugate **62**. This result shows great prospects in chemical biology and immunology, as it may enable, for example, the Ugi multicomponent assembly of *N*-

functionalized helical epitopes and their subsequent conjugation to carrier proteins or immunogenic peptides. Importantly, this type of conjugation of stapled peptides can be executed without affecting other amino acids, besides the Lys and Glu/Asp used to introduce the lactam bridge. Once more, it is worth noting that this is impossible to do with the ring-closing metathesis and lactamization approaches, which do not introduce additional reactive handles during the stapling process.



Scheme 4.3. Bioconjugation of lactam-bridged helical peptides with exocyclic reactive handle derived from the Ugi macrocyclization

## 4.6. Conclusions

We have developed a solid-phase multicomponent methodology that enables, for the first time, the simultaneous stabilization of peptide helical structures and the diversity-oriented functionalization of the resulting lactam bridge. This novel class of peptide stapling technique, herein referred as multicomponent stapling, makes use of an on-resin Ugi reaction-based macrocyclization to lock the peptide conformation into a helical structure at the same time that introduces lipids, carbohydrates, PEGs, fluorescent labels and reactive handles as exocyclic functionalities. The  $\alpha$ -helical character of the Ugi-derived stapled peptides was assessed by CD analysis, while a deeper insight into their three-dimensional structure was achieved by means of NMR and MD simulation. Never before the Ugi reaction had been implemented in solid-phase for peptide stapling purposes, which further enhance the versatility of this MCR in the realm of peptide chemistry. As a demonstration of the synthetic scope, we proved that a lactam-bridge *N*-functionality introduced by the on-resin Ugi macrocyclization can be used for peptide-protein bioorthogonal conjugation without affecting other peptide side chains. In addition, the methodology allowed for the solid-phase construction of bicyclic stapled peptides having two consecutive *N*-functionalized lactam bridges. The feasibility of the solid-phase protocol, including the efficient Ugi multicomponent macrocyclization, shows promise for applications in chemical biology, immunology and peptide drug discovery.

## 4.7. Experimental part

### 4.7.1 Spectroscopic characterization

NMR spectra were recorded at 298 K either on a Varian Mercury 400 NMR spectrometer at 399.94 MHz and 100.57 MHz for  $^1\text{H}$  and  $^{13}\text{C}$ , respectively, or on an Agilent (Varian) VNMRS 600 NMR spectrometer at 599.83 MHz and 150.83 MHz, respectively. Chemical shifts ( $\delta$ ) for intermediates characterized in common organics solvents are reported in ppm relative to the TMS ( $^1\text{H}$  NMR) and to the solvent signal ( $^{13}\text{C}$  NMR). For water-recorded NMR spectra, the chemical shifts are reported relative to TSP-d<sub>4</sub> and  $^{13}\text{C}$  chemical shifts were inferred from  $^1\text{H}$ -1D spectra according to IUPAC recommendations.<sup>[34]</sup> IR spectra were obtained on a Thermo Nicolet 5700 FT-IR spectrometer. Circular dichroism spectra were recorded on a Jasco J-815 spectropolarimeter equipped with a temperature controller at 20° C. A total of 16 accumulations from 260 to 185 nm at 50 nm/sec using 1 mm cuvettes were done.

### 4.7.2 Chromatographic methods

Analytical and preparative RP-HPLC was carried out with an Agilent 1260 Infinity series system equipped with two preparative pumps and one analytical quaternary pump, coupled to a MWD detector and an Agilent 6120 Quadrupole LC/MS detector using API-ES as ion source. Reverse phase YMC-ODS-A column (150 × 4.6 mm I.D., 5 μm particle size) and YMC-ODS-A (150 × 20 mm I.D., 5 μm particle size) columns were used for analytical and preparative scale, respectively. For analytical analysis, unless otherwise stated, a linear gradient from 5% to 80% of solvent B (0.1% (v/v) formic acid (FA) in acetonitrile) in solvent A (0.1% (v/v) formic acid (FA) in water) over 20 min at a flow rate of 0.8 mL min<sup>-1</sup> was used. Flash column chromatography was carried out using Merck silica gel 60 (0.015-0.040 nm) and analytical thin layer chromatography (TLC) was performed on Merck silica gel 60 F254 aluminum sheets.

### 4.7.3 Mass spectrometry characterization

#### ESI-HRMS

The positive- and negative-ion high-resolution ESI mass spectra were obtained with an Orbitrap Elite mass spectrometer (Thermo Fisher Scientific, Germany) equipped with an HESI electrospray ion source (positive spray voltage 4.5 kV, negative spray voltage 3.5 kV, capillary temperature 275 °C, source heater temperature 250 °C, FTMS resolution 30000). A TripleToF

6600-1 mass spectrometer (Sciex) was also used for high-resolution mass spectrometry, which was equipped with an ESI-DuoSpray-Ion-Source (it operated in positive ion mode) and was controlled by the Analyst 1.7.1 TF software (Sciex). The ESI source operation parameters were as follows: ion spray voltage: 5,500 V, nebulizing gas: 60 p.s.i., source temperature: 450 °C, drying gas: 70 p.s.i., curtain gas: 35 p.s.i. Data acquisition was performed in the MS1-ToF mode, scanned from 100 to 1500 Da with an accumulation time of 50 ms.

### **MALDI-TOF-MS**

The measurements were performed in a MALDI-TOF MS (Ultraflex MALDI-TOF/TOF MS, Bruker Daltonics) apparatus equipped with a 337 nm Smartbeam II laser operated at 500 Hz. 1  $\mu$ L of the samples was spotted onto the target plate (MTP 384 target plate ground steel BC, Bruker Daltonics, Bremen, Germany). The samples were mixed with 1  $\mu$ L of matrix solution (30 mg/mL sinapinic acid in 50% (v/v) AcN/0.1% (v/v) TFA).

For protein measurements, the instrument was operated in the positive ionization and linear mode by accumulating 1000 laser shots in the range of  $m/z$  10000-100000 at a detector energy of 2990 V. The ion source 1 voltage was 25 kV, the ion source 2 voltage was maintained at 22.8 kV and the lens voltage was 7 kV. For peptide measurements the instrument was operated in the positive ionization and in reflector mode by accumulating 200 laser shots in the range of  $m/z$  600-5000 at a reflector detector energy of 2472 V. The ion source 1 voltage was 25 kV, the ion source 2 voltage was maintained at 21.65 kV and the lens voltage was 10.5 kV.

Mass spectra were calibrated using Protein Calibration Standard II containing trypsinogen, protein A and bovine serum albumin (BSA) and Peptide Calibration Standard II (Bruker Daltonics, Bremen, Germany). Data acquisition was manually done using the FlexControl 3.4 software and data processing was performed using the FlexAnalysis 3.4 software (both Bruker Daltonik).

#### **4.7.4 General methods for Peptide Synthesis**

**Solid Phase Peptide Synthesis:** Coupling reactions were carried out automatically on an INTAVIS ResPepSL automated peptide synthesizer by a stepwise Fmoc/tBu strategy using with a 5-fold excess of amino acid and PyBop and a 10-fold excess of NMM at R.T. for 15 min. A 25  $\mu$ mol scale on TG-S-RAM (Iris Biotech) resin (104 mg, 0.24 mmol/mg) was utilized.

**Swelling:** The resin is swelled for 20 min in dichloromethane before bring it into the synthesizer. After the coupling of all amino acids, the resin is manually washed with DCM (3×1 min) and DMF (2×1 min) and reacted with 10 eq. of Ac<sub>2</sub>O/DIEA in 2mL of DMF for 30 min. The completeness of the reaction is confirmed through the Kaiser test and the resin is manually washed with DCM (3×1 min). **Alloc/Allyl Removal:** The resin is washed with dry dichloromethane (2×2 min) under a stream of nitrogen. A solution of phenylsilane (20 equiv) in dry dichloromethane and tetrakis(triphenylphosphine) Palladium(0) (0.2 equiv) are added to the resin under a continuous stream of nitrogen. The mixture is stirred in the dark for 10 min, and the procedure is repeated once more. Finally, the resin is washed with 0.5 % of sodium diethyldithiocarbamate trihydrate in DMF (5×2 min) and DCM (2×2 min). **Aminocatalysis-mediated Ugi-4C cyclization:** The side chain deprotected resin-bound peptide is washed with THF (4×1min) and treated with a suspension of paraformaldehyde (4 equiv) and pyrrolidine (4 equiv) in THF/MeOH (1:1) for 30 min. The excess of reagents is removed by washing the beads with THF (4×1min). The resin is then washed with DCM (4×1min) and DCM/TFE 1:1 solution (2×1min). A solution of the isocyanide (4 equiv) in 2 mL DCM/TFE 1:1 (or THF:MeOH 1:1 for relative polar isocyanides) is added to the resin and the suspension is stirred overnight (18hrs). Completion is evaluated by ESI-MS or RP-HPLC monitoring after mini-cleavages. Finally, the system is washed with DCM (3×1 min), DMF (2×1 min), DCM (2×1 min) and Et<sub>2</sub>O (3×1 min). **Minicleavage:** A small amount of the dry resin (less than 10 mg) is transferred to an Eppendorf vial and 400 μL of the cleavage cocktail (TFA/TIS/H<sub>2</sub>O 95:2.5:2.5) is added. The suspension is gently agitated during 45 min and afterwards the cleavage cocktail is concentrated under N<sub>2</sub> flow. The remaining oil is precipitated by addition of 500 μL diethyl ether. The suspension is centrifuged for 5 min after what the solid and liquid phases are separate by settling. The precipitated peptide is dissolved in mixture AcN/H<sub>2</sub>O and analyzed by RP-HPLC. **Cleavage:** The resin is treated with the cleavage cocktail TFA/TIS/H<sub>2</sub>O (95:2.5:2.5, 10mL/g of resin) for 2 hours under gentle shaking. The peptide is precipitated from frozen diethyl ether, then taken up in 1:2 AcN/H<sub>2</sub>O and lyophilized. **Cyclization by peptide coupling:** PyAOP (4 eq.) and DIPEA (6 eq.) are dissolved in DMF and the solution is added to the resin-bound peptide. The suspension is stirred for 12 h and then the resin is washed with DCM (3×1 min), DMF (2×1 min) and Et<sub>2</sub>O (3×1 min).

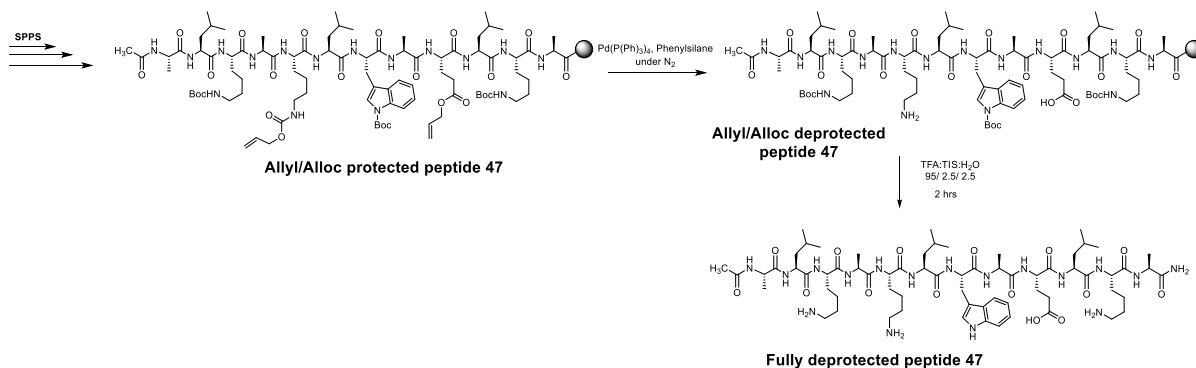
### 4.7.5 Synthesis of isocyanides

#### General protocol for the synthesis of isocyanides from amines

A solution of the amine (25 mmol) in ethyl formate (20 mL) is heated at reflux for 12 h to afford the corresponding formamide. The resulting solution is concentrated under vacuum and used without further purification. The formamide in 40 mL of dry THF (or DCM if not soluble), mixed with Et<sub>3</sub>N (4 eq.) and under N<sub>2</sub> atmosphere is cooled to -20 °C and a solution of POCl<sub>3</sub> (1.3 eq.) in 15 mL of THF is added dropwise during 30 min. The resulting mixture is stirred at -20 °C for 1 h, then allowed to reach room temperature and stirred for additional 2 h. The reaction mixture is quenched with 50 mL of 10% aqueous NaHCO<sub>3</sub> and extracted with EtOAc (2×150 mL). The combined organic phases are washed with brine (50 mL), dried over anhydrous Na<sub>2</sub>SO<sub>4</sub>, and concentrated under reduced pressure to dryness. The crude product is purified by column chromatography. The details of the synthesis of isocyanides are enclosed in the annexes at the end of the manuscript.

### 4.7.6 Synthesis of peptides

#### Linear peptide 47



Allyl/Alloc protected peptide **47** was synthesized in 25 μmol scale on TentaGel S RAM resin (104 mg, 0.24 mmol/g) according to the protocols described in 4.7.4. Cleavage with TFA/H<sub>2</sub>O/TIS 95:2.5:2.5 for 2 h after simultaneous Alloc and Allyl ester removal according to protocol in 4.7.4 afforded the fully deprotected peptide **47** (92% cleavage yield), which was characterized by analytical HPLC (*R*<sub>t</sub> 9.7 min, > 95% purity (crude)); ESI-HRMS, calcd for C<sub>66</sub>H<sub>113</sub>N<sub>17</sub>O<sub>15</sub>: 691.9301 [M+2H]<sup>2+</sup>; Found: *m/z* 691.9281 [M + 2H]<sup>2+</sup>.

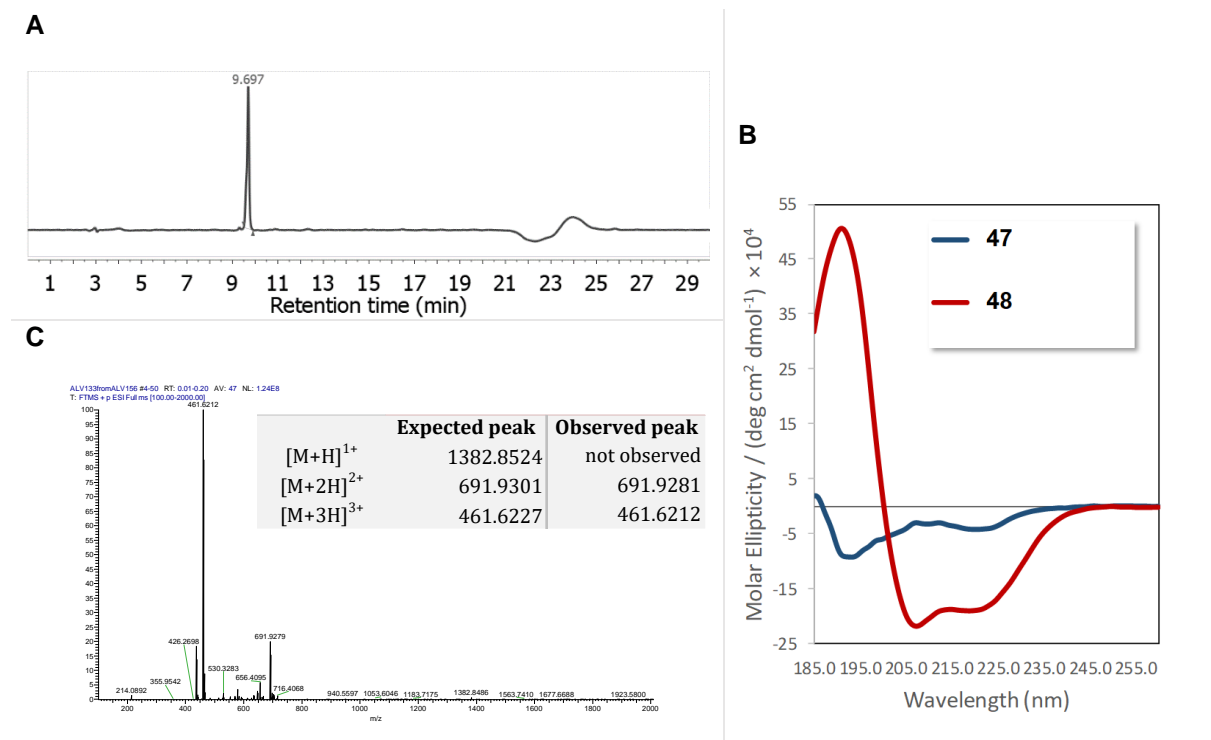


Figure 4.2. A) HPLC trace of deprotected peptide **47**. B) Comparison of CD spectra of deprotected peptide **47** and its MCR-stapled derivative **48** in 10 mM aq. phosphate buffer. C) ESI-HRMS of fully deprotected peptide **47**.

### Lipidated Stapled Peptide **48**

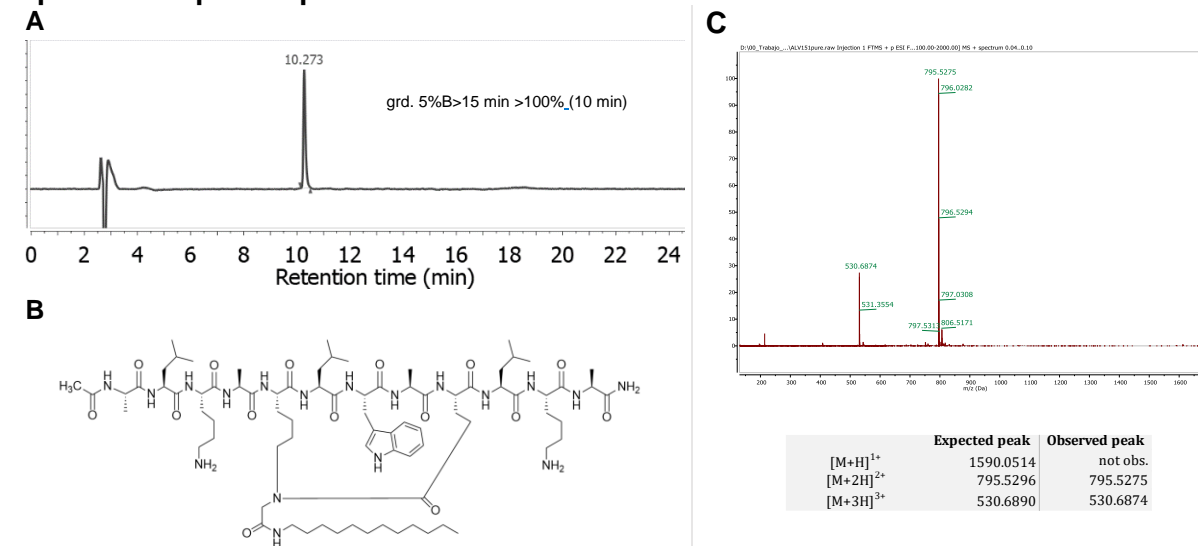
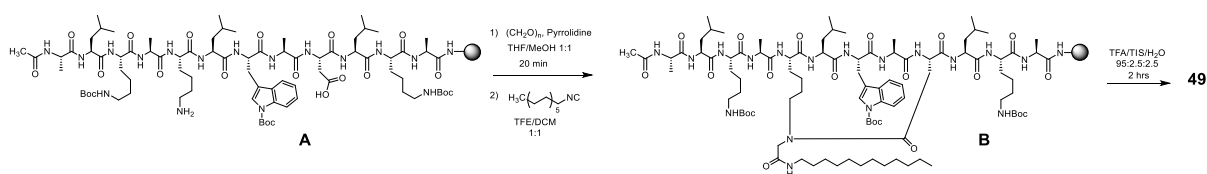


Figure 4.3. A) HPLC trace of purified peptide **48**. B) Structure of peptide **48**. C) ESI-HRMS of stapled peptide **48**

Stapled peptide **48** was produced by on-resin cyclization in a 25  $\mu$ mol scale from peptide **47** according to the aminocatalysis-mediated Ugi macrocyclization protocol described in 4.7.4, in the presence of *n*-dodecylisocyanide. Cleavage with TFA/H<sub>2</sub>O/TIS 95:2.5:2.5 for 2 h afforded peptide **48** (73% cleavage yield), which was purified by semi-preparative RP-HPLC (17.2 mg,

43% isolated yield);  $R_t$  10.3 min, > 95% purity. ESI-HRMS, calcd. for  $C_{80}H_{138}N_{18}O_{15}$ : 795.5296  $[M + 2H]^{2+}$  Found:  $m/z$  795.5275  $[M + 2H]^{2+}$ .

### Lipidated Stapled Peptide 49



The resin-linked fully protected form of peptide **A** was synthesized in a 25  $\mu$ mol scale on TentaGel S RAM resin (104 mg, 0.24 mmol/mg), then deprotected at Lys5 (Alloc) and Asp9 (Allyl) according to the procedures described in 4.7.4. **A** was subjected to the aminocatalysis-mediated on-resin Ugi macrocyclization in the presence of *n*-dodecylisocyanide as described in 4.7.4. Cleavage with TFA/ $H_2O$ /TIS 95:2.5:2.5 for 2 h afforded peptide **49** (73% cleavage yield), which was purified by semi-preparative RP-HPLC (14.6 mg, 37% isolated yield);  $R_t$  15.24 min, > 92% purity. ESI-HRMS, calcd. for  $C_{79}H_{135}N_{22}O_{15}$ : 1576.0354  $[M + H]^+$ . Found:  $m/z$  1576.0350  $[M + H]^+$ .

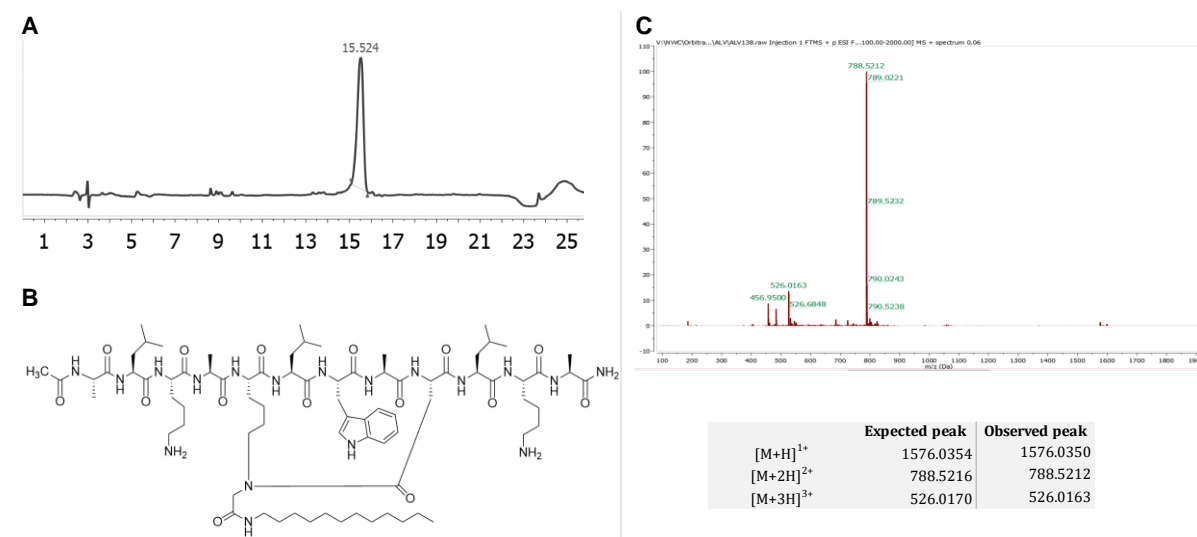


Figure 4.4. A) HPLC trace of purified peptide **49**. B) Structure of peptide **49**. C) ESI-HRMS of peptide **49**

### Ugi-stapled Peptide 50

Stapled peptide **50** was produced by on-resin cyclization in a 25  $\mu$ mol scale from Allyl/Alloc deprotected peptide **47** according to the aminocatalysis-mediated Ugi macrocyclization protocol described in 4.7.4, in the presence of *t*-butyl 3-isocyanopropanoate. Cleavage with TFA/ $H_2O$ /TIS 95:2.5:2.5 for 2 h afforded peptide **50** (78% cleavage yield), which was purified

by semi-preparative RP-HPLC (17.7 mg, 47% isolated yield);  $R_t$  8.8 min, > 94% purity. ESI-HRMS, calcd. for  $C_{71}H_{117}N_{18}O_{17}$ : 1493.8844  $[M + H]^+$ . Found:  $m/z$  1493.8813  $[M + H]^+$ .

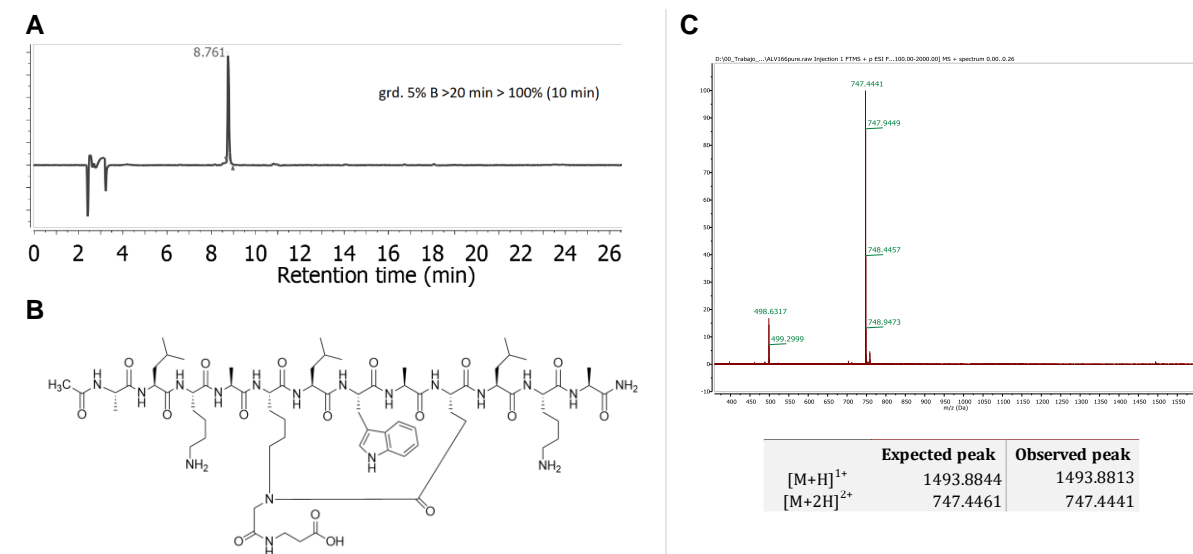


Figure 4.5. A) HPLC trace of purified peptide **50**. B) Structure of peptide **50**. C) ESI-HRMS of peptide **50**

### Glycosylated Stapled Peptide **51**

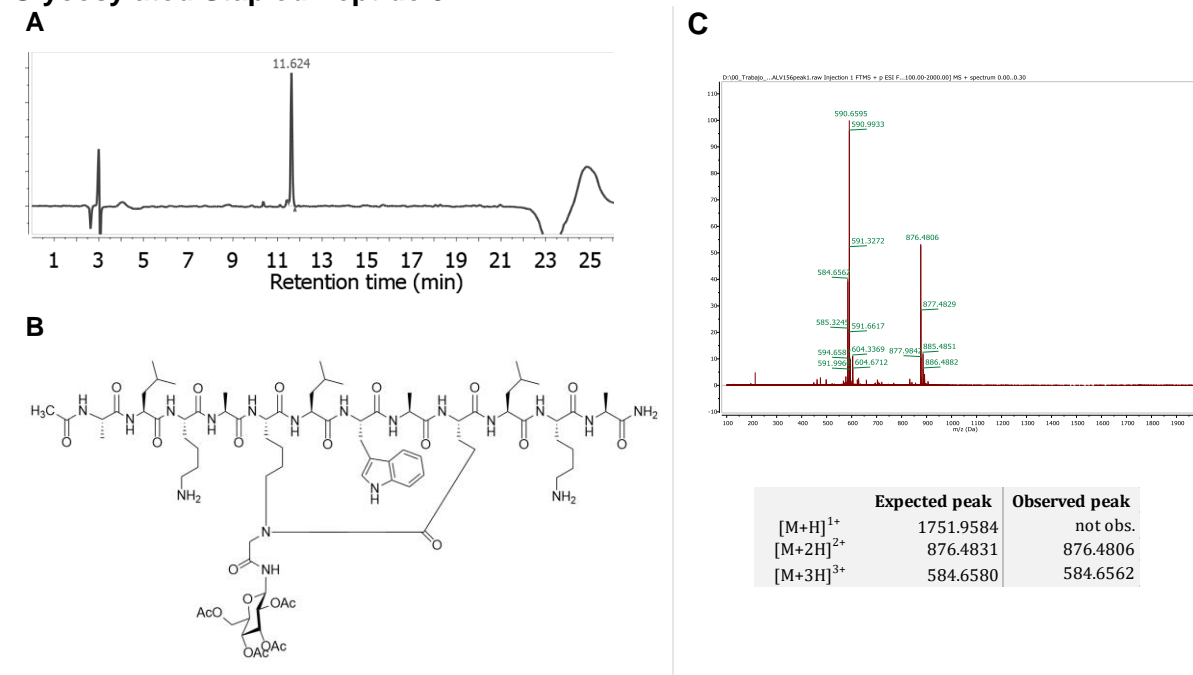


Figure 4.6. A) HPLC trace of purified peptide **51**. B) Structure of peptide **51**. C) ESI-HRMS of peptide **51**

Stapled peptide **51** was produced by on-resin cyclization in a 25  $\mu$ mol scale from Allyl/Alloc deprotected peptide **47** according to the aminocatalysis-mediated Ugi macrocyclization protocol described in 4.7.4, in the presence of 2,3,4,6-tetra-*O*-acetyl- $\beta$ -D-glucopyranosyl

isocyanide. Cleavage with TFA/H<sub>2</sub>O/TIS 95:2.5:2.5 for 2 h afforded peptide **51** (66% cleavage yield), which was purified by semi-preparative RP-HPLC (12.6 mg, 29% isolated yield); *R*<sub>t</sub> 11.6 min, > 88% purity. ESI-HRMS, calcd. for C<sub>82</sub>H<sub>132</sub>N<sub>18</sub>O<sub>24</sub>: 876.4831 [M + 2H]<sup>2+</sup>. Found: *m/z* 876.4806 [M + 2H]<sup>2+</sup>.

Note: The compound proved unstable when kept in slightly acidic aqueous solution.

### PEGylated Stapled Peptide 52

Stapled peptide **52** was produced by on-resin cyclization in a 25 μmol scale from Allyl/Alloc deprotected peptide **47** according to the aminocatalysis-mediated Ugi macrocyclization protocol described in 4.7.4, in the presence of *N*-(OMe-(PEG)<sub>11</sub>ethyl)-2-isocyanoacetamide. Cleavage with TFA/H<sub>2</sub>O/TIS 95:2.5:2.5 for 2 h afforded peptide **52** (69% cleavage yield), which was purified by semi-preparative RP-HPLC (9.5 mg, 19% isolated yield); *R*<sub>t</sub> 14.7.4.3 min, > 92% purity. MALDI-TOF MS, calcd. for C<sub>95</sub>H<sub>166</sub>N<sub>19</sub>O<sub>28</sub>: 2021.215 [M + H]<sup>+</sup>. Found: *m/z* 2021.169 [M + H]<sup>+</sup>.

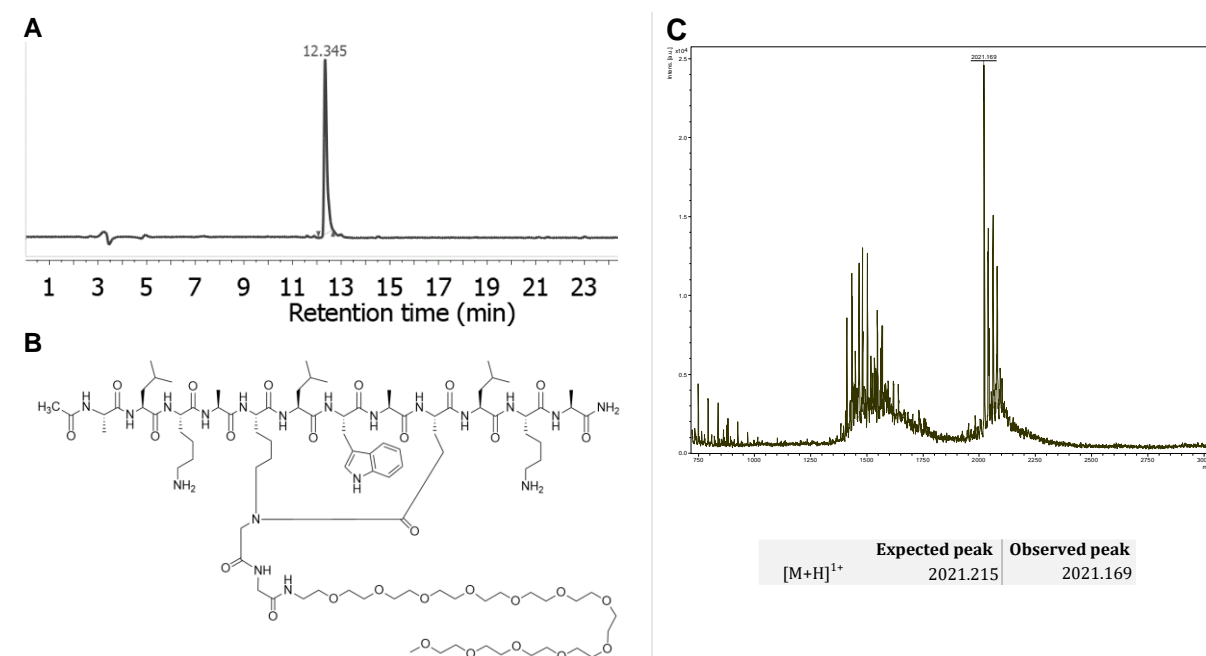
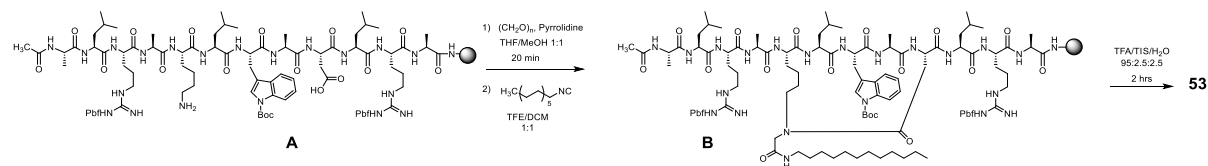


Figure 4.7. A) HPLC trace of purified peptide **52**. B) Structure of peptide **52**. C) MALDI-MS of peptide **52**

## Lipidated Stapled Peptide 53



The resin-linked peptide **A** was synthesized in a 25  $\mu\text{mol}$  scale on TentaGel S RAM resin (63 mg, 0.24 mmol/mg) followed by deprotection at Lys5 (Alloc) and Asp9 (Allyl) according to the procedures described in 4.7.4. **A** was subjected to the aminocatalysis-mediated on-resin Ugi macrocyclization in the presence of *n*-dodecylisocyanide as described in 4.7.4. Cleavage with TFA/H<sub>2</sub>O/TIS 95:2.5:2.5 for 2 h afforded peptide **53** (82% cleavage yield), which was purified by semi-preparative RP-HPLC (14.4 mg, 35% isolated yield);  $R_t$  15.24 min, > 93% purity. ESI-HRMS, calcd. for C<sub>79</sub>H<sub>136</sub>N<sub>22</sub>O<sub>15</sub>: 816.5278 [M + 2H]<sup>2+</sup>. Found:  $m/z$  816.5269 [M + 2H]<sup>2+</sup>.

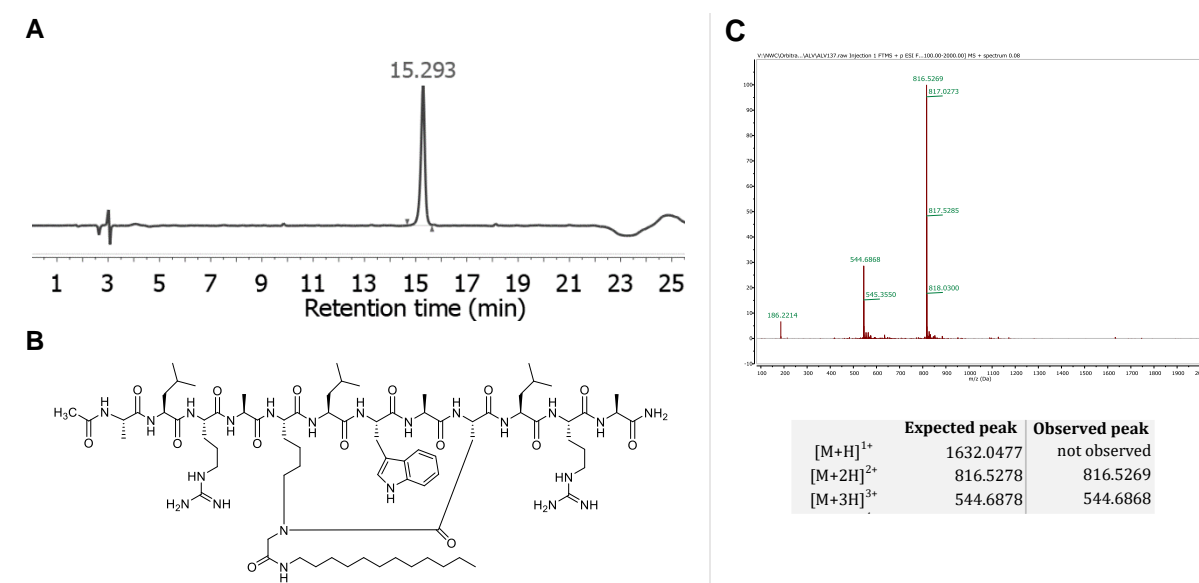
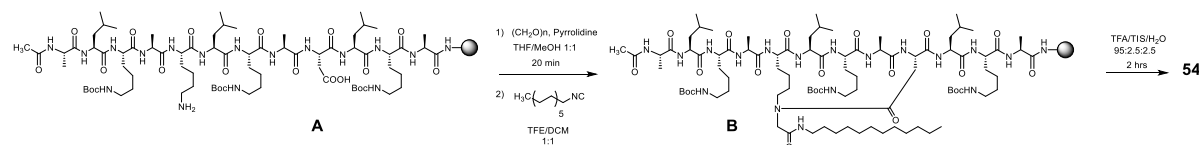


Figure 4.8. A) HPLC trace of purified peptide **53**. B) Structure of peptide **53**. C) ES-HRMS of peptide **53**

## Lipidated Stapled Peptide 54



The resin-linked peptide **A** was synthesized in a 25  $\mu\text{mol}$  scale on TentaGel S RAM resin (104 mg, 0.24 mmol/mg) followed by deprotection at Lys5 (Alloc) and Asp9 (Allyl) according to the procedures described in 4.7.4. **A** was subjected to the aminocatalysis-mediated on-resin Ugi

macrocyclization in the presence of *n*-dodecylisocyanide as described in 4.7.4. Cleavage with TFA/H<sub>2</sub>O/TIS 95:2.5:2.5 for 2 h afforded peptide **54** (87% cleavage yield), which was purified by semi-preparative RP-HPLC (14.2 mg, 35% isolated yield); *R*<sub>t</sub> 15.9 min, > 95% purity. ESI-HRMS, calcd. for C<sub>74</sub>H<sub>137</sub>N<sub>18</sub>O<sub>15</sub>: 1518.0511 [M + H]<sup>+</sup>. Found: *m/z* 1518.0478 [M + H]<sup>+</sup>.

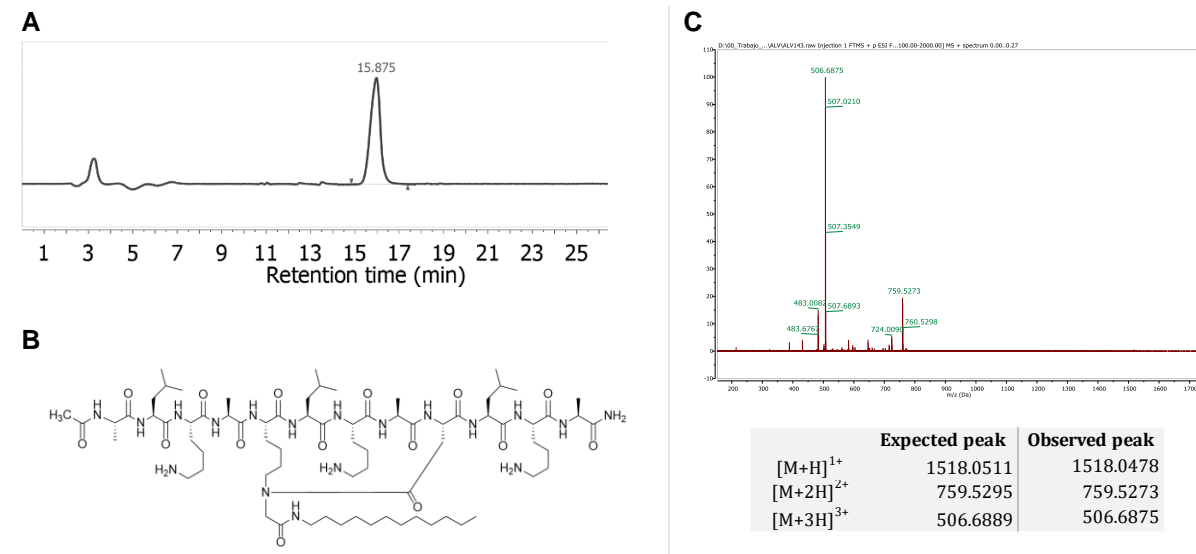
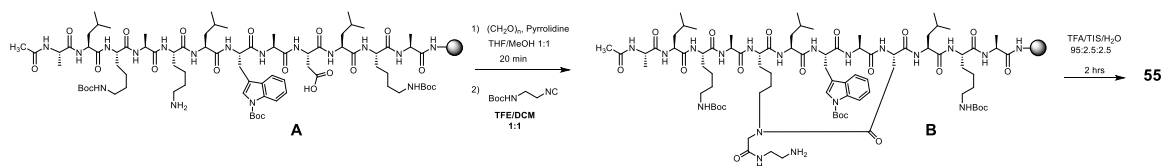


Figure 4.9. A) HPLC trace of purified peptide **54**. B) Structure of peptide **54**. C) ESI-HRMS of peptide **54**

### Ugi-stapled Peptide **55**



The resin-linked peptide **A** was synthesized in a 25 μmol scale on TentaGel S RAM resin (104 mg, 0.24 mmol/mg), deprotected at Lys5 (Alloc) and Asp9 (Allyl) according to the procedures described in 4.7.4. **A** was subjected to the aminocatalysis-mediated on-resin Ugi macrocyclization in the presence of *n*-dodecylisocyanide as described in 4.7.4. Cleavage with TFA/H<sub>2</sub>O/TIS 95:2.5:2.5 for 2 h afforded peptide **55** (78% cleavage yield), which was purified by semi-preparative RP-HPLC (11.8 mg, 33% isolated yield); *R*<sub>t</sub> 8.7 min, > 89% purity. ESI-HRMS, calcd. for C<sub>69</sub>H<sub>117</sub>N<sub>19</sub>O<sub>15</sub>: 725.9488 [M + 2H]<sup>2+</sup>. Found: *m/z* 725.9469 [M + 2H]<sup>2+</sup>.

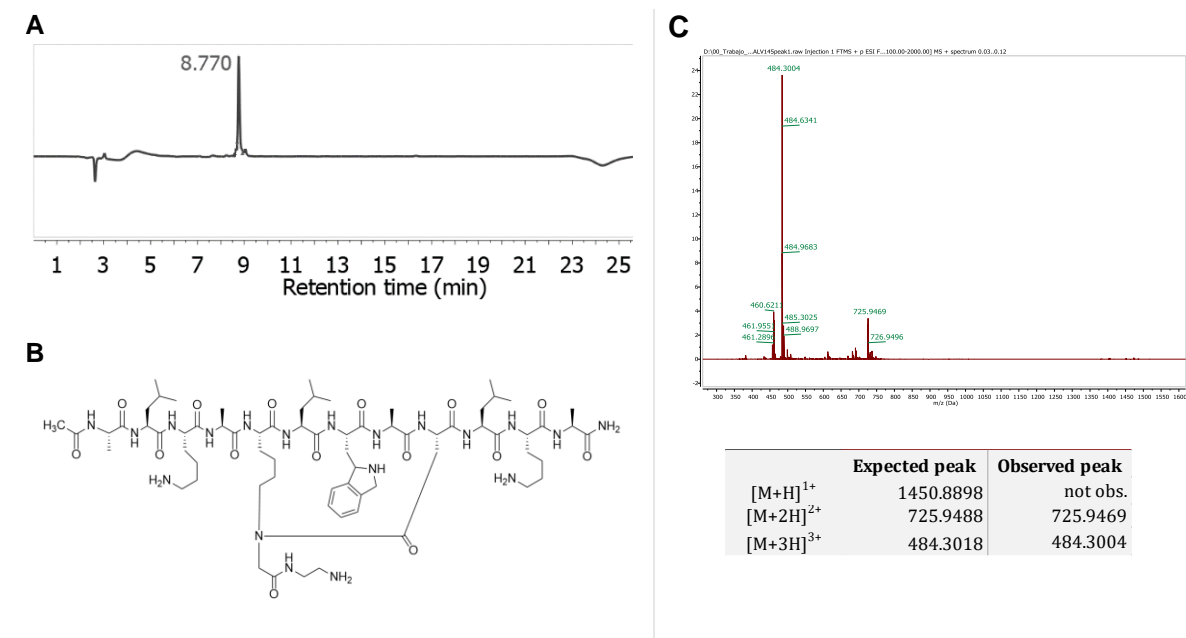


Figure 4.10. A) HPLC trace of purified peptide **55**. B) Structure of peptide **55**. C) ESI-HRMS of peptide **55**

### Ugi-stapled Peptide **56**

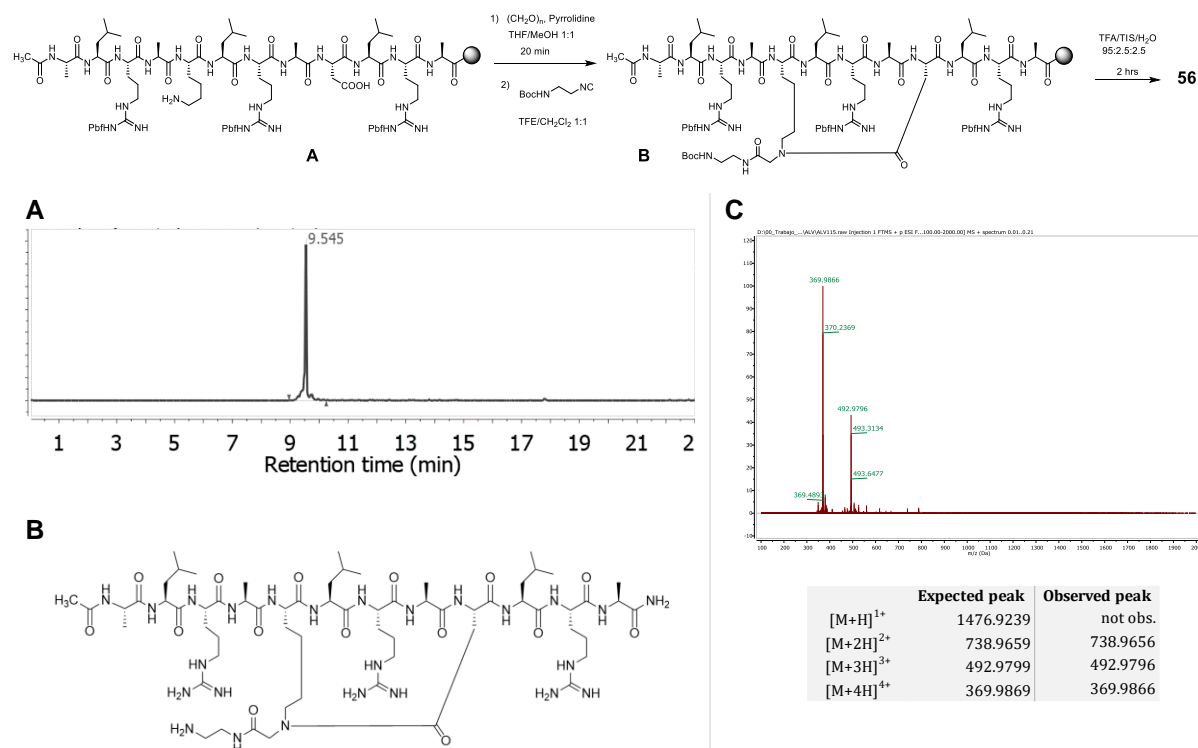


Figure 4.11. A) HPLC trace of purified peptide **56**. B) Structure of peptide **56**. C) ESI-HRMS of peptide **56**

The resin-linked peptide **A** was synthesized in a 25  $\mu$ mol scale on TentaGel S RAM resin (104 mg, 0.24 mmol/mg), deprotected at Lys5 (Alloc) and Asp9 (Allyl) according to the procedures

described in 4.7.4. **A** was subjected to the aminocatalysis-mediated on-resin Ugi macrocyclization in the presence of (*N*-tert-butyloxycarbonyl)-aminoethyl isocyanide as described in 4.7.4. Cleavage with TFA/H<sub>2</sub>O/TIS 95:2.5:2.5 for 2 h afforded peptide **56** (84% cleavage yield), which was purified by semi-preparative RP-HPLC (10.9 mg, 29% isolated yield); *R*<sub>t</sub> 9.5 min, > 87% purity. ESI-HRMS, calcd. for C<sub>64</sub>H<sub>119</sub>N<sub>25</sub>O<sub>15</sub>: 738.9659 [M + 2H]<sup>2+</sup>. Found: *m/z* 738.9656 [M + 2H]<sup>2+</sup>.

### Ugi-stapled Peptide 57

Stapled peptide **57** was produced by on-resin cyclization in a 25 μmol scale from Allyl/Alloc deprotected peptide **47** according to the aminocatalysis-mediated Ugi macrocyclization protocol described in 4.7.4, in the presence of *n*-dodecylisocyanide. Cleavage with TFA/H<sub>2</sub>O/TIS 95:2.5:2.5 for 2 h afforded peptide **57** (65% cleavage yield), which was purified by semi-preparative RP-HPLC (15.0 mg, 41% isolated yield); *R*<sub>t</sub> 12.0 min, > 95% purity. ESI-HRMS, calcd. for C<sub>72</sub>H<sub>121</sub>N<sub>18</sub>O<sub>15</sub>: 1477.9259 [M + H]<sup>+</sup>. Found: *m/z* 1477.9322 [M + H]<sup>+</sup>.

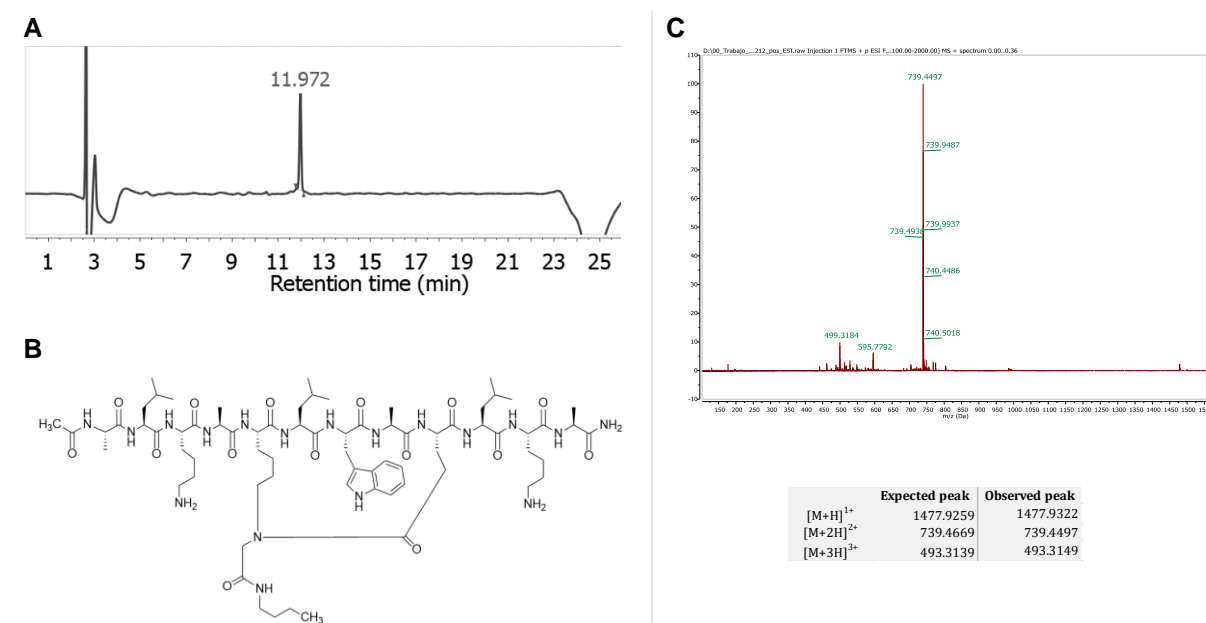


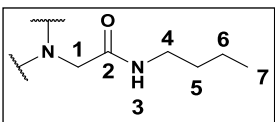
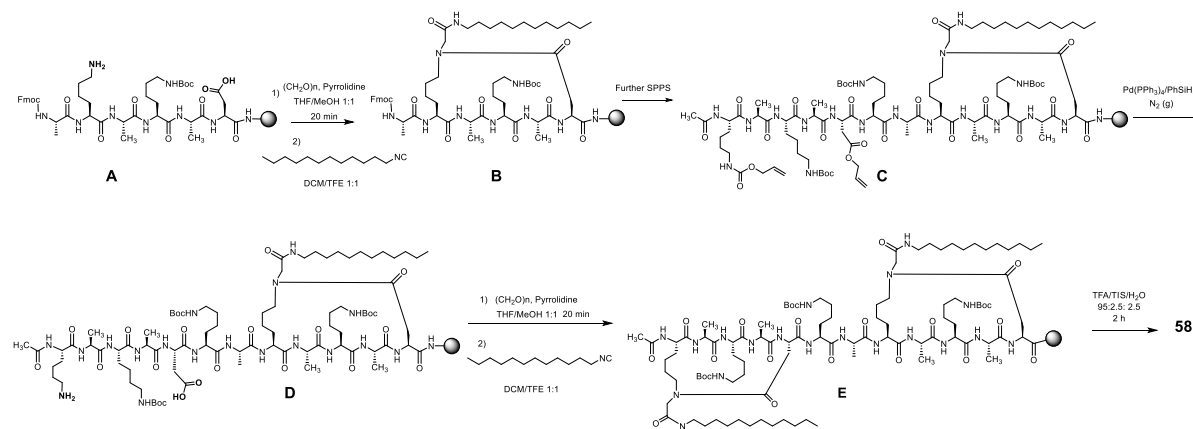
Figure 4.12. A) HPLC trace of purified peptide **57**. B) Structure of peptide **57**. C) ESI-HRMS of peptide **57**

Table 1. Full assignment of the NMR resonances for Ugi-stapled peptide **57** in H<sub>2</sub>O/D<sub>2</sub>O 9:1 at 25 °C and pH 5 (*s-cis* conformer).

Major conformer (~95%)					
Residue	HN( <sup>3</sup> J)	HA/CA	HB/CB	CO	others
Ace <sup>1</sup>	-	2.051/24.55		177.0	
Ala <sup>2</sup>	8.344	4.219/53.372	1.392/19.09	179.0	
Leu <sup>3</sup>	8.334	4.322/56.05	1.652/41.929	177.9	1.657/27.065(γ); 0.954/24.56; 0.904
Lys <sup>4</sup>	8.149	4.114/57.68	1.773/32.61	177.3	1.446, 1.375/25.00(γ); 1.676/29.20(δ); 2.978/42.14(ε)
Ala <sup>5</sup>	8.075	4.236/53.56	1.412/18.83	178.8	
Lys <sup>6</sup>	8.024	4.191/57.96	1.815/32.44	178.1	1.686; 1.293/30.02(δ); 3.025, 3.352/51.95(ε)
Leu <sup>7</sup>	8.272	3.988/57.217	1.651, 1.504/41.63	<i>n.d.</i> ( <sup>†</sup> )	1.657/27.065(γ); 0.780/22.93 (δ1); 0.885(δ2)
Trp <sup>8</sup>	7.571	4.660/57.78	3.323, 3.382/29.80	176.6	129.9(γ); 10.23(ε1); 139.0(ε2); 7.63/121.1(ε3); 7.50/114.6(ζ2); 7.17/122.2 (ζ3); 7.24/124.6(η)
Ala <sup>9</sup>	8.187	4.132/53.87	1.528/18.58	179.5	
Glu <sup>10</sup>	8.446	4.246/57.258	2.237, 1.924/28.817	177.6	2.813, 2.417/31.60 (γ); 177.20(δ)
Leu <sup>11</sup>	8.064	4.258/52.17	1.61, 1.72/42.28	178.3	1.657/27.065(γ); 0.880; 0.908
Lys <sup>12</sup>	8.075	4.164/56.64	1.775, 1.697/32.58	176.7	1.321/24.54(γ); 1.593/28.94(δ); 2.901/42.13(ε)
Ala <sup>13</sup>	7.965	4.251/52.55	1.423/19.43	180.6	Terminal NH <sub>2</sub> : 2.05

<i>N</i> -substitution			
Atom group	δ <sub>H</sub> /δ <sub>C</sub>	Atom group	δ <sub>H</sub> /δ <sub>C</sub>
1	3.815, 4.119/53.00	5	1.461/33.32
2	173.5	6	1.300/22.17
3	7.853	7	0.879/15.82
4	3.203/41.99		


<sup>(†)</sup> *n.d.* = not determinedDouble Lipidated Stapled Peptide **58**

The resin-linked peptide **A** was synthesized in a 25 μmol scale on Rink-Amide AM resin (179 mg, 0.14 mmol/g), deprotected at Lys2 (Alloc) and Asp6 (Allyl) according to the procedures described in 4.7.4. **A** was subjected to the aminocatalysis-mediated on-resin Ugi macrocyclization in the presence of *n*-dodecylisocyanide as described in 4.7.4 to afford **B**. Resin-linked peptide **C** was synthesized by additional SPPS from **B**, then deprotected at Lys1 (Alloc) and Asp5 (Allyl) according to the procedures described in 4.7.4. **D** then was subjected

to the second aminocatalysis-mediated on-resin Ugi macrocyclization in the presence of *n*-dodecylisocyanide as described in 4.7.4. Cleavage with TFA/H<sub>2</sub>O/TIS 95:2.5:2.5 for 2 h afforded peptide **58** (59% cleavage yield), which was purified by semi-preparative RP-HPLC (12.2 mg, 29% isolated yield); *R*<sub>t</sub> 15.0 min, > 93% purity. ESI-HRMS, calcd. for C<sub>83</sub>H<sub>153</sub>N<sub>20</sub>O<sub>17</sub>: 850.5822 [M + 2H]<sup>2+</sup>. Found: *m/z* 850.5823 [M + 2H]<sup>2+</sup>.

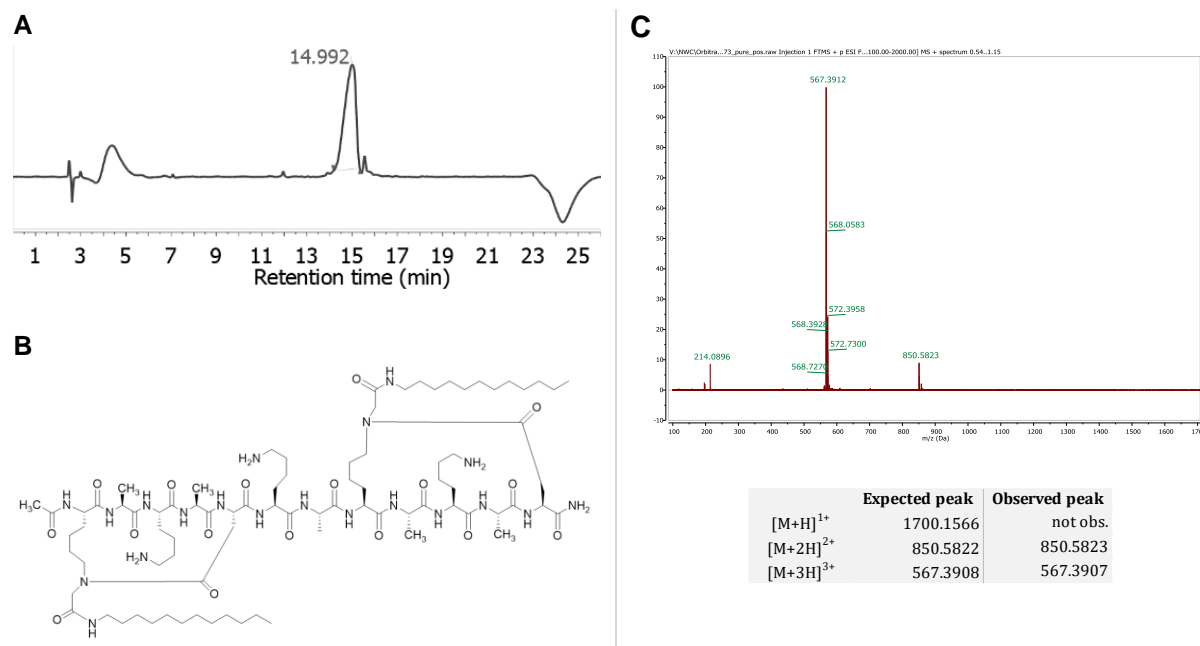
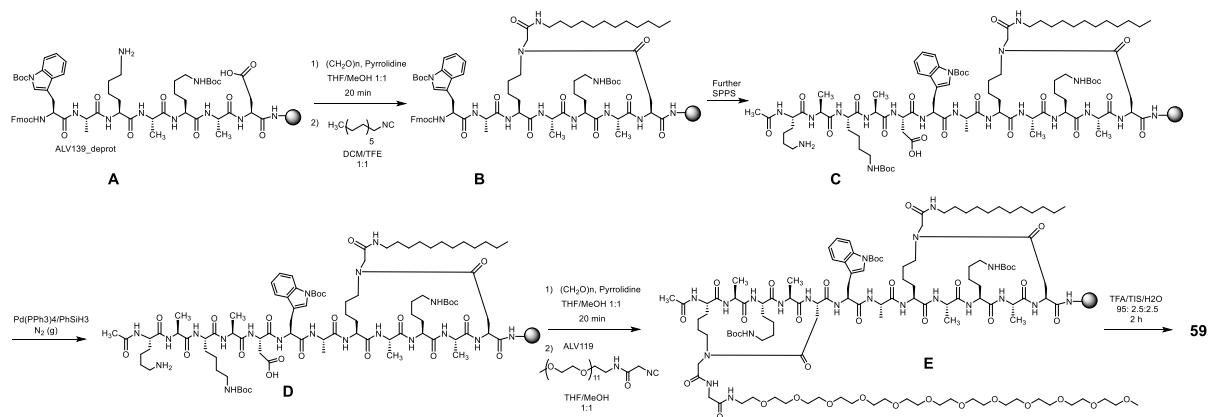


Figure 4.13. A) HPLC trace of purified peptide **58**. B) Structure of peptide **58**. C) ESI-HRMS of peptide **58**

### Lipidated/PEGylated Double Stapled Peptide **59**



The resin-linked peptide **A** was synthesized in a 25 μmol scale on Rink-Amide AM resin (179 mg, 0.14 mmol/g), then deprotected at Lys3 (Alloc) and Asp7 (Allyl) according to the procedures described in 4.7.4. **A** was subjected to the aminocatalysis-mediated on-resin Ugi macrocyclization in the presence of *n*-dodecylisocyanide as described in 4.7.4 to afford **B**.

Resin-linked peptide **C** was synthesized by additional SPPS from **B**, and next deprotected at Lys1 (Alloc) and Asp5 (Allyl) according to the procedures described in 4.7.4. **D** was then subjected to the aminocatalysis-mediated on-resin Ugi macrocyclization in the presence of *N*-(OMe-(PEG)<sub>11</sub>-ethyl)-2-isocyanoacetamide as described in 4.7.4. Cleavage with TFA/H<sub>2</sub>O/TIS 95:2.5:2.5 for 2 h afforded peptide **59** (64% cleavage yield), which was purified by semi-preparative RP-HPLC (9.4 mg, 17% isolated yield); *R*<sub>t</sub> 15.6 min, > 89% purity. ESI-HRMS, calcd. for C<sub>103</sub>H<sub>179</sub>N<sub>21</sub>O<sub>30</sub>: 1095.1563 [M + 2H]<sup>2+</sup>. Found: *m/z* 1095.1559 [M + 2H]<sup>2+</sup>.

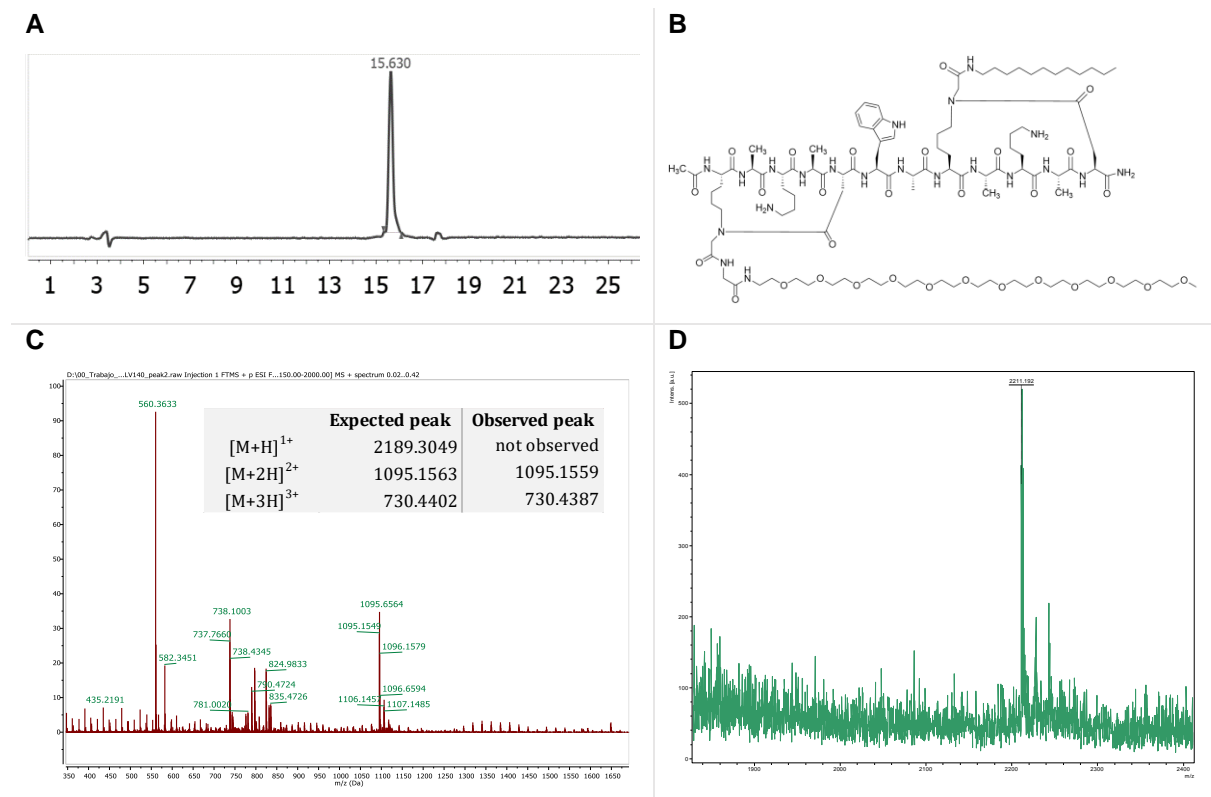


Figure 4.14. A) HPLC trace of purified peptide **59**. B) Structure of peptide **59**. C) ESI-HRMS of peptide **59**; and D) MALDI-TOF MS of stapled peptide **59**.

### Glycosylated/Fluorescent labeled Double Stapled Peptide **60**

The resin-linked peptide **A** was synthesized in a 25  $\mu$ mol scale on Rink-Amide AM resin (179 mg, 0.14 mmol/g), deprotected at Lys3 (Alloc) and Glu7 (Allyl) according to the procedures described in 4.7.4. **A** was subjected to the aminocatalysis-mediated on-resin Ugi macrocyclization in the presence of 2-(4-dimethylamino-1,8-naphthalimido)-ethyl isocyanide as described in 4.7.4 to afford **B**. Resin-linked peptide **C** was synthesized by additional SPPS from **B**, then deprotected at Lys1 (Alloc) and Glu5 (Allyl) according to the procedures described in 4.7.4. **D** was then subjected to the second aminocatalysis-mediated on-resin Ugi

macrocyclization in the presence of 2,3,4,6-tetra-O-acetyl- $\beta$ -D-glucopyranosyl isocyanide as described in 4.7.4.

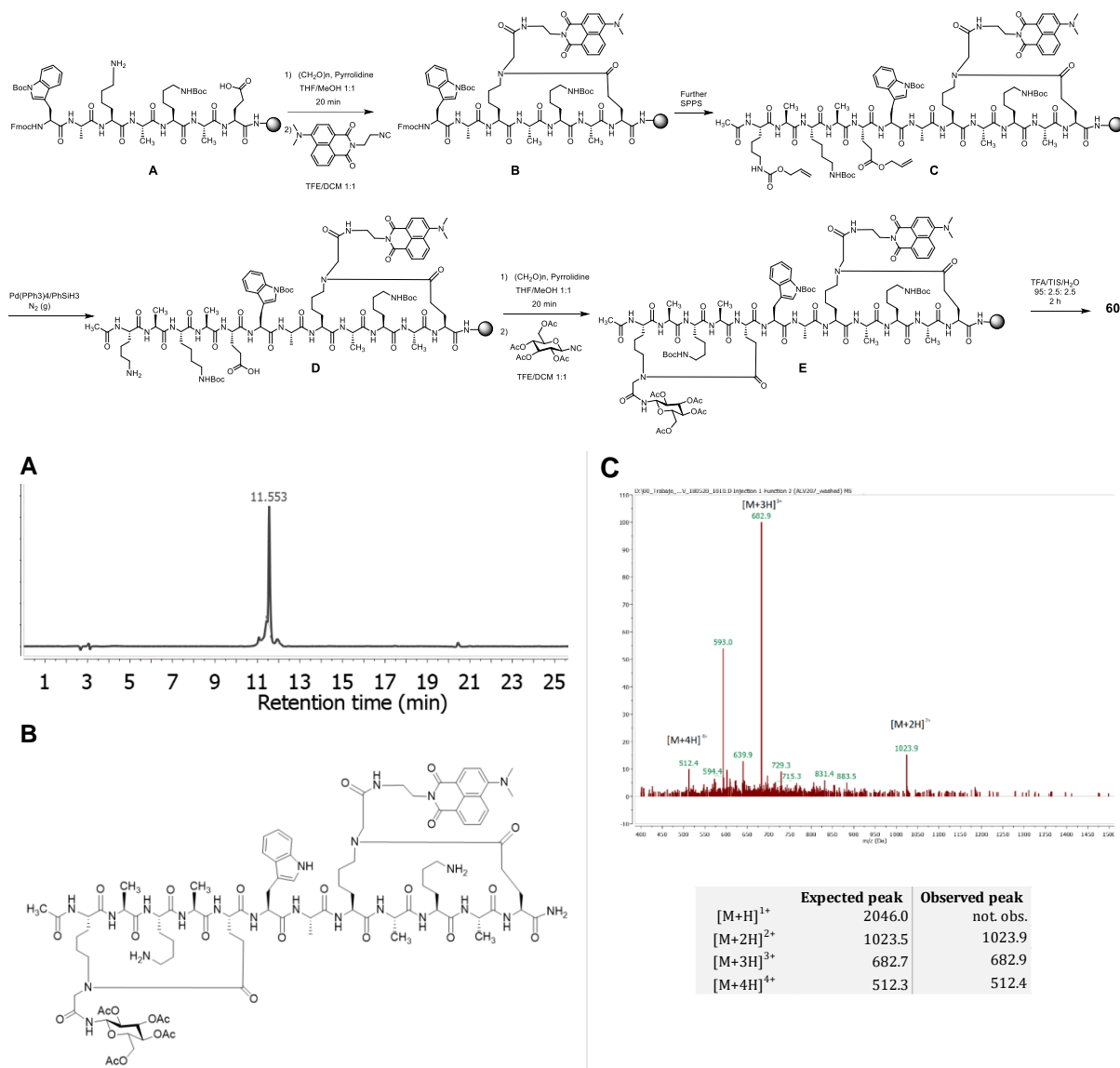


Figure 4.15. A) HPLC trace of purified peptide **60**. B) Structure of peptide **60**. C) ESI-MS of peptide **60**

Cleavage with TFA/H<sub>2</sub>O/TIS 95:2.5:2.5 for 2 h afforded peptide **60** (67% cleavage yield) which was characterized by analytical HPLC ( $R_t$  11.6 min, 9.7 mg (19% isolated yield); > 86% purity after semipreparative HPLC; ESI-MS, calcd. for C<sub>96</sub>H<sub>138</sub>N<sub>22</sub>O<sub>28</sub>: 1023.5  $[\text{M} + 2\text{H}]^{2+}$ . Found:  $m/z$  1023.9  $[\text{M} + 2\text{H}]^{2+}$ . Note: The compound proved unstable when kept in an even only slightly acidic aqueous solution.

### Maleimide Functionalized Stapled Peptide 61

Stapled peptide **61** was produced by on-resin cyclization in a 25  $\mu\text{mol}$  scale from Allyl/Alloc deprotected peptide **47** according to the aminocatalysis-mediated Ugi macrocyclization protocol described in 4.7.4, in the presence of *N*-(6-isocyano-hexanyl)maleimide. Cleavage with TFA/H<sub>2</sub>O/TIS 95:2.5:2.5 for 2 h afforded peptide **61** (73% cleavage yield), which was purified by semi-preparative RP-HPLC (16.5 mg, 41% isolated yield);  $R_t$  13.9 min, > 87% purity. ESI-HRMS, calcd. for C<sub>78</sub>H<sub>127</sub>N<sub>19</sub>O<sub>17</sub>: 800.9829 [M + 2H]<sup>2+</sup>. Found:  $m/z$  800.9803 [M + 2H]<sup>2+</sup>. Note: The compound proved unstable when kept in a slightly acidic aqueous solution.

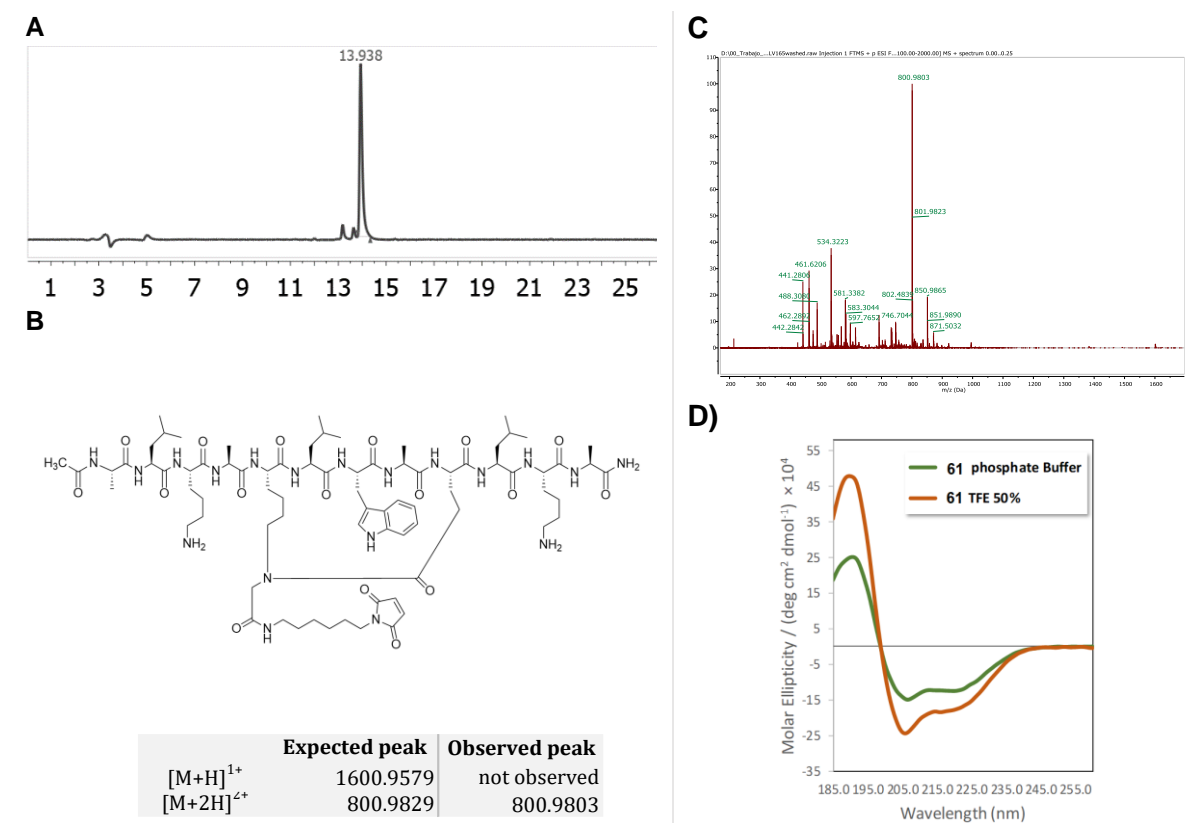


Figure 4.16. A) HPLC trace of purified peptide **61** B) Structure of peptide **61** C) ESI-HRMS of crude peptide **61** D) CD spectrum of pure peptide **61**

### Stapled Peptide-BSA Conjugate 62

Bovine serum albumin (BSA) (10 mg, 0.15  $\mu\text{mol}$ ) and maleimide-armed peptide **61** (1 mg, 0.63  $\mu\text{mol}$ ) were dissolved in a solution containing PBS pH 7.4 and 1 mM EDTA (1 mL). Nitrogen was bubbled into the solution and the reaction mixture was stirred for 4 h at room temperature. The conjugate was purified by membrane ultracentrifugation using a regenerated cellulose membrane (30 kDa) (Amicon® Ultr-15 30 kDa Centrifugal Filter Devices-Merck) with 95% recovery. As depicted in the MALDI-MS shown below, incomplete

consumption of the protein was observed. This observation is consistent with only ca. 50% of the Cys-34 residues in commercial BSA batches being available for reaction due to oxidation with adventitious cysteine, glutathione, etc.<sup>[35]</sup>

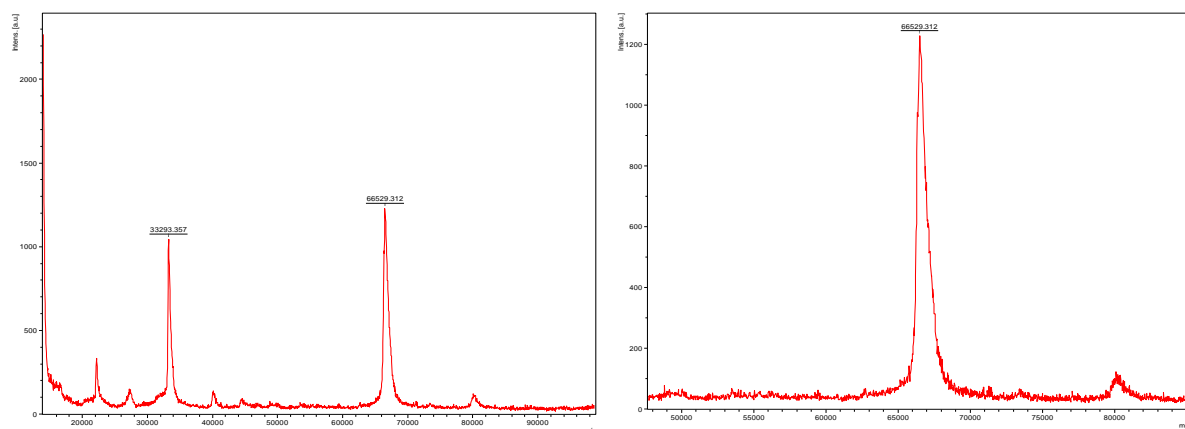


Figure 4.17. MALDI-TOF MS of BSA used for the conjugation

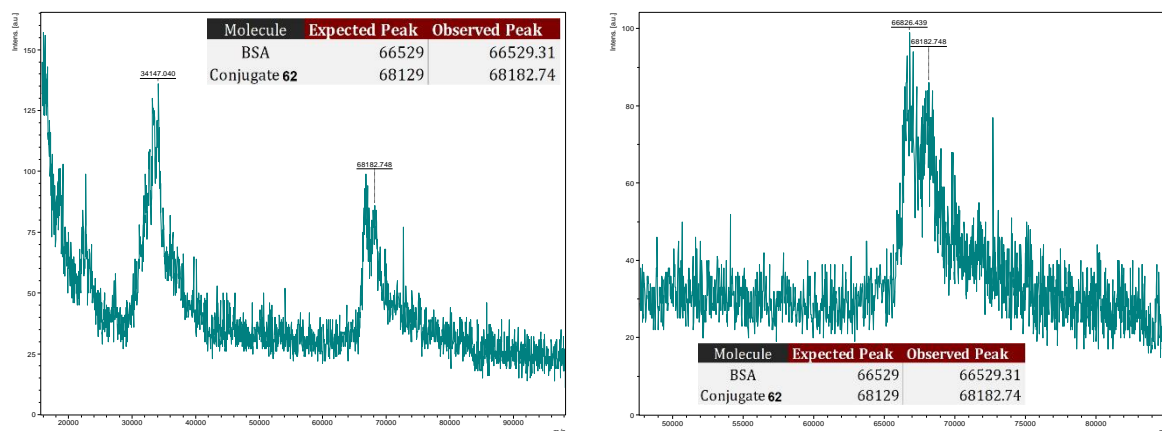


Figure 4.18. MALDI-TOF MS of BSA-peptide conjugate 62

### 4.7.7 Molecular Dynamics Simulations

For Stapled Peptide **57** a PDB structure with a helical conformation was generated within YASARA. According to the NMR data, *s-cis* configuration around the *N*-substituted lactam bridge was set initially. The structure was optimized using the AMBER 12 force field and the obtained coordinates were employed as starting point for a 100 ns MD simulation using AMBER 12 force field within YASARA. The starting model was placed in a water box with a physiological NaCl concentration of 0.9%. Periodic boundary conditions with pressure control at 298 K were utilized. Force field parametrizations for the novel residues based on semi-

empirical calculations were automatically calculated. The final trajectory was analyzed within YASARA, as well as VMD.

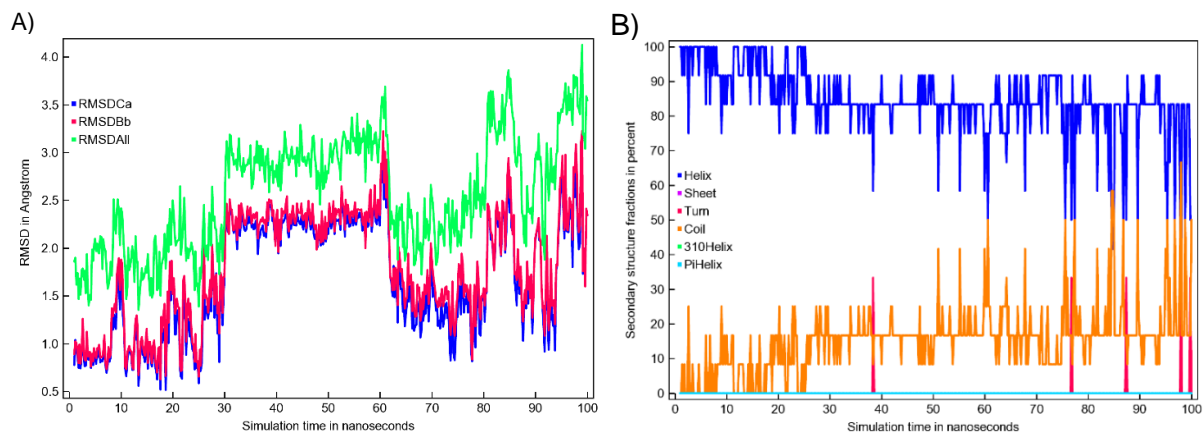


Figure 4.19. A) Solute RMSD from starting structure analysis and B) protein secondary structure analysis during 100 ns MD simulation for stapled peptide **57**

## 4.8. References

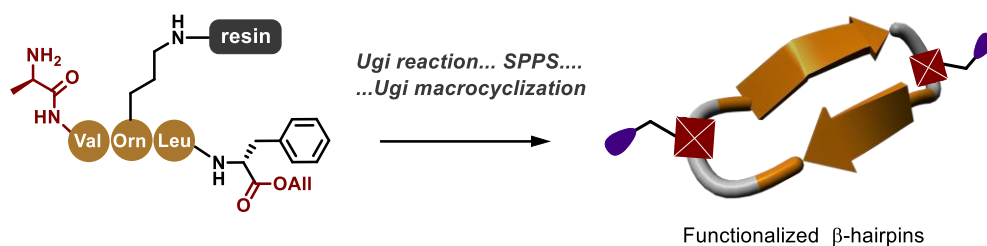
- [1] C. E. Schafmeister, J. Po, G. L. Verdine, *J. Am. Chem. Soc.* **2000**, *122*, 5891–5892.
- [2] L. D. Walensky, A. L. Kung, I. Escher, T. J. Malia, S. Barbuto, R. D. Wright, G. Wagner, G. L. Verdine, S. J. Korsmeyer, *Science (80-. )*. **2004**, *305*, 1466–1470.
- [3] Y. W. Kim, T. N. Grossmann, G. L. Verdine, *Nat. Protoc.* **2011**, *6*, 761–771.
- [4] A. M. Felix, E. P. Heimer, C. T. Wang, T. J. Lambros, A. Fournier, T. F. Mowles, S. Maines, R. M. Campbell, B. B. Wegrzynski, V. Toome, et al., *Int. J. Pept. Protein Res.* **1988**, *32*, 441–454.
- [5] M. E. Houston, C. L. Gannon, C. M. Kay, R. S. Hodges, *J. Pept. Sci.* **1995**, *1*, 274–282.
- [6] A. Bisello, C. Nakamoto, M. Rosenblatt, M. Chorev, *Biochemistry* **1997**, *36*, 3293–3299.
- [7] B. Hargittai, N. A. Solé, D. R. Groebe, S. N. Abramson, G. Barany, *J. Med. Chem.* **2000**, *43*, 4787–4792.
- [8] G. Ösapay, J. W. Taylor, *J. Am. Chem. Soc.* **1990**, *112*, 6046–6051.
- [9] C. Bracken, J. Gulyás, J. W. Taylor, J. Baum, *J. Am. Chem. Soc.* **1994**, *116*, 6431–6432.
- [10] N. E. Shepherd, H. N. Hoang, G. Abbenante, D. P. Fairlie, *J. Am. Chem. Soc.* **2005**, *127*, 2974–2983.
- [11] L. D. Walensky, G. H. Bird, *J. Med. Chem.* **2014**, *57*, 6275–6288.
- [12] P. M. Cromm, J. Spiegel, T. N. Grossmann, *ACS Chem. Biol.* **2015**, *10*, 1362–1375.
- [13] A. D. de Araujo, J. Lim, K.-C. Wu, Y. Xiang, A. C. Good, R. Skerlj, D. P. Fairlie, *J. Med. Chem.* **2018**, *61*, 2962–2972.
- [14] R. S. Harrison, G. Ruiz-Gómez, T. A. Hill, S. Y. Chow, N. E. Shepherd, R. J. Lohman, G. Abbenante, H. N. Hoang, D. P. Fairlie, *J. Med. Chem.* **2010**, *53*, 8400–8408.

- [15] N. L. Mills, M. D. Daugherty, A. D. Frankel, R. K. Guy, *J. Am. Chem. Soc.* **2006**, *128*, 3496–3497.
- [16] N. E. Shepherd, H. N. Hoang, V. S. Desai, E. Letouze, P. R. Young, D. P. Fairlie, *J. Am. Chem. Soc.* **2006**, *128*, 13284–13289.
- [17] Y. H. Lau, P. de Andrade, Y. Wu, D. R. Spring, *Chem. Soc. Rev.* **2015**, *44*, 91–102.
- [18] T. A. Hill, N. E. Shepherd, F. Diness, D. P. Fairlie, *Angew. Chem., Int. Ed.* **2014**, *53*, 13020–13041.
- [19] M. Pelay-gimeno, A. Glas, O. Koch, T. N. Grossmann, *Angew. Chem., Int. Ed.* **2015**, *54*, 8896–8927.
- [20] K. Sharma, D. L. Kunciw, W. Xu, M. M. Wiedmann, Y. Wu, H. F. Sore, W. R. J. D. Galloway, Y. H. Lau, L. S. Itzhaki, D. R. Spring, in *Cycl. Pept. From Bioorganic Synth. to Appl.*, The Royal Society Of Chemistry, **2017**, pp. 164–187.
- [21] K. Holland-Nell, M. Meldal, *Angew. Chem., Int. Ed.* **2011**, *50*, 5204–5206.
- [22] Ø. Jacobsen, H. Maekawa, N. H. Ge, C. H. Görbitz, P. Rongved, O. P. Ottersen, M. Amiry-Moghaddam, J. Klaveness, *J. Org. Chem.* **2011**, *76*, 1228–1238.
- [23] G. Lautrette, F. Touti, H. G. Lee, P. Dai, B. L. Pentelute, *J. Am. Chem. Soc.* **2016**, *138*, 8340–8343.
- [24] S. P. Brown, A. B. Smith, *J. Am. Chem. Soc.* **2015**, *137*, 4034–4037.
- [25] A. M. Spokoyny, Y. Zou, J. J. Ling, H. Yu, Y. S. Lin, B. L. Pentelute, *J. Am. Chem. Soc.* **2013**, *135*, 5946–5949.
- [26] H. Jo, N. Meinhardt, Y. Wu, S. Kulkarni, X. Hu, K. E. Low, P. L. Davies, W. F. Degrado, D. C. Greenbaum, *J. Am. Chem. Soc.* **2012**, *134*, 17704–17713.
- [27] L. Mendive-Tapia, S. Preciado, J. García, R. Ramón, N. Kielland, F. Albericio, R. Lavilla, *Nat. Commun.* **2015**, *6*, 7160.
- [28] A. F. M. Noisier, J. García, I. A. Ionuț, F. Albericio, *Angew. Chem., Int. Ed.* **2017**, *56*, 314–318.
- [29] Y. Wu, F. Villa, J. Maman, Y. H. Lau, L. Dobnikar, A. C. Simon, K. Labib, D. R. Spring, L. Pellegrini, *Angew. Chem., Int. Ed.* **2017**, *56*, 12866–12872.
- [30] Y. Wu, L. B. Olsen, Y. H. Lau, C. H. Jensen, M. Rossmann, Y. R. Baker, H. F. Sore, S. Collins, D. R. Spring, *ChemBioChem* **2016**, *17*, 689–692.
- [31] Y. H. Lau, P. de Andrade, S.-T. Quah, M. Rossmann, L. Laraia, N. Sköld, T. J. Sum, P. J. E. Rowling, T. L. Joseph, C. Verma, et al., *Chem. Sci.* **2014**, *5*, 1804–1809.
- [32] N. Assem, D. J. Ferreira, D. W. Wolan, P. E. Dawson, *Angew. Chem., Int. Ed.* **2015**, *54*, 8665–8668.
- [33] F. E. Morales, H. E. Garay, D. F. Muñoz, Y. E. Augusto, A. J. Otero-González, O. Reyes Acosta, D. G. Rivera, *Org. Lett.* **2015**, *17*, 2728–2731.
- [34] R. K. Harris, E. D. Becker, S. M. Cabral De Menezes, R. Goodfellow, P. Granger, *Concepts Magn. Reson. Part A Bridg. Educ. Res.* **2002**, *14*, 326–346.

[35] D. C. Carter, J. X. Ho, *Adv. Protein Chem.* **1994**, *45*, 153–203.

## Chapter 5.

# Synthesis of novel *N*-backbone modified analogs of Gramicidin S by Ugi-4C reaction



---

**ABSTRACT:** The present chapter describes the synthesis of *N*-functionalized  $\beta$ -hairpin peptides analogs of Gramicidin S through a synthetic approach comprising the on-resin Ugi head-to-tail cyclization of the peptide skeleton. The Ugi-derived *N*-functionalization proved successful to mimic proline's  $\beta$ -turn stabilization effect within this sequence when one or both proline residues were replaced. NMR solution structure in DMSO for the compounds was assessed in order to prove the  $\beta$ -hairpin folding of the peptide backbone.

---

\* The content within this chapter has been accepted for publication in Organic Letters as: Manuel G. Ricardo, Aldrin V. Vasco,<sup>†,§</sup> Daniel G. Rivera, and Ludger A. Wessjohann, "On the Stabilization of Cyclic  $\beta$ -Hairpins by Ugi Reaction-Derived *N*-Alkylated Peptides: The Quest for Functionalized  $\beta$ -Turns". DOI: 10.1021/acs.orglett.9b02592  
Author contribution: Synthesis of half of cyclic peptides, partial NMR analysis, Molecular Dynamics simulations.

## 5.1. Introduction

Tight turns comprise protein motifs characterized for reversing the directionality of the peptide backbone. Such a class of non-repetitive secondary structures possesses significant implications for achieving protein three dimensional structure, since they allow the polypeptide chain to fold into compact globular structures.<sup>[1]</sup> Additionally, their frequent location on exposed protein surfaces makes them to be involved in several molecular recognition processes crucial for triggering biological events. Therefore, extensive efforts have been addressed to the synthesis of  $\beta$ -turn mimetics, some of them depicted in figure 1.<sup>[2–5]</sup> A renowned model to address the suitability of a mimetic of  $\beta$ -turn consists of evaluating their destabilization effect towards ideal head-to-tail cyclic  $\beta$ -hairpins.<sup>[6,7]</sup> Such cyclic peptides – comprising two  $\beta$ -turns flanked by two anti-parallel  $\beta$ -strands– have turned out to be excellent systems for fine mimicking naturally-occurring epitopes mediating medically-relevant protein-protein interactions.<sup>[4,7–9]</sup> Moreover, important antimicrobial peptides found in nature possess a  $\beta$ -hairpin structure stabilized from side chain-to-side chain or head-to-tail cyclization.<sup>[10–12]</sup> Among these antimicrobial peptides, Gramicidin S (GS, **63**) stands as one of the most studied models.<sup>[13–15]</sup> It possesses a cyclic structure in which the  $\beta$ -hairpin structure includes two type II'  $\beta$ -turns featuring a turn inducer D-Phe-Pro motif (Figure 1A). Additionally, the molecule possesses a marked amphiphilic character, bearing two positively-charged ornithine residues in one of the faces and highly hydrophobic side chains in the opposite face.

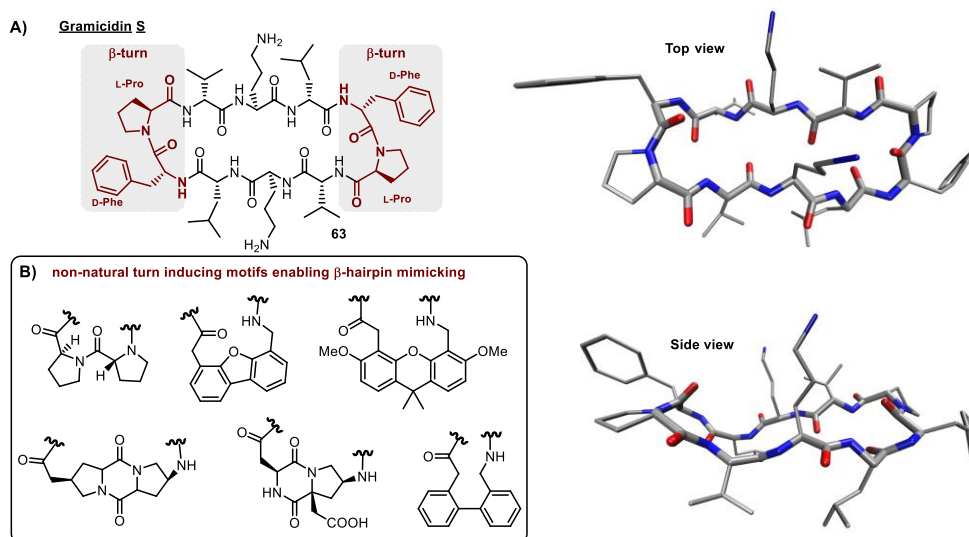


Figure 5.1. A) Structure of Gramicidin S B) Synthetic tight-turns inducers enabling the synthesis of protein mimetics possessing  $\beta$ -hairpin structure

Extensive synthetic approaches to the preparation of mimetics of GS have been addressed, including the modification of the side chains,<sup>[16–20]</sup> the ring size<sup>[21,22]</sup> and the  $\beta$ -turn moiety.<sup>[5,6,22–25]</sup> Based in our previous reports evidencing the ability of Ugi-derived *N*-alkylated fragments to successfully favor the folding of short peptide skeletons into  $\beta$ -turn like structures,<sup>[26]</sup> it seemed reasonably to evaluate the capacity of such motifs for the stabilization of  $\beta$ -hairpins structures. Considering the proved efficacy of Ugi macrocyclization to insert cationic and lipidic derivatization during the peptide tethering,<sup>[27,28]</sup> it resulted interesting to evaluate the effect of such backbone *N*-substitutions in  $\beta$ -hairpins possessing facial amphiphilicity. For this purpose, we chose to mimic the proline residues in Gramicidin S with those coming from the Ugi-reaction.

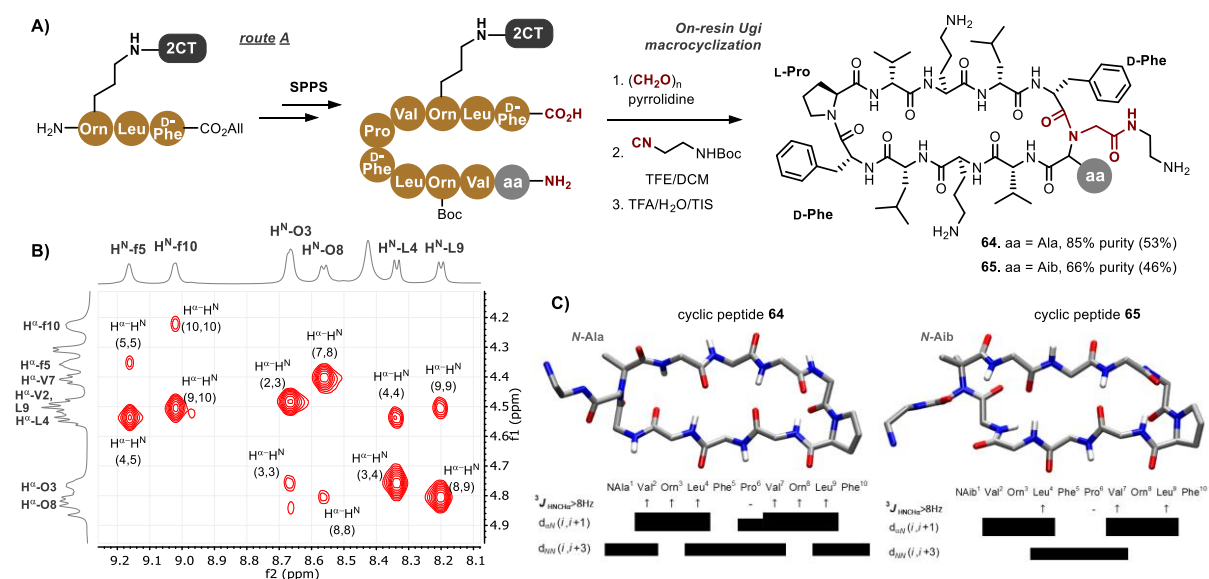
## 5.2. Synthetic plan

In order to successfully substitute the proline residues in GS for Ugi-derived tertiary amides, we decided to design an approach comprising the major synthetic steps to be conducted on-resin. We envisioned that it should be possible to achieve not only the assembly, but also the macrocyclization of the peptide skeleton with the growing chain attached to the solid support. Consequently, the macrocyclic peptide can be cleaved from the resin at the same time that the deprotection of acid-sensitive protecting groups is accomplished. So that the head-to-tail on-resin cyclization could be achieved, the attachment of the peptide to the resin must be conducted through one of the side chains. Therefore, the first step of our approach was the attachment of the tripeptide Fmoc-Orn-Leu-D-Phe-OAll to a 2-chlorotrytilchloride resin, enabling the Pd(0)-mediated selective C-terminal deprotection after peptide growth (Scheme 5.1A, route A). We envisioned that, due to the presence of two  $\beta$ -turns within the targeted peptides, the best cyclization spot would be located at one of the turns. In this way, the spatial proximity of the reacting *N*- and *C*- termini would be favored from the presence of a  $\beta$ -turn inducing moiety in the middle of the sequence.

## 5.3. Mono-substituted GS analogs

Since a recent study has proven that the replacement of proline for *N*-Me-Ala does not affect the activity of the corresponding GS analogues,<sup>[29]</sup> our first approach consisted on utilizing an *N*-terminal alanine residue as amino component of the Ugi-macrocyclization, thus leading to an *N*-substituted Ala residue as for cyclic peptide **64**. To compare whether the side chain of the amino acid bearing the *N*-substitution influences the  $\beta$ -hairpin structure or not, peptide **65**

– bearing an *N*-substituted Aib residue – was synthesized. Due to the known biological (and therefore structural) relevance of cationic residues within these amphiphilic peptides,<sup>[17]</sup> for both compounds an amino-containing isocyanide was utilized for the macrocyclization. To avoid the undesired occurrence of diastomeric mixtures, paraformaldehyde was chosen as oxo-component. As depicted in scheme 5.1, the proposed strategy enables the obtention of the crude peptides in a moderate to good purity considering that a head-to-tail cyclization reaction is achieved. Furthermore, the synthesis of peptide **65** comprises the utilization of a highly hindered Aib as cyclizing *N*-terminal amino acid, which is known to be disfavored by traditional peptide coupling.<sup>[30,31]</sup>



Scheme 5.1. A) Strategy for the on-resin synthesis of mono-substituted Ugi-derived Gramicidin S analogs. In parenthesis are reported the yields of crude products; enough sample was purified to >95% purity in order to measure NMR spectra. B)  $\text{H}^{\text{N}}\text{-H}^{\alpha}$  region of the ROESY spectrum (mix.  $T = 300\text{ms}$ ) of cyclic peptide **64**. C) NMR-derived average structures for cyclic peptides **64** and **65**, and summary of structurally-relevant NMR information. The thickness of the black bars indicates the strength of the observed ROE contact and the arrows represent coupling constants higher than 8 Hz. Side chains are excluded for better clarity.

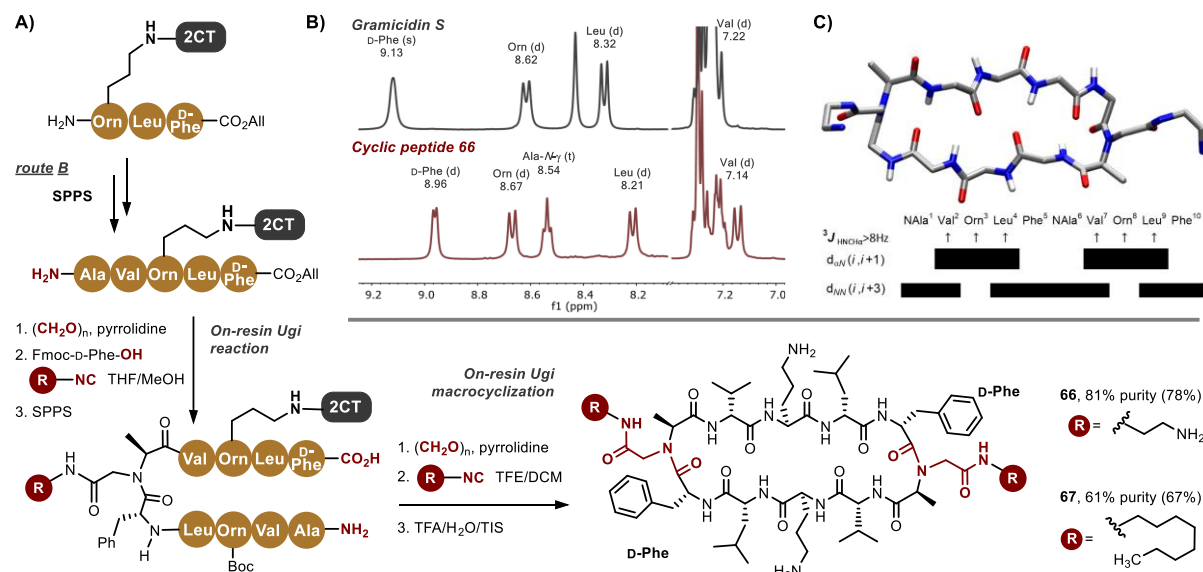
Analysis of the NMR spectra of cyclic peptide **64** in DMSO agrees with that expected for a  $\beta$ -hairpin structure. As clearly seen in the ROESY spectrum (Scheme 5.1B), inter-residue  $\text{H}^{\alpha}_i \leftrightarrow \text{H}^{\text{N}}_{i+1}$  ROE crosspeaks are much more intense than the intra-residue  $\text{H}^{\alpha}_i \leftrightarrow \text{H}^{\text{N}}_i$  which, in conjunction with the observation of  $^3J_{\text{HN-H}\alpha}$  higher than 8 Hz, indicate an extended conformation for the segments 2-4 and 7-9.<sup>[5]</sup> Additionally, inter-strand  $\text{H}^{\text{N}}_i \leftrightarrow \text{H}^{\text{N}}_{i+3}$  NOEs between Leu4-Val7 and Leu9-Val2 were detected, confirming the turn structure comprising these segments. Also indicative of a turn structure was the  $^3J_{\text{HN-H}\alpha}$  value lower than 4Hz found

for both D-Phe residues.<sup>[32]</sup> Moreover, inter-strand crosspeaks between the alpha hydrogens of both ornithine residues were also present in the ROESY spectrum which confirms the spatial proximity of both strands characteristic of a hairpin-like conformation. The NMR-derived structural information was employed for a structure refinement protocol within XPLOR-NIH<sup>[33]</sup> as previously described in Chapter 2. The average from the best structures is represented in scheme 5.2C. As expected, the molecule occurs in a  $\beta$ -hairpin conformation in which the Ugi-derived tertiary amide incorporates an additional amino group. Nevertheless, the *N*-substituent doesn't seem to interact intramolecularly and therefore doesn't influence the  $\beta$ -hairpin structure. In contrast, the insertion of an *N*-functionalized Aib as proline mimetic as in cyclic peptide **65** clearly distorts the ideal hairpin conformation. In this case only Leu4, Val7 and Leu9 amide protons show  $^3J_{\text{HN-H}\alpha}$  higher than 8 Hz. Furthermore,  $\text{H}^{\text{N}}_{i} \leftrightarrow \text{H}^{\text{N}}_{i+3}$  NOEs indicative of  $\beta$ -turns are only observed between the residues in the turn region enclosing the proline residue. The resulting NMR structure shows a distorted  $\beta$ -hairpin with an open turn involving the *N*-substituted Aib residue, while the opposite side of the molecule encompasses a  $\beta$ -turn stabilized by the D-Phe-Pro motif. Even when Aib is known to favor helical turns, in this case additional steric hindrance arising from the  $\alpha,\alpha$ -dialkylation towards the *N*-substitution seems to force the backbone to twist apart from the  $\beta$ -turn-stabilizing conformation, thus leading to the subsequent rupture of the ideal  $\beta$ -hairpin structure. It has also been described that the heterochirality at positions *i*+1 and *i*+2 is essential for the stabilization of type II'  $\beta$ -turns.<sup>[34]</sup>

#### 5.4. Di-substituted GS analogs

A slightly different synthetic route as that described in scheme 5.1A can be implemented in order to substitute not one, but both proline residues in GS (Scheme 5.2A, route B). After tripeptide attachment to the resin, valine and alanine are respectively coupled by traditional SPPS using the Fmoc/tBu strategy. The resulting *N*-terminal deprotected pentapeptide is submitted to on-resin Ugi reaction leading to the *N*-substitution of the Alanine and the incorporation of the D-Phe moiety. Further solid phase peptide synthesis and selective C-terminal deprotection enables the peptide to be subjected to a final Ugi-mediated macrocyclization with the subsequent *N*-functionalization of the cyclizing tertiary amide depending on the nature of the reacting isocyanide. While in cyclic peptide **66** the cationic nature of the *N*-substitution was maintained, cyclic peptide **67** was intended to incorporate two hydrophobic residues coming from the utilization of *n*-octyl-isocyanide. It should be

noticed that the yield and purity obtained for these cyclic peptides are comparable, and even better, than those reported in the synthesis of peptides **64** and **65**, where only one of the proline residues of GS was replaced. The latter could be indicative of the capacity of the first *N*-substitution inserted by the Ugi reaction to induce a turn-like conformation of the peptide skeleton which favours the spatial proximity of the cyclizing *N*- and *C*- termini. The turn inducing effect of Ugi-derived tertiary amides has been previously reported by our group. [26,35]



Scheme 5.2. A) Strategy for the synthesis of di-substituted analogs of Gramicidin S by double Ugi reaction. In parenthesis are reported the yields of crude products; enough sample was purified to >95% purity in order to measure NMR spectra. B) Amide region of the  $^1\text{H-NMR}$  spectra of Gramicidin S and cyclic peptide **66**. C) NMR-derived average structure of cyclic peptide **66**, and summary of structurally-relevant NMR information. Side chains are excluded for better clarity.

As perceived in scheme 5.2B, for cyclic peptide **66** only five amide protons are observed in the  $^1\text{H-NMR}$  spectrum. This latter is indicative of molecular symmetry which is a characteristic of Gramicidin S (i.e., one spin system is found for every amino acid type).<sup>[5,36]</sup> Moreover,  $^1\text{H}$  chemical shifts and  $^3J_{\text{HN-H}\alpha}$  for amide protons of cyclic peptide **66** and Gramicidin S possess high similarity, which points to conformational resemblance between the compounds. The higher difference between amide chemical shift is observed for the D-Phe residue (0.17 ppm) which is logical since the major structural differences correspond to this region of the molecule. As could be seen in Scheme 5.2C,  $^3J_{\text{HN-H}\alpha}$  values higher than 8 Hz as well as strong inter-residue  $\text{H}^{\alpha}_i \leftrightarrow \text{H}^{\text{N}}_{i+1}$  ROE crosspeaks confirmed the extended conformation for Val, Orn and Leu residues. In the same way, inter-strand  $\text{H}^{\text{N}}_i \leftrightarrow \text{H}^{\text{N}}_{i+3}$  NOEs between Leu and Val residues confirmed the turn-like conformation enclosed by these residues. The NMR-derived

three dimensional structure in solution was proposed after simulated annealing and refinement protocols within Xplor-NIH. In agreement with the NMR information, the peptide backbone appears to occur in a  $\beta$ -hairpin conformation featuring two amino groups inserted as *N*-backbone substitutions at the  $\beta$ -turn regions. Interestingly, the  $^1\text{H-NMR}$  spectrum of cyclic peptide **67**, containing two *N*-lipidated moieties, resulted very similar to that of cyclic peptide **66** (see annexes). Consequently, we did not consider necessary to perform an MD-assisted NMR-based structure refinement to conclude that this peptide also occurs in a  $\beta$ -hairpin conformation. Apparently, the nature of the *N*-substitution doesn't affect dramatically the  $\beta$ -hairpin conformation. This results are in accordance with those observed in Chapter 2 for cyclic  $\beta$ -turn peptides.

In agreement with the NOE and  $^3J_{\text{HN-H}\alpha}$  data, the temperature coefficients of amides of Leu and Val residues in compounds **64**, **65** and **66** were in the range expected for hydrogen-bonding, confirming the occurrence of a close beta-turn in compounds **64** and **66**. In contrast with these compounds, the irregular turn described for peptide **65** comprises the observation of a very low temperature dependence of Phe10 amide (the residue next to the *N*-substituted amino acid). Careful inspection of the NMR structures shows the possible hydrogen-bonding interaction of this amide with the carbonyl of the Val2, thus leading to a  $\gamma$ -turn.

In contrast to the expected reinforcement of the amphiphilicity for compounds **64**, **65** and **66** containing a *N*-substituted moiety with cationic character, the obtained NMR structures show the extra amino groups pointing to the face of the  $\beta$ -hairpin opposite to the side chains of the ornithine residues (Figure 5.2A). A deeper analysis of the Ugi-stabilized  $\beta$ -turn within peptides **64** and **66** revealed a preferential disposition of the tertiary amide to occur in an axial conformation respect to the plane defined by the  $\beta$ -hairpin. In contrast with the ideal type II'  $\beta$ -turn found in GS, the replacement of proline for *N*-Ala at the  $\beta$ -turn inducing moiety supposes the substitution of a chiral "cyclic" *N*-substituted aminoacid for a chiral "open" – and therefore less constrained – *N*-substituted one. The direct consequence is the preferred accommodation of the Phe side chain, the *N*-substitution and the Ala-side chain in an equatorial-axial-equatorial disposition respect to the plane defined by the hairpin. The latter contrasts with the equatorial-axial disposition of the side-chains of residues  $i+1$  and  $i+2$  in ideal type II'  $\beta$ -turns, firstly postulated by Rose *et. al.*<sup>[37]</sup> and supported by Wishart and coworkers.<sup>[7]</sup> An observation supporting the idea of an equatorial disposition of the D-Phe sidechain is the big chemical shift anisotropy affecting the diastereotopic  $N^{\alpha}$  methylene protons of the *N*-Ala. This anisotropic effect has been described for  $\delta$  hydrogens of proline in type II'

$\beta$ -turns and can be directly correlated with the  $\beta$ -sheet content of  $\beta$ -hairpins, i.e. the higher the chemical shift separation of the geminal hydrogens, the higher the  $\beta$ -sheet content on the peptides.<sup>[7]</sup> As evidenced in the NMR spectra, this difference is higher than 1 ppm in cyclic peptides **64**, **66** and **67**. In the case of cyclic peptide **65**, the difference between the  $N^\alpha$  methylene protons chemical shifts is less than 0.2 ppm, supporting the occurrence of the turn far away from the “ideal” type II'  $\beta$ -turn conformation reflected in a lesser  $\beta$ -sheet content.

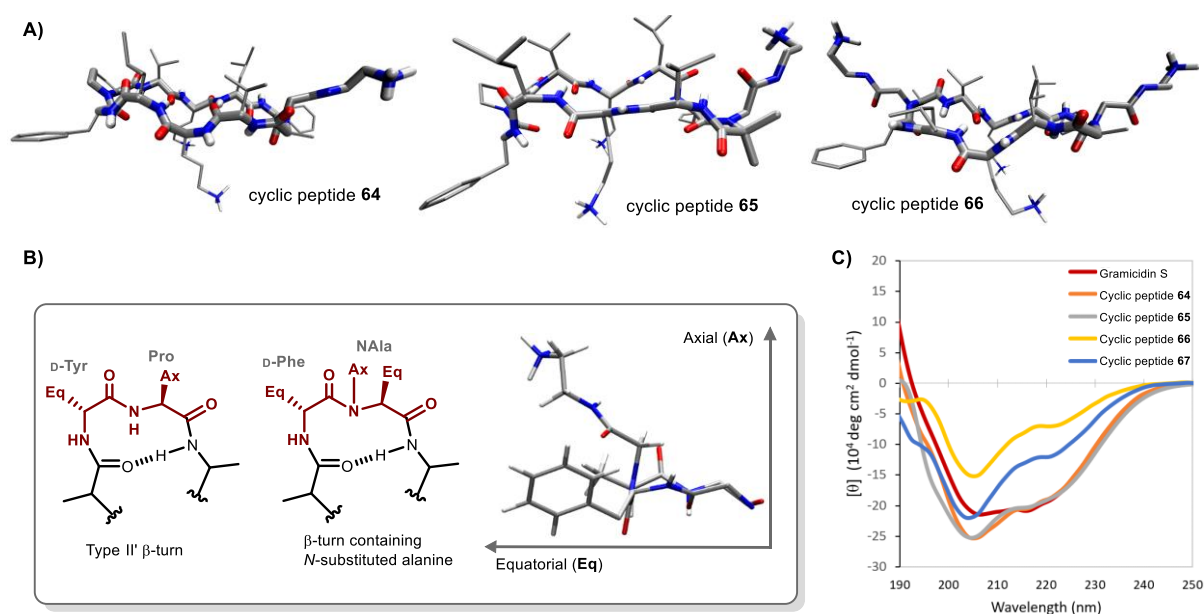


Figure 5.2. A) Side chain orientation of the average structures for cyclic peptides **64**, **65** and **66**. B) Comparison between the spatial disposition of the side chains and  $N$ -substitution within the turn region and that expected for an ideal disposition in type II'  $\beta$ -turns according to Wishart and coworkers.<sup>[7]</sup> C) CD of the compounds in phosphate buffer at 25 °C and pH 7.2

Inconsistently, the CD spectra in water of the synthesized compounds show that only cyclic peptides **64** and **65** seem to occur in a conformation close to that of GS. In double-substituted peptides **66** and **67**, a clear decrease of the  $\beta$ -sheet content is evidenced by a lower intensity of the band around 220 nm, while the predominant band at 205 nm – arising from its type II'  $\beta$ -turn in the case of GS –<sup>[7]</sup> is maintained in cyclic peptide **67** and partially reduced in peptide **66**. A possible rationalization could be that the additional  $N^\beta$  amide group inserted at the tertiary amide influences the shape of the expected bands towards a more “random coil-like” CD spectrum. The effect should be expected to be higher in those peptides containing two  $N$ -substitutions. Nevertheless, it should not be excluded the possibility that these compounds occur in a different conformation in water, since the solvation effects could differ substantially. Moreover, as previously evidenced in other chapters of this thesis, a change in the solvent

could enable the occurrence of *s-cis/s-trans* isomerism around the Ugi-derived tertiary amide, and this phenomenon is likely to be more critical in compounds containing two *N*-substitutions where up to four possible conformers could be present.

## 5.5. Conclusions

A new type of cyclic  $\beta$ -hairpin comprising the on-resin Ugi head-to-tail macrocyclization of peptides has been synthesized. Enough NMR data supports that the incorporation of *N*-alkylated amino acid residues by Ugi reactions may induce  $\beta$ -turn conformations and, thereby, stabilize the  $\beta$ -hairpin architecture. Thus, the incorporation D-Phe at *i*+1 position and *N*-substituted Ala at *i*+2 opposed to the native D-Phe-Pro retains the overall  $\beta$ -hairpin conformation of GS. However, the substitution of Pro (*i*+2) by *N*-alkylated Aib leads to partially distorted  $\beta$ -hairpin conformation. The D-Phe-*N*Ala motif could be effectively employed for the substitution of both native  $\beta$ -turns in GS with preservation of the  $\beta$ -hairpin conformation. We foresee as the most relevant result the fact that this Ugi reaction-based approach allows the stabilization of a  $\beta$ -hairpin and its simultaneous functionalization at the  $\beta$ -turn motifs. This structural modification could be used not only to modulate the bioactivity of  $\beta$ -hairpin peptides (e.g., polarity and cationic/anionic character), but also to install bioconjugation handles, fluorescent tags, etc., in  $\beta$ -hairpins designed as mimetics of protein epitopes.<sup>9</sup>

## 5.6. Experimental part

### **5.6.1 General Information:**

All starting materials were purchased from commercial sources and used without further purification. <sup>1</sup>H NMR and <sup>13</sup>C NMR spectra were recorded either in a Varian Mercury 400 NMR spectrometer at 399.94 MHz and 100.57 MHz, respectively or in an Agilent (Varian) VNMR 600 NMR spectrometer at 599.83 MHz and 150.83 MHz, respectively. Chemical shifts ( $\delta$ ) are reported in ppm relative to the TMS (<sup>1</sup>H NMR) and to the solvent signal (<sup>13</sup>C NMR). The positive- and negative-ion high-resolution ESI mass spectra were obtained with an Orbitrap Elite mass spectrometer (Thermo Fisher Scientific, Germany) equipped with an HESI electrospray ion source (positive spray voltage 4.5 kV, negative spray voltage 3.5 kV, capillary temperature 275 °C, source heater temperature 250 °C, FTMS resolution 30000). A TripleToF 6600-1 mass spectrometer (Sciex) was also used for high-resolution mass spectrometry, which was equipped with an ESI-DuoSpray-Ion-Source (it operated in positive ion mode) and

was controlled by Analyst 1.7.1 TF software (Sciex). The ESI source operation parameters were as follows: ion spray voltage: 5,500 V, nebulizing gas: 60 p.s.i., source temperature: 450 °C, drying gas: 70 p.s.i., curtain gas: 35 p.s.i. Data acquisition was performed in the MS1-ToF mode, scanned from 100 to 1500 Da with an accumulation time of 50 ms. Analytical RP-HPLC analysis was performed with an Agilent 1100 system in a reverse-phase C18 column (4.6 × 150 mm, 5 μm) with a PDA detector. A linear gradient from 5% to 80% of solvent B in solvent A over 20 min at a flow rate of 0.8 mL/min was used. The preparative purification was performed on Knauer 1001 system with UV detector K-2501. Separation was achieved using an RP C18 column (25 × 250 mm, 25 μm). A linear gradient from 15% to 40% of solvent B in solvent A over 20 min at a flow rate of 5 mL/min was used. Detection was accomplished at 210 nm. Solvent A: 0.1% (v/v) formic acid (FA) in water. Solvent B: 0.1% (v/v) FA in acetonitrile.

### **5.6.2 General methods for the Solid Phase Peptide Synthesis**

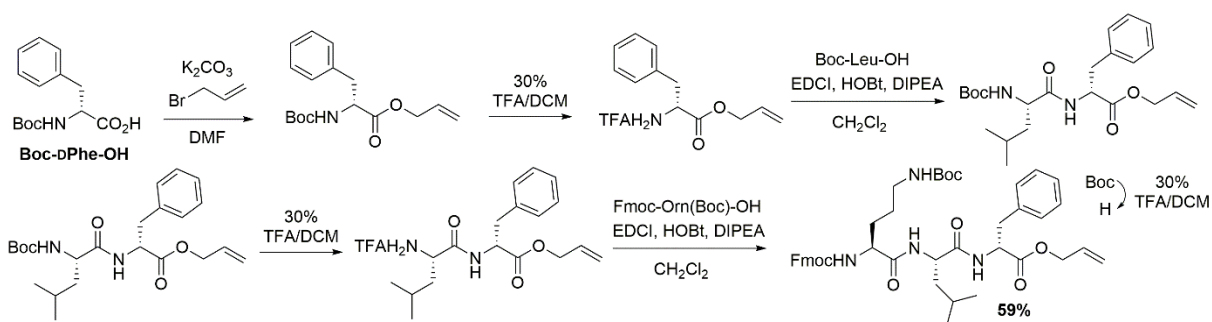
Coupling reactions were carried out manually on TG-S-RAM (Iris Biotech) resin (0.4 g, 0.24 mmol/g) by a stepwise Fmoc/*t*Bu strategy. **Swelling:** The resin is swelled for 20 min in DCM. **Fmoc removal:** The resin is treated with a solution of 20% piperidine in DMF (2×10 min), then washed with DCM (3×1 min) and DMF (2×1 min). **DIC/HOBt coupling:** Fmoc protected amino acid (4.0 eq.) and HOBt (4.0 eq.) are dissolved in DMF, then DIC (4 eq.) is added. The mixture is pre-activated for 5 min, added to the resin, and stirred at room temperature until completion as indicated by the Kaiser test.<sup>[38]</sup> The resin is washed with DCM (3×1 min) and DMF (2×1 min). **Allyl Removal:** The resin is washed with dry DCM (2×2 min) under a stream of nitrogen. A solution of phenylsilane (20 eq.) in dry DCM and tetrakis(triphenylphosphine) palladium(0) (0.2 eq.) are added to the resin under a continuous stream of nitrogen. The reaction mixture is stirred in the dark for 15 min, and the procedure is repeated once and then washed with 0.5% of sodium diethyldithiocarbamate trihydrate in DMF (5×2 min) and DCM (2×2 min). **Aminocatalysis-mediated Ugi reaction:** The free *N*-terminal resin-bound peptide is subjected to imine formation by treating the resin beads with a suspension of paraformaldehyde (4 eq.) and pyrrolidine (4 eq.) in THF/MeOH (1:1) for 30 min. The excess of reagents is removed by washing the beads with THF (4×1 min). A solution of the Fmoc-protected amino acid (4 eq.) in 2 mL of THF/MeOH (1:1) and another of the ω-functionalized isocyanide (4.0 eq.) in 2 mL of THF/MeOH (1:1) are added to the resin and the mixture is stirred for 24 h-72 h. For macrocyclizations by Ugi-reaction, no Fmoc-protected amino acid is

needed and the solvent used is DCM/TFE (1:1). Completion is indicated either by ESI-MS or by RP-HPLC monitoring after mini-cleavages. Finally, the system is washed with DCM (3×1 min) and DMF (2×1 min). **Cleavage:** The resin is treated with the cocktail TFA/TIS/H<sub>2</sub>O (95:2.5:2.5). The peptide is precipitated from cold (-20°C) diethyl ether, then taken up in AcN/H<sub>2</sub>O 1:2 (v/v) and lyophilized.

### 5.6.3 Synthesis of resin-attached tripeptide Fmoc-Orn(NH-2CT)-Leu-D-Phe-OH

**General protocol for solution-phase peptide synthesis:** Boc-protected amino acid (1.0 eq.), HOBt (1.1 eq.), EDC (1.1 eq.) and the allyl ester amino acid/dipeptide hydrochloride are suspended in dry CH<sub>2</sub>Cl<sub>2</sub> (15 mL). Et<sub>3</sub>N (1.4 eq.) is syringed in one portion and the resulting solution is stirred at room temperature overnight (~12 h). The reaction mixture is diluted with 100 mL EtOAc, transferred to a separatory funnel and sequentially washed with 1 M aqueous solution of KHSO<sub>4</sub> (2×20 mL) and saturated aqueous suspension NaHCO<sub>3</sub> (2×20 mL). The organic phase is dried over Na<sub>2</sub>SO<sub>4</sub>, filtered and concentrated under reduced pressure.

**General Boc removal procedure:** The crude peptide is exposed to high vacuum for 1 h before dissolving it in a 1:3 mixture of TFA/DCM for Boc removal. As the material is dissolved, gas evolution could be detected and the pressure that built up inside the reaction flask is regularly released by opening the reaction flask. After 2 h, usually no starting material is detected by thin layer chromatography and the reaction is concentrated under reduced pressure and then placed under high vacuum. If required, the hydrochloride salt can be crystallized from ice cold diethyl ether.



**FmocNH-Orn(NH<sub>2</sub>)-Leu-D-Phe-OAlyl:** Boc-D-Phe-OH (3 g, 11.3 mmol) and K<sub>2</sub>CO<sub>3</sub> (2.34, 17.0 mmol, 1.5 eq) were suspended in dry DMF (20 mL). The mixture was heated at 100 °C, Allyl-Br (1.24 mL, 14.7 mmol, 1.3 eq.) was added dropwise and the reaction was stirred for 4 h. The mixture was cooled until room temperature, diluted with EtOAc (100 mL), transferred

to a separatory funnel and washed with saturated aqueous suspension of  $\text{NaHCO}_3$  (2×15 mL) and brine (2×15 mL). The organic phase was dried over  $\text{MgSO}_4$ , filtered and concentrated under reduced pressure. The fully protected amino acid obtained was subject to Boc removal following the described procedure and sequentially coupled to Boc-Leu-OH (2.61 g, 11.3 mmol) and Fmoc-Orn(Boc)-OH (5.1 g, 11.3 mmol) without previous purification and according to the general peptide coupling procedure. Flash column chromatography purification ( $\text{CH}_2\text{Cl}_2/\text{EtOAc}$  2:1) furnished the pure peptide (5.0 g, 59%) as a white solid.  $R_f = 0.65$  (DCM/MeOH).  $^1\text{H}$  NMR (400 MHz,  $\text{DMSO}-d_6$ ),  $\delta = 8.53$  (d,  $J = 8.1$  Hz, 1H), 7.93 (d,  $J = 7.5$  Hz, 2H), 7.82 (d,  $J = 8.6$  Hz, 1H), 7.75 (dd,  $J = 7.5, 3.4$  Hz, 1H), 7.53 (d,  $J = 8.3$  Hz, 1H), 7.45 (td,  $J = 7.5, 1.1$  Hz, 2H), 7.36 (td,  $J = 7.4, 1.2$  Hz, 2H), 7.33 – 7.24 (m, 5H), 6.81 (t,  $J = 5.7$  Hz, 1H), 5.88 (ddt,  $J = 17.4, 10.6, 5.3$  Hz, 1H), 5.31 (dd,  $J = 17.2, 1.7$  Hz, 1H), 5.22 (dd,  $J = 10.5, 1.5$  Hz, 1H), 4.59 (dt,  $J = 5.5, 1.6$  Hz, 2H), 4.58 – 4.47 (m, 1H), 4.35 (d,  $J = 7.0$  Hz, 1H), 4.31 – 4.24 (m, 2H), 4.05 – 3.96 (m, 1H), 3.12 (dd,  $J = 13.6, 4.8$  Hz, 1H), 2.96 – 2.88 (m, 3H), 1.68 – 1.51 (m, 1H), 1.40 (s, 9H), 0.81 – 0.70 (m, 6H).  $^{13}\text{C}$  NMR (101 MHz,  $\text{DMSO}-d_6$ ),  $\delta = 172.4, 171.9, 171.52, 170.8, 156.4, 156.0, 144.3, 144.2, 141.1, 137.6, 132.3, 129.6, 128.6, 128.0, 127.5, 126.9, 125.7, 120.5, 118.2, 77.8, 66.1, 65.3, 60.2, 54.7, 53.9, 51.0, 47.1, 29.69, 28.7, 26.6, 24.3, 23.2, 22.2, 21.2, 14.5$ . The resulting peptide was then subjected to Boc removal and crystallization of its hydrochloride salt from ice cold diethyl ether. **Attachment to 2CTC resin:** The peptide containing free Orn side chain amino group (1 mmol, 1 eq.) is dissolved with DIPEA (0.34 mL, 2 mmol, 2 eq.) in dry DCM (10 mL). 2CTC Resin 1.3 mmol/g (0.77 g, 1 mmol, 1 eq., 1.3 mmol/g) is placed in 10 mL solid-phase reaction vessel and pre-swelled with dry DCM (2×8 min). The solution containing the peptide is transferred into the 2CTC-containing vessel and the reaction mixture is stirred during 4 h. The liquid face is removed and the resin is washed with DCM (3×1 min) and  $\text{Et}_2\text{O}$  (2×1 min). Lastly, 2CT-bound peptide is capped with MeOH (2×1 min) for 1 h, washed again with DCM (3×1 min) and  $\text{Et}_2\text{O}$  (2×1 min) and dried in a desiccator for 1 d. **Loading calculation:** 2CT loaded resin (10 mg) is mixed in an Eppendorf tube with 20% piperidine/DMF (1 mL), stirred for 20 min and centrifuged. 100  $\mu\text{L}$  were transferred to a tube containing 10 mL DMF and mixed and triplicate determinations of the absorbance at 310 nm are recorded. Substitution of the resin =  $[101 \times (\text{Absorbance})] / [7.8 \times (\text{weight in mg})]$ . Final resin loading for FmocNH-Orn(NH-2CT)-Leu-DPhe-OAllyl: 0.41 mmole/g.

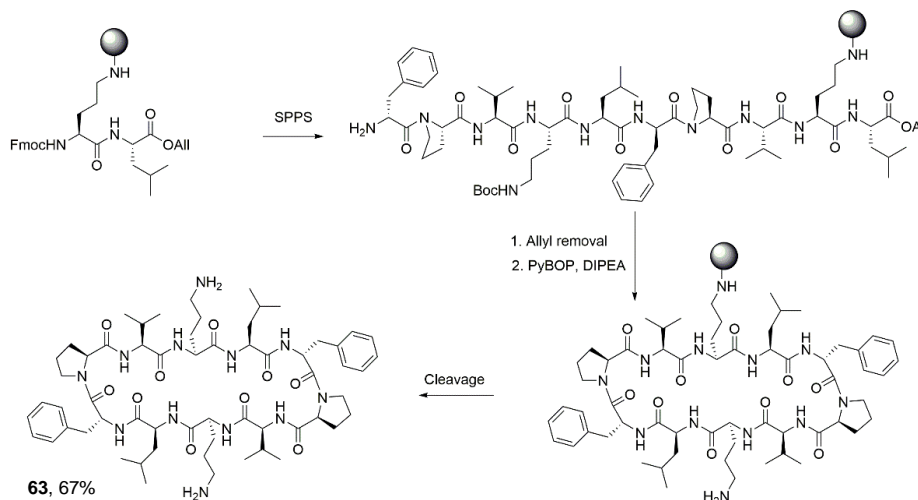
### 5.6.4 Synthesis of isocyanides

#### General protocol for the synthesis of isocyanides from amines

A solution of the amine (25 mmol) in ethyl formate (20 mL) is heated at reflux for 12 h to afford the corresponding formamide. The resulting solution is concentrated under vacuum and used without further purification. The formamide in 40 mL of dry THF (or DCM if not soluble), mixed with Et<sub>3</sub>N (4 eq.) and under N<sub>2</sub> atmosphere is cooled to -20 °C and a solution of POCl<sub>3</sub> (1.3 eq.) in 15 mL of THF is added dropwise during 30 min. The resulting mixture is stirred at -20 °C for 1 h, then allowed to reach room temperature and stirred for additional 2 h. The reaction mixture is quenched with 50 mL of 10% aqueous NaHCO<sub>3</sub> and extracted with EtOAc (2×150 mL). The combined organic phases are washed with brine (50 mL), dried over anhydrous Na<sub>2</sub>SO<sub>4</sub>, and concentrated under reduced pressure to dryness. The crude product is purified by column chromatography. The details of the synthesis of isocyanides are enclosed in the annexes at the end of the manuscript.

### 5.6.5 Synthesis of cyclic peptides

#### Gramicidin S (63)



Starting from Fmoc-Orn(NH-2CT)-Leu-OAll resin (190 mg, 0.1 mmol), Fmoc-Val-OH (136 mg, 0.4 mmol), Fmoc-Pro-OH (135 mg, 0.4 mmol), Fmoc-D-Phe-OH (155 mg, 0.4 mmol), Fmoc-Leu-OH (141 mg, 0.4 mmol), Fmoc-Orn(Boc)-OH (182 mg, 0.4 mmol), Fmoc-Val-OH, Fmoc-Aib-OH (125 mg, 0.4 mmol) and Fmoc-D-Phe-OH (155 mg, 0.4 mmol) are sequentially incorporated following the general methodology given above. After removing the Fmoc and allyl protecting groups, a head-to-tail macrolactamization, is performed using PyBOP (208 mg,

0.4 mmol) and DIPEA (139  $\mu$ L, 0.8 mmol) in DMF for 2 h. The resulting product is cleaved from the resin to obtain after lyophilization the Gramicidin S (91 mg, 81% crude yield, 67% purity) as an amorphous white solid. An analytical sample was purified by preparative RP-HPLC for NMR and HR-MS characterization.  $R_t = 17.8$  min. HR-MS  $m/z$ : 1141.7186  $[M+H]^+$ , calcd. for  $C_{59}H_{93}N_{12}O_{10}$ : 1141.7171.

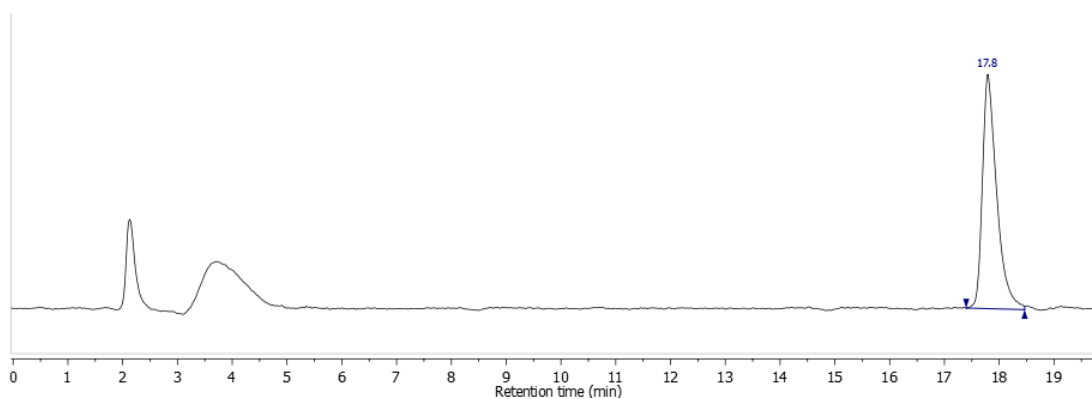
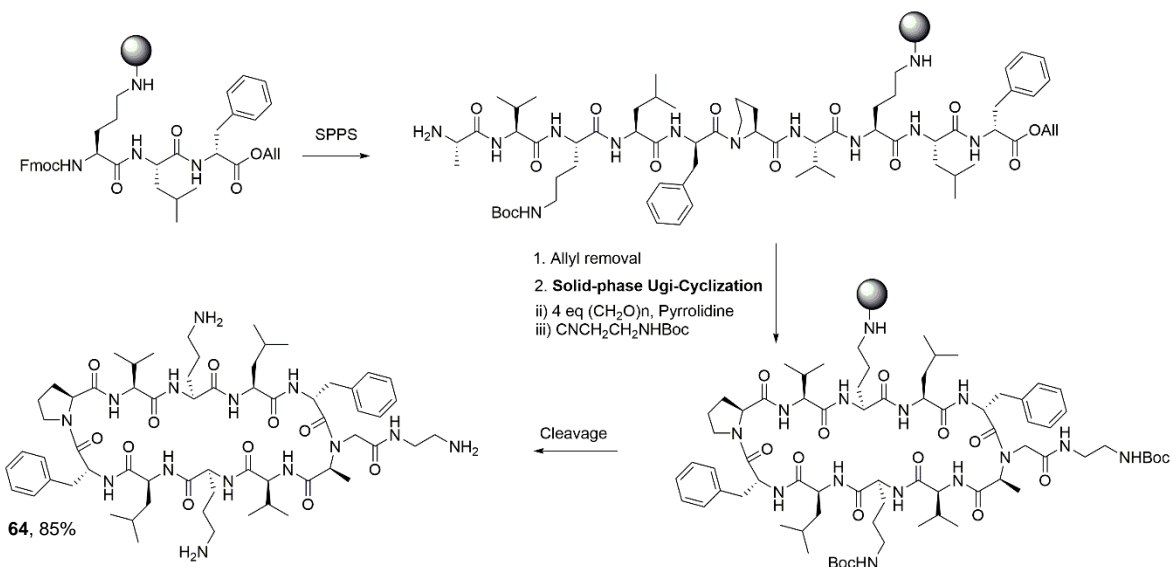


Figure 5.3. RP-HPLC trace of pure cyclic peptide Gramicidin S.

### Cyclic Peptide 64



Starting from Fmoc-Orn(NH-2CT)-Leu-OAll resin (210 mg, 0.1 mmol), Fmoc-Val-OH (136 mg, 0.4 mmol), Fmoc-Pro-OH (135 mg, 0.4 mmol), Fmoc-D-Phe-OH (155 mg, 0.4 mmol), Fmoc-Leu-OH (141 mg, 0.4 mmol), Fmoc-Orn(Boc)-OH (182 mg, 0.4 mmol), Fmoc-Val-OH, Fmoc-Ala-OH (132 mg, 0.4 mmol) and Fmoc-D-Phe-OH (155 mg, 0.4 mmol) are sequentially incorporated following the general methodology given above. After removing the Fmoc and

allyl protecting groups, a head-to-tail cyclization by aminocatalysis-mediated Ugi reaction, is performed using paraformaldehyde (12 mg, 0.4 mmol) and *t*-butyl 2-isocyanoethylcarbamate (68 mg, 0.4 mmol) as described above. The resulting product is cleaved from the resin to obtain after lyophilization the crude cyclic peptide **64** (94 mg, 77% crude yield, 85% purity) as an amorphous white solid. An analytical sample was purified by preparative RP-HPLC for NMR and HR-MS characterization.  $R_t = 13.2$  min. HR-MS  $m/z$ : 1215.7613  $[M+H]^+$ , calcd. for  $C_{62}H_{99}N_{14}O_{11}$ : 1215.7618.

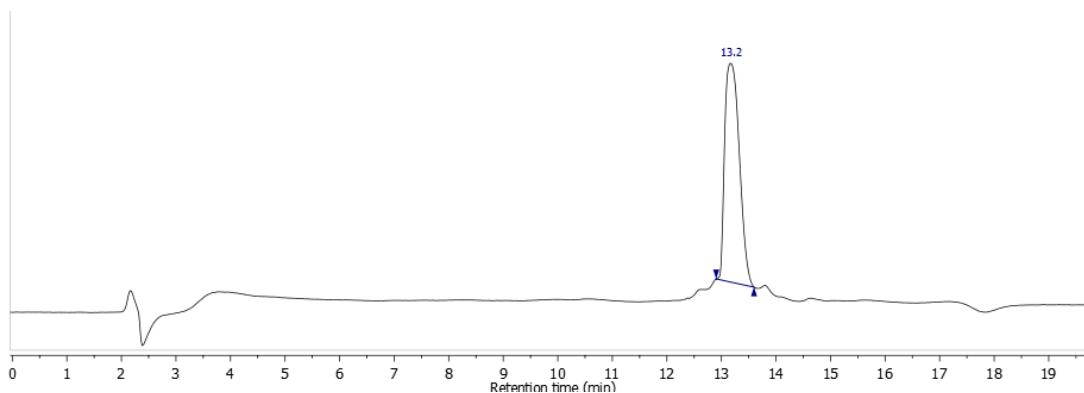
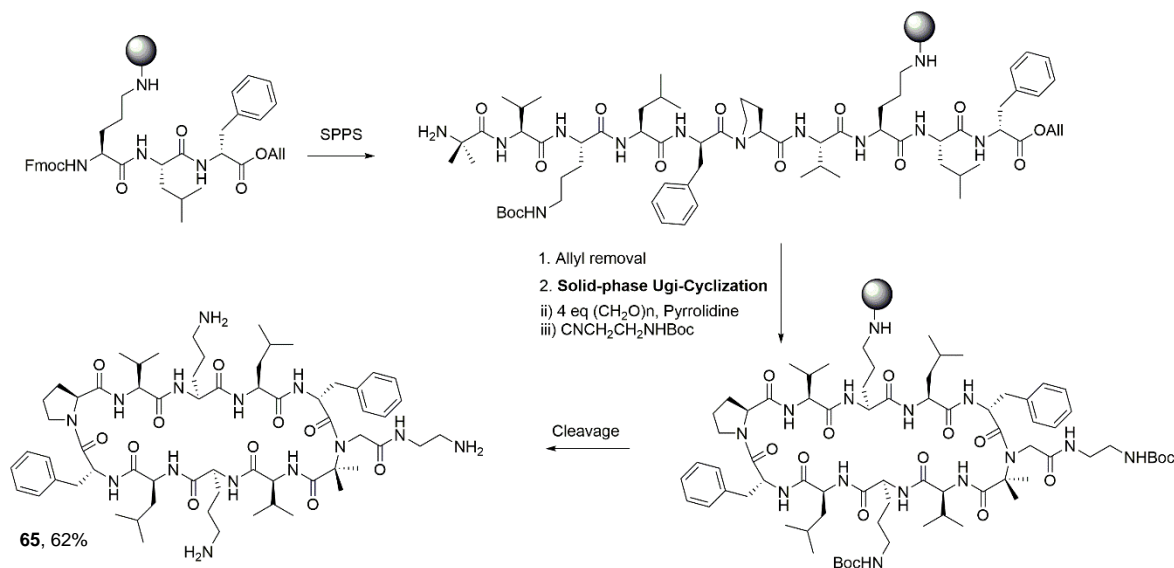


Figure 5.4. RP-HPLC trace of pure cyclic peptide **64**.

### Cyclic peptide **65**



Starting from Fmoc-Orn(NH-2CT)-Leu-OAll resin (210 mg, 0.1 mmol), Fmoc-Val-OH (136 mg, 0.4 mmol), Fmoc-Pro-OH (135 mg, 0.4 mmol), Fmoc-D-Phe-OH (155 mg, 0.4 mmol), Fmoc-Leu-OH (141 mg, 0.4 mmol), Fmoc-Orn(Boc)-OH (182 mg, 0.4 mmol), Fmoc-Val-OH, Fmoc-Aib-OH (125 mg, 0.4 mmol) and Fmoc-D-Phe-OH (155 mg, 0.4 mmol) are sequentially

incorporated following the general methodology given above. After removing the Fmoc and allyl protecting groups, a heat-to-tail cyclization by aminocatalysis-mediated Ugi reaction, is performed using paraformaldehyde (12 mg, 0.4 mmol) and *t*-butyl 2-isocyanoethylcarbamate (68 mg, 0.4 mmol) as described above. A second Ugi reaction cycle is required for this compound. The resulting product is cleaved from the resin to obtain after lyophilization the crude cyclic peptide **65** (80 mg, 65% crude yield, 62% purity) as an amorphous white solid. An analytical sample was purified by preparative RP-HPLC for NMR and HR-MS characterization.  $R_t = 11.4$  min. HR-MS  $m/z$ : 1229.7765  $[M+H]^+$ , calcd. for  $C_{63}H_{101}N_{14}O_{11}$ : 1229.7774.

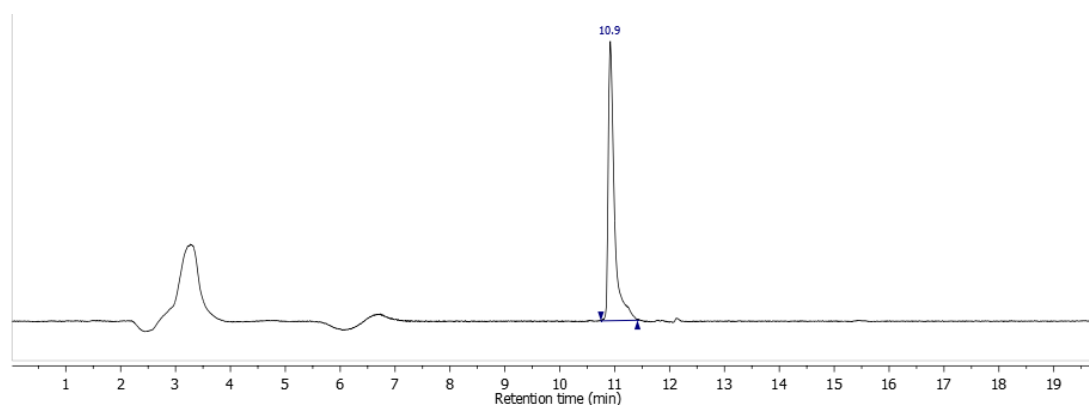
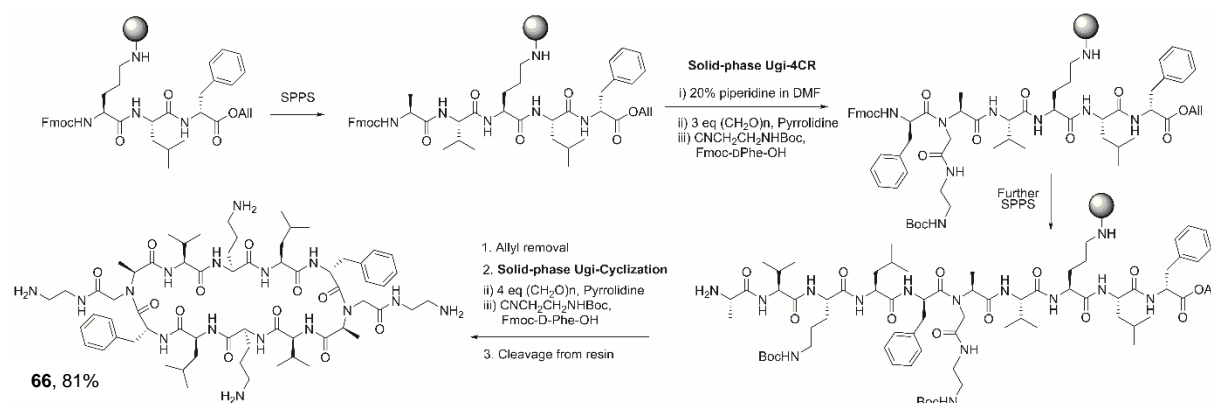


Figure 5.5. RP-HPLC trace of pure cyclic peptide **65**.

### Cyclic peptide **66**



Starting from Fmoc-Orn(NH-2CT)-Leu-DPhe-OAll resin (210 mg, 0.1 mmol), Fmoc-Val-OH (136 mg, 0.4 mmol) and Fmoc-Ala-OH (132 mg, 0.4 mmol) are sequentially incorporated following the general methodology given above. After removing the Fmoc protecting group, an aminocatalysis-mediated Ugi reaction is performed using Fmoc-D-Phe-OH (155 mg, 0.4 mmol), paraformaldehyde (12 mg, 0.4 mmol) and *t*-butyl 2-isocyanoethylcarbamate (68 mg,

0.4 mmol) as described above. Then, Fmoc-Leu-OH (141 mg, 0.4 mmol), Fmoc-Orn(Boc)-OH (182 mg, 0.4 mmol), Fmoc-Val-OH (136 mg, 0.4 mmol) and Fmoc-Ala-OH (132 mg, 0.4 mmol) are sequentially coupled. After removing the Fmoc and allyl protecting groups, a head-to-tail cyclization by aminocatalysis-mediated Ugi reaction, is performed using paraformaldehyde (12 mg, 0.4 mmol) and *t*-butyl 2-isocyanoethylcarbamate (68 mg, 0.4 mmol) as described above. The resulting product is cleaved from the resin to obtain after lyophilization the crude cyclic peptide **66** (101 mg, 78% crude yield, 81% purity) as an amorphous white solid. An analytical sample was purified by preparative RP-HPLC for NMR and HR-MS characterization.  $R_t = 11.7$  min. HR-MS  $m/z$ : 1289.8108  $[M+H]^+$ , calcd. for  $C_{64}H_{105}N_{16}O_{12}$ : 1289.8098.

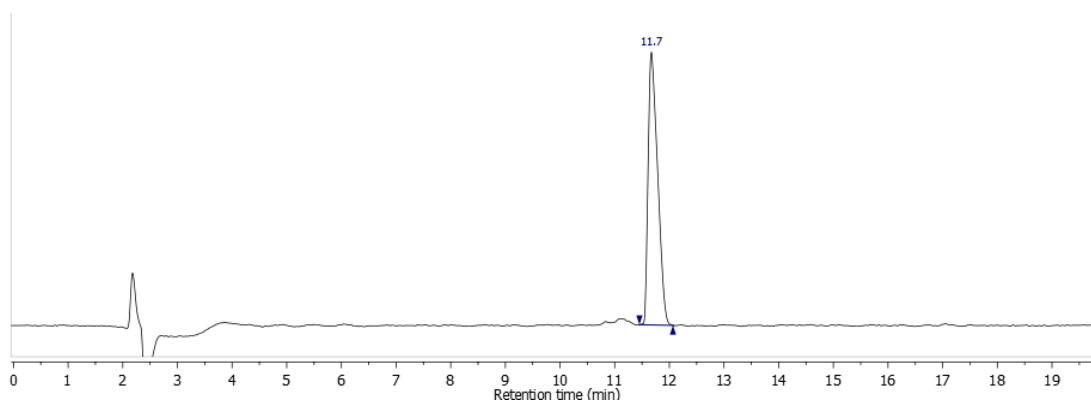
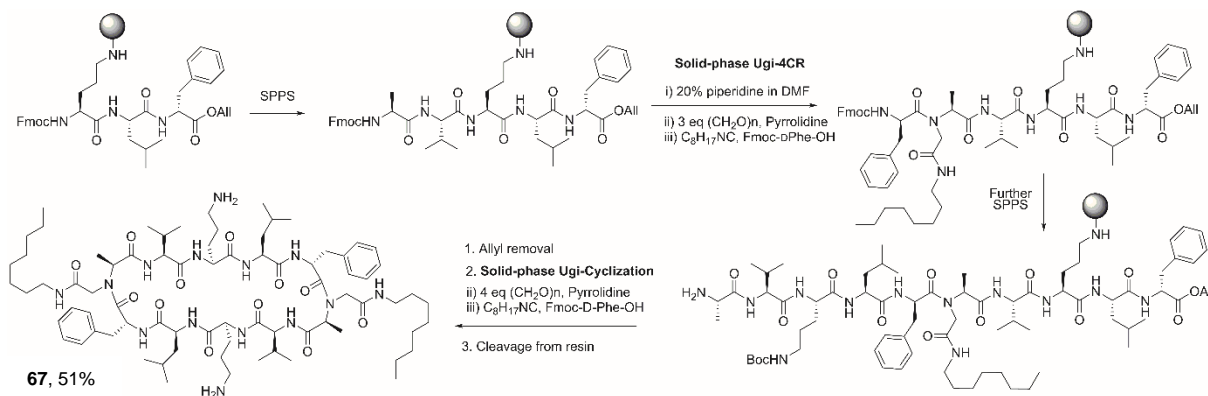


Figure 5.6. RP-HPLC trace of pure cyclic peptide **66**.

### Cyclic peptide **67**



Starting from Fmoc-Orn(NH-2CT)-Leu-DPhe-OAll resin (210 mg, 0.1 mmol), Fmoc-Val-OH (136 mg, 0.4 mmol) and Fmoc-Ala-OH (132 mg, 0.4 mmol) are sequentially incorporated following the general methodology given above. After removing the Fmoc protecting group, an aminocatalysis-mediated Ugi reaction is performed using Fmoc-D-Phe-OH (155 mg, 0.4

mmol), paraformaldehyde (12 mg, 0.4 mmol) and *n*-octyl isocyanide (56 mg, 0.4 mmol) as described above. Then, Fmoc-Leu-OH (141 mg, 0.4 mmol), Fmoc-Orn(Boc)-OH (182 mg, 0.4 mmol), Fmoc-Val-OH (136 mg, 0.4 mmol) and Fmoc-Ala-OH (132 mg, 0.4 mmol) are sequentially coupled. After removing the Fmoc and allyl protecting groups, a head-to-tail cyclization by aminocatalysis-mediated Ugi reaction, is performed using paraformaldehyde (12 mg, 0.4 mmol) and *n*-octyl isocyanide (56 mg, 0.4 mmol) as described above. The resulting product is cleaved from the resin to obtain after lyophilization the crude cyclic peptide **67** (95 mg, 67% crude yield, 51% purity) as an amorphous white solid. An analytical sample was purified by preparative RP-HPLC for NMR and HR-MS characterization.  $R_t = 18.7$  min. HR-MS  $m/z$ : 1427.9753  $[M+H]^+$ , calcd. for  $C_{76}H_{127}N_{14}O_{12}$ : 1427.9758.

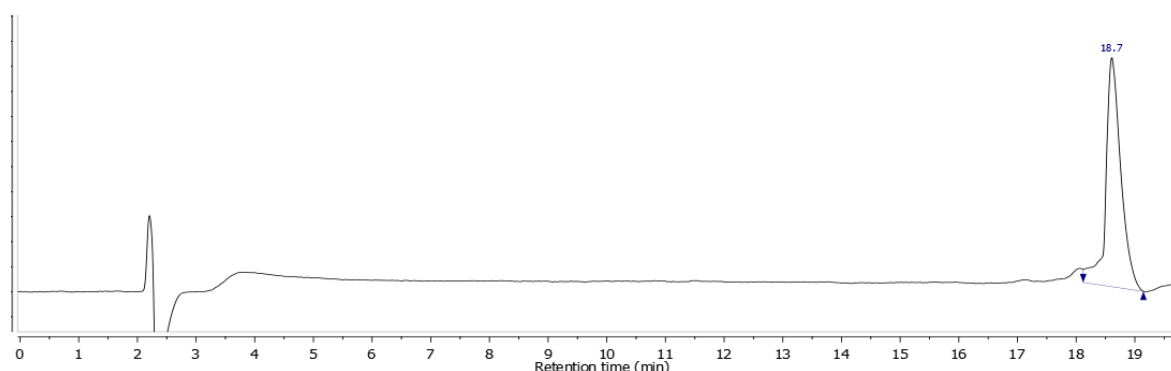


Figure 5.7. RP-HPLC trace of pure cyclic peptide **67**.

### **5.6.6 NMR-based structure calculations**

NMR structure determination was performed in Xplor-NIH<sup>[33,39]</sup> through simulated annealing regularization and refinement in torsion angle space, using experimental data as inter-proton distances and dihedral angles restraints. Observed  $^3J_{\text{HNCH}\alpha}$  coupling constants higher than 8 Hz were translated into  $\phi = -120 \pm 30^\circ$  dihedral constraints. Only ROE-derived restraints coming from the backbone resonances were used as distance restraints. The normalization of ROE-intensities was performed by averaging of  $\alpha\text{N}(i, i+1)$  intensities assuming a distance of 2.2 Å.

For simulated annealing regularization, 200 starting structures were randomly generated. Geometric bond, angle and improper energy contributions were scaled to 1.0, 0.4, and 0.1 respectively. Non-bonded van der Waals contributions were set to 0.004 and experimental NOE and dihedral constraints were scaled to 2 and 10 respectively. An initial 100 steps conjugated gradient Powell minimization was performed. A 100 ps molecular dynamics simulation at 3500 K was performed with a time-step of 3 fs. Before the cooling stage, the

energy function due to experimental dihedral restraints was scaled to 200. The system was cooled from 3500 to 25 K, with a temperature step of 12.5 K. At each temperature step, 0.2 ps of molecular dynamics simulation was performed. During this stage the van der Waals energy term was progressively scaled from 0.004 to 4, and the experimental NOE potential was climbed to 30. Angle and improper terms were both progressively scaled to 1.0. A 500 steps torsion angle minimization was performed and finally the system was optimized by means of 500 steps conjugated gradient Powell Cartesian minimization. The refinement protocol consisted in a slow cooling simulated annealing from the regularized structures. The initial weights of the energy functions were 0.4, 0.1 and 1.0 for the angle, improper, and bond terms; 10 and 2 respectively for the NOE and dihedral experimental restraints; and 0.004 for the non-bonded van der Waals term. A 10 ps molecular dynamics simulation at 3000 K was achieved with a time-step of 3 fs, afterwards dihedral restraints contribution was set to 200. The system was cooled with a temperature step of 12.5 K and a simulation time of 0.2 ps at each temperature. During this simulation, the van der Waals energy term was scaled from 0.003 to 4. During this stage the van der Waals energy term was progressively scaled from 0.004 to 4, and the experimental NOE potential was climbed to 30. Angle and improper terms were both progressively scaled to 1.0. A 500 torsion angle minimization was performed afterwards a second 500 steps minimization was achieved in cartesian coordinates. A finally 1000 steps Powell minimization with an energy function non-dependent of experimental restraints was executed. Final RMSD was calculated with the plugin *RMSD calculator* within *VMD 1.9.2*,<sup>[40]</sup> excluding *N*- and *C*-terminal residues in the calculation. Final average structures were minimized within MOPAC2012 (<http://openmopac.net/>) software using PM7 semi-empirical method.<sup>[41]</sup> The superimposition of the 10 best structures obtained after NMR-based simulated annealing and refinement protocols for compounds **64**, **65** and **66** are depicted in Figure 8.

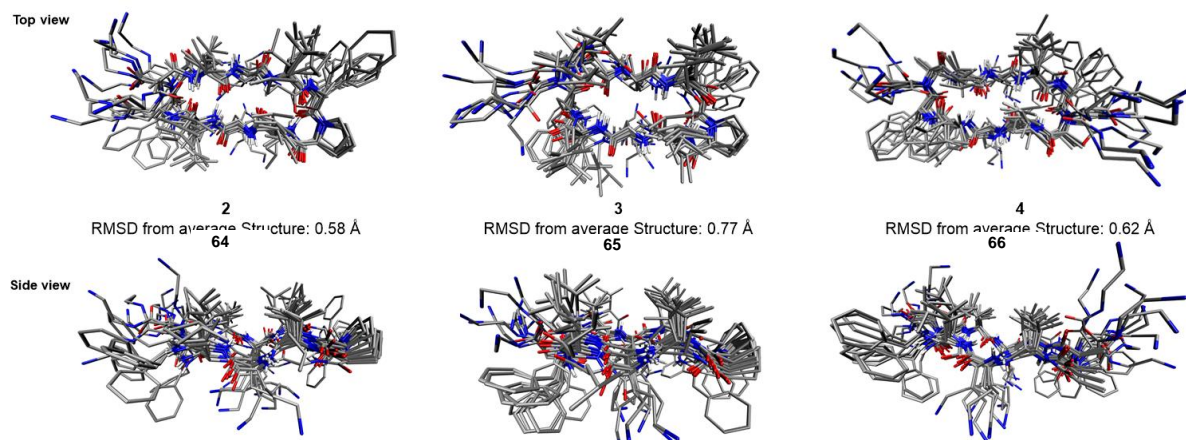


Figure 5.8. Superimposition of the 10 lowest energy NMR-derived structures for cyclic peptides **2**, **3** and **4**.

### Variable Temperature NMR experiments

Temperature coefficients for amide protons were determined by measuring chemical shifts between 298K and 323K with temperature steps of 5K. Temperature calibration was conducted by measuring the shift of the resonance signals of ethylene glycol standard. The chemical shifts are reported relative to TMS, whose chemical shift was corrected according to the data reported from Hoffmann and Becker.<sup>[42]</sup> The data utilized for the determination of the temperature coefficients can be found in the annexes.

	$-\Delta\delta/T$ in ppb/K									
	Val <sup>2</sup>	Orn <sup>3</sup>	Leu <sup>4</sup>	dPhe <sup>5</sup>	NH_Ugi	Val <sup>7</sup>	Orn <sup>8</sup>	Leu <sup>9</sup>	dPhe <sup>1</sup>	
Peptide <b>64</b>	2.1	5.1	2.9	10.1	8.1	1.1	5.0	2.7	9.9	
Peptide <b>65</b>	3.9	6.0	2.9	10.2	13.6	2.7	6.4	3.0	1.0	

	$-\Delta\delta/T$ in ppb/K				
	Val <sup>2,7</sup>	Orn <sup>3,8</sup>	Leu <sup>4,9</sup>	dPhe <sup>5,10</sup>	NH_Ugi
GS	2.9	5.7	3.4	11.4	-
Peptide <b>66</b>	1.7	4.7	2.7	8.0	3.5

## 5.7. References

- [1] K. C. Chou, *Anal. Biochem.* **2000**, *286*, 1–16.
- [2] L. Jiang, K. Moehle, B. Dhanapal, D. Obrecht, J. A. Robinson, *Helv. Chim. Acta* **2000**, *83*, 3097–3112.
- [3] J. A. Robinson, *Acc. Chem. Res.* **2008**, *41*, 1278–1288.
- [4] J. A. Robinson, S. DeMarco, F. Gombert, K. Moehle, D. Obrecht, *Drug Discov. Today* **2008**, *13*, 944–951.
- [5] W. C. Ripka, G. V. De Lucca, A. C. Bach, R. S. Pottorf, J. M. Blaney, *Tetrahedron* **1993**, *49*,

- 3609–3628.
- [6] D. Andreu, S. Ruiz, C. Carren, J. Alsina, F. Albericio, M. Á. Jiménez, N. de la Figuera, R. Herranz, M. T. García-López, R. González-Muñiz, *J. Am. Chem. Soc.* **1997**, *119*, 10579–10586.
- [7] A. C. Gibbs, T. C. Bjorndahl, R. S. Hodges, D. S. Wishart, *J. Am. Chem. Soc.* **2002**, *124*, 1203–1213.
- [8] J. A. Robinson, *Acc. Chem. Res.* **2008**, *41*, 1278–1288.
- [9] R. Fasan, R. L. A. Dias, K. Moehle, O. Zerbe, J. W. Vrijbloed, D. Obrecht, J. A. Robinson, *Angew. Chemie - Int. Ed.* **2004**, *43*, 2109–2112.
- [10] S. V. Sychev, S. V. Sukhanov, P. V. Panteleev, Z. O. Shenkarev, T. V. Ovchinnikova, *Biopolymers* **2017**, e23093.
- [11] P. V. Panteleev, I. A. Bolosov, S. V. Balandin, T. V. Ovchinnikova, *Acta Naturae* **2015**, *7*, 37–47.
- [12] G. F. Gause, M. G. Brazhnikova, *Nature* **1944**, *3918*, 703.
- [13] S. Pal, U. Ghosh, R. S. Ampapathi, T. K. Chakraborty, in *Pept. II. Top. Heterocycl. Chem.*, Springer, Cham, **2015**, pp. 159–202.
- [14] X. Wu, X. Bu, K. M. Wong, W. Yan, Z. Guo, *Org. Lett.* **2003**, *5*, 1749–1752.
- [15] M. van der Knaap, E. Engels, H. J. Busscher, J. M. Otero, A. L. Llamas-Saiz, M. J. van Raaij, R. H. Mars-Groenendijk, D. Noort, G. A. van der Marel, H. S. Overkleeft, et al., *Bioorganic Med. Chem.* **2009**, *17*, 6318–6328.
- [16] M. Tamaki, K. Fujinuma, T. Harada, K. Takanashi, M. Shindo, M. Kimura, Y. Uchida, *J. Antibiot. (Tokyo)*. **2011**, *64*, 583–585.
- [17] M. Tamaki, I. Sasaki, Y. Nakao, M. Shindo, M. Kimura, Y. Uchida, *J. Antibiot. (Tokyo)*. **2009**, *62*, 597–599.
- [18] V. V. Kapoerchan, A. D. Knijnenburg, P. Keizer, E. Spalburg, A. J. De Neeling, R. H. Mars-groenendijk, D. Noort, J. M. Otero, A. L. Llamas-saiz, M. J. Van Raaij, et al., *Bioorg. Med. Chem.* **2012**, *20*, 6059–6062.
- [19] V. V. Kapoerchan, A. D. Knijnenburg, M. Niamat, E. Spalburg, A. J. De Neeling, P. H. Nibbering, R. H. Mars-Groenendijk, D. Noort, J. M. Otero, A. L. Llamas-Saiz, et al., *Chem. - A Eur. J.* **2010**, *16*, 12174–12181.
- [20] S. Afonin, R. W. Glaser, M. Berdichevskaja, P. Wadhvani, K. H. Gührs, U. Möllmann, A. Perner, A. S. Ulrich, *ChemBioChem* **2003**, *4*, 1151–1163.
- [21] L. H. Kondejewski, S. W. Farmer, D. S. Wishart, C. M. Kay, R. E. Hancock, R. S. Hodges, *J. Biol. Chem.* **1996**, *271*, 25261–8.
- [22] E. Spalburg, A. J. De Neeling, R. H. Mars-groenendijk, D. Noort, G. M. Grotenbreg, G. A. Van Der Marel, H. S. Overkleeft, M. Overhand, *Helv. Chim. Acta* **2012**, *95*, 2544–2561.
- [23] K. Yamada, M. Kodaira, S. S. Shinoda, K. Komagoe, H. Oku, R. Katakai, T. Katsu, I. Matsuo, *Medchemcomm* **2011**, *2*, 644–649.
- [24] V. V. Kapoerchan, E. Spalburg, A. J. De Neeling, R. H. Mars-Groenendijk, D. Noort, J. M. Otero, P. Ferraces-Casais, A. L. Llamas-Saiz, M. J. Van Raaij, J. Van Doorn, et al., *Chem. - A Eur. J.* **2010**, *16*, 4259–4265.
- [25] B. Legrand, L. Mathieu, A. Lebrun, S. Andriamanarivo, V. Lisowski, N. Masurier, S. Zirah, Y. K. Kang, J. Martinez, L. T. Maillard, *Chem. - A Eur. J.* **2014**, *20*, 6713–6720.
- [26] D. G. Rivera, A. V. Vasco, R. Echemendía, O. Concepción, C. S. Pérez, J. A. Gavín, L. A. Wessjohann, *Chem. - A Eur. J.* **2014**, *20*, 13150–13161.
- [27] A. V. Vasco, C. S. Pérez, F. E. Morales, H. E. Garay, D. Vasilev, J. A. Gavín, L. A. Wessjohann, D. G. Rivera, *J. Org. Chem.* **2015**, *80*, 6697–6707.
- [28] A. V. Vasco, Y. Méndez, A. Porzel, J. Balbach, L. A. Wessjohann, D. G. Rivera, *Bioconjug. Chem.* **2019**, *30*, 253–259.

- [29] Y. Li, N. Bionda, A. Yongye, P. Geer, M. Stawikowski, P. Cudic, K. Martinez, R. A. Houghten, *ChemMedChem* **2013**, *8*, 1865–1872.
- [30] J. Pastuszak, J. H. Gardner, J. Singh, D. H. Rich, *J. Org. Chem.* **1982**, *47*, 2982–2987.
- [31] J. S. Davies, *J. Pept. Sci.* **2003**, *9*, 471–501.
- [32] M. Van Der Knaap, E. Engels, H. J. Busscher, J. M. Otero, A. L. Llamas-saiz, M. J. Van Raaij, R. H. Mars-groenendijk, D. Noort, G. A. Van Der Marel, H. S. Overkleeft, et al., *Bioorg. Med. Chem.* **2009**, *17*, 6318–6328.
- [33] C. D. Schwieters, J. J. Kuszewski, N. Tjandra, G. M. Clore, *J. Magn. Reson.* **2003**, *160*, 65–73.
- [34] L. H. Kondejewski, S. W. Farmer, D. S. Wishart, C. M. Kay, R. E. W. Hancock, R. S. Hodges, *J. Biol. Chem.* **1996**, *271*, 25261–25268.
- [35] A. R. Puentes, M. C. Morejón, D. G. Rivera, L. A. Wessjohann, *Org. Lett.* **2017**, *19*, 4022–4025.
- [36] C. R. Jones, C. T. Sikakana, S. Hehir, M. C. Kuo, W. A. Gibbons, *Biophys. J.* **1978**, *24*, 815–832.
- [37] G. D. Rose, L. M. Glerasch, J. A. Smith, *Adv. Protein Chem.* **1985**, *37*, 1–109.
- [38] E. Kaiser, R. L. Colescott, C. D. Bossinger, P. I. Cook, *Anal. Biochem.* **1970**, *34*, 595–598.
- [39] C. D. Schwieters, J. J. Kuszewski, G. Marius Clore, *Prog. Nucl. Magn. Reson. Spectrosc.* **2006**, *48*, 47–62.
- [40] W. Humphrey, A. Dalke, K. Schulten, *J. Mol. Graph.* **1996**, *14*, 33–38.
- [41] J. J. P. Stewart, **2012**.
- [42] R. E. Hoffman, E. D. Becker, *J. Magn. Reson.* **2005**, *176*, 87–98.

## Annexes

**Note:** Detailed experimental and spectroscopic information for compounds within chapters 2 and 4 can be found in the Supporting information files published online under:

[https://pubs.acs.org/doi/suppl/10.1021/acs.joc.5b00858/suppl\\_file/jo5b00858\\_si\\_001.pdf](https://pubs.acs.org/doi/suppl/10.1021/acs.joc.5b00858/suppl_file/jo5b00858_si_001.pdf)

[https://pubs.acs.org/doi/suppl/10.1021/acs.bioconjchem.8b00906/suppl\\_file/bc8b00906\\_si\\_001.pdf](https://pubs.acs.org/doi/suppl/10.1021/acs.bioconjchem.8b00906/suppl_file/bc8b00906_si_001.pdf)

For chapters 3 and 5 the same information can be found in the upcoming publications.

### **Table of contents**

Annexes.....	113
Synthesis of Isocyanides.....	114
General protocol for the synthesis of isocyanides from amines.....	114
( <i>N</i> -tert-butyloxycarbonyl)-aminoethyl isocyanide .....	114
<i>n</i> -dodecylisocyanide .....	114
2,3,4,6-tetra-O-acetyl- $\beta$ -D-glucopyranosyl isocyanide .....	115
allyl 2-isocyanoethylcarbamate .....	115
<i>N</i> -(6-isocyanoethyl) maleimide .....	116
<i>n</i> -octylisocyanide .....	118
<i>t</i> -butyl 3-isocyanopropanoate .....	119
<i>N</i> -( $\omega$ -O-Me-PEG <sub>11</sub> -ethyl)-2-isocyanoacetamide.....	121
2-(4-dimethylamino-1,8-naphthalimido) ethyl isocyanide.....	123
NMR data of selected compounds .....	124
Variable Temperature Analysis for amide protons .....	132
Internal IPB codes for the compounds within the thesis .....	135

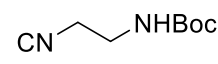
---

## Synthesis of Isocyanides

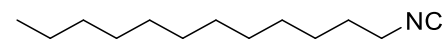
### General protocol for the synthesis of isocyanides from amines

A solution of the amine (25 mmol) in ethyl formate (20 mL) is heated at reflux temperature for 12 h to afford the formamide. The resulting solution is concentrated under vacuum and used without further purification. The formamide in 40 mL of dry THF, mixed with Et<sub>3</sub>N (4 eq.) and under N<sub>2</sub> atmosphere is cooled to 0 °C and a solution of POCl<sub>3</sub> (1.3 eq.) in 15 mL of THF is added dropwise during 30 minutes. The resulting mixture is stirred at 0 °C for 1 h, then allowed to reach room temperature and stirred for additional 2 h. The reaction mixture is quenched with 50 mL of 10% aqueous NaHCO<sub>3</sub> and extracted with EtOAc (2x50 mL). The combined organic phases are washed with brine (20 mL), dried over anh. Na<sub>2</sub>SO<sub>4</sub>, and concentrated under reduced pressure to dryness. The crude product is purified by column chromatography.

### (*N*-tert-butyloxycarbonyl)-aminoethyl isocyanide

 The compound was synthesized according to the protocol published in Ref. <sup>1</sup> with a total yield of 67%.

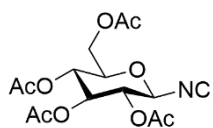
### *n*-dodecylisocyanide

 The compound was synthesized according to the protocol published in Ref. <sup>2</sup>.

---

(<sup>1</sup>) Szymański, W.; Velema, W. A.; Feringa, B. L. *Angew. Chemie Int. Ed.* **2014**, *53*, 8682–8686.

(<sup>2</sup>) Pérez-Labrada, K.; Brouard, I.; Méndez, I.; Rivera, D. G. *J. Org. Chem.* **2012**, *77*, 4660–4670.

**2,3,4,6-tetra-O-acetyl- $\beta$ -D-glucopyranosyl isocyanide**

The compound was synthesized as described in Ref. <sup>3</sup> with a total yield of 67%.

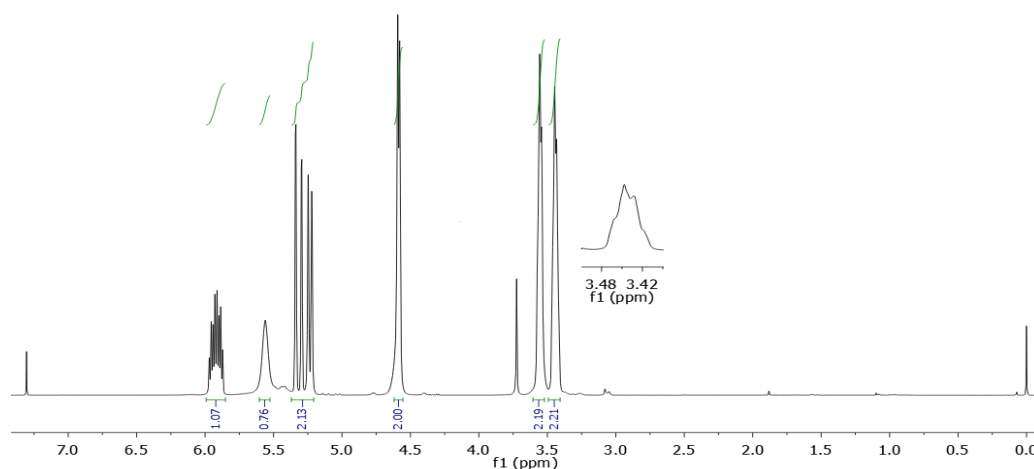
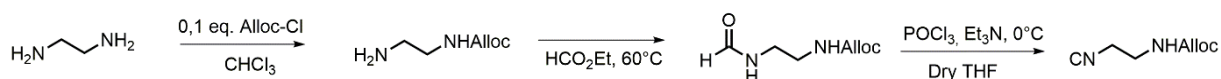
**allyl 2-isocyanoethylcarbamate**

Figure A1. <sup>1</sup>H NMR (400 MHz, CDCl<sub>3</sub>) spectrum of the allyl 2-isocyanoethylcarbamate.

Allyl 2-isocyanoethylcarbamate (1.9 g, 59%) was obtained following the general procedure described before, starting from 3 g of mono alloc-ethylenediamine.  $R_f$  = 0.59 (DCM). IR (KBr,  $\text{cm}^{-1}$ ):  $\nu_{\text{max}}$  = 3326, 2949, 2149, 1698, 1649, 1525, 1255, 1235. <sup>1</sup>H NMR (400 MHz, CDCl<sub>3</sub>):  $\delta$  = 5.92 (m, 1H), 5.56 (s, 1H), 5.32 (dd,  $J$  = 17.2, 1.6 Hz, 1H), 5.23 (dd, 10.4, 1.6 Hz, 1H), 4.59 (d,  $J$  = 5.7 Hz, 2H), 3.56 (t,  $J$  = 5.8 Hz, 2H), 3.48-3.41 (m, 2H). <sup>13</sup>C NMR (101 MHz, CDCl<sub>3</sub>):  $\delta$  = 157.4 (t,  $J$  = 5.2 Hz, CN), 156.1 (C=O), 132.4 (CH), 117.8 (CH), 65.7 (CH<sub>2</sub>), 41.7 (t,  $J$  = 6.6 Hz, CH<sub>2</sub>-N), 40.0 (CH<sub>2</sub>).

(<sup>3</sup>) Proserpi, D., Ronchi, S., Lay, L., Rencurosi, A. and Russo, G. *Eur. J. Org. Chem.* **2004**, 2004, 395-405.

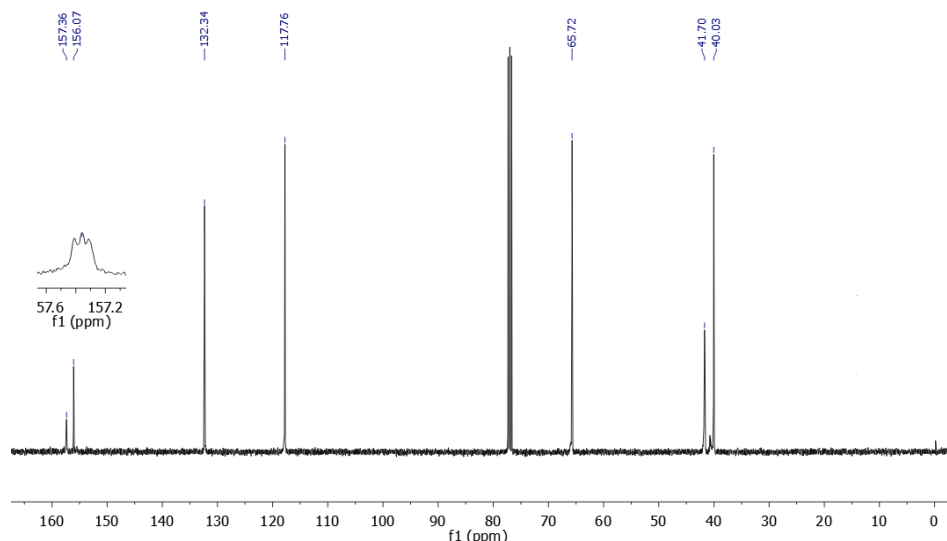
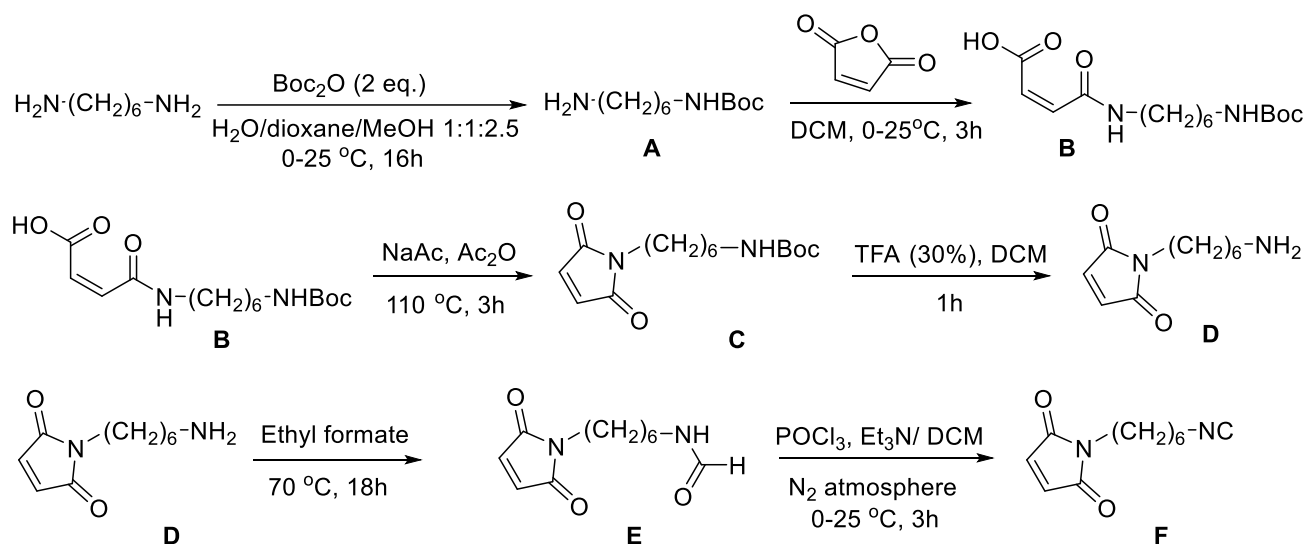


Figure A2.  $^{13}\text{C}$  NMR (100 MHz,  $\text{CDCl}_3$ ) spectrum of the allyl 2-isocyanoethylcarbamate.

### ***N***-(6-isocyanohexyl) maleimide



A solution of  $\text{Boc}_2\text{O}$  (3 g, 13,8 mmol) in 5 mL dioxane was added dropwise to 1,6-diaminohexane (8 g, 69 mmol) in 90 mL of a mixture of  $\text{H}_2\text{O}$ /dioxane/MeOH 1:1:2.5 at  $0^\circ\text{C}$ . The reaction mixture was stirred overnight at RT. Thereupon, the dioxane was evaporated and the residue extracted with EtOAc (3  $\times$  50 mL). The organic layer was dried over  $\text{Na}_2\text{SO}_4$  and the solvent was evaporated under reduced pressure to furnish monoprotected hexylidenediamine **A** (2.58 g, 87 %);  $R_f = 0.52$  (DCM/MeOH/FA, 1.6:0.4:0.05), which was employed without further purification.

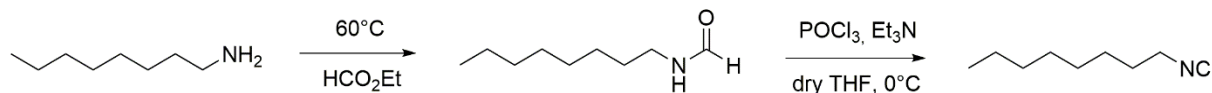
Compound **A** (2.58 g, 11.9 mmol) was dissolved in DCM (50 mL) and this solution was added dropwise to maleic anhydride (1.17 g, 11.3 mmol) in DCM (25 mL) at 0 °C. The reaction mixture was stirred for 3 h and washed with H<sub>2</sub>O (20 mL) and brine (20 mL). The organic layer was dried over Na<sub>2</sub>SO<sub>4</sub> and the solvent removed under reduced pressure. Column chromatography (EtOAc/*n*-hexane 4:1 – 7:1) afforded **B** (2.0 g, 53 %) as a colorless oil; *R<sub>f</sub>* = 0.31 (EtOAc/*n*-hexane 4:1). <sup>1</sup>H NMR (400 MHz, CDCl<sub>3</sub>): δ = 1.28 – 1.40 (m, 4H, 2 × CH<sub>2</sub>); 1.42 (s, 9H, C(CH<sub>3</sub>)<sub>3</sub>); 1.45 – 1.52 (m, 2H, CH<sub>2</sub>); 1.60 (p, 2H, *J* = 6.9 Hz, CH<sub>2</sub>); 3.12 (q, 2H, *J* = 6.6 Hz, CH<sub>2</sub>); 3.35 (q, 2H, *J* = 6.4 Hz, CH<sub>2</sub>); 4.70 (t, 1H, *J* = 6.4 Hz, NH); 6.29 (d, 1H, *J* = 12.8 Hz, CH); 6.50 (d, 1H, *J* = 12.8 Hz, CH); 8.25 (s, 1H, NH); <sup>13</sup>C NMR (100 MHz, CDCl<sub>3</sub>): δ = 25.1, 25.4, 28.2 (CH<sub>2</sub>); 28.6 (CH<sub>3</sub>); 30.1, 39.7, 53.6 (CH<sub>2</sub>); 79.6 (C); 132.1, 135.8 (CH); 156.8, 166.0, 166.4 (C=O).

A mixture of compound **B** (2 g, 6.37 mmol), anhydrous NaAcO (0.47 g, 5.73 mmol) and acetic anhydride (7.8 mL, 82.75 mmol) was heated to 110 °C and kept under reflux for 3 h. After the reaction was complete, it was cooled to 22 °C, and an ice cooled saturated NaHCO<sub>3</sub> solution (20 mL) was slowly poured into the reaction mixture to neutralize the excess of acid. The mixture was extracted with DCM (5 × 30 mL), washed with H<sub>2</sub>O (20 mL) and brine (20 mL). The organic layer was dried over Na<sub>2</sub>SO<sub>4</sub> and the solvent removed under reduced pressure. Column chromatography (*n*-hexane/EtOAc 3:1 – 1:1) afforded **C** (1.12 g, 59 %) as a colorless oil; *R<sub>f</sub>* = 0.66 (EtOAc/*n*-hexane 1.5:1). <sup>1</sup>H NMR (400 MHz, CDCl<sub>3</sub>): δ = 1.22 – 1.38 (m, 4H, 2 × CH<sub>2</sub>); 1.43 (s, 9H, C(CH<sub>3</sub>)<sub>3</sub>); 1.44 – 1.50 (m, 2H, CH<sub>2</sub>); 1.57 (p, 2H, *J* = 7.4 Hz, CH<sub>2</sub>); 3.08 (q, 2H, *J* = 6.7 Hz, CH<sub>2</sub>); 3.49 (t, 2H, *J* = 7.2 Hz, CH<sub>2</sub>); 4.51 (s, 1H, NH); 6.67 (s, 2H, 2 × CH); <sup>13</sup>C NMR (100 MHz, CDCl<sub>3</sub>): δ = 25.1, 25.4, 28.2 (CH<sub>2</sub>); 28.6 (CH<sub>3</sub>); 30.1, 39.7, 53.6 (CH<sub>2</sub>); 79.6 (C); 132.1, 135.8 (CH); 156.8, 166.0, 166.4 (C=O).

Compound **C** was dissolved in TFA (30 % in DCM) and the completion of the reaction was assessed by TLC (EtOAc/MeOH 3:1) and ESI-MS. The TFA was removed by successive co-evaporations with DCM to afford **D** in quantitative yields. Compound **D** (428 mg, 2.18 mmol) was subjected to the standard POCl<sub>3</sub> procedure for isocyanide synthesis to afford maleimido hexyl isocyanide **F** as a pale yellow oil (180 mg, 40 %) over two steps. Column chromatography: for the formamide (DCM/MeOH 20:1; *R<sub>f</sub>* = 0.83 (DCM/MeOH 10:1); yield = 59 %); for the isocyanide (EtOAc/ *n*-hexane 2:1; *R<sub>f</sub>* = 0.95 (EtOAc/*n*-hexane 2:1); yield = 68 %). <sup>1</sup>H NMR (400 MHz, CDCl<sub>3</sub>): δ = 1.32 (p, 2H, *J* = 7.2 Hz, CH<sub>2</sub>); 1.41 – 1.53 (m, 2H, CH<sub>2</sub>); 1.56 – 1.72 (m, 4H); 3.38 (tt, 2H, *J* = 6.6/1.9 Hz, CH<sub>2</sub> α); 3.52 (t, 2H; *J* = 7.2 Hz, CH<sub>2</sub>); 6.69 (s,

2H, 2 × CH)  $^{13}\text{C}$  NMR (100 MHz,  $\text{CDCl}_3$ ):  $\delta$  = 26.0, 28.4, 29.1, 37.8 ( $\text{CH}_2$ ); 41.6 (t,  $J$  = 6.5 Hz,  $\text{CH}_2$ ); 134.2 (CH); 156.1 (t,  $J$  = 5.7 Hz,  $\text{C}\equiv\text{N}$ ); 171.0 ( $\text{C}=\text{O}$ ).

### *n*-octylisocyanide



*n*-octyl amine (4 mL, 0.024 mol) is dissolved in ethyl formate (30 mL) and the system is stirred at reflux for 12 h. After removing the solvent until dryness, the formamide (3.8 g, 0.024 mol) is dissolved in 40 mL of dry THF and mixed with  $\text{Et}_3\text{N}$  (11.8 mL, 0.85 mol). The reaction mixture is connected with a stream of  $\text{N}_2$ , cooled to 0 °C and a solution of  $\text{POCl}_3$  (2.7 g, 0.029 mol) in 15 mL of THF is added dropwise during 30 minutes. The system is stirred at 0 °C for 2 h, then allowed to reach room temperature, quenched with 50 mL of 10 % aqueous  $\text{Na}_2\text{CO}_3$  and extracted with  $\text{EtOAc}$  (2×50 mL). The combined organic phases are combined, washed with brine (20 mL), dried over anhydrous  $\text{Na}_2\text{SO}_4$ , and concentrated under reduced pressure. The crude product is purified by column chromatography (DCM) to afford the pure *n*-octylisocyanide (2.7 g, 82%) as a pale yellow oil.  $R_f$  = 0.82 (DCM). IR (KBr,  $\text{cm}^{-1}$ ): 2951.6, 2924.8, 2856.6, 2145.8, 1455.9.  $^1\text{H}$  NMR (400 MHz,  $\text{CDCl}_3$ )  $\delta$  3.40 – 3.35 (m, 1H), 1.75 – 1.61 (m, 2H), 1.48 – 1.39 (m, 2H), 1.36 – 1.23 (m, 8H), 0.89 (t,  $J$  = 6.8 Hz, 3H).  $^{13}\text{C}$  NMR (101 MHz,  $\text{CDCl}_3$ )  $\delta$  155.67, 41.65, 31.78, 29.20, 29.11, 28.75, 26.41, 26.40, 22.68, 14.13.

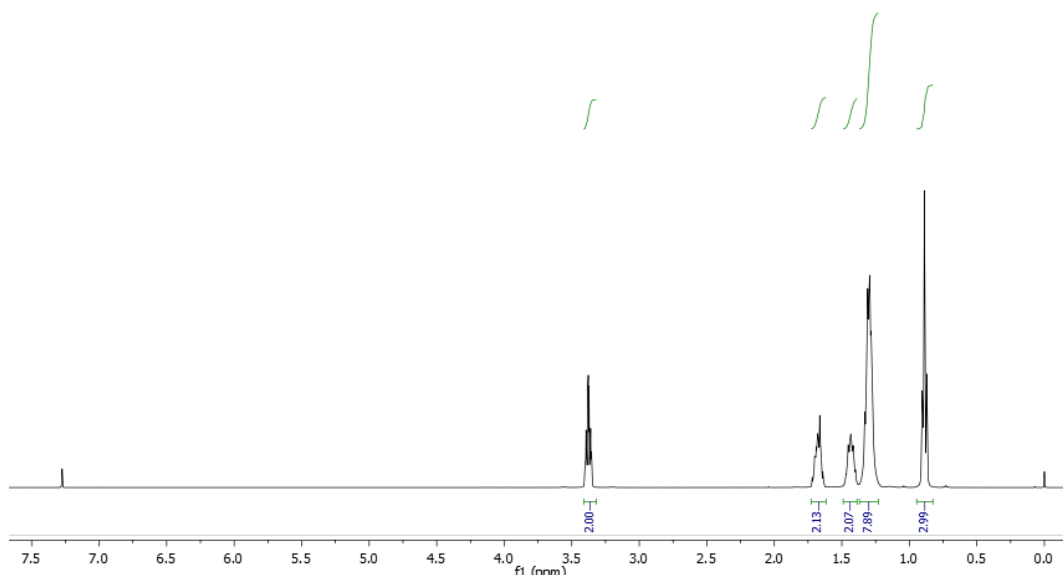


Figure A3.  $^1\text{H}$  NMR (400 MHz,  $\text{CDCl}_3$ ) spectrum of *n*-octylisocyanide.

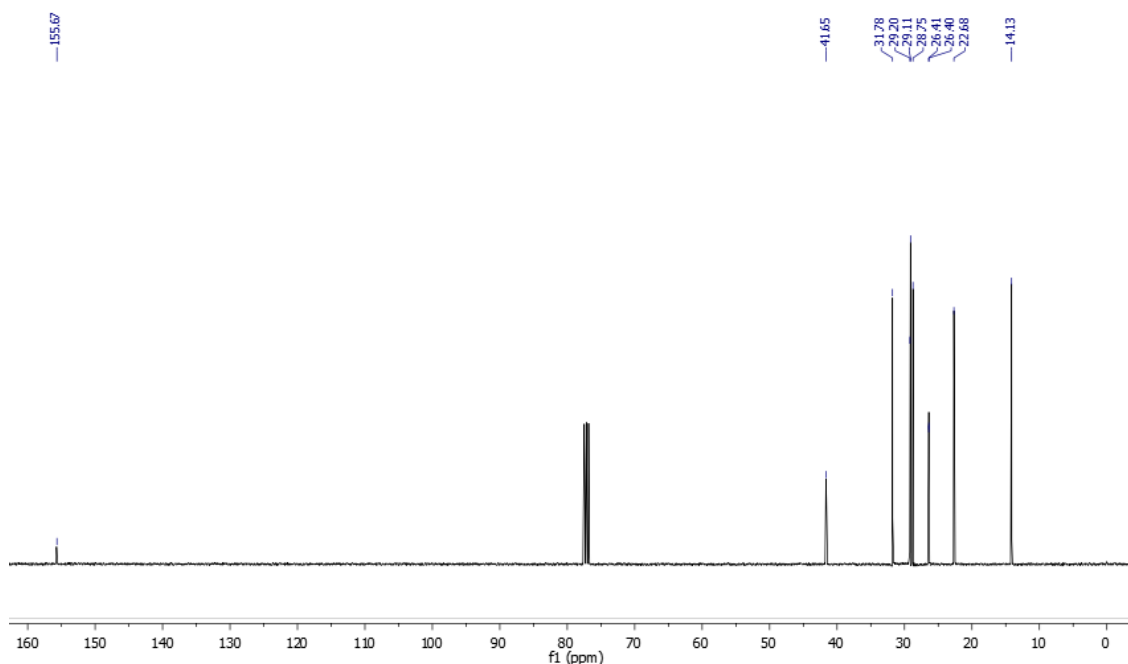
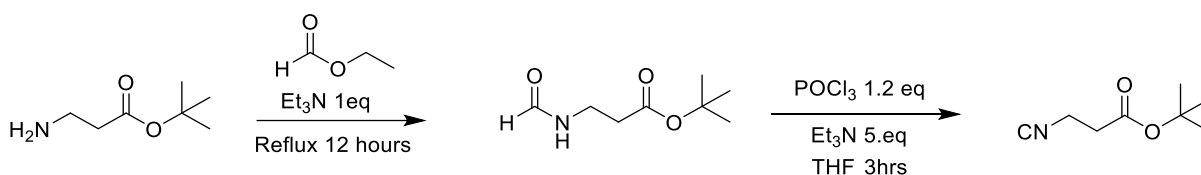


Figure A4.  $^{13}\text{C}$  NMR (100 MHz,  $\text{CDCl}_3$ ) spectrum of *n*-octylisocyanide.

### ***t*-butyl 3-isocyanopropanoate**



A solution of  $\beta$ -alanine *t*-butyl ester hydrochloride (27.5 mmol, 5.00 g) in ethyl formate (20 mL) was heated at reflux for 3 hours. The solvent was evaporated, yielding the formamide product as a clear colourless oil, which was not further purified. This latter product (4.8 g) and triethylamine (137.6 mmol, 19.2 mL) were dissolved in freshly distilled THF (20 mL) and the solution was cooled to  $-60\text{ }^\circ\text{C}$ . Phosphorus oxychloride (33.0 mmol, 3.08 mL) was added dropwise, keeping the temperature below  $-55\text{ }^\circ\text{C}$ . The cooling was removed and the reaction mixture was allowed to warm up to room temperature and stirred for additional 2 h. The reaction mixture was then poured into ice-cooled satd. aq.  $\text{NaHCO}_3$  (40 mL) and the organic phase was separated. The aqueous phase was washed with chloroform ( $2 \times 25\text{ mL}$ ). The collected and combined organic phases were dried ( $\text{MgSO}_4$ ) and the solvent was evaporated. The product was purified by flash chromatography (*n*-hexane/ $\text{AcOEt}$ , 8:1, *v/v*;  $R_f = 0.68$ ). Yield (3.8 g) 87%; yellow oil.  $^1\text{H}$  NMR (400 MHz,  $\text{CDCl}_3$ )  $\delta = 3.57$  (tt,  $J = 6.8, 1.9\text{ Hz}$ , 2H), 2.56

(tt,  $J = 6.8, 2.1$  Hz, 2H), 1.41 (d,  $J = 1.2$  Hz, 9H).  $^{13}\text{C}$  NMR (101 MHz,  $\text{CDCl}_3$ )  $\delta$  167.59 (CO), 156.16 (t,  $J = 5.4$  Hz), 80.86 ( $\text{C}(\text{CH}_3)_3$ ), 36.40 (t,  $J = 7.1$  Hz,  $\text{CH}_2$ ), 34.24 ( $\text{CH}_2$ ), 27.00 ( $\text{C}(\text{CH}_3)_3$ ).

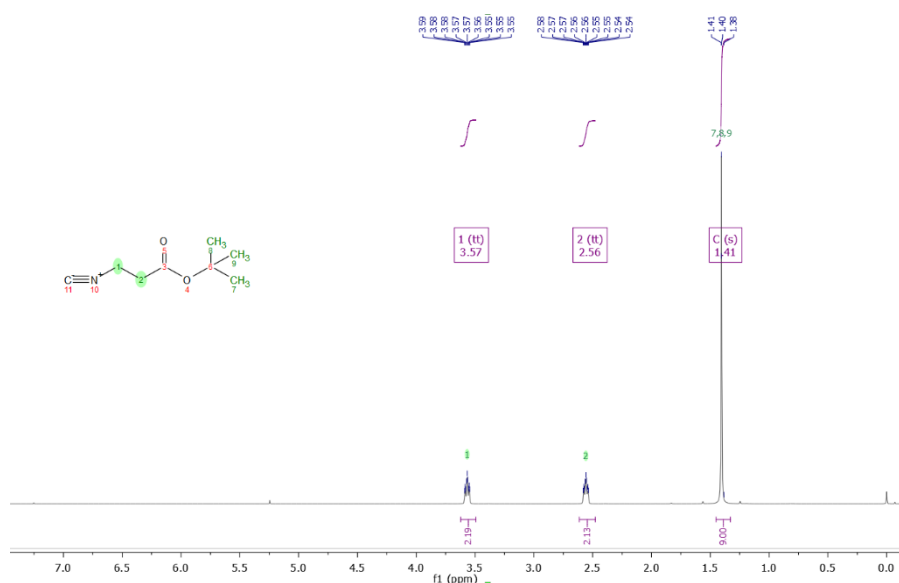


Figure A5.  $^1\text{H}$ -NMR spectrum of *tert*-butyl 3-isocyanopropanoate

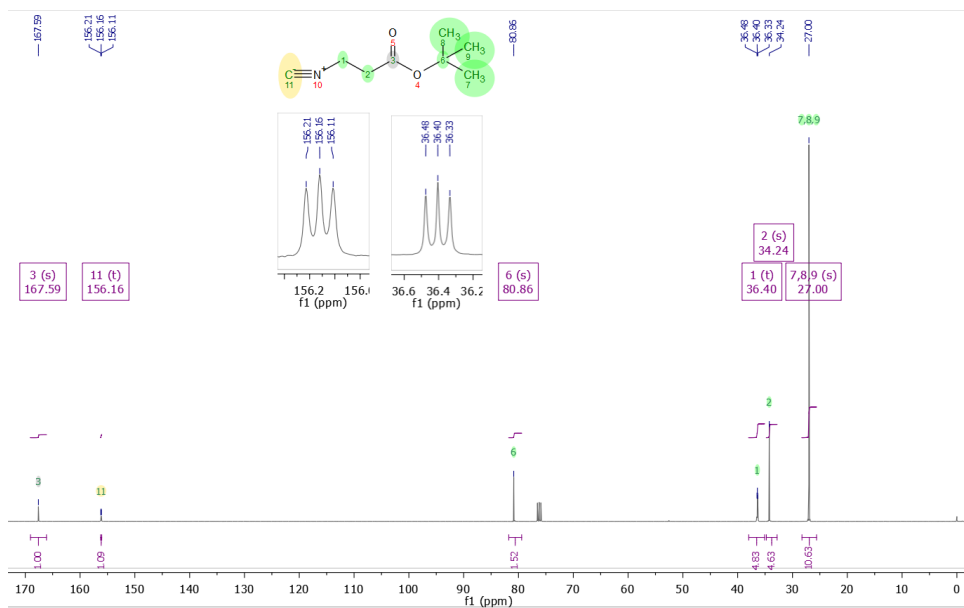


Figure A6.  $^{13}\text{C}$ -NMR spectrum of *tert*-butyl 3-isocyanopropanoate



Commercial MA(PEG)<sub>12</sub> amine (560 mg, 1 mmol, 1 equiv.) was dissolved in 1 mL DCM and methyl isocyanoacetate (0.1 mL, 109 mg, 1.1 mmol, 1.5 equiv.) was added. The reaction mixture was stirred overnight and then lixiviated with 10 ml of *n*-heptane to remove any excess of methyl isocyanoacetate. The PEG-derived isocyanide was employed without further purification. <sup>1</sup>H NMR (400 MHz, CDCl<sub>3</sub>): δ 7.23 (br. s, 1H), 4.21 (s, 2H), 3.78-3.59 (m, 44H), 3.57 – 3.45 (m, 4H), 3.38 (s, 3H). <sup>13</sup>C NMR (101 MHz, CDCl<sub>3</sub>): δ 162.70 (CO), 161.40 (br. s, CN), 71.94, 70.55, 70.33, 69.27, 59.03, 39.73. RP-HPLC R<sub>t</sub>. 11.09 min.

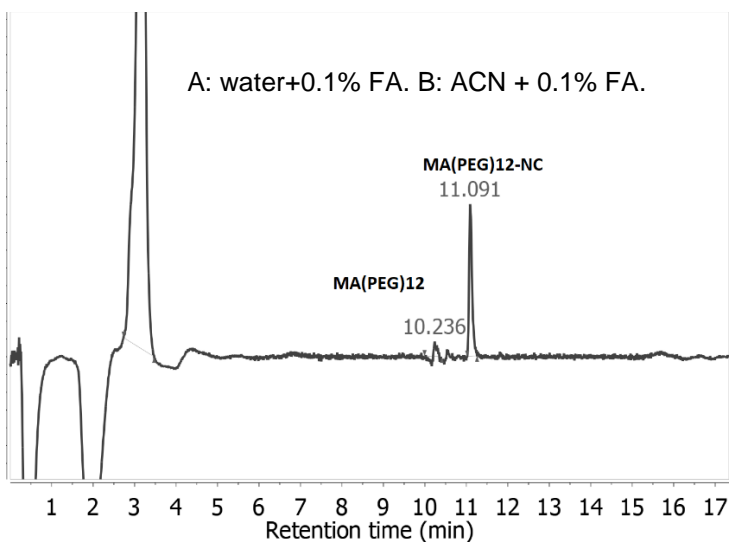


Figure A7. HPLC trace of the crude of *N*-(36-methoxy-β-(PEG)<sub>11</sub>-ethyl)-2-isocyanoacetamide

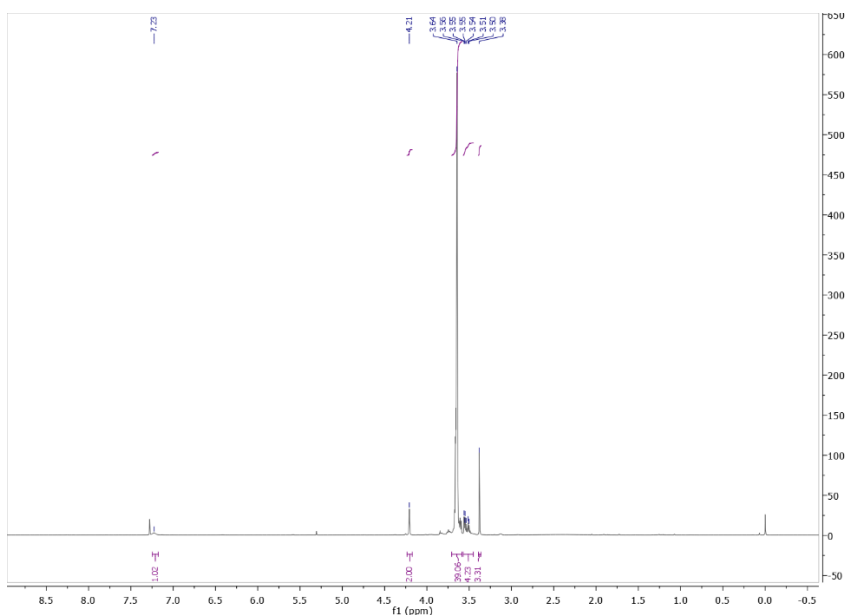


Figure A8. <sup>1</sup>H-NMR spectrum of *N*-(36-methoxy-β-(PEG)<sub>11</sub>-ethyl)-2-isocyanoacetamide

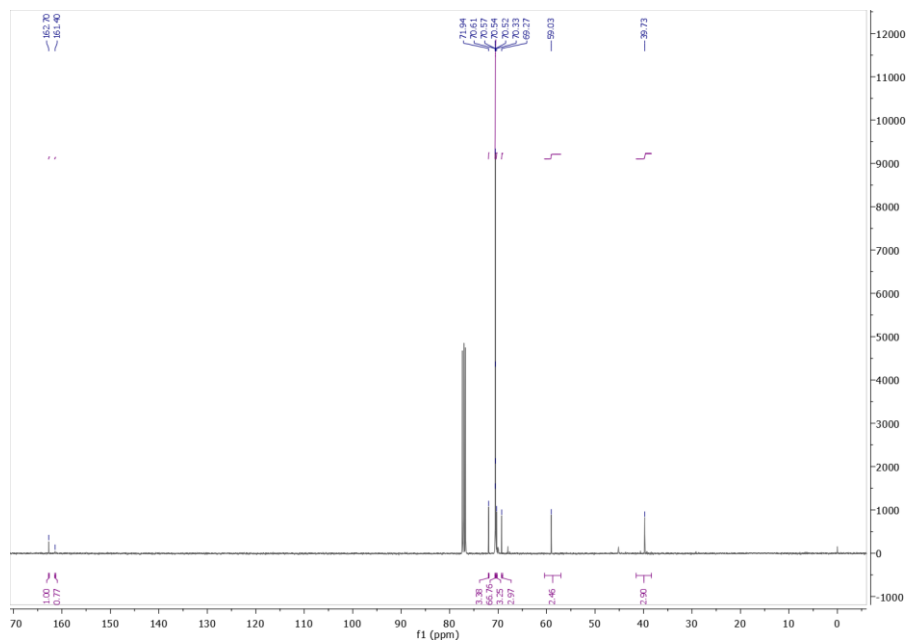
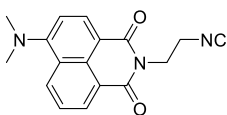


Figure A9.  $^{13}\text{C}$ -NMR spectrum of *N*-(36-methoxy- $\beta$ -(PEG)<sub>11</sub>-ethyl)-2-isocyanoacetamide

### **2-(4-dimethylamino-1,8-naphthalimido) ethyl isocyanide**



This fluorescent isocyanide was produced from 4-*N,N*-dimethylamino-1,8-naphthalic anhydride as described in Ref. <sup>4</sup> in a total yield of 26%.

<sup>4</sup> Rotstein, B. H., Mourtada, R., Kelley, S. O. and Yudin, A. K. *Chem. Eur. J.* **2011**, *17*, 12257-12261

## NMR data of selected compounds

Table A1. Full assignment of the NMR resonances for cyclic peptide **30**

Residue	Peptidic Region								Others		
	Amide		$\alpha$		$\beta$		$\gamma$		H (assignment)	C (assignment)	
NH (m, J)	CO	H	C	H	C	H	C				
Leu	7.36 (d, )	171.8	4.02	52.9	1.20; 1.38	40.9	1.56	24.2	0.81, 0.85 (2 × CH <sub>3</sub> δ)	21.3, 23.2 (2 × CH <sub>3</sub> δ)	
Lys	7.87 (d, )	171.4	4.30	52.4	1.69; 1.42	32.9	1.25; 1.35	22.6	1.52; 1.41 (Hδ), 2.90; 3.45 (Hε)	28.1 (Cδ), 48.4 (Cε)	
Phe	8.73 (d, )	170.2	4.42	54.3	2.77; 3.15	37.3	-	137.9	Ar: 7.17 (o), 7.20 (m), 7.13 (p)	Ar: 128.8 (o), 128.2 (m), 126.2 (p)	
Val	6.72 (d, )	172.4	4.30	56.0	2.00	31.4	0.83, 0.90	17.4, 19.2	-	-	
Glu	8.32 (d, )	170.4	4.30	50.5	1.57; 2.21	27.1	2.35; 2.40	27.7	-	171.4 (CO ε)	
Ala	8.23 (d, )	172.5	4.03	49.0	1.21	17.0	-	-	3.64 (OCH <sub>3</sub> )	52.0 (OCH <sub>3</sub> )	
<i>N</i> -alkylated substituent produced by cyclization	CH <sub>2</sub>		NH		C=O		Cyclohexane ring				
	H	C					H (assign.)		C (assign.)		
		3.72; 3.90	48.7	7.54	167.3	3.50 (α), 1.65, 1.63, 1.21, 1.11, 1.19, 1.17, 1.15				47.5 (α), 32.3, 32.4	
Cbz protective group	CH <sub>2</sub>		C=O		Aromatic signals						
	H	C			H (assign.)		C (assign.)				
		5.01	65.3	155.9	7.34 (o), 7.35 (m), 7.30 (p)						137.2 (quat), 127.6 (o), 128.4 (m), 127.8 (p)

Table A2. Full assignment of the NMR resonances for cyclic peptide **32**

Residue	Peptidic Region								Others	
	Amide		$\alpha$		$\beta$		$\gamma$		H (assign.)	C (assign.)
NH (m, J (Hz))	CO	H	C	H	C	H	C			
Val	7.92 (d, 9.0)	171.10	4.18	57.7	1.93	30.4	0.79, 0.81	18.2, 19.3	-	-
Ile	7.84 (d, 8.8)	170.38	4.15	56.7	1.69	36.6	1.41; 1.05 (CH <sub>2</sub> ), 0.79 (CH <sub>3</sub> )	24.4 (CH <sub>2</sub> ), 15.2 (CH <sub>3</sub> )	0.79 (CH <sub>3</sub> δ)	11.07 (CH <sub>3</sub> δ)
Glu	7.96 (d, 7.1)	170.30	4.26	51.9	1.75; 1.84	27.7	2.26; 2.61	28.3	-	171.84 (CO δ)
Ala	8.15 (d, 6.4)	171.90	4.07	48.9	1.26	17.8	-	-	-	-
Gln	7.82 (d, 6.7)	171.19	4.02	53.1	1.76; 2.08	27.1	1.76; 2.07	31.3	7.31; 6.80 (NH <sub>2</sub> )	173.83 (CO δ)
Lys	7.94 (d, 9.4)	171.68	4.25	51.7	1.55; 1.35	31.9	1.16	21.9	1.48; 1.36 (δ), 3.21 (ε)	27.4 (δ), 47.9 (ε)
Phe	8.03 (d, 8.1)	171.26	4.49	54.0	3.03; 2.80	37.4	-	137.6	Ar: 7.22 (o), 7.24 (m), 7.17 (p)	Ar: 129.2 (o), 128.1 (m), 126.3 (p)
Gly	8.31 (t, 6.0)	170.72	3.56; 3.65	41.9	-	-	-	-	7.18; 7.08 (terminal NH <sub>2</sub> )	-
<i>N</i> -alkylated substituent produced by cyclization	CH <sub>2</sub>		NH (m)		C=O		<i>tert</i> -Butyl group			
	H	C					H (assign.)		C (assign.)	
		3.70; 3.85	47.5	7.40 (s)	167.65	1.23 (CH <sub>3</sub> )		50.06 (C), 28.6 (3 × CH <sub>3</sub> )		
<i>N</i> -terminal acetyl group		H (assign.)		C (assign.)						
		1.85 (CH <sub>3</sub> )		165.90 (CO), 22.5 (CH <sub>3</sub> )						

Table A3. Full assignment of the NMR resonances for cyclic peptide **34**

Residue	Peptidic Region									
	Amide		$\alpha$		$\beta$		$\gamma$		Others	
	NH (m, J (Hz))	CO	H	C	H	C	H	C	H (assign.)	C (assign.)
Phe	8.03 (d, 8.5)	170.95	4.52	53.8	2.93; 2.68	37.7	-	138.0	Ar: 7.23 (o), 7.25 (m), 7.18 (p)	Ar: 129.2 (o), 128.1 (m), 126.2 (p)
Lys	8.05 (d, 8.4)	171.56	4.34	52.1	1.68; 1.44	31.5	1.30	22.2	1.69; 1.42 ( $\delta$ ), 3.06; 3.42 ( $\epsilon$ )	27.37( $\delta$ ), 48.61( $\epsilon$ )
Gly	8.44 (m)	169.55	4.38; 3.72	41.1	-	-	-	-	-	-
Pro	-	172.74	4.16	61.4	2.19; 1.82	29.1	1.93; 1.89	24.5	3.73; 3.51 ( $\delta$ )	46.6 ( $\delta$ )
Ala I	8.24 (d, 6.3)	172.55	4.14	49.7	1.30	16.2	-	-	-	-
Asp	7.53 (d, 7.6)	170.87	4.59	50.6	3.12; 2.54	34.0	-	170.36	-	-
Ala II	7.60 (d, 7.5)	173.76	4.09	48.4	1.23	17.9	-	-	7.01; 7.04 (terminal NH <sub>2</sub> )	-
<i>N</i> -alkylated substituent produced by cyclization	CH <sub>2</sub>		NH (m)		C=O		Others (assigned respect to amide group)			
	H	C	H	C	H	C	H (assign.)		C (assign.)	
		4.08; 3.60	48.5	7.65 (s)	168.01		3.11; 3.02 (CH <sub>2</sub> $\alpha$ ), 1.63 (CH <sub>2</sub> $\beta$ ), 2.20 (CH <sub>2</sub> $\gamma$ ), 3.58 (OCH <sub>3</sub> )		38.0 (CH <sub>2</sub> $\alpha$ ), 24.4 (CH <sub>2</sub> $\beta$ ), 30.6 (CH <sub>2</sub> $\gamma$ ), 173.21(CO), 51.3 (OCH <sub>3</sub> )	
<i>N</i> -terminal acetyl group	H (assign.)		C (assign.)							
	1.85 (CH <sub>3</sub> )		165.90 (CO), 22.5 (CH <sub>3</sub> )							

Table A4. Full assignment of the NMR resonances for cyclic peptide **40a**

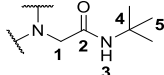
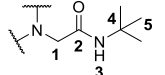
Major conformer( <i>s-cis</i> ) 63%					Minor conformer( <i>s-trans</i> ) 37%																																								
Residue	HN( $^{\circ}$ J)	HA/CA	HB/CB	CO	others	Residue	HN( $^{\circ}$ J)	HA/CA	HB/CB	CO	others																																		
Ace	-	1.99/21.57	-	176.8	-	Ace	-	2.07/24.4	-	177.6	-																																		
Lys <sup>1</sup>	8.19(5.9)	4.19/56.4	1.68, 1.78/ 33.7	177.5	1.49/ 24.9 $\gamma$ ; 1.60, 1.71/ 31.1 $\delta$ ; 3.28, 3.60/ 52.8 $\epsilon$	Lys <sup>1</sup>	8.28 (3.6)	4.12/ 57.8	1.77, 1.80/ 31.8	n.d	1.13, 1.57/ 24.8 $\gamma$ ; 1.84, 1.36/ 28.1 $\delta$ ; 2.69, 3.97/ 52.0 $\epsilon$																																		
Ala <sup>2</sup>	8.64 (4.6)	4.29/52.6	1.47/ 19.2	178.7	-	Ala <sup>2</sup>	8.42 (3.7)	4.07/ 54.9	1.42/ 17.9	180.2	-																																		
Ala <sup>3</sup>	8.50 (3.5)	4.14/54.5	1.45/ 18.4	179.3	-	Ala <sup>3</sup>	7.82 (5.9)	4.18/ 53.7	1.41/ 18.6	179.5	-																																		
Ala <sup>4</sup>	8.10 (5.0)	4.25/53.1	1.40/ 18.3	174.7	-	Ala <sup>4</sup>	7.96 (5.3)	4.15/ 54.1	1.43/ 18.5	179.3	-																																		
Asp <sup>5</sup>	7.84 (7.2)	4.60/53.8	2.79, 3.32/ 36.8	179.0	174.7 $\gamma$ ; 7.30, 7.16 (terminal NH <sub>2</sub> )	Asp <sup>5</sup>	8.14 (6.5)	4.59/ 53.7	2.78, 2.93/ 37.4	n.d	7.28, 7.04 (terminal NH <sub>2</sub> )																																		
																																													
<table border="1"> <thead> <tr> <th><i>N</i>-substitution</th> <th>Atom group</th> <th><math>\delta_H/\delta_C</math></th> </tr> </thead> <tbody> <tr><td></td><td>1</td><td>3.95/ 52.8</td></tr> <tr><td></td><td>2</td><td>/172.3</td></tr> <tr><td></td><td>3</td><td>7.37/ -</td></tr> <tr><td></td><td>4</td><td>/ 54.3</td></tr> <tr><td></td><td>5</td><td>1.32/ 28.6</td></tr> </tbody> </table>					<i>N</i> -substitution	Atom group	$\delta_H/\delta_C$		1	3.95/ 52.8		2	/172.3		3	7.37/ -		4	/ 54.3		5	1.32/ 28.6	<table border="1"> <thead> <tr> <th><i>N</i>-substitution</th> <th>Atom group</th> <th><math>\delta_H/\delta_C</math></th> </tr> </thead> <tbody> <tr><td></td><td>1</td><td>.89, 4.16/ 56.9</td></tr> <tr><td></td><td>2</td><td>/172.1</td></tr> <tr><td></td><td>3</td><td>7.65/ -</td></tr> <tr><td></td><td>4</td><td>/ 54.6</td></tr> <tr><td></td><td>5</td><td>1.32/ 30.5</td></tr> </tbody> </table>					<i>N</i> -substitution	Atom group	$\delta_H/\delta_C$		1	.89, 4.16/ 56.9		2	/172.1		3	7.65/ -		4	/ 54.6		5	1.32/ 30.5
<i>N</i> -substitution	Atom group	$\delta_H/\delta_C$																																											
	1	3.95/ 52.8																																											
	2	/172.3																																											
	3	7.37/ -																																											
	4	/ 54.3																																											
	5	1.32/ 28.6																																											
<i>N</i> -substitution	Atom group	$\delta_H/\delta_C$																																											
	1	.89, 4.16/ 56.9																																											
	2	/172.1																																											
	3	7.65/ -																																											
	4	/ 54.6																																											
	5	1.32/ 30.5																																											

Table A5. Full assignment of the NMR resonances for cyclic peptide **40c**

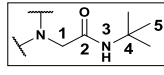
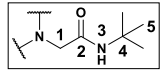
Major conformer (~69%)					Minor conformer (~31%)																																								
Residue	HN( $^{\circ}$ J)	HA/CA	HB/CB	CO	others	Residue	HN( $^{\circ}$ J)	HA/CA	HB/CB	CO	others																																		
Ace <sup>1</sup>	-	2.03/24.5	-	176.0	-	Ace <sup>1</sup>	-	2.09/24.6	-	176.1	-																																		
Arg <sup>2</sup>	8.24(6.7)	4.27/56.1	1.64/27.1	177.4	1.73-1.81/31.1 $\gamma$ ; 3.20/43.40 $\delta$ ; 159.7 $\zeta$	Arg <sup>2</sup>	8.41	4.16/57.9	n/d	n/d	3.21/43.5 $\delta$																																		
Lys <sup>3</sup>	8.35 (6.0)	4.24/56.4	1.69-1.82/33.7	176.3	1.51/24.9 $\gamma$ ; 1.71-1.59/24.9 $\delta$ ; 3.59-3.29/52.8 $\epsilon$	Lys <sup>3</sup>	8.38	4.22/57.6	1.73-1.82/33.4	177.1	n/d																																		
Ala <sup>4</sup>	8.67 (4.8)	4.28/52.5	1.46/19.2	177.7	-	Ala <sup>4</sup>	8.27 (3.0)	4.09/54.6	1.41/19.3	179.6	-																																		
Ala <sup>5</sup>	8.49 (2.7)	4.15/54.4	1.45/18.7	179.1	-	Ala <sup>5</sup>	7.69 (6.1)	4.20/53.6	1.44/18.9	178.9	-																																		
Ala <sup>6</sup>	8.11 (4.9)	4.25/53.1	1.40/18.3	177.5	-	Ala <sup>6</sup>	8.04 (5.4)	4.19/53.4	1.45/18.6	179.1	-																																		
Asp <sup>7</sup>	7.83 (7.3)	4.60/53.8	2.79-3.31/39.1	177.9	174.7 $\gamma$ ; 7.32-7.16 (terminal NH <sub>2</sub> )	Asp <sup>7</sup>	8.21 (6.8)	4.60/53.8	2.92-2.78/37.4	n/d	173.9 $\gamma$ ; 7.27-7.12 (terminal NH <sub>2</sub> )																																		
																																													
<table border="1"> <thead> <tr> <th><i>N</i>-substitution</th> <th>Atom group</th> <th><math>\delta_H/\delta_C</math></th> </tr> </thead> <tbody> <tr><td></td><td>1</td><td>3.95/53.0</td></tr> <tr><td></td><td>2</td><td>172.4</td></tr> <tr><td></td><td>3</td><td>7.38</td></tr> <tr><td></td><td>4</td><td>54.3</td></tr> <tr><td></td><td>5</td><td>1.32/30.8</td></tr> </tbody> </table>					<i>N</i> -substitution	Atom group	$\delta_H/\delta_C$		1	3.95/53.0		2	172.4		3	7.38		4	54.3		5	1.32/30.8	<table border="1"> <thead> <tr> <th><i>N</i>-substitution</th> <th>Atom group</th> <th><math>\delta_H/\delta_C</math></th> </tr> </thead> <tbody> <tr><td></td><td>1</td><td>4.15-3.93/56.6</td></tr> <tr><td></td><td>2</td><td>n/d</td></tr> <tr><td></td><td>3</td><td>7.67</td></tr> <tr><td></td><td>4</td><td>n/d</td></tr> <tr><td></td><td>5</td><td>1.33/30.6</td></tr> </tbody> </table>					<i>N</i> -substitution	Atom group	$\delta_H/\delta_C$		1	4.15-3.93/56.6		2	n/d		3	7.67		4	n/d		5	1.33/30.6
<i>N</i> -substitution	Atom group	$\delta_H/\delta_C$																																											
	1	3.95/53.0																																											
	2	172.4																																											
	3	7.38																																											
	4	54.3																																											
	5	1.32/30.8																																											
<i>N</i> -substitution	Atom group	$\delta_H/\delta_C$																																											
	1	4.15-3.93/56.6																																											
	2	n/d																																											
	3	7.67																																											
	4	n/d																																											
	5	1.33/30.6																																											

Table A6. Full assignment of the NMR resonances for cyclic peptide **40d**

Major conformer (~71.5%, s-cis)						Minor conformer (~28.5%, s-trans)					
Residue	HN( $\delta$ )	HA/CA	HB/CB	CO	others	Residue	HN( $\delta$ )	HA/CA	HB/CB	CO	others
Ace <sup>1</sup>	-	1.99/24.5	-	176.9	-	Ace <sup>1</sup>	-	2.06/24.6	-	177.7	-
Lys <sup>2</sup>	8.19 (5.8)	4.18/56.5	1.68-1.77/33.7	176.8	1.48/30.0 $\gamma$ ; 1.74-1.59/29.9 $\delta$ ; 3.29/52.9 $\epsilon$	Lys <sup>2</sup>	8.29 (3.6)	4.12/57.9	1.80/37.9	n/d	1.87-1.36/28.0 $\delta$ ; 3.95-2.70/51.6 $\epsilon$
Ala <sup>3</sup>	8.60 (4.7)	4.28/52.6	1.46/19.2	178.8	-	Ala <sup>3</sup>	8.43 (3.7)	4.06/55.2	1.40/19.3	180.2	-
Ala <sup>4</sup>	8.51 (3.5)	4.14/54.6	1.44/18.6	179.4	-	Ala <sup>4</sup>	7.82 (5.7)	4.18/53.9	1.41/18.0	179.5	-
Ala <sup>5</sup>	8.12 (4.8)	4.24/53.3	1.40/18.4	177.6	-	Ala <sup>5</sup>	7.95 (6.4)	4.15/54.2	1.43/18.0	179.3	-
Asp <sup>6</sup>	7.84 (7.1)	4.58/53.9	2.80-3.32/36.9	178.2	174.9 $\gamma$ ; 7.30-7.20 (terminal NH <sub>2</sub> )	Asp <sup>6</sup>	8.15 (6.5)	4.59/53.9	2.80-2.93/37.5	179.1	173.8 $\gamma$ ; 7.05-7.28 (terminal NH <sub>2</sub> )

N-substitution			N-substitution		
Atom group	$\delta_H/\delta_C$		Atom group	$\delta_H/\delta_C$	
1	4.10-3.96/52.4		1	4.27-3.96/56.2	
2	173.50		2	173.20	
3	7.92 (6.0)		3	8.10 (5.9)	
4	3.45/39.0		4	3.46/39.2	
5	2.51/37.9		5	2.50/38.0	
6	181.00		6	181.10	

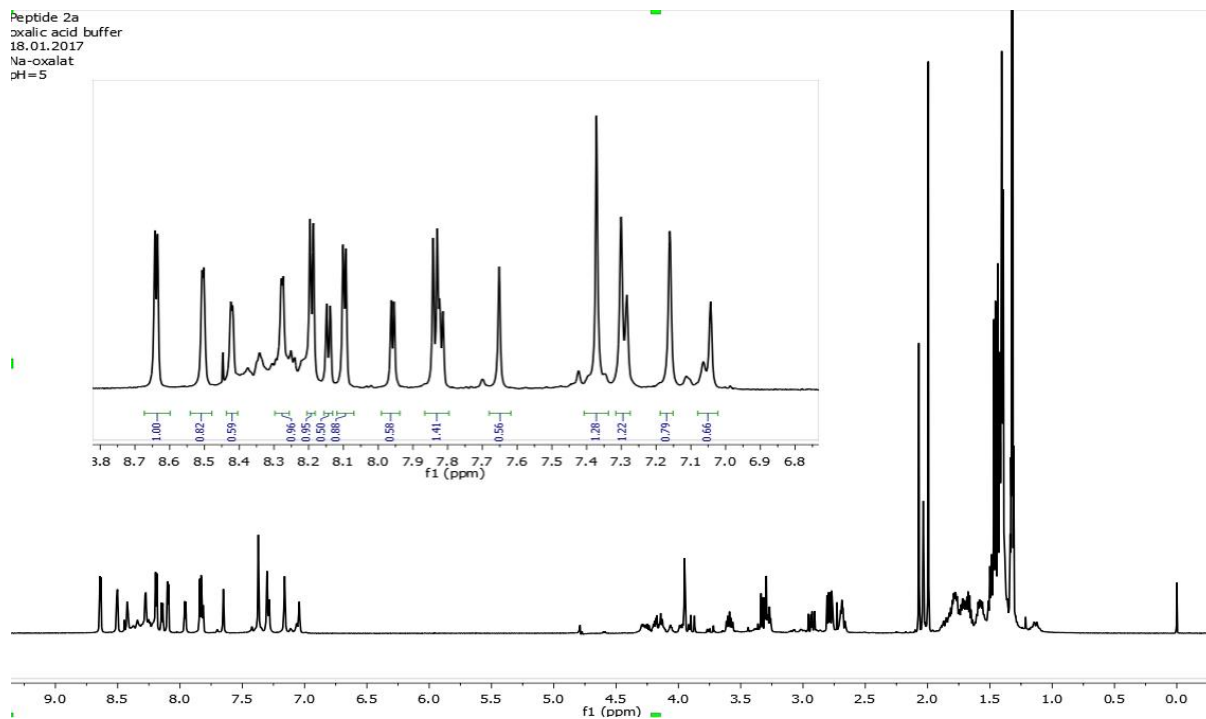


Figure A10. <sup>1</sup>H-NMR spectrum of peptide **40a** in a pH 5 oxalic acid/oxalate buffer in Water/D<sub>2</sub>O 9:1 obtained using the WATERGATE pulse sequence for water suppression.

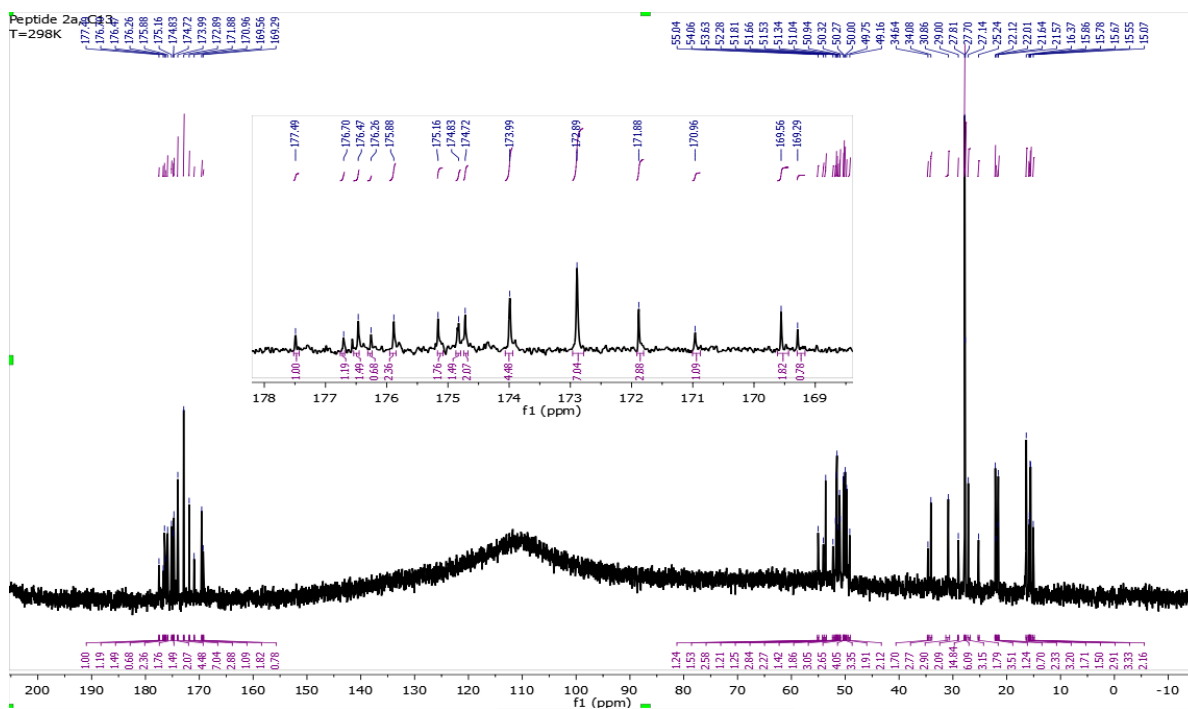


Figure A11.  $^{13}\text{C}$ -NMR spectrum of peptide **40a** in a pH 5 oxalic acid/oxalate buffer in Water/ $\text{D}_2\text{O}$  9:1

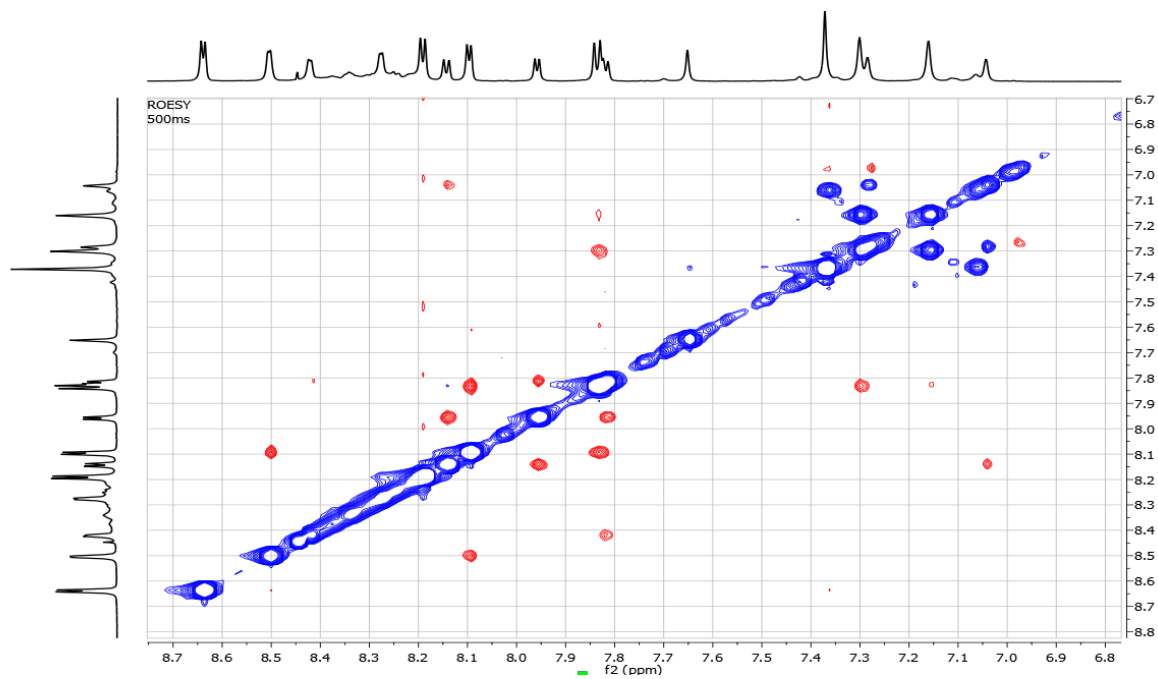


Figure A12.  $^1\text{H}$ - $^1\text{H}$  section of the ROESY spectrum of peptide **40a** in a pH 5 oxalic acid/oxalate buffer in Water/ $\text{D}_2\text{O}$  9:1

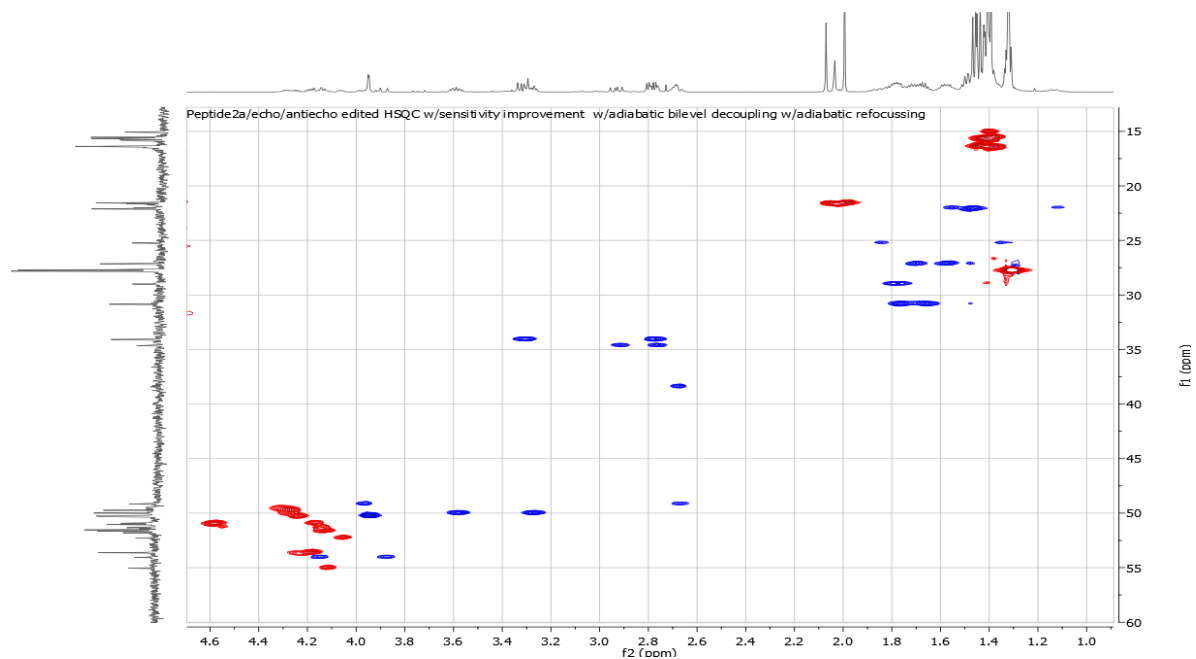


Figure A13. HSQC spectrum of peptide **40a** in a pH 5 oxalic acid/oxalate buffer in Water/D<sub>2</sub>O 9:1.

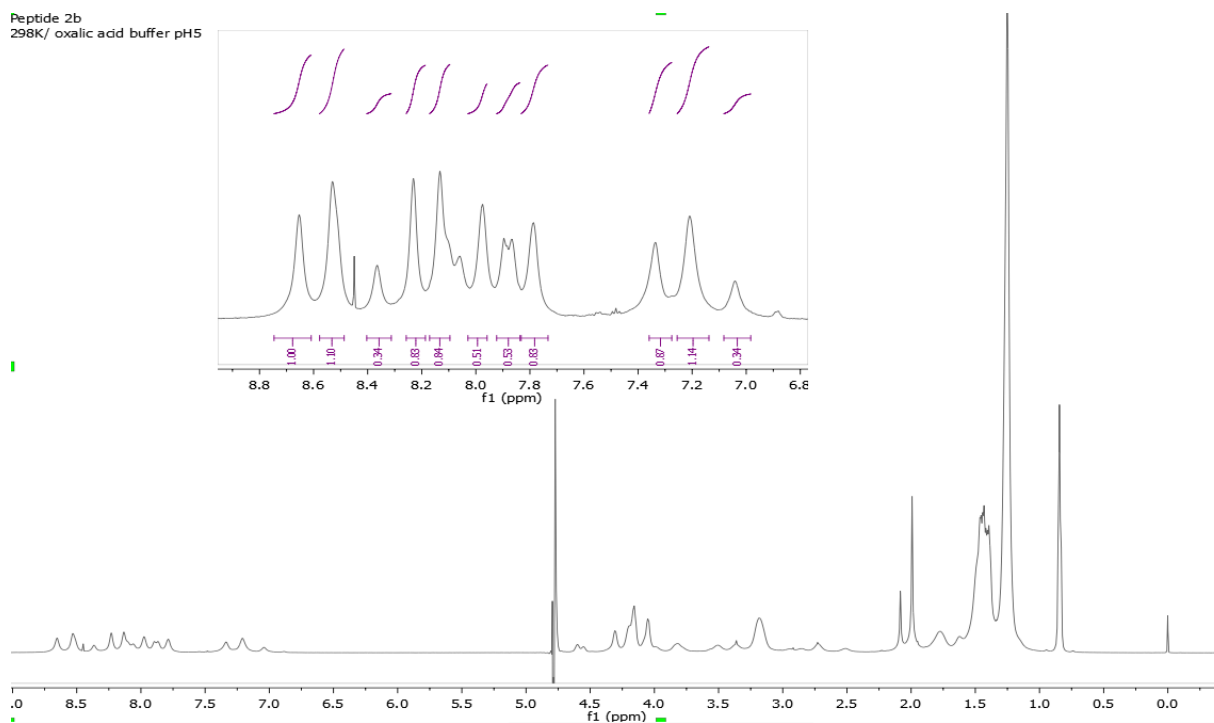


Figure A14. <sup>1</sup>H-NMR spectrum of peptide **40b** in a pH 5 oxalic acid/oxalate buffer in Water/D<sub>2</sub>O 9:1 obtained using the PRESAT pulse sequence for water suppression.

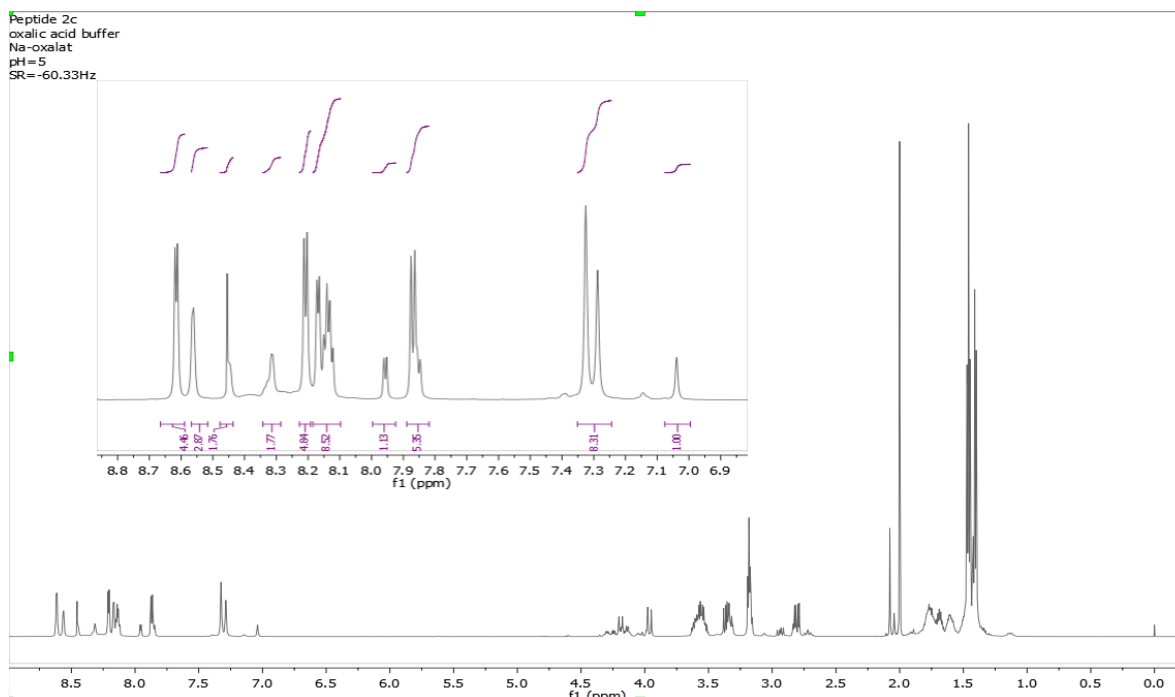


Figure A15.  $^1\text{H-NMR}$  spectrum of peptide **40c** in a pH 5 oxalic acid/oxalate buffer in Water/ $\text{D}_2\text{O}$  9:1 obtained using the WATERGATE pulse sequence for water suppression.

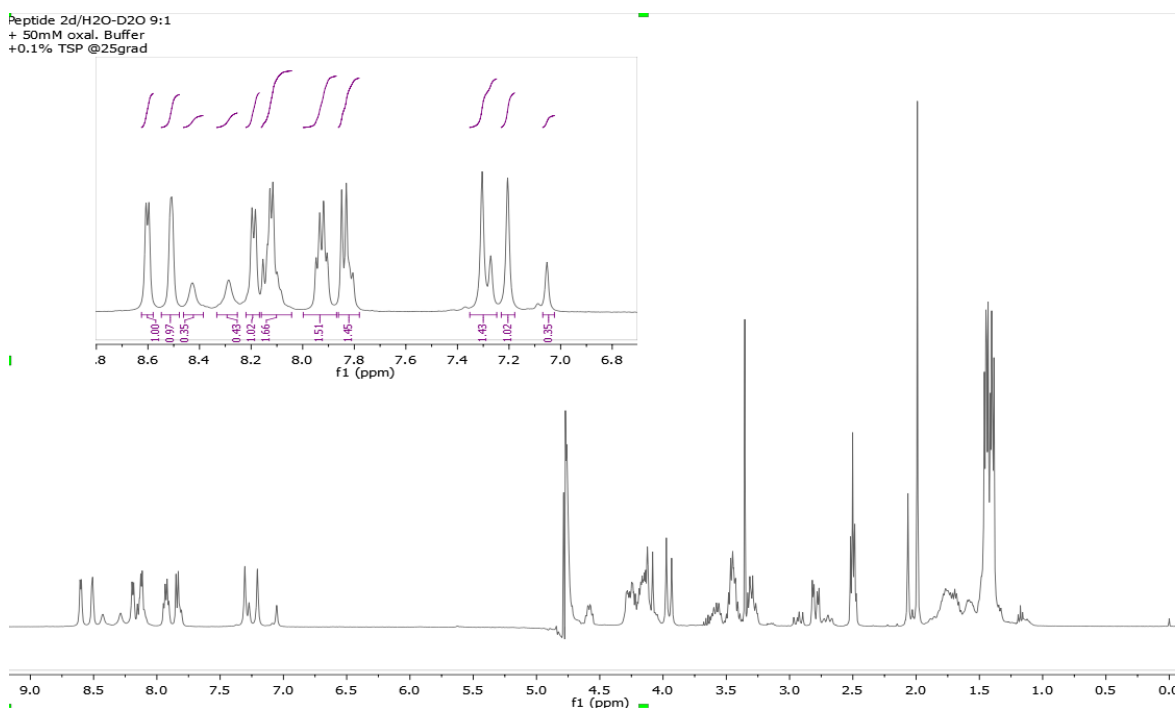


Figure A16.  $^1\text{H-NMR}$  spectrum of peptide **40d** in a pH 5 oxalic acid/oxalate buffer in Water/ $\text{D}_2\text{O}$  9:1 obtained using the PRESAT pulse sequence for water suppression.

Table A7. Full assignment of the NMR resonances for cyclic peptide **64**

Residue	HN( $^3J$ )	HA/CA	HB/CB	CO	others
Ala <sup>1</sup>	-	5.19/52.49	1.20/13.77	169.4	-
Val <sup>2</sup>	7.18(9.6)	4.50/56.66	2.07/31.42	170.9	0.86/19.20 0.90/18.34
Orn <sup>3</sup>	8.66(8.8)	4.77/51.07	1.71;1.57/29.48	170.3	1.57/23.95 2.73/38.63
Leu <sup>4</sup>	8.33(8.8)	4.55/49.72	1.34/40.97	171.6	1.41/23.93 0.80/ 22.59
DPhe <sup>5</sup>	9.17	4.36/53.74	2.90, 2.94/35.56	170.8	136.2; 7.25/129.1; 7.28/128.1; 7.25/128.1
Pro <sup>6</sup>	-	4.30/59.79	1.52, 1.95/29.01	169.7	1.51/23.04 2.52, 3.58/ 45.90
Val <sup>7</sup>	7.19(9.6)	4.42/56.66	2.05/31.08	170.8	0.76/18.94 0.80/ 17.81
Orn <sup>8</sup>	8.55(9.1)	4.82/51.07	1.56/29.55	170.3	1.44/24.59 2.67/39.02
Leu <sup>9</sup>	8.19(8.5)	4.52/49.78	1.23/41.24	172.5	1.19/24.00 0.69/22.07; 22.59
DPhe <sup>10</sup>	9.02	4.23/52.23	2.87, 3.10/34.82	170.8	138.3; 7.29/128.9; 7.25/127.98; 7.19/126.1

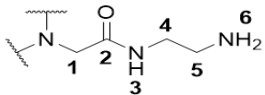
<i>N</i> -substitution	Atom group	$\delta_H/\delta_C$
	1	3.69, 4.85/47.45
	2	-
	3	8.69
	4	3.26/39.97
	5	2.73/39.78
	6	8.47

Table A8. Full assignment of the NMR resonances for cyclic peptide **65**

Residue	HN( $^3J$ )	HA/CA	HB/CB	CO	others
Aib <sup>1</sup>	-	-	1.15/25.88; 1.17/22.07	175.5	-
Val <sup>2</sup>	8.56	4.42/56.9	2.06/30.88	172.1	0.78/22.69, 18.93
Orn <sup>3</sup>	8.58	4.84/51.01	1.66/30.20	170.3	1.65/23.91 2.81/38.99
Leu <sup>4</sup>	8.39(9.0)	4.60/49.9	1.43,1.27/41.32	171.6	1.27/24.22; 0.84/22.93
DPhe <sup>5</sup>	9.33	4.34/53.89	2.88,2.97/35.54	170.8	136.3; 7.24/129.2; 7.29/128.0; 7.25/126.8
Pro <sup>6</sup>	-	4.29/59.67	1.51, 1.92/28.92	169.8	1.48/23.00; 2.50, 3.58/45.78
Val <sup>7</sup>	7.33(9.4)	4.25/57.31	2.05/30.88	171	0.75, 0.81/20.85
Orn <sup>8</sup>	8.94	4.41/51.78	1.70, 1.78/28.43	170.3	1.57/24.79; 2.76/39.30
Leu <sup>9</sup>	8.16(8.8)	4.19/51.89	1.55, 1.44/39.35	170.0	1.45/23.91; 0.71/19.28; 0.73/18.70
DPhe <sup>10</sup>	7.03	4.67/50.48	2.77/38.83	170.4	136; 7.13/129.1; 7.27/128.1; 7.25/126.6

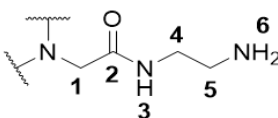
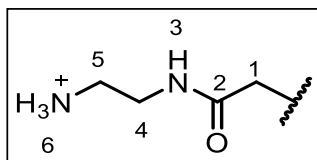
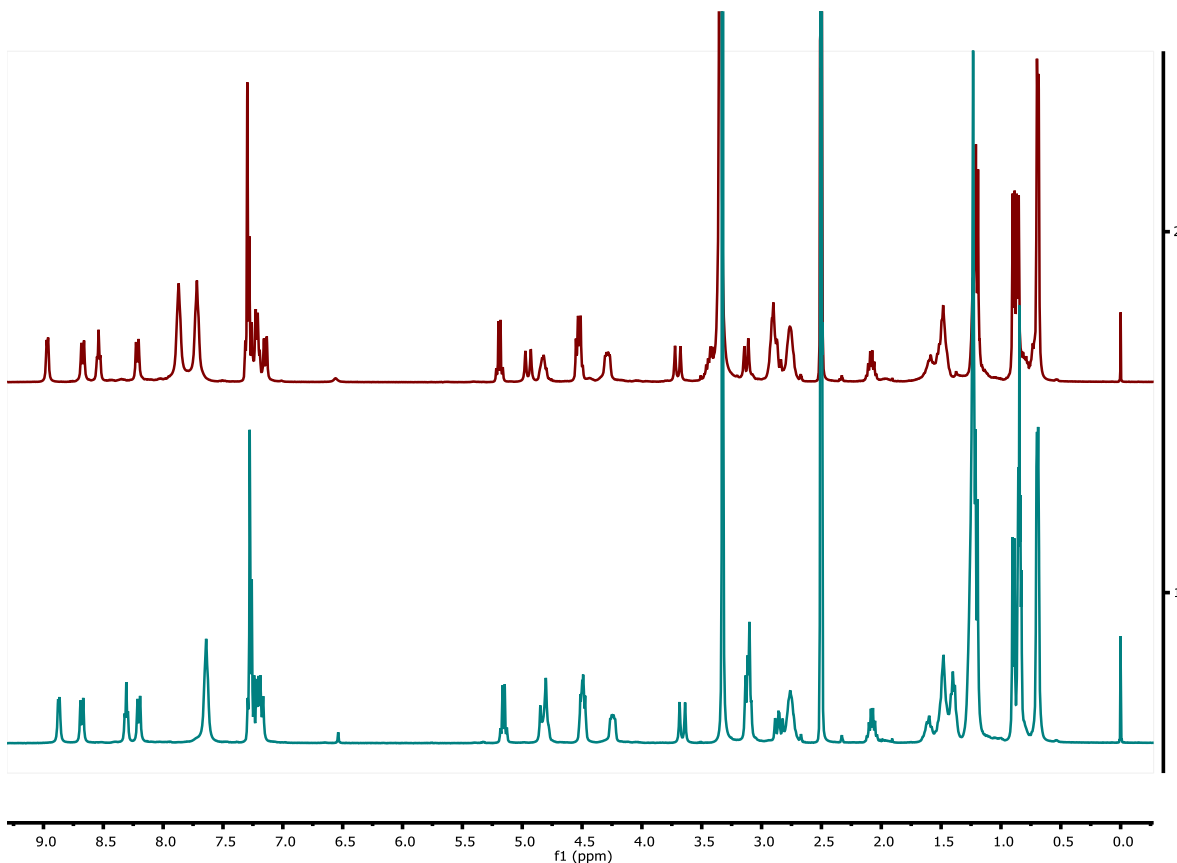
<i>N</i> -substitution	Atom group	$\delta_H/\delta_C$
	1	3.65, 3.82/45.37
	2	-
	3	8.91
	4	3.15/39.89
	5	2.72/39.18
	6	n.d

Table A9. Full assignment of the NMR resonances for cyclic peptide **66**

Residue	HN( $^3J$ )	HA/CA	HB/CB	others
<i>N</i> Ala <sup>1&amp;6</sup>	-	5.19/53.12	1.20/14.33	
Val <sup>2&amp;7</sup>	7.15 (9.5 Hz)	4.53/57.09	2.08/32.02	0.86/19.76 $\gamma$ ; 0.90/18.60 $\gamma$
Orn <sup>3&amp;8</sup>	8.67 (9.1 Hz)	4.82/51.49	1.48/23.80	2.76/39.18 $\gamma$ ; 7.71(bs) $\delta$
Leu <sup>4&amp;9</sup>	8.22 (8.7 Hz)	4.52/50.24	1.23/41.73	1.22/24.46 $\gamma$ ; 0.69/22.88 $\delta$
D-Phe <sup>5&amp;10</sup>	8.97 (5.3 Hz)	4.29/52.5	3.13;2.87/35.38	137.8 $\gamma$ ; 7.30/129.2 $\delta$ ; 7.28/128.5 $\epsilon$ ; 7.21/126.8 $\zeta$

*N*-substitution *N*Ala

Atom group	$\delta_H/\delta_C$
1	4.95;3.70/48.11
2	/
3	8.53(5.7 Hz)
4	3.43;3.34/36.95
5	2.90/39.04
6	7.87(bs)

Figure A17.  $^1\text{H}$ -NMR spectra of cyclic peptides **66** (top) and **67** (bottom)

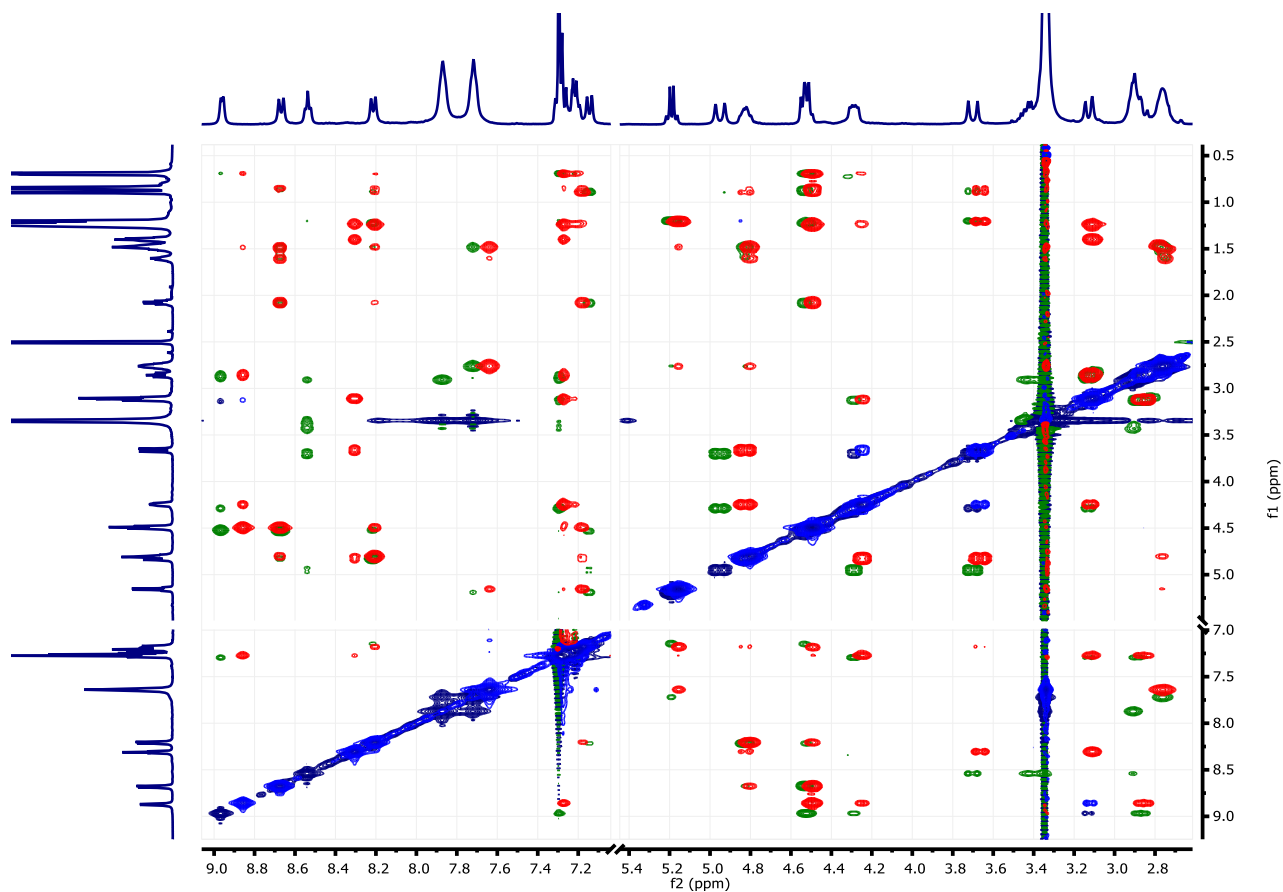


Figure A18. Superimposition of the ROESY spectra (tm= 300ms) for cyclic peptides **66** (green) and **67** (red). Horizontal trace corresponds with 1H-NMR spectrum of cyclic peptide **66** while vertical corresponds to that of peptide **67**. Irrelevant zones of the spectra are omitted for clarity.

## Variable Temperature Analysis for amide protons

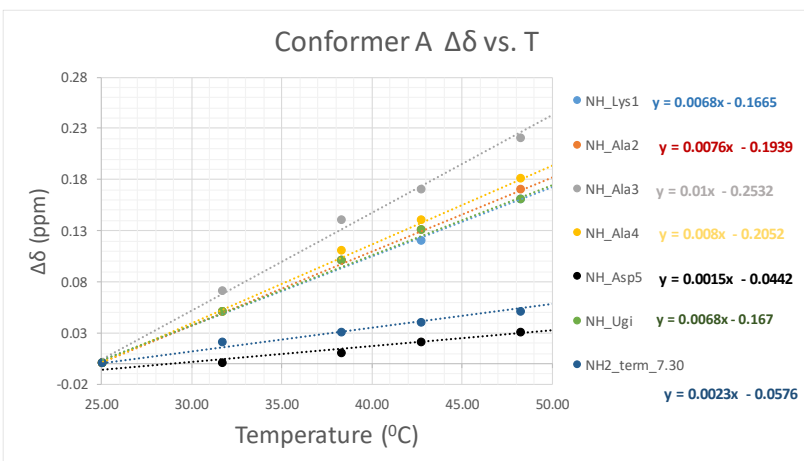


Figure A19. Temperature dependence of amide chemical shifts for the Conformer A of Peptide **40a**

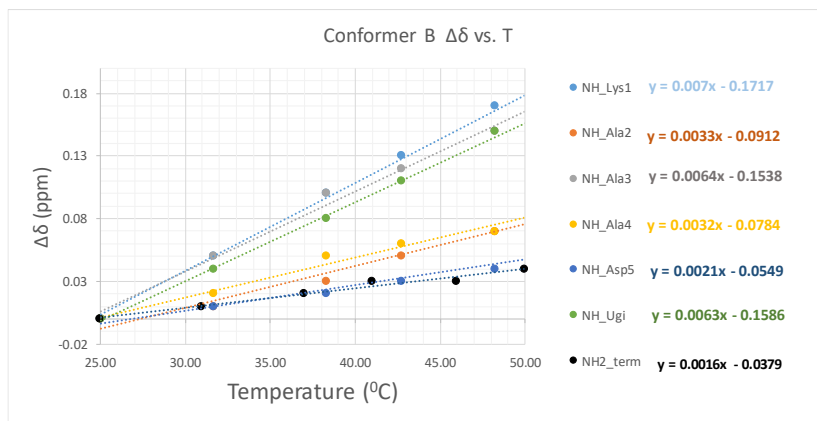


Figure A20. Temperature dependence of amide chemical shifts for the Conformer B of Peptide 40a

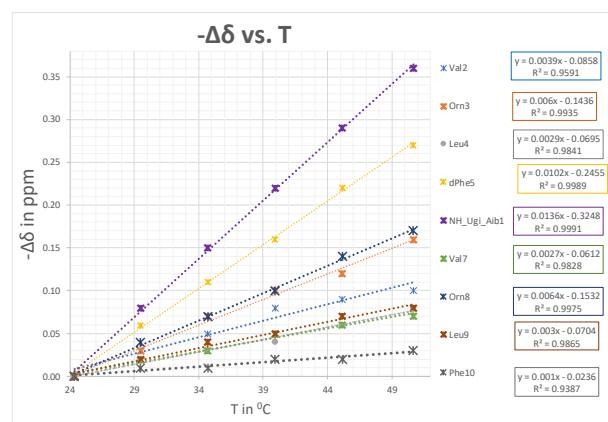
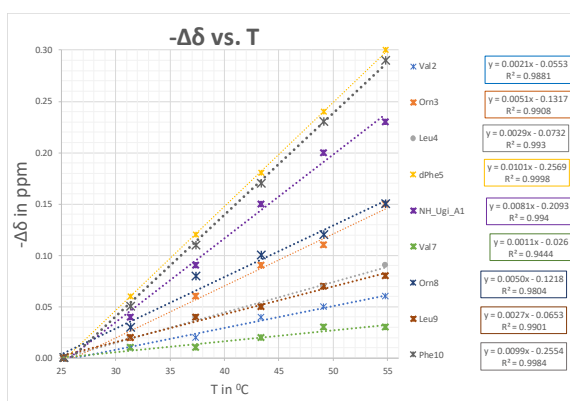


Figure A21. Temperature dependence of amide chemical shifts for compound 64

Figure A22. Temperature dependence of amide chemical shifts for compound 65

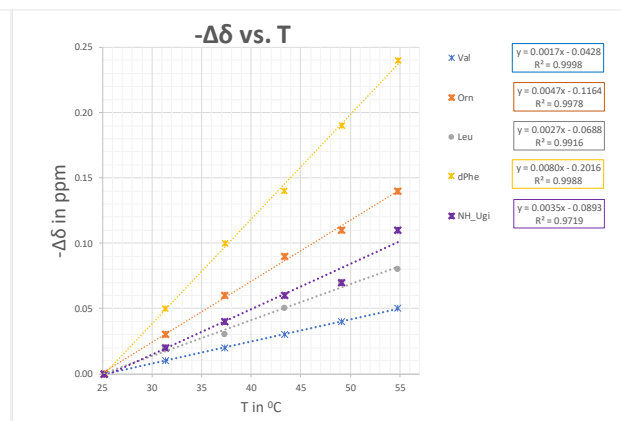
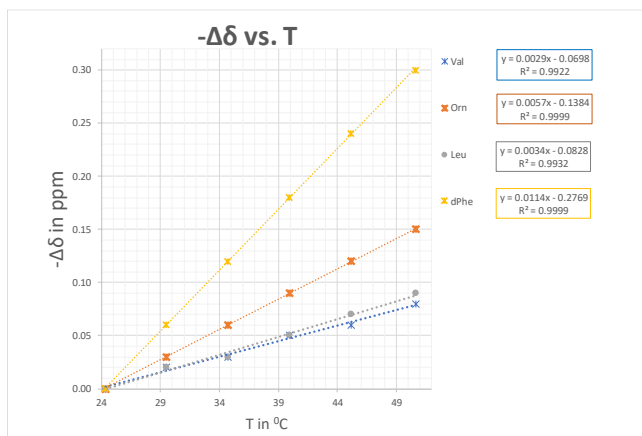


Figure A23. Temperature dependence of amide chemical shifts for Gramicidin S

Figure A24. Temperature dependence of amide chemical shifts for compound 66

---

Internal IPB codes for the compounds within the thesis

	Code Thesis	IPB-Code		Code Thesis	IPB-Code
<b>Chapter 2</b>	29	VAD312	<b>Chapter 4</b>	47	ALV133, ALV159
	30	VAD315		48	ALV151
	36	VAD299		49	ALV138
	38	VAD335		50	ALV166
<b>Chapter 3</b>	39	ALV023, ALV046, ALV077		51	ALV156
	40a	ALV026, ALV080		52	ALV193
	40b	ALV032		53	ALV137
	40c	ALV064, ALV092		54	ALV143
	40d	ALV033, ALV066 ALV092		55	ALV145
	41	ALV065		56	ALV115
	42a	ALV053, ALV061		57	ALV212
	42b	ALV085		58	ALV073
	43	ALV111		59	ALV140
	44	ALV144		60	ALV207
	45	ALV213		61	ALV165
	46	ALV117		62	YAM213
					<b>Chapter 5</b>
			64	RID424	
			65	RID425	
			66	RID410	
			67	RID406	

---

Lic. Aldrin Vasco Vidal (Cuba, 15. November 1989)

## Leibniz Institute of Plant Biochemistry

Weinberg, 3

06120. Halle (Saale). Germany

Tel.: +49 157 59667556. E-mail: aldrinvasco@gmail.com

### CURRICULUM VITAE (08/2019)

University Studies	<b>2008-2013</b> - Diploma in Chemistry, University of Havana. First Honors (5.54 out of 5) Diploma Thesis: Peptide Cyclization. Mention: Excellent
Postgraduate Studies	<b>2015</b> - Master at University of Havana – NMR structural elucidation of cyclopeptides
Positions	<b>2013-2015</b> - Teaching assistant of General Chemistry for Engineers at the Technological University of Havana  <b>2016-present</b> - Ph.D. student at Leibniz Institut of Plant biochemistry (DAAD scholarship)
Awards/Honors	2007 – Silver Medal at the XII Iberoamerican Chemistry Olympiad 2010 – Special Award of the Higher Education Ministry to the best scientific work presented for a novel student in the Faculty of Chemistry's Science Fair 2010, 2011, 2012, 2013 – Several Prizes at the Faculty of Chemistry's Science Fair 2014 – University of Havana Award to the Best Scientific Article
Scientific Interest	<ul style="list-style-type: none"><li>– Synthetic Methods for Biological and Chemical Applications</li><li>– Stabilization of regular and non-regular secondary structures of peptides</li><li>– Molecularly targeted therapy</li><li>– Site-selective protein modification</li><li>– NMR-based 3D structure elucidation of peptides</li><li>– Bioconjugation and Macrocyclization Chemistry</li></ul>
Publications	8 scientific publications, 2 papers in preparation, H-index 3
Research mentoring	4 Master and 1 Diploma thesis co-supervised
Scientific expertise	<ul style="list-style-type: none"><li>– Solid Phase Peptide Synthesis/ Peptide cyclization</li><li>– NMR acquisition on Varian/Agilent spectrometer</li><li>– NMR-based structure elucidation/NMR of peptides</li><li>– MD simulations</li><li>– Organic Synthesis</li></ul>

## Languages

- HPLC chromatography on Agilent/Waters/Knauer/Äkta systems with UV and or MS detection
- Spanish (native)
- English (fluent)
- German (B2)

## Selected conferences and specialized courses

**2019** – 4th Iberoamerican Symposium On Organic Chemistry (SIBEAQO-IV) “Multicomponent Stapling Approaches to Conformationally Constrained Peptides: The Quest for Functionalized Secondary Structures” (Poster Presentation)

**2018** – 35<sup>th</sup> European Peptide Symposium. “Targeting Peptide Secondary Structures with Multicomponent Ligation and Cyclization Strategies”(Poster Presentation)

**2017** – 13<sup>th</sup> German peptide Symposium. “Targeting Peptide Secondary Structures with Multicomponent Ligation and Cyclization Strategies” (Oral Presentation)

**2016** – GNMR School, Goethe-University Frankfurt.

**2015**- International Conference Material Science in the Age of Sustainability, IMRE. “MCR-based cyclization strategies for the secondary structure stabilization of peptide skeletons.” (Oral Presentation)

**2015** – 10<sup>th</sup> Seminars of Advanced Studies on Molecular Design and Bioinformatics. “Structural analysis by NMR and molecular dynamics of side-chain cross-linked cyclopeptides derived from Ugi-4C reaction.” (Poster Presentation)

**2013** – 9<sup>th</sup> Seminars of Advanced Studies on Molecular Design and Bioinformatics. “Structural analysis by NMR and molecular dynamics of a novel peptidosteroid analogue.” (Poster Presentation)

**2012** – Humboldt Kolleg 2012: Challenges and Frontiers of Physics and Chemistry to Modern Biology. “On the cyclization of peptides by the Ugi-4C reaction.” (Poster Presentation)

**2012** – 8<sup>th</sup> Congress of Chemical Sciences, Technology, and Innovation Quimicuba’2012. “On the cyclization of peptides by the Ugi-4C reaction.” (Poster presentation)

**2012** – 8<sup>th</sup> Congress of Chemical Sciences, Technology and Innovation Quimicuba’2012. “Modeling and visual displaying of key mechanisms for supporting Organic Chemistry teaching.” (Oral Presentation)

## Publications List

- **A. V. Vasco**, C. González, S. Gröger, W. Brandt, Jochen Balbach, C. S. Pérez, L. A. Wessjohann, D. G. Rivera. "Insights into *s-cis/s-trans* isomerism and the influence of the lactam bridge *N*-substituent in the secondary structure of Ugi-stapled peptides" *In preparation*
- **A. V. Vasco**, M. Brode, Y. Méndez, O. Valdés, D. G. Rivera, L. A. Wessjohann. "Synthesis of Lactam-Bridged and Lipidated Cyclo-Peptides as Promising Anti-Phytopathogenic Agents". *Molecules*, **2020**, 25, 811. doi:10.3390/molecules25040811
- M. G. Ricardo, **A. V. Vasco**, L.A. Wessjohann, D. G. Rivera. "On the Stabilization of Cyclic  $\beta$ -Hairpins by Ugi Reaction-Derived *N*-Alkylated Peptides: The Quest for Functionalized Proline Surrogates". *Organic Letters*. **2019**, 21, 7307-7310. **Shared first authorship**
- **A. V. Vasco**, Y. Méndez, A. Porzel, J. Balbach, L. A. Wessjohann, D. G. Rivera. "A Multicomponent Stapling Approach to Exocyclic Functionalized Helical Peptides: Adding Lipids, Sugars, PEGs, Labels and Handles to the Lactam Bridge". *Bioconjugate Chem.* **2019**, 30, 253-259.
- Méndez, Y.; De Armas, G.; Pérez, I.; Rojas, T.; Valdés-Tresanco, M. E.; Izquierdo, M.; Alonso del Rivero, M.; Álvarez-Ginarte, Y. M.; Valiente, P. A.; Soto, C. de León, L.; **Vasco, A. V.**; Scott, W. L.; Westermann, B.; González-Bacerio, J.; Rivera, D. G. "Discovery of Potent and Selective Inhibitors of the Escherichia Coli M1-Aminopeptidase via Multicomponent Solid-Phase Synthesis of Tetrazole-Peptidomimetics". *Eur. J. Med. Chem.* **2019**, 163, 481–499.
- Centorame, D. D. E. M.; Senczuk, A. F. G.; Alemán, G. H. J.; **Vidal, A. V.**; Méndez, Y.; Ehrlich, A.; Wessjohann, L. A.; Francioso, A. "Iridoids and Volatile Pheromones of Tapinoma Darioi Ants: Chemical Differences to the Closely Related Species Tapinoma Magnum". *Chemoecology* **2019**, 1–10.
- Y. Méndez, J. Chang, A. R. Humpierre, A. Zanuy, R. Garrido, **A. V. Vasco**, J. Pedroso, D. Santana, L. M. Rodríguez, D. García-Rivera, Y. Valdés, V. Vérez-Bencomo, Daniel G. Rivera\*. "Multicomponent Polysaccharide-Protein Bioconjugation in the Development of Antibacterial Glycoconjugate Vaccine Candidates". *Chemical Science* **2018**, 9, 2581-2588.
- **Aldrin V. Vasco**, Carlos S. Pérez, Fidel E. Morales, Hilda Garay, Dimitar Vasilev, José A. Gavín, Ludger A. Wessjohann, Daniel G. Rivera "Macrocyclization of Peptide Side Chains by Ugi Reaction: Achieving Peptide Folding and Exocyclic *N*-Functionalization in One Shot". *Journal of Organic Chemistry* **2015**, 80, 6697-6707.
- Daniel G. Rivera\*, **A. V. Vasco**, R. Echemendía, O. Concepción, F. E. Morales C. S. Pérez, J. A. Gavín, L. A. Wessjohann, "A Multicomponent Conjugation Strategy to Unique *N*-Steroidal Peptides: First Evidence of the Steroidal Nucleus as a beta-Turn Inducer in Acyclic Peptides". *Chemistry – A European Journal* **2014**, 20, 13150-13161. **Selected as VIP.**